THE UNIVERSITY
of EDINBURGH

New Culture Systems

For Mesenchymal Stem Cells

Cairnan Duffy

Thesis for the Degree of Doctor of Philosophy

University of Edinburgh

March 2015

ABSTRACT

Mesenchymal stem cells are the stem cells that replace the bone, fat and cartilage tissues of the human body. In addition, these cells can form muscles, ligaments and neurons. This wide multipotency has made mesenchymal stem cells of particular interest in the fields of tissue engineering and regenerative medicine. Furthermore, mesenchymal stem cells can modulate the immune system by reducing factors that increase inflammation and immune recognition. This immune recognition suppression has resulted in their application as part of bone marrow transplantation in the prevention of 'graft versus host' disease. There are hundreds of on-going clinical trials using these cells for the treatment of autoimmune diseases such as type I diabetes, arthritis and multiple sclerosis. The increasing importance of these cells has brought in to focus the culture methods used to for their expansion and manipulation. Currently, animal derived components are used as surfaces for their growth and as components in the culture media. This exposes these cells to animal pathogens and antigens that can be passed to the recipients of these cells.

In the first part of this thesis, polymer microarrays were employed to identify alternatives to the biological surfaces currently used for mesenchymal stem cell culture. This platform allowed hundreds of polyacrylates/acrylamides and polyurethanes to be simultaneously scrutinised to identify surfaces that could support their growth and maintain their stem cell characteristics. Identified polymer surfaces were monitored in long-term culture (10 passages) and were shown to retain the cell phenotype and capacity to differentiate, thus providing chemically defined substrates for long-term mesenchymal stem cell culture.

In the second part of this thesis, a 'smart' polymer microarray of hydrophilic cross-linked polymers (hydrogels) were used to remove another key biological component of culture, trypsin. These 'smart' hydrogels modulated their properties depending on the temperature. Hydrogels that could trigger mesenchymal stem cell release after a reduction in temperature were identified. A unique passaging system using a modest temperature reduction for 1h was developed as a passaging method. Cells were

maintained and monitored for 10 passages using this novel enzyme free passaging method. Analysis of the mesenchymal stem cell phenotype and differentiation capacity revealed this method superior than conventional culturing methods.

In the final part of this thesis, a ‘knowledge-based’ small molecule library was designed, which could potentially yield small molecules to manipulate/enhance the mesenchymal stem cell state without the use of biological components. The key protein pathways that control the stem cell state were examine with the bioinformatics tool GeneGo was used to identify compounds that affected these pathways, resulting in selection of 200 small molecules. The effect of the small molecules on the mesenchymal phenotype was examined and 5 small molecules were identified that enhanced the phenotype of these cells. The anti-inflammatory properties associated with the hit compounds led to the investigation of their effects on key surface proteins associated with the immune-modulatory state of the cells. In this preliminary study, two of the small molecules, estriol and spermine, increased the expression of a key mesenchymal stem cell marker STRO-1 and down regulated ICAM-1, a critical component of the immune modulation capacity of this cell type.

TABLE OF CONTENTS

DECLARATION OF AUTHORSHIP

This thesis has been composed by the author, and describes research carried out by the author under the supervision of Dr Paul de Sousa and Professor Mark Bradley at the University of Edinburgh. Where work has been performed either jointly or wholly by others, this is clearly attributed. No part of this thesis has been previously submitted for any other degree or professional qualification.

Parts of this thesis were published previously or have been submitted as:

Duffy, C.R.E., Zhang, R., How, S.E., Lilienkampf, A., De Sousa, P.A. & Bradley, M., (2014) Long term mesenchymal stem cell culture on a defined synthetic substrate with enzyme free passaging. *Biomaterials*, 35(23), 5998–6005. doi: 10.1016/j.biomaterials.2014.04.013. Reproduced by permission of Elsevier.

Duffy, C.R.E., Zhang, R., How, S.E., Lilienkampf, A., Tourniaire, G., Hu, W., West, C.C., De Sousa, P.A. & Bradley, M., (2014) A high-throughput polymer microarray approach for identifying defined substrates for mesenchymal stem cells. *Biomater Sci*, 2014, 2, 1683–1692. doi: 10.1039/c4bm00112e- Reproduced by permission of The Royal Society of Chemistry.

ACKNOWLEDGEMENTS

First of all I would like to thank my Supervisors Dr Paul De Sousa and Professor Mark Bradley for the privilege of working in one of the most exciting fields in science. I would like to thank them for the intellectual growth and change in perspective that comes with the challenges that face every Ph.D. student and also because we could have a laugh at the same time. Disagreement, challenge, encouragement and the clarity of thought that comes with honed critical thinking have been the hallmark of my experience. I have to thank Professor Rong Zhang, colleague, collaborator and most of all friend. A very humble man with massively understated talent who applies a constant pressure on ideas forcing them into reality. I would also like to thank Dr Sew Eng How for her brilliantly timed appearance and the productive work we achieved together and also Kay Samuel for her patients and help with the flow cytometry measurements and analysis. I would also like to thank my friends who made the experience a fantastic one. Dr Anne Hansen for her encouraging words on first arriving 'What are you doing here?', an attitude she continues until this day and Dr Frank Thielbeer for his friendship and help in turning what was a positive current account balance into a negative one before the end of the month.

I would also like to thank Dr Emma Johansson for being herself. There are so many of the little people too numerous to mention (Martin, Martha, Aurelie, Salvo, Neil, Matt) and the newer faces Holly, Matt and the Great Mangani and others and of course my comedy compadres Sesha, who's made me laugh and cry at the same time but for different reasons and Alex who made me cry and laugh at different times for the same reasons. My non-uni posse Emily, Valaria, Kev & Badger, and Soliman for nourishing my soul and stomach.

I would like to give an enormous thanks to my friend Dr Annamaria Lilienkampf whose help over the last year with the preparation of our publications and the input and advice during this thesis has been for some time un-repayable. I suppose would just like to thank the Bradley group members and De Sousa group members for

making this one of the best experience of my life. Finally and above all things Me Ma for her unfailing kindness, making all this possible and my family members for their support and unsentimental outlook on life. I would also like to thank my late father whom I continually miss.

LIST OF PUBLICATIONS

Duffy, C.R.E., Zhang, R., How, S.E., Lilienkampf, A., de Sousa, P.A. & Bradley, M., (2014) Long term mesenchymal stem cell culture on a defined synthetic substrate with enzyme free passaging. *Biomaterials*, 35(23), p5998–6005. doi: 10.1016/j.biomaterials.2014.04.013. Reproduced by permission of Elsevier

Duffy, C.R.E., Zhang, R., How, S.E., Lilienkampf, A., Tourniaire, G., Hu, W., West, C.C., De Sousa, P.A. & Bradley, M., (2014) A high-throughput polymer microarray approach for identifying defined substrates for mesenchymal stem cells. *Biomater Sci*, 2, p1683–1692. doi: 10.1039/c4bm00112e- Reproduced by permission of The Royal Society of Chemistry

Zhang, R., Mjoseng, H.K., Hoeve, M.A., Bauer, N.G., Pells, S., Besseling, R., Velugotla, S., Tourniaire, G., Kishen, R.E., Tsenkina, Y., Armit, C., Duffy, C.R., Helfen, M., Edenhofer, F., de Sousa, P.A. & Bradley, M., (2013) A thermoresponsive and chemically defined hydrogel for long-term culture of human embryonic stem cells. *Nat Commun*, 4, p1335–1345. doi: 10.1038/ncomms2341.

Velugotla, S., Pells, S., Mjoseng., H.K., Duffy. C.R., Smith, S., de Sousa, P. & Pethig, R., (2012) Dielectrophoresis based discrimination of human embryonic stem cells from differentiating derivatives. *Biomicrofluidics*, 6(4), 44113. doi: 10.1063/1.4771316.

CHAPTER 1

INTRODUCTION

1.1 REGENERATIVE MEDICINE, STEM CELLS AND SCAFFOLDS

1.1.1 Regenerative medicine

Regenerative medicine has been defined as a '*therapeutic intervention, which replaces or regenerates cells, tissues or organs, to restore or establish normal function*' (Ducheyne & Qui 1999; Mason 2007). In recent decades, it has emerged as a 'great new hope' for dealing with the medical issues arising from an aging population and because of its theoretical ability to overcome the limitations of conventional medicine. In the future, regenerative medicine will be increasingly applied to the treatment of degenerative and autoimmune diseases, and to the replacement/repair of organs and tissues.

Pharmaceutical drugs often operate by blocking disease processes, such as cholesterol-lowering 'statin' drugs used to block HMG-CoA reductase, a key enzyme in the production of cholesterol. They also operate by preventing other processes that cause injury, such as anti-inflammatory drugs that prevent inflammation, thereby manipulating the body's machinery to achieve a desired aim. Where drug treatments and surgical techniques fail, synthetic implants, mechanical devices and machines such as dialysis can be used to restore some function.

Conventional medical techniques, such as surgery, are framed around the body's inherent regenerative capacity. When surgical treatments alone are insufficient, organ and tissue transplantation can be employed. Transplantation has significant drawbacks, such as the requirement of immune suppression and a limited supply of organs and tissues. Even when tissue matched organs and tissues are available, they have a limited lifespan and will ultimately be rejected by the host immune system.

Regenerative medicine offers great promise, not only because it can overcome some of the limitations conventional medicine, but also because it offers the possibility of circumventing immune rejection completely. Furthermore, regenerative medicine

allows the development of entirely novel strategies that can open up new branches of medicine.

1.1.2 Stem cells

Stem cells are defined as cells with a capacity to "self-renew" and in response to intrinsic and extrinsic determinants, differentiate into more than one cell type with specialised function. The number of tissues and cell types that the cell can produce defines the 'potency' of a stem cell (Fig. 1.1). The newly fertilised egg is 'totipotent' because it can form all the embryonic and extra-embryonic cell types (Tarkowski 1959). It is not a stem cell as with each cellular division that follows fertilisation the resulting cells differ and become more restricted in their potency than the cell from which they derived – there is no self-renewal. However, early in embryo development, it is possible to extract and perpetuate *in vitro* stem cell populations. In mammals, embryo stem cells, with a capacity to give rise to all of the cell types and organs, can be isolated from the inner cell mass cells of a pre-implantation blastocyst conceptus. This includes the three embryonic lineages, the ectoderm layer or 'outside skin' that forms neural tissues and skin, the mesoderm or 'middle skin' that forms muscles and connective tissues and the endoderm or 'inner skin' that forms the intestines and lungs. Together these layers form all the cells of the human body (Fig. 1.1). The renewal of such "pluripotent" stem cells in an unspecified state is dependent on core set of transcription factors. A similar form of pluripotent stem cell can be extracted from a sub-region of the inner cell mass known as the epiblast, which forms after implantation. In some species, such as the mouse, neither pre-implantation inner cell mass or post-implantation epiblast derived stem cells can form extra-embryonic tissues, which constitute the embryo contribution to the placenta. These lineages are dependent on other transcription factors such as ($Gata4^{+}/6^{+}$, Cdx2+) first expressed in the outer cells of a blastocyst stage embryo known as the trophectoderm (Cockburn & Rossant 2010).

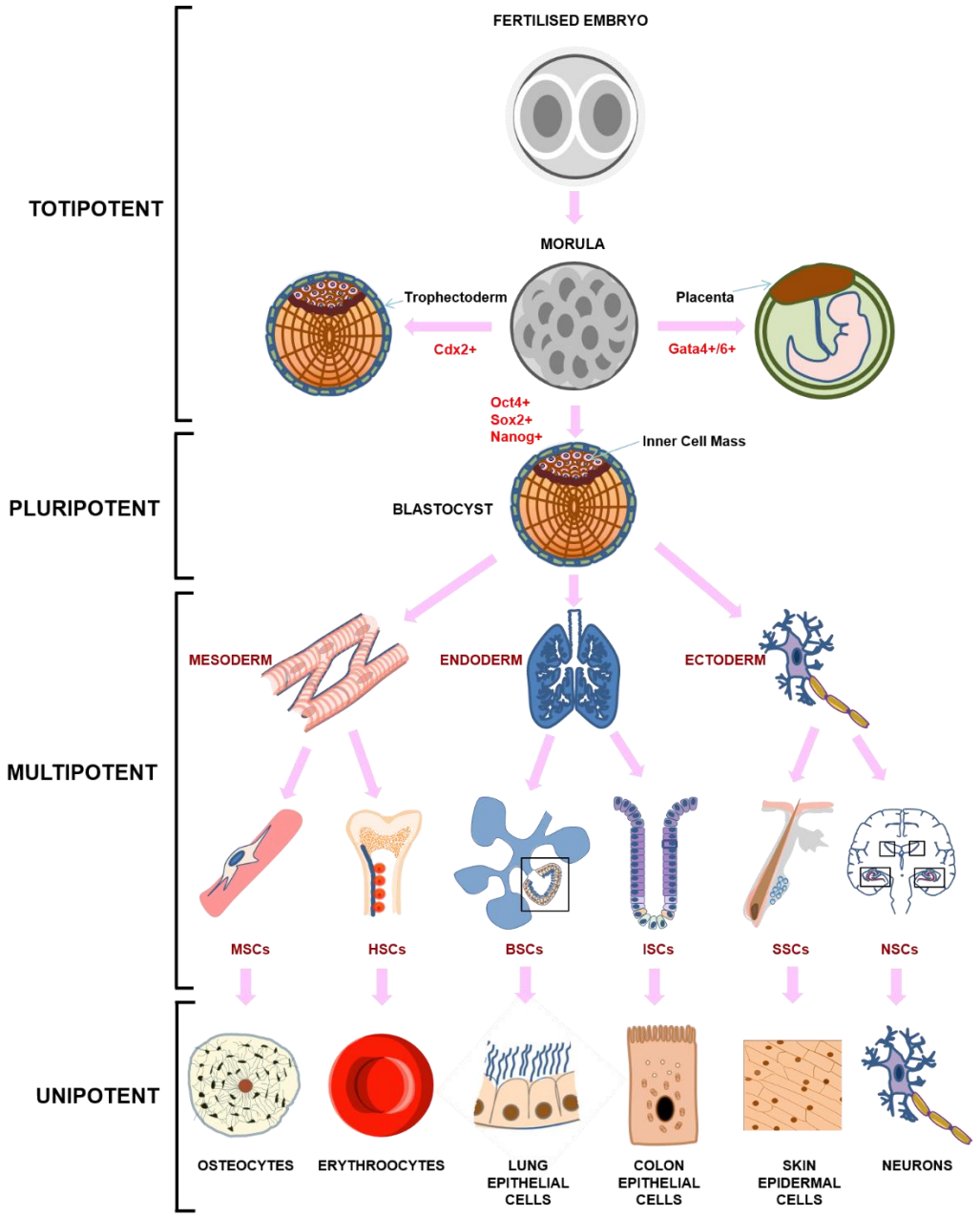

Figure 1.1. *Hierarchy of potency. The fertilised embryo and the morula is totipotent due to its ability to make all the cells of the organism including the extra-embryonic tissues of the placenta (Gata4+/6+) and trophoblast (Cdx2+). The inner cell mass cells are pluripotent, i.e., they can form the three primary germ layers; mesoderm, endoderm and ectoderm and hence all the cells of the body, including the multipotent stem cells and the unipotent differentiated somatic cells (>200). Multipotent stem cells maintain tissue homeostasis after development and reside within specific niches. Mesenchymal stem cells (MSCs) reside next to the vasculature (peri-vascular), hematopoietic stem cells (HSCs) form the lineages of the blood and reside next to the MSCs in trabecular bone. Basil stem cells (BSCs) reside in the lung epithelium. Intestinal stem cells (ISCs) reside in the base of the crypts of intestinal cilia. Skin stem cells (SSCs) reside in the hair follicle and neural stem cells (NSCs) reside in the lateral ventricles (top squares) and the dentate gyrus (bottom squares). These cells go on to form fully differentiated unipotent cells such as osteocytes and neurons.*

1.1.3 Adult stem cells

Once the organism is fully formed, a state of homeostasis emerges where the maintenance and repair of the adult tissues depends on a small subpopulation of stem cells (Fig. 1.1). One of the principle characteristics of stem cells is their ability to self-renew. When they divide they produce one stem cell and one rapidly dividing cell called a trans-amplifying cell that divides a finite number of times before differentiating into the various cell types of the tissue/organ. The low cell turnover or quiescence of the remaining stem cell allows the stem cell phenotype to be maintained over the lifetime of the adult. Stem cells in some adult tissues, which maintain tissue homeostasis generally differ from stem cells which are perpetuated *in vitro*, particularly pluripotent stem cells extracted from early embryos, by being extremely slow growing (*i.e.* long cell division "cycling" times). It was this slow cycling characteristic that allowed many of the stem cell niches to be identified through their retention of radio labelled 5-bromo-2'-dioxyuradine (BrdU) as so-called label retaining cells (LRCs) (Bickenbach et al. 1981). Once localised, the contribution that these cells and their descendants made to the surrounding tissues could be scrutinised in detail to reveal their true stem cell nature. For example, intestinal stem cells were verified in their location in the crypts (Fig. 1.1) by following inheritance patterns of changes introduced at random into gut epithelial cells to reveal single crypt cells that contributed to the entire crypt (Bjerknes & Chang 2002; Winton & Ponder 1990).

More recently, a population of leucine-rich G protein-couple receptor-5 positive cells ($Lgr5^+$ an orphan GPCR receptor of unknown function) were found to be responsible for the generation of the label retaining cell (paneth cell) and for the regeneration of the colon epithelium (Fig. 1.2). The $Lgr5^+$ cells are able to produce mini-guts *in vitro* making them particularly promising for regenerative medicine (Buczacki et al. 2013). In the skin a similar label-retaining experiments identified slow-cycling cells located in the bulge region of the hair follicle (Fig. 1.2E); however, these cells ($CD34^+$, $K15^+$) do not contribute to the epidermis in the absence of injury (Cotsarelis et al. 1990; Braun et al. 2003).

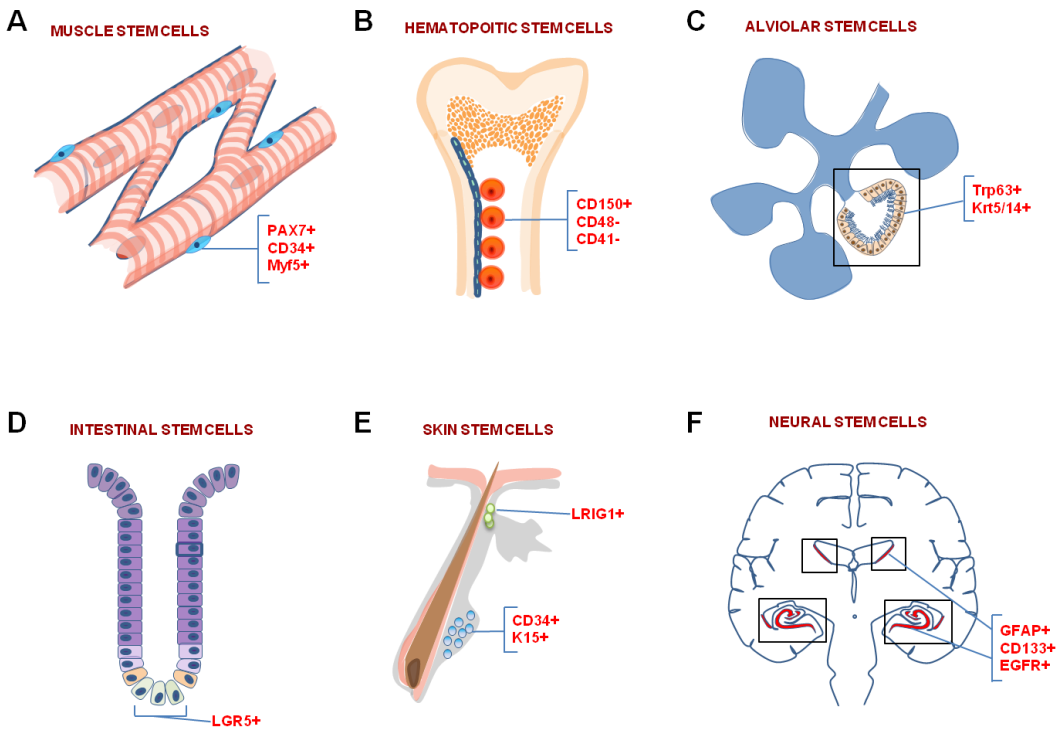

Figure 1.2. *Stem cell niches and associated markers for representative organs and tissues. A) Muscle stem cells also known as satellite stem cells due to their peripheral location on the myotubule are characterised by the expression of Pax7, CD34 and Myf5. B) HSCs located in the bone marrow niche with the 150^{+}, CD48^{-}, CD41^{-} phenotype that characterise all HSCs, they reside specifically near the arterioles and cell permeable vasculature (sinusoids) of the trabecular bone. C) Alveolar stem cells known as basal cells reside in the lung epithelium of the alveoli, identified by their TRP63^{+}, Krt5/14^{+} phenotype are a label retaining cell that reconstitutes the lung epithelium after injury. D) LGR5^{+} intestinal stem cells reside at the base of the intestinal crypts adjacent to paneth (yellow) cells. E) The hair follicle is the niche of two populations of stem cell responsible for the regeneration of hair follicle and skin, one population resides in the bulge region (CD34^{+} and K15^{+}) and the other lies close to the skin surface (LRIG1^{+}). F) Neural stem cells reside in two primary locations, the dentate gyrus (lower boxes) in the hippocampus and in the lateral ventricles (upper boxes) and are signified by GFAP^{+}/CD133^{+}/EGFR^{+} phenotype.*

Another population, LRIG1^{+} cells, contributes to the epidermis but not the hair follicles. The existence of more than one population of stem cells that contribute to various lineages depending on whether the tissue has been exposed to injury is common to both the intestinal and skin stem cell niches (Buczacki et al. 2013; Braun et al. 2003).

Identifying stem cells in organs with slow cell turnover, *i.e.*, stem cell niches in 'terminally differentiated' organs such as the heart and brain required the opposite approach (identification of cells undergoing renewal). In the brain, early studies to identify renewal involved the application of tritiated thymidine, which incorporates into the DNA of dividing cells and is detected by autoradiography (Smart & Leblond 1961). This work identified the sub ventricular zone (SVZ) (Fig. 1.2F) as one of the main reservoirs of neural stem cells. Later work identified the dentate gurus (DG) and olfactory bulb as a second location for these cells (Kaplan & Hinds 1977). Neural stem cells primarily differentiate into astrocytes, oligodendrocytes and neurons. The niche contains activated neural stem cell identified by the markers $GFAP^+$ (glial fibrillary acidic protein), $CD133^+$ (prominin, a transmembrane glycoprotein expressed on the cilia), $EGFR^+$ (epidermal growth factor receptor), as well as a quiescent neural stem cell identified by the markers $GFAP^+$ and $CD133^+$ (Codega et al. 2014) (Fig. 1.2F). Resident stem cell populations that repair the peripheral nervous system have yet to be isolated. However, Swann cells have demonstrated extensive plasticity and even dedifferentiation in response to injury through the activation of Sox2 (Le et al. 2005) and cJun (Arthur-Farrage et al. 2012). Injury causes the Swann cells to take on an undifferentiated 'Büngner' cell phenotype (where Sox2 and cJun are up-regulated) to proliferate allowing regenerating axons to create a nerve bridge and restore function (Kim et al. 2013).

Where skin and intestinal stem cells reside in high turnover organs and neural stem cells reside in 'terminally differentiated' organs, other stem cell niches reside in organs that have relatively low cell turnover but retain impressive regenerative capability, such as the liver, muscle and lungs. This is highlighted by the fact that two thirds of the liver can be removed and it will regenerate. In skeletal muscles, injury results in very efficient regeneration through the activation of normally quiescent cells known as satellite cells, which are located on the outer part of the muscle fibres (Fig. 1.2A). These cells were first implicated through the distribution of thymidine in the muscle fibres (Moss & Leblond 1971) with later experiments using isolated myofibrils showing their definitive contribution (Bischoff 1975; Bischoff 1986) and their ability to self-renew (Collins et al. 2005). Injury of the muscle cells causes these cells to exit their quiescent phase to self-renew to produce

a daughter satellite cell and a trans-amplifying cell that become myoblasts and eventually the myofibre. This process is characterised by the concerted up regulation and down regulation of a number of different genes at different stages. Genes CD34, PAX7 and Myf5 characterise the quiescent phase of the satellite cells (Fig.2). Pax7 is a transcription factor that is essential for the formation and maintenance of functional satellite cells (Kuang et al. 2006). Pax7 has been shown to associate with the Wdr5–Ash2L–MLL2 histone methyltransfease (HMT) complex that directs methylation of histone H3 lysine 4 (H3K4). Pax7 associates with the Myf5 (among other myogenic development genes) gene resulting in H3K4 trimethylation of the surrounding chromatin and transcriptional activation (McKinnell et al. 2008). Myf5 is expressed in quiescent satellite cells (Kuang et al. 2007), however, they are prevented from entering the myogenic program through the sequestration of Myf5 mRNA in messenger ribonucleoprotein (mRNP) granules. In activated cells the mRNP granules dissociate and the satellite cells enter the myogenic program (Crist et al. 2012).

During activation of satellite stem cells the myogenic transcription factor MyoD is also up regulated through Six1 (Sine oculis homeobox gene 1) (Liu et al. 2013). MyoD targets a large number of myogenic differentiation genes, 1.4k in myoblasts and 9.3k in myotubes. Initial expression of MyoD does not initiate differentiation as the targets of MyoD are blocked through the transcriptional repressor Snail by the recruitment of histone deacetylases HDAC1 and HDAC2. This results in continued myoblast proliferation until expression of two miRNAs, miR30a and miR206 that target snail1 and snail2 respectively resulting in their removal and activation by MyoD target genes (Soleimani et al. 2012). Terminal differentiation ensues with the up-regulation of myogenin and the formation of the myotube. At this point the quiescent stem cell markers CD34 and PAX7 are down regulated signifying commitment to differentiation and fusion of the cells into the myotubule. The final maturation phase is signified by the expression of MLC3F and the down regulation of Myf5, MyoD and Myogenin (Zammit et al. 2006). The age associated degeneration of muscle fibres resulting in sarcopenia (muscle loss) has recently been demonstrated to be the result of alterations of fibroblast growth factor receptor 1, p38α and p38β mitogen-activated protein kinase signalling in satellite cells. This study showed that muscle loss was due to the loss of the satellite cells ability to self-

renew. Remarkably, pharmacological manipulation of the pathways was able to ameliorate the age associated muscle loss and restore the satellite stem cells capacity for self-renewal (Bernet et al. 2014).

In the lung, turnover is relatively low, but again the lung has the capacity to regenerate after removal of large sections of tissue (unilateral pneumectomy) (Esenhauer et al. 2013). The lungs harbour label retaining cells known as basal stem cells. These cells are signified by the markers, transformation related protein 63 (Trp63) and cytokeratin 5 and/or 14 (Krt5/14) (Hong et al. 2004). Basal stem cells repopulate the lung epithelium after injury. Regaining the precise dimensions of the damaged tissue is important to restore lung function. Patterning of the lung tissue during development occurs primarily through secretion of FGF10 by progenitor cells in the developing bud (Nyeng et al. 2008), and the distance of the cells from the FGF10 determines the ability of the cells to differentiate with cells furthest away able to fully differentiate. Likewise, in the adult lung basal cells produce FGF10 after injury allowing progenitor cells to expand in the surrounding areas (Volckaert et al. 2013) until a state of homeostasis is re-established (Hsu et al. 2012).

Finally, the most well-known and applied stem cells are hematopoietic stem cells in the bone marrow, the critical cells in bone marrow transplantation. The ability to isolate these cells using surface markers dates back to 1988 (Spangrude et al. 1988). These non-label retaining cells (Kiel et al. 2007) are identified by their $CD150^{+}CD48^{-}CD41^{-}/CD41^{low}$ immunophenotype (Kiel et al. 2005). *In vivo* the hematopoietic stem cell niche is composed of mesenchymal stem cells (Méndez-Ferrer et al. 2010) and endothelial cells in the perivascular niche adjacent to the blood vessels in the trabecular bone (Fig. 1.2B). The maintenance of the niche operates through the production of CXCL12 and stem cell factor (SCF) by mesenchymal stem cells and endothelial cells (Ding et al. 2012).

The structure of the niche is composed of the interface of the trabecular bone with the bone marrow called the endosteum. HSCs are mainly located near the sinusoidal endothelial cells and arterioles peripheral to the central vein. Sinusoids are structures in the bone marrow composed of endothelial cells that are a discontinuous reticulum with holes that allow cells to move freely from the bone marrow into the vascular

system. Located on the surface of endothelial sinusoidal cells are a number of other phenotypes that have been shown to be critical to maintaining the hematopoietic stem cell niche, including CXCL12-abundant reticular (CAR) cells (Sugiyama et al. 2006) and lepr^{+} perivascular cells. CXCL12 (also known as SDF-1) and its receptor CXCR-4 have been shown to be critical in HSC engraftment. Disruption of this axis through chronic G-CSF followed by acute treatment with plerixafor (AMD3100) results in rapid HSC mobilisation (Pitchford et al. 2009).

Secretion of stem cell factor (scf) has also been shown to be important in this niche with the lepr+ cells expressing the highest levels and the endothelial cells expressing lower levels (Ding et al. 2012). Elimination of scf from endothelial (Tie2^{+}) and lepr^{+} cells in the sinusoidal niche results in the elimination of 85% of the HSC population (Oguro et al. 2013). Other locations in the bone marrow have also been shown to effect the HSC niche. Arterioles are small arteries located peripherally to the central vein and supply the bone marrow with nutrients and oxygen. Quiescent HSCs are located next to the arterioles which are in sheathed in nestin^{+} NG2^{+} perivascular cells distinct from the lepr^{+} cells located on the sinusoids (Kunisaki et al. 2013).

Isolation of the location of adult stem cells, identification of unique markers for resident stem cell populations, and understanding of the niche within which the stem cell resides, has advanced considerably in the last decade. In terms of regenerative medicine, where an autologous source of stem cells is intended for use in a particular application, knowing the location and the identity of the stem cell population, and the factors affecting its maintenance, is critical. This was clearly demonstrated by the pharmaceutical manipulation of the signalling pathways for the satellite stem cell to restore function (Bernet et al. 2014). When the identifying markers of the stem cell population are on the cell surface, as with LGR5^{+} intestinal stem cells, the cells can be isolated using flow cytometry, and manipulated and differentiated *in vitro* under the appropriate conditions (in the case of LGR5^{+} cells to produce 'mini colons'). The use of autologous stem cells for the recapitulation of organs and tissues has the advantage of avoiding immune rejection and use of immunosuppressant medication. A biopsy followed by the isolation of the stem cell population and subsequent expansion *ex vivo* is the preferable route where possible. However, in some cases the

sources of the stem cells can be limited or inaccessible (e.g. neural stem cells and cardiac stem cells). In addition, the 'autologous route' does not offer 'off the shelf' treatments, which is one of the goals of regenerative medicine.

1.1.4 *In vitro* pluripotent stem cells

One of the most important achievements in regenerative medicine has been the isolation of the human cells of the inner cell mass in pluripotent state, and their maintenance for extended passage *in vitro* (Thomson et al. 1998). This has provided an *in vitro* model for mammalian and human development and disease processes. Importantly, it provided a potentially unlimited source of cells for regenerative medicine as these human embryonic stem cells (hESCs) had seemingly unlimited *in vitro* expansion capacity. Consequently, the ability of human embryonic stem cells to differentiate into the various cells of the human body such as cardiomyocytes, osteoblasts, neurons, and hepatocytes has been demonstrated (Kehat et al. 2001; Sottile et al. 2003; Zeng et al. 2004; Duan et al. 2010). It has also been possible to differentiate hESCs into cells that display the stem cell phenotype, providing a potentially unlimited source of multipotent stem cells (Ardehali et al. 2013; Karlsson et al. 2009).

A significant advance in pluripotent stem cell research involved the reprogramming of fully differentiated human fibroblasts using retrovirus transfection containing the genes that encode for the four reprogramming factors Oct4, Sox2, Klf4 and cMyc (Takahashi et al. 2007). This work followed on from the identification of these 4 factors in the reprogramming of MEFs into cells indistinguishable from mouse embryonic stem cells (Takahashi & Yamanaka 2006). The ability to reprogram differentiated adult cells into pluripotent stem cells (called induced pluripotent stem cells or iPS) avoided the ethical issues surrounding hESC derivation (from fertilised human embryos) and provided a source of stem cells that have the potential to reduce immune rejection. iPS also offer a means for deriving pluripotent stem cells from patients with genetic diseases providing more accurate *in vitro* models for diseases such as Huntington's disease (Park et al. 2008). iPS are particularly advantageous for

the study of human neural disorders due to the inability to access the tissues at various stages of disease progression. iPS generated from genetic neural disorders gives the further advantages that the observed response/behaviour of cells can be directly attributed to identified mutations. Neural diseases that can be non-hereditary or hereditary are particularly active areas of research, for example familial Parkinson's disease (PD) arises due to mutations in the LRRK2, PINK1, SNCA, PARKIN, DJ-1, ATP1A3, UCHL1 and GBA genes (Imiazumi & Okano 2014). These genes are also implicated in the pathogenesis of sporadic PD. Motor symptoms do not appear until 70% of dopaminergic neurons in the substantia nigra have been lost, iPS has allowed for the generation of cell models of familial PD associated with mutations such as PARKIN (Imiazumi et al. 2012) to provide better models of this disease and of PD in general. The increased understanding of resident stem cells, the ability to derive pluripotent stem cells from fertilised embryos, and through the reprogramming of differentiated fibroblasts, gives the field of regenerative medicine a number of different tools to be applied to the myriad of human diseases and degenerative disorders

1.2 MESENCHYMAL STEM CELLS

Mesenchymal stem cells (MSCs) were first isolated from a bone marrow aspirate by Friedenstein as a rare population of fibroblastic cells termed 'colony forming units' (Friedenstein et al. 1974). These cells were later identified as a multipotent stem cell population that can give rise to bone, fat and cartilage tissues (Pittinger et al. 1999). The identification of the *in vivo* niche as well as *in vivo* phenotype was much later identified as PDGFR-b, CD146 and NG2 positive cells located next to the vasculature (Crisan et al. 2008) (Fig. 1.2). Within the bone marrow, MSCs act as a supportive stromal layer for hematopoietic stem cells (section 1.1.2). The importance of this cell type for regenerative medicine and tissue engineering arises from their wide multilineage potential, immune-modulation properties, ease of isolation, and the growing number of sources from which they can be obtained. Their diverse

response to material properties is also making MSCs a particularly useful model system for cell/substrate interactions (Engler et al. 2006).

1.2.1 Embryonic origins from mesenchyme and neural crest lineages

Although MSCs have been extensively researched for their regenerative potential, the embryonic origin of this stem cell *in vivo* is not fully understood. What is known is that these cells come from both the ectoderm (Takashima et al. 2007) and mesoderm lineages (Dennis & Charbord 2002b). The mesoderm is seen as the primary source of MSCs that form the bone and connective tissues (Dennis & Charbord 2002b). Pericytes that develop around the trunk vessels in the axial and lateral plate are thought to come from the mesoderm (Hungerford & Little 1999). Evidence for their mesodermal origins stems from the fact that they show the same markers during development as other cells of mesodermal origins (*e.g.* vascular smooth muscle) (Remy-Martin et al. 1999; Owens 1995). MSCs also localise with other stem cells of mesodermal origin such as hematopoietic stem cells (Mendes et al. 2005; Mendes-Ferrer et al. 2010). MSCs from ectodermal origin are derived from neural crest cells (Le Douarin et al. 2004). After the formation of the three primary germ layers, the ectoderm splits into two, forming the surface ectoderm and the neural ectoderm. The neural ectoderm goes on to form the neural tube (precursor to the brain and spinal cord). The dorsal part of the tube that is in contact with the surface ectoderm is where the neural crest cells reside. These migratory cells have wide multilineage potential and form neurons, glial cells of the peripheral nervous system, smooth muscle cells of the heart and bone, cartilage cells of the face and mesenchymal stem cells (Morikawa et al. 2009). MSCs derived from neural crest cells retain some of their neural lineage capacity (Shi et al. 2013). The mixed embryonic origins may explain the wide range of cell types that MSCs are capable of differentiating into as well as the variety of sources (Nery et al. 2013).

1.2.2 Applications of MSCs

The potential of MSCs in stem cell therapy has grown with increasing numbers of accessible and more readily obtainable sources of these cells including adipose tissue (Zuk et al. 2001), umbilical cord blood (Lee et al. 2004), and Wharton's Jelly (Wang et al. 2004). In addition, the range of cell types that MSCs can generate has expanded from the originally characterised adipocytes, chondrocytes and osteocytes (Pittenger et al. 1999) to smooth muscle cells (Wakitani et al. 1995) and neurons (Tropel et al. 2006). Furthermore, MSCs have also been shown to be capable of modulating the immune response, attenuating inflammation and graft *versus* host responses (Lazarus et al. 2005). Hundreds of clinical trials (http://clinicaltrails.gov, accessed 2nd June 2014) are underway investigating MSCs ability to modulate the immune system in a number of diseases as well as for tissue repair (Uccelli & Prockop 2010; Singer & Caplan 2011). The discovery that MSCs prevented T cell proliferation *in vitro* and *in vivo* to promote skin graft survival (Bartholomew et al. 2002) has resulted in these cells being applied to many other autoimmune diseases including type 1 diabetes (Fiorina et al. 2009), arthritis (Augello et al. 2007), Crohn's disease (Dala et al. 2012) and multiple sclerosis (Cohen 2013).

In tissue engineering, MSCs have long been used for bone repair in conditions such as critical bone defect repair (Long et al. 2014) and cartilage repair (Gopal et al. 2014). Their use has also expanded into periodontal applications (Tobita & Mizuno 2013), myocardial infarction (Yannarelli et al. 2014) and wound healing (Maxson et al. 2012). Surgical stitches have been filled with adipose derived MSCs to accelerate healing (Reckhenrich et al. 2014; Casado et al. 2014). MSCs have been successfully applied in the clinical transplantation of a tissue engineered trachea (Macchiarini et al. 2008). In this ground breaking study, a donor trachea was first decellularised and subsequently reseeded with MSCs and endothelial cells that were extracted from the patient's bone marrow and brachial mucosa respectively. The cells were expanded *in vitro* and in the case of MSCs, differentiated toward chondrocytes, and then injected onto the decellularised trachea where they were further cultured in a bioreactor. Transplantation resulted in the restoration of normal function in what was once a fatal prognosis. A 5 year follow up study found that a cicatricial stenosis had

developed in the native trachea which required repeat stinting. However, the tissue engineered trachea had completely recellularised and vascularised with normal respiratory function and no anti-donor antibodies had developed (in the absence of any immune-suppression treatment). To date this procedure provides the best treatment option with patients with a long segmental airway disorder (Gonfiotti et al. 2014).

The growing number of applications, and therefore increasing importance of MSCs in stem cell biology, has made it crucial to develop fully defined culture systems to allow the expansion of these cells for research and therapeutic purposes. The maintenance of MSCs in their 'stem cell' state in the absence of undefined components remains a challenge and represents a major limitation for their long-term clinical potential.

1.2.3 MSC sources

MSCs populations are heterogeneous populations containing undifferentiated MSCs as well as various progenitor cell types with varying degrees of multipotency (Pevsner-Fischer et al. 2011). Although the criteria for identifying cells as MSCs include the ability of cells to differentiate towards the adipogenic, osteogenic and chondrogenic lineages, the proportion of cells that are multipotent within a population remains unknown. Without functional MSCs markers, the criteria for defining and isolating MSCs are based solely on consensus which lack meaningful correlation to the multipotent state (Dominici et al. 2006). Currently, the phenotype of MSCs is defined as the ability to adhere to tissue culture plastic, being positive for CD90, CD105, CD73, negative for CD45, CD34, CD14, CD19 and HLA-DR, and the ability to differentiate down the osteogenic, adipogenic and chondrogenic lineages (Dominici et al. 2006). In the development of more selective defined systems, which specifically selects for a homogenous multipotent sub-population, the readout in terms of positive markers for the MSC phenotype and markers for progenitor and differentiated cell types will be critical. Markers that reflect multipotency will determine the success or failure of these culture environments.

Some strategies have attempted to sidestep MSC *in vitro* culture all together by using freshly isolated MSCs from adipose tissue, an abundant source of MSCs. This is possible due to the fact that *in vivo* pericyte markers (a perivascular cell type with the MSC phenotype) are known (PDGF-Rβ, NG and CD146). Direct isolation of these pericytes using flow cytometry can theoretically provide the cell numbers required for MSC therapies (James et al. 2012). However, the quantity of the antibodies required makes this approach impractical.

The heterogeneity of MSC culture is further complicated by the large variety of tissues that MSCs have been isolated from. This in itself is not an issue, but considerable marker variation occurs depending on the source of the MSCs (Table 1.1) (Nery et al. 2013; Murray et al. 2014).

Table 1.1 *MSC marker expression of MSCs derived from a variety of sources.*

MSC MARKER	hMSC	PLACENTA	hADMSC	SYNOVIAL TISSUE	UMBILICAL CORD	DENTAL PULP
CD14	X		X			
CD34			X			
CD58	X	X	X	X		
CD73			X		X	X
CD90	X		X	X	X	X
CD105	X		X			X
CD146	X					X
CD271						
STRO-1						
HLA-DR					X	
PDGF-Rβ						
REF	Niehage (2011)	Brooke (2008)	Gimble (2007)	Fickert (2003)	Kerstendjiea (2008)	pivoruuinas (2010)

In addition, the source of the MSCs can result in differences in differentiation capacity. Adipose derived MSCs (ADMSCs) and bone marrow derived MSCs (BDMSCs) differentiation capacity reflect the source of the tissue. ADMSCs and BDMSCs differentiate significantly better into adipocytes and osteocytes, respectively (Peng et al. 2008). Some of these differences are due differences in receptor signalling, such as the requirement for BMP-2 and TGF-β signalling for chondrogenic differentiation. Weak chondrogenic differentiation with ADMSCs can be compensated for by addition of both factors in the chondrogenic diffentiation media (Mehlhorn et al. 2007).

1.2.4 Development of hES-MPs from human ESCs

An alternative and potentially unlimited source of MSC has emerged with the development of protocols for obtaining mesenchymal progenitors (MPs) from hESCs. This can potentially produce cells of consistent phenotype and multipotency (Karlsson et al. 2009; Kopher et al. 2010). The three principle methods for obtaining mesenchymal stem cells (MSCs) from hESCs are via embriod body (EB) formation (Brown et al. 2009), via substrate outgrowth culture (Karlsson et al. 2009), or by co-culture with more differentiated cell types (Barberi et al. 2005). Very often EB formation is followed by plating and differentiation, similar to outgrowth culture (Sottile et al. 2003). In terms of clinical applicability and simplicity, the outgrowth culture method has an advantage due to the lack of an EB step. For example, Karlsson et al. plated hESCs on 0.1% gelatin feeding the cells with MSC medium consisting of DMEM with 10% fetal calf serum (FCS) supplemented with 10ng/mL of human recombinant basic fibroblast growth factor (hrbFGF). Serial passaging produced a homogeneous fibroblast morphology of hES-MPs with the characteristic markers of MSCs (Dominici et al. 2006) and chondrogenic, adipogenic and osteogenic differentiation potential. The hES-MPs can passaged for > 20 passages without sinesence (Karlsson et al. 2009). hESC derived MSCs can supply ‘off the shelf’ therapies but the potential of immune rejection and the accessibility of

autologous MSCs means that present research is primarily focused on autologous sources of MSCs. hESCs do present a consistent and unlimited supply of MSCs for research purposes without the need for primary sources.

1.2.5 MSC markers

A review of the literature would indicate that some markers are better indicators of MSC potency. It has been suggested that CD146 could be used as a single marker for MSC potency; however, this is also a marker of endothelial cells. Furthermore, MSCs from the tunica (adventitial cells) are negative for CD146 and positive for CD34 (Corselli et al. 2012). CD271 (low affinity nerve growth factor receptor) has become commercially popular marker due to its high expression and ability to isolate the entire CFU-F fraction of cells from bone marrow aspirate (Buhring et al. 2007). The ability of MSCs to form colonies is critical component for expansion and multipotency (Castro-Malaspina et al. 1980). When over expressed, CD271 inhibits the differentiation of MSCS into osteogenic, adipogenic, chondrogenic, and myogenic lineages indicating an important role in maintaining the MSC state (Mikami et al. 2011).

STRO-1 was the first MSC marker used to isolate MSCs from bone marrow aspirate as opposed to tissue culture plastic adherence. The STRO-1 antibody was generated by raising antibodies against the stromal fraction of bone marrow aspirate (Simmons & Torok-Storb 1991) and has also been used to isolate the CFU-F fraction of freshly sorted MSCs (Gronthos et al. 1994). This has made it one of the most widely used Markers. Cells isolated purely on STRO-1 intensity have increased expression of the cytokine stromal derived factor 1 (SDF-1) and PDGF-ββ. The addition of PDGF-ββ and SDF-1 to media results in a significant increase in CFU-F frequency and reduced IL-4 induced apoptosis (Kortesidis et al. 2005). The STRO-1 fraction has also been shown to be the one responsible for the immune modulation capability of MSCs (Nasef et al. 2009). This, combined with the extensive characterisation of the STRO-1, makes it a good ‘functional’ MSC marker.

Jian et al. demonstrated that the marker CD105 correlates to increased chondrogenic potential of freshly isolated MSCs. The adherent fraction of adipose derived MSCs were removed after 16 hours adherence and FACS sorted using the CD105 marker to isolate the $CD105^+$ and $CD105^-$ fractions of the adherent populations. The $CD105^+$ fraction was differentiated down the adipogenic, osteogenic and chondrogenic lineages. Distinct differences emerged between the $CD105^+$ and $CD105^-$ groups with the $CD105^+$ fraction showing significantly higher levels of the chondrogenic markers collagen II and aggrecan. The most important observation was that the CD105 cells where able to form homogenous cartilage tissue when seeded onto PGLA scaffolds compared to the CD105- fraction. This indicated that the CD105 marker is an important indicator of cartilage differentiation in freshly isolated ADMSCs (Jiang et al. 2010).

Other markers such as CD146, in combination with NG2, PDGF-Rβ, $CD56^-$ and $CD34^-$, selects specifically for pericytes, which have been proposed as the *in vivo* source of MSCs. In addition, these cells go down the myo, chondro, adipo and osteo lineages after being clonally derived, a key distinction between these cells and many other studies (Crisan et al. 2008). A high-throughput assay showed that sorting of MCSs based on this marker resulted in enrichment in the trilineage differentiation potential when compared with CD73 and CD271 indicating greater multi-lineage capacity with MSCs that have this marker (Russel et al. 2010). In addition, FACS isolation of cells with the CD146 marker from adipose tissue also showed enhanced CFU-F capacity (Zannettino et al. 2008). Isolation of MSCs from the umbilical cord using the CD146 marker gave a stable phenotype over 10 passages (Schugar et al. 2009).

For characterisation studies, particularly those involving long-term culture, a selection of well-characterised markers, *i.e.*, markers consistently associated with the MSC phenotype, potency and function, are required.

1.3 POLYMERS AS BIOMATERIALS

1.3.1 Biomaterials

Biomaterials are materials intended to interface with biological systems. Biomaterials include ceramics, metals, glass, polymers or any material that is applied in a biological context without adverse effects. The required properties of a biomaterial depend on its intended purpose, for example, synthetic hips are widely used biocompatible devices that are tailored for manoeuvrability and load bearing functions while heart valves are chosen for their mechanical reliability and neutrality to blood factors over the lifetime of the patient. The ability to fine tune a material to its end use and therefore improve its compatibility gives synthetic polymers an enormous advantage over other materials. Stiffness, elasticity, load bearing capacity, biodegradability, surface structure and chemistry, and biomolecule incorporation can all be considered and tuned to match the desired function.

1.3.2 Polymers

Polymers are molecules composed of repeating units. There are many commonly found in nature (*e.g.* DNA, proteins, polysaccharides) and in synthetic chemistry (*e.g.* polystyrene, polyurethane, polyethene). The most widely used synthetic polymers for tissue engineering are aliphatic polyesters such as poly(glycolic acid) (PGA), poly(lactic acid) (PLA) and poly(caprolactone) (PCL), which are biodegradable through hydrolysis of the ester linkages. PGA was first applied in biomedicine as resorbable stitches (Katz & Tumer 1970). Lactic acid is a chiral molecule and poly(L-lactic acid) and poly(DL-lactic acid) have been extensively applied in tissue engineering. Poly(L-lactic acid) forms a semi crystalline structure with a high Young's modulus and has been applied as a bone substitute. Poly(DL-lactic acid) is amorphous and is less resistant to hydrolysis (by H_2O) than Poly(L-lactic acid) causing it to biodegrade faster. PCL degrades much more slowly than the other polymers. The differences in the rates of degradation (PGA fast, PLA intermediate and PCL slow) and the ability to adjust the physical properties *e.g.* by blending, allows fine tuning through the formation of co-polymers such as

poly(lactic-co-glycolic acid) (PLGA). PLGA (which has FDA approval for clinical use in medical devices) has been used extensively in tissue engineering and drug delivery (Kasuya & Tanishita 2012, Fioretta et al. 2012; Liu et al. 2012; Romagnoli et al. 2013). To some extent the wide current application of these polymers arises from the fact that they are known to be biocompatible. As the demands of the field of regenerative medicine increases what is expected of polymers, this necessarily requires the expansion in the number, type and diversity biocompatible polymers.

1.3.3 Hydrogels

Hydrogels are a group of polymeric materials in which hydrophilic structure allows them to retain amounts of water in their three-dimensional networks. Hydrogels have been used for a wide variety of tissue engineering applications because they resemble soft tissues and can have good biocompatibility (Van Vlierberghe et al. 2011). The hydrophilicity of the cross-linked polymer network arises from hydrophilic groups such as -OH, -COOH, -CONH, $-CONH_2$, $-SO_3H$ (Baroli et al. 2007). Interaction with water causes the hydrogel to swell to many times its un-hydrated size.

The most commonly used synthetic hydrogels are formed from acrylate and acrylamide monomers. They are usually cross-linked through the addition of a cross linker such as *N*,*N*-methylenebisacrylamide (MBA), gluteraldehyde or ethylene glycol dimethacrylate (EGDMA). Another method of hydrogel formation is through ionic interactions. Hydrogels of this type (*e.g.* alginate, chitosan and hyaluronin) are composed of linear saccharides that 'cross-link' through ions such as Ca^{2+}. There has been increasing interest on these hydrogels as they are formed without harsh conditions making them amenable to protein and cell encapsulation (Burdick & Prestwich 2011). Ionic and covalent double-networked hydrogels have been successfully combined to give hydrogels that are highly stretchable and strong (Sun et al. 2012).

Other types of hydrogel networks are also possible. Of particular importance is gelatin, which forms through heat-mediated denaturation of the triple helix of collagen fibres. Upon cooling the denatured strands interact and intermingle to form

hydrogen bonded interwoven strands (gelation). The overlapping nodules 'cross-link' these gels (Joly-Duhamel et al. 2002). These denatured and renatured extracellular matrix proteins make excellent substrates for cell growth as they retain the features (*e.g.* RGD binding sequences) that cells normally interact with *in vivo* (see Section 1.3.1).

The ability of a hydrogel to interact with the solvent though hydrogen bonds and ionic interactions means that changes in the surrounding environment can alter the hydrogel. Changes in pH, temperature and light have all been used to alter the properties of hydrogels (Yin et al. 2006; Hu et al. 1995; Wells et al. 2011). In this thesis the alteration of the properties of hydrogels through changes in temperature is employed to identify thermo responsive hydrogels that trigger cellular release (see Chapter 4).

1.3.4 Thermo-responsive hydrogels

The transition between a solution and a gel is called the 'sol-gel transition'. For hydrogels that form upon cooling, such as gelatin and agarose, the point at which the polymer transitions from solution to a gel is called the upper critical solution temperature (UCST). Polymers that separate from a solution to form a 'solid' above a certain temperature exhibit 'a lower critical solution temperature' (LCST). These transitions result from a change in solubility resulting from an overall change in the hydrophilicity of the hydrogel, thus the polymer becomes 'insoluble' above a certain temperature and forms a gel. If the temperature is reduced below the LCST the polymer will become soluble and re-liquefy. Hydrogen bonding and hydrophobic effects are temperature dependent. At the transition to gel, hydrogen bonding between the polymer and water becomes unfavourable compared to the corresponding polymer–polymer and water–water interactions. This results in a rapid change as the hydrated polymer quickly dehydrates becoming 'insoluble' and forming a solid network (Wischerhoff et al. 2000).

The most investigated thermo-responsive hydrogels are based on poly(*N*-isopropylacrylamide) (pNiPAAm) (Hirokawa et al. 1984). The LCST of the

pNiPAAm homo polymer is 32 °C, making it particularly amenable to the formation of *in situ* hydrogels at physiological temperature (Ruel-Gariepy et al. 2004). NiPAA-based nanoparticles have also been employed for encapsulation and release of proteins and small molecules (Fan et al. 2011). Other poly(*N*-alkylacrylamide) hydrogels, such as poly(*N*,*N*-diethylacrylamides) (DEAA), have been investigated for drug delivery and as thermally adjustable sieves for DNA separation (Ngadaonye et al. 2012).

1.3.5 Scaffolds in tissue engineering

Scaffolds are biocompatible materials that support 3-dimentional tissue formation through cell recruitment, physical and/or biological cues. Scaffolds are either composed of, or mimic, the components of the extracellular matrix such as collagen, fibronectin, chitan, or hydroxyapitite allowing the cells within them to behave as they do in native tissue. Scaffolds have been fabricated by a variety of methods such as electrospinning (Lao et al. 2011), freeze drying (Budyanto et al. 2009), solvent separation (Heijkants et al. 2006), self-assembly (Nagahama et al. 2008) and 3D printing (Serra et al. 2013). Typically, scaffolds can either consist of a scaffold template alone, or be preloaded with cells.

In one study (Quarto et al. 2001), autologous MSCs were expanded and seeded onto a scaffold of macroporus hydroxyapitite. This was then used to fill sections of bone in three patients with a critical bone defect. Critical bone defect occurs when a patient loses a substantial section of bone (> 3.5 cm). The size is critical because beyond this body's native bone repair mechanism is impaired, leaving a substantial gap in the bone. Traditional treatment often uses autologous bone, but on site tissue morbidity and complications from the additional surgery make this a less than ideal option (Younger & Chapman 1989). Furthermore, in cases where the missing bone section is large, the bone graft approach is impractical. Over the period of observation the patients showed significant bone repair.

Much of the subsequent bone repair scaffold work from other groups followed this basic format albeit with different materials (Khan et al. 2010). Factors that influence

vascularisation, such as vascular endothelial growth factor (VEGF) have also been incorporated in the scaffolds. This was possible due to use of supercritical CO_2 and the biodegradable polymer poly(DL-lactic acid) in the scaffold formation, allowing the incorporation of temperature and solvent sensitive growth factors as no solvents are required and the temperature of the process never exceeds 35°C. These scaffolds were pre-loaded with MSCs to facilitate bone formation. The ability to incorporate sensitive proteins added a new level of sophistication into the scaffold and showed significantly improved levels of bone formation (Kanczler et al. 2007).

A protein or small molecule can be physically trapped, adsorbed or covalently bonded (degradable linkers) within hydrogel scaffolds (Censi et al. 2012). The release mechanisms are diffusion, degradation, swelling or use of a trigger (*e.g.* temperature). For most applications diffusion offers the most practical and efficient option (Boerckel et al. 2011). The ability of hydrogels to encapsulate small molecules and growth factors in a temporal manner gives them an advantage over other scaffolds. This approach has been taken further with the additional incorporation of micro carriers (hydrogel microspheres) with varying degrees of release to allow multiple factors to be released at different times (Chen et al. 2009). The controlled release of factors from scaffolds have used polyethylene glycol (PEG) hydrogel scaffolds that encapsulated VEGF to promote vascular growth for the treatment of hind limb ischemia in mice (Phelps et al. 2010).

Scaffolds for tissue engineering have been fabricated from nanofibres made from polymers such as PLA, PLGA and PCL, with the nanofibres closely resembling the nanostructure of ECM proteins such as collagen and chitosan. Combining these synthetic polymers with ECM proteins in 3D scaffolds allows for the mechanical properties to be better designed as well as allowing the controlled release of growth factors and small molecules (Carbone et al. 2014).

One of the most important developments in tissue engineering has been the application of decellularised tissues as scaffolds (Uygun et al. 2010; Elder et al. 2009; Song et al. 2013). Decellularised tissues have had their cell components removed through detergent and enzymatic treatments. The subsequent recellularisation of these tissues has given impressive results when applied to tissues

and organs. In the first study of transplantation of a recellularised trachea, considerable effort was put into completely decellularise the tissue to remove any potential antigens that could result in immune rejection (Macchiarini et al. 2008). Recellularisation of whole organs, such as the liver and kidney, resulted in the formation of microstructure and the partial restoration of function (Song et al. 2013). Although this technology has generated considerable excitement, a donor organ is still required and the strategy does not represent a solution for replacement organs. However, for some tissues, such as skin where large amounts of tissue is available, this does offer an alternative non-immunogenic source of tissue.

Advances have been made with scaffolds for regenerative medicine, however, these have been applied only to the 'simple targets', such as bone, skin and cartilage (Falanga & Sabolinski 1999). The current applications usually consist of tissues with limited complexity, *i.e.*, they require a limited number of cell types that are readily identifiable and expandable *in vitro.* This has allowed the partial restoration of function in these tissues but falls far short of clinical need.

In order for scaffolds to make a real impact in tissue engineering and regenerative medicine, new generic platforms are required that can incorporate a wide range of synthetic and natural biomaterials in high resolution architectures, allowing controlled release/incorporation of small molecules and proteins. If the intention is for these scaffolds to be fully absorbed, the biodegradability of the biomaterial must match the rate it is being replaced by native extracellular matrix. In addition, the increased understanding of the *in vivo* stem cell niche needs to be transferred to *in vitro* culture. For *in vitro* tissues, scaffolds should effectively specify cell growth only at their intended location as well as provide the required nutrients in the form of a functional vasculature. As with *in vivo* development, scaffolds should facilitate temporal changes, *i.e.*, facilitate growth of a stem cell progenitor and subsequently stimulate differentiation. Finally, these constructs should ultimately restore function of the replaced tissue or organ.

1.4 DEFINED ENVIRONMENTS FOR STEM CELL CULTURE

The culture conditions used in *in vitro* expansion of stem cells should be ideally in the absence of animal derived products. With cells aimed for clinical use, all elements of culture need to be defined for both consistency and traceability (EU directives 2003/94/EC and 2004/24/EC). The need to remove animal products arises from the underlying risk that these products contain pathogens or antigens that could be transferred to humans. The biological nature of these components, and methods involving co-culture cells, means that they cannot be sterilised and require time-consuming procedures to verify their disease free status. Animal derived products in stem cell culture have also resulted in immunogenic reactions due to the incorporation of xeno epitopes such as siliciac acid (Martin et al. 2005). Verification of substrates, such as lactate-dehydrogenase-elevating virus (LDV) free Matrigel™ (derived from mouse sarcomas), are acceptable for research purposes but clearly insufficient in a clinical setting. In addition, batch-to-batch variation of biological substrates and serum make quality control difficult as well as confounding the outcomes of research. Due to their clinical potential, hESCs and MSCs have been the focus of defining stem cell culture.

1.4.1 Defined media for hESC culture

hESCs were originally derived on a feeder layer of mouse embryonic fibroblasts (MEFs) in serum containing media (Thomson et al. 1998). The initial advances towards a more defined system involved the removal of the feeder layers with the basal lamina substitute Matrigel™ in combination with MEF conditioned media allowing the separation of human and animal cells (Zuk et al. 2001). This was quickly followed by the use of the conditioned media from human sources (Richards et al. 2002; Amit et al. 2003). The critical components in this media required by hES cells were subsequently identified and used to formulate the first xeno-free fully defined media, mTESR (Ludwig et al. 2006). This has been further refined to eight minimal media components (insulin, selenium, transferrin, l-ascorbic acid, FGF2 and

TGFβ in DMEM/F12 with pH adjusted with NaHCO3) known as E8 media (Chen et al. 2011).

1.4.2 Defined media for MSC culture

The standard culture conditions for the expansion of MSCs rely on supplementation of the media with 10% FCS. As described previously, the removal of animal products is a requirement for MSC clinical applications. The ability to isolate the colony forming unit fraction of bone marrow using the surface marker STRO-1 (Simmons & Torok-Storb 1991) allowed the freshly isolated STRO-1 positive population to be investigated under low serum conditions. Expansion using 2% FCS identified key factors that are critical for the colony formation, namely TGF-B, bFGF and EGF (Gronthos et al. 1994). Examination of these factors in long-term culture under low serum conditions resulted in the cells differentiating towards the osteogenic lineage (Apel et al. 2009) and in a failure to differentiate down the chondrogenic lineage (Girdlestone et al. 2009). However, long-term studies also showed that serum-containing medium, supplemented with bFGF, enhances long-term growth (Walsh et al. 2000). Eventually, it was shown that the presence of TGF-β, bFGF and PDGF-ββ under serum free conditions could maintain MSCs for up to 8 passages (after an initial 5 passages in 10% FBS containing media) and retain their potency (Ng et al. 2008; Chase et al. 2010). Jung (2010) fully described a defined formulation for the maintenance and isolation of MSCs. This study indicated that PDGF-ββ had a significant effect on growth, but reduced both the size and efficiency of colony formation indicating that PDGF-ββ may up-regulate the proliferation of the non-MSC fraction. TGFb and bFGF, but not PDGF-ββ, was included in their final media formulation. The study by Chase (2010) in contrast indicated a synergistic relationship between the different growth factors and showed that the presence of PDGF-ββ, BFGF and TGF-β, insulin and 'other factors' resulted in colony forming unit efficiencies similar to that of serum containing medium. Commercial media formulations soon followed with three defined media formulations, STEMPRO MSC™ (Invitrogen), Mesencult™ (Stem cell technologies) and MSCGM-CD™ (Lonza). Interestingly, the defined media mTESR used for the expansion of hESCs

has also been demonstrated to maintain hMSCs. This media contains a high level of both bFGF and TGFb and many of the other factors of the Jung (Lonza) media formulation (Hudson et al. 2011).

1.4.3 MSC surface interactions

Although standard tissue culture plastic (composed of plasma treated polystyrene) is sufficient to support attachment and isolation of MSC from a heterogeneous primary tissue isolate, it is insufficient to maintain the growth and properties of these cells for long-term culture (Mauney et al. 2004 & 2005). The complex factors controlling cell fate in MSCs have been shown to be due to the rigidity of the matrix it occupies (Engler et al. 2006), cell–material interactions (Khalil et al. 2014), nanostructure interactions (Dalby et al. 2007), cytoskeletal tension (McBeath et al. 2004), and the components in the media (Discher et al. 2009). The effect of matrix rigidity was demonstrated using collagen coated polyacrylamide gels with varying degree of stiffness (obtained through varying the proportion of cross linkers). After one week of culture, the softer matrix, similar to brain tissue (with a tensile strength of 0.1-1 kilopascals (kPa)) resulted in MSCs with a morphology similar to primary neurons grown on Matrigel™. Stiffer substrates (8-17kPa) resulted in myoblast morphology, whereas the stiffest matrices (25-40kPa) produced cells with an osteoblast morphology (Engler et al. 2006). It was also demonstrated using a NMMII ATPase inhibitor blebbistatin that matrix-mediated differentiation occurred through the cytoskeletal filament non-muscle myosin 2 (NMMII). Mechanotransduction (communication of the extracellular matrix properties to the cells) is mediated through focal adhesion tension by myosin filaments acting on actin filaments. Alteration of the cytoskeleton occurs through focal adhesion kinase (FAK) and Rho-associated kinases (ROCKs) (Schaller 2010).

Surface chemistry also directly influences the differentiation potential of cultured cells. Curran *et al*. examined the effect of methyl ($-CH_3$), amino ($-NH_2$), thiol (-SH), hydroxyl (-OH) and carboxy (-COOH) modified glass surfaces (Curran et al. 2006). Here, MCSs were grown for 28 days in basal, osteogenic and chondrogenic media.

The cells grown on the amino and -SH modified surfaces showed promotion of osteogenisis with and in the absence of osteogenic stimulus. Conversely, these surfaces did not promote chondrogenisis with or without chondrogenic stimuli. The cell viability of hMSCs on the amino modified substrates with chondrogenic stimulus was significantly reduced. The hydroxy and carboxy modified surfaces promoted chondrogenisis under both basal and chondrogenic stimulus, but did not support osteogenisis. Only the methyl and unmodified surfaces seemed to maintain the MSC phenotype (Curran et al. 2006). A follow up study of the methyl modified silane surfaces showed that the chain length had a significant effect on the ability of the surface to support hMSC growth directly related to induced FGF release, with the best performing having a $CH_3(CH_2)_6$- motif (Curran et al. 2011).

A study by Benoit and Anseth (2008) used PEG hydrogels in which MSCs were encapsulated to quantify the effect of various small functional groups. In addition to the PEG monomer, 5 other acrylate monomers containing different functional groups were added at 3 different concentrations. The five functional groups where amino, t-butyl, phosphate, fluoro andcarbolylic acid, all of which having a common methacrylate group. The concentrations of the functional group monomers where chosen so as not to effect the material properties such as stiffness and swelling. UV treatment (~4mW cm^{-2}) encapsulated the MSCs in a rounded morphology. The results showed that the phosphate groups significantly elevated levels of osteopontin and CBFA1 (markers of osteogenisis) and the t-butyl groups resulting in elevated levels PPAR-γ (a regulator of adipogenisis). The chondrogenic markers collagen II and aggrecan were significantly elevated with the carboxyl monomer correlating to the increased chondrogenic differentiation observed by Curran (2006) described above.

1.4.4 Integrins and extracellular matrix proteins

Polymer surfaces vary in their ability to bind extracellular matrix proteins such as fibronectin, vitronectin and collagen, which facilitate MSC binding (Danmark et al. 2012). It has been well established that cells bind to extracellular matrix through

interaction with the integrins (Fig. 1.3). Integrins are surface receptors composed of two non-covalently bound subunits (αand β). These transmembrane receptors have a large extracellular domain and a short cytoplasmic tail. Mammals have 18 different α-units and 8 β-units that combine to produce 24 heterodimers that can bind to cell surface, extracellular matrix or protein ligand domains (Table 1.2). The various subunit combinations determine which ligand the receptor will bind to. The extracellular matrix contains a host of binding motifs including the arginine-glycine-aspartic acid (RGD) binding motif. The intracellular domain is connected to the cytoskeleton through actin filaments (Fig 1.3).

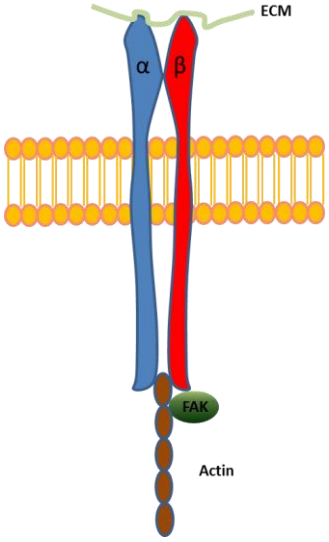

***Figure 1.3**. Basic structure of the integrin heterodimers with the α and β subunits, an extracellular domain that interacts with the extracellular matrix (ECM) proteins and the cytoplasmic tail with actin filaments and focal adhesion kinase (FAK) that transduce the mechanical tension and alter the cytoskeleton according though the action of Rho-associated kinase (ROCK).*

Recently, it has been demonstrated that MSCs don't interact with a polymer surface directly but through the proteins that are bound to it (Li et al. 2013). The mechanical tension between the integrins and the proteins bound to the polymer indirectly determined the polymer stiffness. MSCs proactively pull on the extracellular matrix fibres, which are more stretched on rigid structures than on softer materials (Li et al. 2013). Furthermore, the density of the integrin contacts points with the extracellular matrix play a critical role in determining cell fate.

Table 1.2. *List of the 24 known integrin combinations expressed in mammals, the extracellular matrix/ligands that they bind to and whether these integrins are expressed in MSCs.*

INTEGRINS		EXTRACELLULAR MATRIX/LIGANDS	EXPRESSION IN MSCs
β1	**α1**	Collagens, laminins	Gronthos et al. 2001 (α&β)
	α2	Collagens, laminins	Majumdar et al. 2000 (α)
	α3	Collagens, laminins, fibronectin, entactin	Heckmann et al. 2006 (α)
	α4	Fibronectin, VCAM-1	Walsh et al. 2001 (α)
	α5	Fibronectin	Gronthos et al. 2001 (α)
	α6	Laminins	Gronthos et al. 2001 (α)
	α7	Laminins	
	α8	Vitronectin, fibronectin, tenascin	
	α9	Vitronectin, fibronectin, tenascin	
	α10	Collagens ‡	Goessler et al. 2006 (α)
	α11	Collagens ‡	Foster et al. 2005 (α)
	αV	Fibronectin, vitronectin	Klees et al. 2005 (α)
β2	**αL**	ICAM-1, ICAM-2, ICAM-3	Majumdar et al. 2000 (α&β)
	αM	iC3b, fibrinogen, ICAM-1, coagulation factor X	Dominici et al. 2006 (α)
	αX	Fibrinogen, iC3b	
	αD	ICAM-3	
β3	**αIIβ**	Fibrinogen, fibronectin, von Willebrand factor vitronectin, thrombospondin, tenascin	Gronthos et al. 2001 (β)
	αV	Fibrinogen, fibronectin, von Willebrand factor, vitronectin, thrombospondin, osteopontin, collagens	Gronthos et al. 2001 (α&β)
β4	**α6**	Laminins	Klees et al. 2005 (α)
β5	**αV**	Vitronectin, fibronectin	Reyes et al. 2001 (α&β)
β6	**αV**	Fibronectin, tenascin	Chastain et al. 2006 (β)
β7	**α4**	Fibronectin, VCAM-1, MAdCAM-1	
	αE	E-Cadherin	
β8	**αV**	Vitronectin	

When extracellular matrix contact points are varied under constant stiffness in a polyacrylamide matrix coated with collagen (as described in the Engler paper above), the stem cell fate altered with higher densities giving bone morphology and lower densities the neural morphology (Trappmann et al. 2012). Synthetic substrates with RGD containing peptide sequences (GRGDSP) have also shown a correlation with

density and cell fate where high-density GRGDSP surfaces (2.5%) resulted in higher levels of osteogenic differentiation compared to low-density surfaces (0.27%) (Koepsel et al. 2012).

MSC bind to the extracellular matrix through focal adhesions. The integrins at focal adhesions are clustered. One study varied both the density of the RGD containing sequence (YRGD) and the number of sequences per cluster (1, 5, and 9). This showed that the most efficient binding occurred with clusters of nine sequences at distances of 190 nm (Maheshwari et al. 2000). Both surface chemistry and contact of the extracellular matrix play a critical role in binding and determining MSC stem cell fate.

1.4.5 Polymer substrates for long-term MSC culture

It has been shown that continued culture of MSCs on tissue culture plastic results in loss of osteogenic (Mauney et al. 2004) and adipogenic (Mauney et al. 2005) differentiation potential. To overcome these limitations, hMSCs are typically cultured on biological substrates such as gelatin (Mauney et al. 2004) and fibronectin (Kisiday et al. 2011), and little work has been reported regarding defined synthetic substrates for long-term culture. One of the few studies to do this built on previous work that showed that 150 nm pits in a square at distances of 300 nm from centre to centre showed osteogenic differentiation when the squares were offset by 50 nm (Dalby et al. 2007). Using electron beam lithography and a PCL substrate, 150 nm pits in an asymmetrical arrangement (300 nm centre to centre) were able to maintain the MSCs for 8 weeks, however, the markers used to characterise the cells were limited (STRO-1, CD166 and CD63) passaging experiments however did examine STRO-1 expression at each passage with the offset of 50 maintaining the phenotype where the symmetrical square had lost it (McMurray et al. 2011).

Curran et al. used dip pen nanolithography (DPN) to interrogate the effect of both nano-topography *and* functional group presentation. This technology used thiolated molecules on gold (nano-structured self-assembled monolayers (SAMs)) presenting different functional groups on nano-scale spots (>40 nm in diameter). This

corroborated previous studies showing the $–CH_3$ functional group maintained the MSC phenotype. In addition, the study also revealed that the distance between presentation of the functional group was critical to this property. The DPN dots were 70nm in diameter to allow for the formation of a single focal adhesion known to be between 60-67nm (Poole et al. 2005), and only a distance of 280 nM between spot centres could maintain the phenotype (Curran et al. 2010).

Currently, all 'defined' culture systems require the use of biological substrates (Frith et al. 2012) as tissue culture plastic cannot support MSC growth with defined media. To date, a polymer substrate able to maintain MSCs in serum free media is not known. Recently, a peptide–acrylate substrate has been reported for defined hMSC culture, however, the details of the substrate were not disclosed, whether the substrate was a polymerised version of extracellular matrix protein sequences or *de novo* sequences remains unknown (Dolley-Sonneville et al. 2013). Given what is now known about MSC–substrate interactions, it is not surprising that media containing no serum components, and therefore no extracellular matrix components containing the RGD binding sequence, cannot support MSCs in completely synthetic substrates. The requirements for purely synthetic substrate are considerably higher in the absence of serum components as the polymer will have to directly interact with the cell surface integrins in a way that can maintain the hMSCs in their stem cell state.

1.5 POLYMER MICROARRAYS

As described in section 1.3, stem cells represent a particularly difficult problem when designing/identifying substrates that maintain them in their stem cell state. The problem arises from the many factors that influence their stem cell state including surface chemistry, protein adsorption, material stiffness, nano-topography, and integrin contact point density. Characterisation of all the biomaterials that support stem cells in short-term rather than in long-term culture is a high risk, low reward

strategy. As more stem cells types become isolable, a strategy for the identification biomaterials for a diverse range of stem cells with different sets of environmental cues becomes necessary. Indeed, with the added criteria of the next generation of scaffolds (see section 1.3) any strategy for identifying these materials will require a high-throughput component to cover the combinatorial chemical space needed to identify advanced materials that fit all the necessary criteria.

Polymer science has produced a wide range of potential biocompatible materials for regenerative medicine. In particular, methods incorporation combinatorial chemistry have advanced the field. Using combinatorial approach, Brocchini created polymer libraries by combining different monomers. Here, the first monomer group (A) containing 14 monomers (tyrosine derived diphenols) was polymerised with to the second monomer group (B) containing 8 monomers (aliphatic diacids) to give a library of 112 structurally related polyarylates (Brocchini 1997). Turning these libraries into a usable platform (polymer microarrays) that could interrogate cell material interactions was achieved by applying the printing technology developed in the microelectronics and graphic design industries (Roth et al. 2004).

Polymer microarrays were originally developed by Bradley and Langer (Mizomoto 2004; Anderson et al. 2004; Tourniare et al. 2006). Two primary methods are used for the production of polymer microarrays, contact printing and inkjet printing. Both these methods involve the printing of the polymer libraries onto glass slides. Polymer microarrays typically consist of printed circular polymer features of ~350 μm in diameter printed in a predefined grid with approximately 800 μm between features to represent each polymer in the library. For cell studies, the incubation of cells on the polymer microarray allows the simultaneous scrutiny of cell interactions with polymer libraries using nL volumes of polymers.

1.5.1 Applications of polymer microarrays

Langer applied a polymer microarray composed of 576 polymers made up from 25 different acrylate monomers to hESCs. Glass slides were coated with poly(HEMA) to prevent cell binding between features. hESC were formed into embroid bodies

(embryonic stem cells grouped into rounded spheres), harvested, plated onto the arrays, and incubated for 6 days in the presence of the differentiation factor retinoic acid. The cells that attached to the polymer features were subsequently stained for cytokeratin 7 (epithelial marker) and vimentin (a mesoderm marker). This work identified some substrates that showed enhanced cytokeretin 7 in the presence of retinoic acid (Anderson et al. 2004). These studies demonstrated the potential power of the polymer microarray method; however, the lack of follow up meant that, although polymer microarrays could bind diverse cell types, whether these particular polymers could maintain growth and phenotype at a large scale remained unknown. A different approached by Bradley used a polyurethane-based polymer microarray. The 120-member polymer library was constructed using a polymerisation of a polyol and a diisocyanate monomers with a chain extender (Appendix 1.1C). This polymer microarray format was tested with human tubular renal epithelial cells with a culture period of 5 days. 'Hit' candidates were identified but no large-scale follow up studies were performed (Tourniaire et al. 2006). The same 120-polymer microarray was used to identify polymer candidates that promoted the adhesion of bone derived dendritic cells. Scale-up studies were performed by spin coating glass coverslips with 'hit' polymer solutions. Importantly, functional studies showed the cells had retained their phagocytosis capability on the synthetic polymer substrates. This was the first example that demonstrated the technology beyond 'proof of principle' experiments (Mant et al. 2006).

Zhang (2008) expanded the polymer microarrays to include hydrogel microarrays. The use of inkjet printing in array fabrication allowed for *in situ* photo-initiated polymerisation. In contrast to previous inkjet methods, the monomers were mixed *in situ* with the cross linker and UV photo initiator. Exposure of the arrays to UV for 30 minutes after printing polymerised the mixture to produced hydrogel features. The power and versatility of the new hydrogel array was demonstrated using an array containing 2280 different hydrogels. This hydrogel array included *N*-alkyl substituted acrylamides monomers, such as *N*,*N*-diethylacrylamide (DEAA) and *N*-isopropylacrylamide (NIPAA), with known thermo-responsive abilities (Hirokawa & Tanaka 1984). Incubation of the hydrogel array with HeLa cells followed by a temperature reduction (from 37 to 27 °C) identified hit candidates that could trigger

cellular release of up to 90% of cells in 30 min. The top three hydrogels were subsequently scaled up and cultured with different cell types (Zhang et al. 2008), one of which, a mouse embryonic cell line (E14tg2a), did not grow. These were rescreened to identify a thermo-responsive hydrogel capable of supporting these cells. This demonstrated the power of the array to identify cell specific substrates that could trigger cellular release.

Up to this point much of the research into polymer microarrays concentrated on development of the technology (Liberski et al. 2009), or expanding the chemical 'space' that these arrays covered. Since then, the emphasis has shifted to the practical application of this technology. These applications have included identification of polymers for the isolation of osteoblasts for bone tissue engineering (Tare et al. 2008), polymers that capture protozoan pathogens (Wu et al. 2012), anti-bacterial polymers (Pernagallo et al. 2011; Hook et al. 2012), platelet activating polymers (Hansen et al. 2011) and polymers for the isolation and growth of functional hepatocytes (Hay et al. 2011).

Polymer microarrays have also been applied to stem cells, particularly for those of clinical importance. Anderson applied the polymer microarrays to primary pancreatic islet cells (Mei et al. 2010b). Hit polymers were identified and scale-up experiments performed. However, it should be noted that the arrays and subsequent scale up experiments were coated with fibronectin, an extracellular matrix protein known to support many cell types. Furthermore, comparisons of various extracellular matrix proteins were made, demonstrating that these cells could be maintained on Matrigel, Laminin (sigma), polylysine and G408 supernatant (the standard coating for maintaining primary pancreatic cells). Fibronectin was not compared, it is therefore difficult to ascertain whether the 'hit' polymers act as 'true' surfaces or if the fibronectin coating is the primary source of cell binding and maintenance (Mei et al. 2010).

The identification of the defined components of hESC media had now shifted the focus towards defining the substrate (Baker 2011). The most successful strategies involved the use of recombinant extracellular components such as laminin 511 (Rodin et al. 2010) or specific vitronectin sequences (Melkoumian et al. 2010).

Although successful at maintaining hESC in defined conditions, these substrates would be economically prohibitive for clinical application. Mei et al. used polymer microarrays to identify a 'defined' substrate for hESCs long term culture, however, the substrates were coated with FCS, which is the primary undefined component that defined media such as mTESR (the media that the cells were cultured in) was designed to replace. Indeed, almost all of the publications that have applied the polymer library originally described by Langer et al. for cell studies have required some form of augmentation with extracellular matrix proteins or FCS. This would suggest that the chemical diversity of this array is too limited for cell studies. Perhaps in recognition of this, the authors of these papers have published a new array format (Celiz et al. 2014). By contrast Bradley et al. have developed and applied arrays containing over 7000 polymers (Hansen et al. 2014).

Brafman (2010) applied polymer microarrays to identify a poly(methyl vinyl ether-alt-maleic anhydride) PMVE-alt-MA that could maintain hESCs and iPS for 5 passages. To avoid extracellular matrix protein interference, the polymer microarray screening was performed with hESCs cultured in the defined media StemPro, Subsequent long-term culture and characterisation was performed in serum containing media. The first fully defined hESCs culture system using a polymer substrate used the hydrogel polymer microarray described above (Zhang et al. 2013). hESCs were screened using a 609 hydrogel polymer microarray cultured in defined mTESR media. 25 'Hit' hydrogel candidates were examined for their ability to support hESCs in scale-up culture. The top 10 candidates were then further tested to reveal hydrogels that support hESC and trigger cellular released based upon temperature reduction (15 °C for 30 min). One hydrogel based on 2-(diethylamino)ethyl acrylate termed (HG21) supported hESC growth in defined conditions for over 20 passages while retaining pluripotentcy. In addition, this was achieved in the absence of chemical and enzymatic passaging. In a subsequent study, a polymer substrate that could support hESCs in defined mTESR media was identified using a novel large polymer array (7000 polymers) (Hansen et al. 2014).

In this thesis, the application of the microarray platform is applied to the clinically important MSCs to achieve culture in the absence of biological substrates and enzymatic passaging.

1.6 THESIS AIMS

The aim of this thesis is to develop new chemically defined culture systems for mesenchymal stem cells and to identify small molecule factors that could enhance/manipulate the stem cell phenotype. High-throughput methods were employed which

- Could identify synthetic polymer alternatives to the use of animal derived biological substrates for the long-term culture and maintenance of MSCs.
- Could identify 'smart' hydrogels that allowed MSCs to be passaged in the absence of harsh enzyme treatment.
- Could identify small molecules that could substitute for growth or enhance/alter the MSC marker phenotype of MSCs.

Taken together these achievements would represent a definite advance in the development of new culture systems for MSCs.

CHAPTER 2

MATERIALS AND METHODS

2.1. POLYMER MICROARRAYS

2.1.1 Polymer and Hydrogel Libraries

The polyacrylate/acrylamide library was synthesised by Dr. Mizomoto (Appendix 1A and B) and the polyurethane library was synthesised by Dr. Thaburat (Appendix 1C) under the supervision of Professor Mark Bradley.

2.1.2 Polymer microarray fabrication

2.1.2.1 Slide preparation

Glass microscope slides (76 × 26 mm) were cleaned with oxygen plasma (Europlasma, Belgium) at 20 °C for 5 min, treated with 2% (3-aminopropyl)trimethoxysilane in acetonitrile (w/v) for 1 h, washed with acetonitrile and acetone, and oven dried at 100 °C for 2h. For agarose coating, slides were dipped into a 2% agarose solution (w/v) at 65 °C. The slides were air dried and stored at room temperature.

2.1.2.2 Contact printing

Polymers were contact printed onto agarose coated slides by using a Qarrayer^{mini} (Genetix, UK) with aQu solid pins (K2785, Genetix) inked from 384-well plates filled with 1% (w/v) polymer solutions in *N*-methylpyrrolidone (NMP). Each spot was stamped 5 times with 200 ms inking time and 100 ms stamping time, resulting in ~ 310 μm spots in diameter. For the initial screen the arrays of the polymers (n = 4) were printed in a 32 × 32 pattern. The slides were dried in a vacuum oven at 40 °C

overnight. The 'hit arrays' were fabricated in a similar way as described above (polymer n = 6).

2.1.3 Hydrogel microarray fabrication

2.1.3.1 Slide preparation

Glass microscope slides (76 × 26 mm) were cleaned with oxygen plasma (Europlasma, Belgium) with 1.5 bar oxygen pressure. Slides were washed with water and acetone. Sucrose solution (30% w/v) was printed onto the glass slide as 2 nL spots in a 28 × 38 array with a pitch of 800 µm between spots. The sucrose printed slides were coated with 15 µL of tridecafluoro-1,1,2,2-tetrahydrooctyl-dimethylchlorosilane (FDS) for 12 hours in a sealed container. Slides were washed in acetone before printing.

2.1.3.1 Preparation of polymer hydrogel microarrays

A MicroDrop MD-E-401 printer with an autodrop pipette in conjunction with a MD-O-538-85 CCD camera was used. The humidity of the printing chamber was carefully controlled using a v5100N vicks ultrasonic humidifier with a TH-810 humidity controller. Arrays were fabricated by printing aqueous solutions of 18 acrylate/acrylamide monomers (Table 4.1) in drops on a masked glass slide using a MicroDrop inkjet printer and polymerised *in situ* in the presence of a cross-linker *N*,*N*'-methylenebisacrylamide (MBA 5% v/v) and photo-initiator 1-hydroxyclyclohexyl phenyl ketone (9% v/v). Each array had 28 × 87 features giving 609 different polymers each printed in quadruplicate with 7 different ratios of 2 monomers (plus the cross-linker) in each line of 28 polymers.

2.1.4 Microarray screening

2.1.4.1 Cell culture

Cell culture reagents were purchased from Invitrogen unless otherwise stated. hES-MPs were grown 0.1% gelatin coated 75 cm tissue culture flasks (Corning) in DMEM supplemented with 10% FCS, bFGF (4 ng/mL), L-glut (100 units/mL) and pen/strep (100 units/mL), and incubated at 37 °C with 5% CO_2.

2.1.4.2 Binding assay

A suspension of hES-MPs (4 mL) was added to the microarray slides (initial screen n = 2 for polymer microarrays and n = 3 for hydrogels) at 1.2×10^4 cells/cm^2, placed in a 4-well rectangular chamber. After 24h incubation, the slides were washed with PBS and the cells fixed with 4% formaldehyde in PBS for 10 min, stained with DAPI (0.1 μg/mL in PBS) for 10 min, and washed 3 times with PBS. Image capture was carried out using a Nikon Eclipse 50i microscope with the Pathfinder software (IMSTAR, France). Cell counts were determined by Pathfinder image analysis software.

2.1.4.3 Hydrogel binders

The combined results of the 3 arrays were used to select the best binding hydrogels. Hydrogel binding and cell morphology were analysed to select candidates for the 88 'hit' array.

2.1.4.4 Polymer binders

Polymers with ≥ 5 cells per feature were selected (Fig.3.2) resulting in 171 candidates being taken forward to a 'focused' array.

2.1.5 Second focused screen

The top candidates from the binding array were used to construct hydrogels and polymer arrays containing only the identified 'hits'. Each time point was represented by 3 microarrays giving a total of 9 slides for the polymer array and 9 slides for the hydrogel array. For the analysis each hydrogel/polymer feature was imaged 4 times to give a bright field, DAPI ($\lambda_{Ex}/\lambda_{Em}$ 358/461 nm), FITC ($\lambda_{Ex}/\lambda_{Em}$ 495/519 nm) and RHOD? ($\lambda_{Ex}/\lambda_{Em}$ 555/565 nm) image. A circle was drawn around the spot to define the size of the feature. Image analysis was performed by IMSTAR Pathfinder software. The 'focused arrays' were also assessed for cell viability (CellTracker^{TM}Green) at the day 7 time point.

2.1.5.1 Immunocytochemistry

Cells on the arrays were stained using standard immunocytochemistry protocols. hES-MPs were blocked for 1h with 10% FCS in PBS. They were then incubated overnight at 4 °C with primary antibodies against STRO-1 (mouse anti-human, Millipore), CD105 (goat anti-human, R&D systems) both at 1:100 dilution, and for the scale-up experiment also with CD271 (rabbit anti-human, Millipore) at 1:50 dilution. The cells were incubated for 4 h with the appropriate AlexaFluor®-conjugated secondary antibodies; STRO-1 (donkey anti-mouse 488) at 1:200, CD105 (donkey anti-goat 555) at 1:400 and CD271 (chicken anti-rabbit) at 1:100 dilution. Excess antibody was removed by washing 3 times with PBS. Finally, cells were stained with DAPI (0.1µg/mL in PBS) and washed 3 times with PBS.

2.2 SCALE-UP STUDIES

2.2.1 Coating of polymers on coverslips

Glass coverslips (Menzel-Gläser, Germany), 10 mm (scale-up experiments) and 32 mm diameter (long-term culture), were washed with tetrahydrofuran (THF) and spin-coated with 1% (w/v) polymer solutions in THF or NMP for 2 s at 2000 rpm. The

coverslips were dried overnight in a vacuum oven (200 mbar) at 40 °C. The coated coverslips were sterilised with UV light for 20 min prior to cell culture.

2.2.2 Preparation of polymer treated coverslips

Glass coverslips were placed in 1M NaOH solution overnight on a shaker. The NaOH solution was removed and the coverslips were washed with water and acetone after which the coverslips were air-dried. Next, the coverslips were placed in a container with 97.5 mL of acetonitrile, 2 mL of trimethoxysilylmetacrylate and 0.5 mL of triethylamine, covered and placed on a shaker overnight. The solvent was removed and the coverslips were rinsed with acetone and air dried and stored at −20 °C until required.

2.2.3 Preparation of hydrogel coated cover slips

Monomer, photo-initiator and cross-linker solutions were prepared in NMP and placed on acrylate treated coverslips (10, 19 and 32 mm in diameter with 1, 1.6 and 10 µL of solution used, respectively). The coverslips were exposed to UV irradiation (Model B 100AP, Black-Ray) for 30 min before incubation overnight at 40 °C. The coated coverslips were then washed with ethanol and acetone before air drying. The coated coverslips were sterilised with UV for 20 min and washed with PBS two times (5 min per wash) prior to cellular studies.

2.2.4 Preparation of agarose coated well plates

A 0.5% Agarose (type B) solution was prepared in 200 mL of deionised water. The solution was heated in a microwave to dissolve the agarose. Agarose was heated prior to coating of well plates (100µL/48-well). Once coated, the plates were put in 4 °C for 1h and moved to a 50 °C oven to dry overnight.

2.2.5 Scale-up culture and cell analysis on polymer/hydrogel coated coverslips

For both the polymer and hydrogel screens, 30 candidates were identified for further analysis in scale-up cell culture. 48-Well plates were coated with 0.5% agarose solution (100 µL/well) and dried overnight at 50 °C. The polymer or hydrogel coated coverslips (n = 4) were placed into the wells and sterilised by UV irradiation for 20 min and washed twice with PBS. The tissue culture plastic controls consisted of 3 wells of a 48-well plate, and the gelatin controls consisted of 3 well of a 48-well plate coated with a 500 µL 0.1% gelatin solution (in PBS). This was followed by seeding with hES-MPs at 1×10^4 cells per well. Media was changed every 2 days. At day 7, cells were washed with PBS, fixed with 4% formaldehyde, stained with DAPI (1 µg/mL in PBS) and triple immunostained for STRO-1, CD105 and CD271. Each well was imaged 9 times on four channels: λ_{Ex} 360 nm (DAPI), λ_{Ex} 488 nm (STRO-1), λ_{Ex} 555 nm (CD105) and λ_{Ex} 649 nm (CD271). Stained nuclei were counted and the fluorescence intensity measured for each image to give cells/mm^2 and intensity/mm^2 (the intensity was normalised to the cell number). The background fluorescence for each candidate was calculated using a replicate stained only with the secondary antibody and deducted from the sample fluorescence to give a corrected fluorescence intensity value for each surface.

2.2.6 Identification of thermo-modulatable hydrogels

Based on the results of the scale up study, 10 hydrogels were tested for their capacity to trigger cellular release. hES-MPs were seeded onto 10 mm hydrogel coated coverslips placed into agarose coated 48-well plates, and cultured for 7 days. To trigger release, the hES-MPs on hydrogels were removed from the incubator and left at 21 °C for 1h, after which detached cells were collected by gentle pipetting and transfer to Eppendorf tubes. The remaining cells were detached by trypsinisation. Both, thermo-detached and trypsinised cells were centrifuged (1000 rpm for 5 min), the cells re-suspended in 50 µL of media, and the cells counted with a Neubauer cell counter. Two counts were performed using 9 squares and the cell count was adjusted

according to the volume. Comparison between trypsin detached cells and thermo-detached cells determined the % detachment. The average and standard deviation for each hydrogel was obtained.

2.3 LONG-TERM CULTURE

2.3.1 Source of hES-MPs and ADMSCs

For long-term culture studies hES-MPs and ADMSCs were used. Ethical approval for the collection of adipose tissue and subsequent research was granted by the South East Scotland Research Ethics Committee (Ref 10/S1103/45h) and hES-MPs were purchased (hES-MP™002.5, Cellectis bioresearch). The ADMSCs were derived from the stromal vascular fraction of lipoasperate from adipose tissue (Zuk et al. 2001).

2.3.2 Long-term passaging

hES-MPs and ADMSCs were seeded at 3×10^4 cells/well onto 32 mm diameter polymer and hydrogel coated coverslips (n = 3), which were placed into agarose coated 6-well plates (0.5% agarose, 500 µL/well). For gelatin controls, 6-well tissue culture plates were treated with 0.1% gelatin in PBS (3 mL/well) for 5 min, and the excess solution removed prior to the application of cells and media. Media was changed every 2–3 days and cells were passaged every 5–6 days at a 1:6 splitting ratio.

2.3.3 Long-term enzyme free passage (Hydrogels)

hES-MPs and ADMSCs were cultured on hydrogel-coated coverslips in 6-well plates where removed from the incubator and plated in a tissue culture hood for 1h. Using a p1000 pipette, the media within the well was gently pipetted 10 times over the surface of the coverslip. Finally the cell suspension was removed and cells were

centrifuged for 5 min at 1000rpm. Cells were re-suspended in DMEM supplemented with 10% FCS, bFGF (4 ng/mL), L-glut (100 units/mL) and pen/strep (100 units/mL) and split in a 1:6 ratio and replated onto fresh coverslips.

2.4 CHARACTERISATION

2.4.1 Flow cytometry

At passage 5 (hES-MPs and ADMSCs) and passage 10 (ADMSCs) cells were stained for CD105, STRO-1, CD271, CD90, CD73, CD34, CD14, CD146, CD140b, and HLA-DR, and analysed by flow cytometry.

For flow cytometry analysis, cells from each replicate (n = 3) were trypsinised. After removing media and washing with PBS, TrypLE™ Express (500 µL) was added to each well for 5 min and subsequently neutralised with media (2 mL). The cells were spun down (5 min, 1000 rpm) and resuspended in 600 µL of FACS-PBS (PBS with 0.1% of BSA and NaN3). To 100 µL of cell suspension 2 µL of the designated fluorescent-conjugated antibody was added; CD105–FITC (Biolegend), STRO-1–APC (Biolegend), CD73–PE (BD Bioscience), HLA-DR–FITC (BD bioscience), CD14–PE (BD Biosciences), CD34–PE (Biolegend) CD140b–APC (BD Biosciences), CD271–PE (BD Bioscience), CD146–FITC (eBiosciences) and CD90–FITC (Biolegend). After incubation for 20 min at 4 °C, 2 mL of FACS-PBS was added to each tube and the tubes centrifuged for 7 min (475 rpm). The PBS was gently decanted ensuring the pellet was not dislodged and the cells resuspended in 250 µL of FACS-PBS and analysed on a FACSCalibur flow cytometer. Flow cytometry histograms were generated using FlowJo.

2.4.2 Osteogenic and adipogenic differentiation

After 5 passages on **HGL1, PU157**, **PU108**, **PA338**, tissue culture plastic and gelatin, ADMSCs were plated at 1.9×10^4 cells per well (n = 3) in standard tissue culture 12-well plates for osteogenic differentiation, and 3.8×10^4 cells per well (n =

3) for adipogenic differentiation. After 24 h the media was changed to StemPro osteogenic or adipogenic differentiation media and the cells were cultured for 28 days with media changes every 3–4 days. After washing with PBS, the cells were fixed in 4% formaldehyde and stained with DAPI (1 μg/mL). Osteo-induced cells were stained with 2% Alizarin red S solution (pH 4.2) and adipo-induced cells with Oil Red O solution (3 parts of 0.5% Oil Red O in isopropanol to 2 parts of water). Adipocyte differentiation was quantified by comparing the number of DAPI stained nuclei with the number of differentiated cells.

2.4.3 Image capture

ADMSCs and HE-SMPs grown before and after long-term passaging on 32mm diameter coverslips (for 6-well plates) were imaged with a Zeiss Observer microscope.

HGL1, **P338**, **PU157** and **PA108** adipogenic quantification was evaluated by comparing total cells with differentiated cells. For the two channels (bright field and DAPI) 12 images were taken for each of the replicate wells (n=3). Firstly, cell counts where made of the DAPI stained nuclei for each of the images in image J. Secondly, merged images of the DAPI stained and bright field images where produced. Differentiated cells were marked and counted. Comparison with the DAPI channels gave a percentage of differentiation for each image. The data for the 12 images of each well where combined. The data for the 3 wells were averaged and the standard deviation determined.

PA338, **PU157** and **PU108** osteogenic differentiation was evaluated by amount of Alizarin red S positive pixels in osteogenic differentiation images. This was quantified using ImageJ by setting the image/adjust/colour threshold option. The ‘analyse option’ (analyse particles) calculated the percentage of pixels above threshold. The best and poorest Alizarin red S stained wells were used as reference points (Mehlem et al. 2013; Yang et al. 2011).

2.4.4 Protein extraction from polymer surfaces

Polymer coated coverslips (n = 3) were placed into a 12-well tissue culture plate and sterilised with UV for 10 min. The coverslips were washed twice (10 min) with PBS and 3 mL of culture media (DMEM supplemented with 10% FCS, 4 ng/mL bFGF, 100 units/mL of L-glutamine, and 1% pen/strep) was added to each well. Plates were placed in an incubator at 37 °C with 5% CO_2 for 24 h. The media was removed and the coverslips washed twice with PBS. Each coverslip was placed into 1.5 mL Eppendorf tube and broken up into small pieces using tweezers. For the gelatin and tissue culture plastic controls, surfaces were removed using curved scalpels. For the culture media control, 40 µL of media was added to a tube. The tubes were centrifuged at 11000 rpm for 5 min. To each tube, 40 µL of sample buffer (0.5 M Tris-HCl (pH 8.8), 4% SDS (w/v), 20% glycerol (v/v), 2% 2-mercaptoethanol (v/v), and 0.0025% bromophenol blue in distilled water) was added and the tubes heated at 100 °C for 10 min. The proteins were separated on a Novex Mini Cell in TGS buffer (Tris 0.025 M, Glycine 0.192 M, 0.1% SDS (w/v)) using a NuPAGE 4–12% Bis-Tris Gel (1mm × 12 well). Gels were run for 40 min at 200 V, 120 mA. For silver staining, gels were placed in deionised water and stained with Sigma ProteoSilver Silver Stain Kit (PROTSIL1-1KT) following the manufacturer's instructions. For Oriole fluorescent staining, gels were placed directly into 100 mL of premixed fluorescent gel stain (Biorad 161-0496) for 90 min and transferred to deionised water and stored in the dark. Gels were imaged using a BIORAD image analyser and analysed with the Biorad image lab 3.0 software.

2.4.5 Polymer and monomer structures

Polymer and monomer structures were made using the software programme ChemDraw.

2.5 SMALL MOLECULE HIGH-THROUPUT SCREENING

2.5.1 Identification of the small molecule library

The GeneGo bioinformatics software allowed searches of the key pathways and markers identified with MSC 'stemness' (Table 5.1, Appendix 3). Pathways in GeneGo highlight (with a blue hexagon) the points of the pathways that are known to be affected by small molecules. By right clicking the blue hexagons, the small molecule(s) are listed with their properties. These can then be compared with the selection criteria (FDA/EU approved, toxicity and solubility). Candidates that fulfilled these criteria were selected for the library.

2.5.2 Preparation of the small molecule library

The members of the small molecule library were mainly ordered from sigma (see appendix 4.1). The majority of the small molecules were dissolved in DMSO with some compounds requiring the addition of 1M HCl or 1M NaOH. The compounds were weighed and dissolved in 2 mL glass vials to make 1.5 mL of 100 mM stock solution of each small molecule. To organise the library small molecule location maps where produced. The maps corresponded to fluidX 1.1 mL Data Matrix Screw-top, robot rack-96 barcoded tubes (v-bottom). 3 maps covered the 200 small molecule library. 1mL of a small molecule solution was transferred to its corresponding vile in the rack. The 1mM solution library was stored at -80 °C.

2.5.3 Preparation of media for small molecule screen and optimisation plate

Master feeder plates (Axygen deep well plates, 96-well, clear) were constructed corresponding to the 3 small molecule maps. 2 mL of hES-MP media was added to each well and to each well 20 µL of stock solution (thawed and well mixed) was added to give a 1 mM concentration. This master plate was used to make the 96-well feeder plate at 100 µM concentration. The 100µM feeder plate had 1800 µL of media

added to each well. Using a multi-channel pipette, media with small molecule solution were mixed well (pipetting up and down 8 times) and 200 µL of solution was transferred to the corresponding well containing 1800 µL of media in the 100 µM feeder plate. Once complete the 100 µM solution of this feeder plate was then used to construct the 10 µM plate using the same procedure. In total 3 feeder plates were made for each concentration (9 plates). Note that the preparation for the small molecule screen in defined media is the same as stated above with the exception of using the define media formulation.

2.5.4 Defined cell culture

hES-MPs and ADMSCs, on gelatin substrate, were transitioned onto the defined media formulation over ~10 days by increasing the proportion of defined media to undefined (serum containing) media. The media was changed every 2–3 days by raising the defined media component in increments (25:75, 50:50, 75:25, 100%).

2.5.5 Plating, fixing and staining 384 well plates

384-Well black clear bottomed plates (PerkinElmer Cell Carrier, 6007430) were coated with 0.1% gelatin solution. 100 µL of hES-MP cell suspension (1×10^4 cells/mL) was added to each well using a 12 tip multi-channel pipette. Making sure cells are in suspension at this point requires continuous mixing of the cell suspension. Cells were incubated for 24h, media removed, and 200 µL of the small molecule containing media was added to the wells. Note the media has to be well mixed before adding it to the cells (pipetting 8 times). Cells were incubated for 7 days with media changes every 2 days after which they were washed with PBS and fixed with 4% formaldehyde. Cells were stained with DAPI nuclear stain, STRO-1, CD105 and CD271 immunostaining (see Immunohistochemistry).

2.5.6 Scanning and analysis with Opera and ACAPELLA

384-well plates were scanned using the Opera high-throughput microscope. Each was imaged 9 times from different representative areas of the well in the DAPI channel ($\lambda_{Ex}/\lambda_{Em}$ 340/488 nm), FITC (STRO-1 antibody $\lambda_{Ex}/\lambda_{Em}$ 495/519 nm), RHOD (CD105 antibody $\lambda_{Ex}/\lambda_{Em}$ 555/565 nm) and far red (CD271 antibody $\lambda_{Em}/\lambda_{Em}$ 650/668 nm) channels. The parameters of the analysis script used by ACAPELLA to produce the data are given below. Each florescent channel required separate analysis. For each screen the parameters were checked and adjusted if necessary for nuclear and cytoplasm detection.

General	
	0
Image Field	3
Number Of Channels	3
Channel number of neclear channel	1
Channel number for cytoplasm channel	3
Show Illustrations	0
Nuclear Detection	
Nuclei Detection Algorithm	F
Theshold Adjustment	6
Minimum Nuclei Distance	8
Nuclear Splitting Adjustment	6
Individual Threshold Adjustment	0.4
Minimum Nuclear Area	60
Minimum Nuclear Contrast	0.03
Parameter SCAN	None
Cytoplasm Detection	
Cytoplams Threshold Adjustment	0.5
Cytoplasm Individual Threshold Adjustment	0.1
Cytoplam Region	
CytoplasmOuterBorderShift	0
CytoplasminnerBorder Shift	0
NucleusBorderShift	
Filters	
Intesity Threshold	500
Upper Area Threshold	15000
Lower Area Threshold	500
Lower Roundness Threshold	0.9
Lower WidthToLength Threshold	0.14

2.5.7 Preparation of defined media

The defined serum free media was prepared as outlined by Jung (see table 2.1) (Jung et al. 2010). DMEM/F-12 (1:1) (Gibco 31331) was used a base media. Media (1 L) was placed in the upper cup of a filter unit. To this was added 50 µL of progesterone stock solution (1mg/8.83mL, in chloroform), 10 mL L-glutamine (200 mM), 1 mL of chemically defined lipoconcentrate (Gibco STEMPRO-LipoMax, A10850), 20 mL sodium bicarbonate (17.22 g/100mL), 10 mL of HEPES (4.12g/100mL, Sigma H4034), 20 mL insulin (69.3g/60mL) form a bovine pancreas (Sigma I1882), 0.5g of human apo-transferrin (Sigma T2252), 1 mL of putrescine dihydrochloride (0.09g/10mL) (Sigma P6024), and 40 g of human serum albumin (Sigma A1653), consecutively.

***Table 2.1**. Defined media components in the serum free media (Jung et al. 2010).*

COMPONENT	SOLVENT	CONCENTRATION
DMEM/Ham's F12 medium (1:1)		
Progesterone	Chloroform	0.018µM
L-Glutamine	Media	4 mM
Chemically defined lipoconcentrate		100µl/100ml
Sodium bicarbonate	Media	20.5 mM
HEPES	Media	4.9 mM
Bovine insulin	H_2O at pH 2	4.9 mM
Human apo-transferrin	Media	0.5g/L
Putrescrine dihydrochloride	Media	55.9 µM
Human serum albumin	Media	40g/L
Ascorbic acid	Media	284 µM
Hydrocortisone	DMSO	100 nM
Fetuin	Media	20.7 µM
bFGF	H_20	2ng/mL
TGF-β	H_20	1ng/mL

Note, the human serum albumin was difficult to dissolve and required repeated mixing by pipetting. To this solution, 10 mL of ascorbic acid (500mg/100mL) (A4403), 18 µL (10mg/mL) hydrocortisone (Sigma H0888), 200 µL of bFGF (10ng/µL) (R&D systems), and 3.3 mL of TGF-β (300ng/mL) (R&D systems) were added. Finally, the solution was mixed using a 50 mL pipette and sterilised by filtering. 40 mL aliquots of the media were frozen and used within 7 days of thawing.

2.6 SMALL MOLECULE SCALE-UP STUDIES

2.6.1 IFN-γ, TNF-α and small molecules treatment of ADMSCs in serum containing and serum free media

ADMSCs were seeded onto 6-well plates coated with 0.1% Gelatin, at a density of 3 × 10^4 cells per well. To determine whether the ADMSCs would respond to IFN-γ and TNF-α treatment would be effective at the published concentrations (English et al. 2007; Chan et al. 2008) and optimisation experiment was performed. In this experiment the treatments were tested in serum containing (hESMP media) and serum free media (Table 2.1). The concentrations chosen for this experiment were 20ng/mL IFN-γ and 10ng/mL TNF-α. Treatment was initiated after 24 hours incubation at 37 °C. Defined media and undefined (Serum containing) media were prepared with the stated concentrations of each protein. The six conditions testes were, INF-γ defined, TNF-γ defined, untreated defined, INF-γ undefined, TNF-γ undefined, untreated undefined. ADMSCs where incubated with these conditions for 4 days. Media was changed after 2 days and on the fourth day cells were trypsinised and stained for ICAM-1, HLA-DR, HLA-ABC, B7-1 and B7-2 (Appendix 4.3). For each of the 5 drugs, 2 drug concentrations were selected based on the most effective concentrations from the third screen. In undefined media small molecules estriol (50μM, 100μM), telmisartan (50 μM, 100 μM), spermine (1μM, 3 μM), IFNγ (20ng/mL), TNF-α (10ng/mL) were prepared. In defined media, niacin (1 μM, 3 μM), atenolol (50 μM, 100 μM), IFN-γ (20ng/mL) and TNF-α (10ng/mL) were prepared. Defined and undefined media were used as untreated controls. ADMSCs were seeded for 24h in defined and undefined media, after these cells were washed twice in PBS and drug and cytokine containing media was added. This media was changed after 2 days and on the 4^{th} day cells were prepared and stained with flow cytometry antibodies for ICAM-1–PE (BD Biosciences), HLA-DR–FITC (Biolegend), HLA-ABC–PE (BD Bioscience), B7-1–FITC (BD Bioscience), B7-2–PE (BD Bioscience) and STRO-1–FITC (Biolegend). Analysis of the optimisation experiment and small molecule treatment experiments was done using flowJo (see flow cytometry for staining method).

2.7 STATISTICAL ANALYSIS

2.7.1 Statistical analysis for small molecule screens

For each drug concentration 4 wells used to determine the average and standard deviation for cell counts and for florescent measurements. Using the Instat software package (Graphpad), the data was compiled to give the average, sample number and standard deviation. Small molecules where compared to control wells using the Dunnett's test (one way ANOVA). This allows large data sets to be compared to a control. Unpaired t tests where performed between drug treatment groups at a given concentration (e.g. 100µM) with the controls at that same concentration for the 3rd screen of the small molecule assessment (chapter 5).

2.7.2 Statistical analysis for polymer and hydrogel screens

For the adipogenic quantification data a one way ANOVA was performed between the differentiated hydrogels and polymers and the gelatin controls (n= 3).

For the thermo detachment experiment using different monomer proportions, cells from the replicates were detached using the thermo-detachment procedure (see enzyme free passaging). The remaining cells where detached by trypsinisation. Detached and trypsinised cells where centrifuged (1000 rpm for 5 min) and cell counts were made by re-suspending cells in 50µL of media. Comparison between trypsin detached cells and thermo-detached cells determined the % detachment. The average for each hydrogel was obtained with the standard deviation and where compared with the untreated gelatin control. A one way ANOVA was performed using Instat software and the p values determined.

Unpaired t tests where performed between to compare the flow cytometry data between the various passages (p0, p5, p10) for a particular marker (e.g. CD105).

CHAPTER 3

A Polymer Microarray Approach for Identifying Defined Substrates for Mesenchymal Stem Cells

Parts of this chapter were previously published in:

Duffy, C.R.E., Zhang, R., How, S.E., Lilienkampf, A., Tourniaire, G., Hu, W., West, C.C., de Sousa, P. & Bradley, M,. (2014) A high-throughput polymer microarray approach for identifying defined substrates for mesenchymal stem cells. *Biomaterials Science*, 2, p1683–1692. doi: 10.1039/c4bm00112e.

ADMSCs were supplied by Dr Chris West Ethical and approval for the collection of adipose tissue and subsequent research was granted by the South East Scotland Research Ethics Committee (Ref 10/S1103/45h).

3.1 INTRODUCTION

Given the clinical importance of MSCs, their culture is crucial for any downstream application. MSCs grown on tissue culture plastic have been shown to lose both osteogenic and adipogenic potential compared to those grown on gelatin (Mauney et al. 2004; Mauney et al. 2005). However, the use of animal derived substrates such as gelatin, collagen or fibronectin is problematic due to the presence of a multitude of undefined factors, batch variation and the potential for pathogen transfer. In order to realise the full clinical potential of MSCs there is a pressing need for defined synthetic substrates for long-term culture. Since MSC populations contain cells of varying degrees of multipotency (Pevsner-Fischer et al. 2011), the ideal substrates should not only maintain the cells, but enrich also the most multipotent cell type.

Polymer microarrays allow the high-throughput interrogation of hundreds to thousands of defined surfaces for various biomedical applications. They have been applied in the identification of polymer substrates that can maintain hESCs in

undefined (Brafman et al. 2010) and defined media (Zhang et al. 2013; Hansen et al. 2013). The ability to isolate and expand stem cells *in vitro* of clinically relevant numbers requires the identification of substrates that not only bind cells and facilitate growth but also maintain stem cell phenotype over multiple passages. The polymer microarray platform offers an approach whereby substrates that promote adhesion and growth can be rapidly identified, and enables the identification of substrates that can maintain or enhance the stem cell phenotype, *i.e*., cells can be evaluated for multiple markers and characteristics in a high-throughput manner.

The use of a high-throughput system to some extent allows multiple components to be taken into consideration simultaneously. Surface chemistry in terms of functional group presentation can be represented to a much greater extent than the -CH3 (methyl), -NH2 (amino), -OH (hydroxyl), -COOH (carboxyl), -SH (thiol), -F (fluoro), and $–PO_4$ (phosphate) functional groups presented in other studies (See appendix 2.1A-C for a full list of monomers) (Curran et al. 2006; Benoit et al. 2008). In the Curran study, 'bulk' presentation resulted in heterogeneous cell growth due to a lack of control with the polymerisation process, i.e. there was an inherent variability and a lack of control over how little or how much 'functional' group was presented on the surface.

This was considerably improved in a latter study in which the distance between functional groups was controlled using dip pen nanolithography (Curran et al. 2010). These chemical functionalities were deposited at the nanometer scale with thiolated molecules of gold that formed self-assembling monolayers (SAMs). This added the dimension of control between functional group presentation that allowed nano-scale modification of the distance between the deposited spots. This confirmed the previous works finding that the –CH3 functionality was able to maintain the MSC phenotype but in addition it was shown that a 'minimal' spot diameter of 70nm was required for cell adhesion. A pitch between spots of 280nm was also necessary to maintain the cell phenotype. The 70nm diameter is similar to the periodicity of type 1 collagen (Das et al. 2013) and close to the minimal area for focal adhesion formation of 60-67nm (Poole et al. 2005). This 'pitch' between centres is also remarkably close to the 'pitch' between nano-structured pits that McMurray et al, showed to be able to

maintain MSCs in there stem cell fate over multiple passages (McMurray et al. 2011). It has been shown that nano-topographical features less than 10nm in diameter can be sensed by the cells though so called ‘nanopodia’ (Dalby et al. 2004).

The important role that nano-topography plays in maintaining and controlling stem cell fate is highlighted in these and many other studies (Dalby et al. 2014). The control provided by such nano-surfaces over topography and functional group presentation is restricted to surfaces with a uniform stiffness. ECM varies in both nano-topography and stiffness/elasticity. The effect of variation of stiffness on MSC fate has been dramatically demonstrated (Engler et al. 2006), this makes comparisons of different studies looking at the same surface chemistries on surfaces of different stiffness/elasticity difficult to interpret. The disadvantage with complete control of the nano-topography means that the structures have to be hypothesised and tested on surfaces with uniform stiffness.

The advantage with the microarray format is that no presuppositions are required prior to the experiment about surface chemistry, nano-topography or surface stiffness. The polymer microarray format allows a large variety of surface chemistries to be concurrently scrutinized by cells. The ability to vary the proportion of different monomers allows variation of functional group presentation. The wide variety of monomer combinations will necessary result in surfaces with a wide range of topographies and stiffness’s. The readout of the screening process can then be used to make connections between the cell behaviour and the surface which is causing the cell to exhibit a particular phenotype.

The aim of this study was to apply the polymer microarray platform to MSCs to identify substrates that can maintain/promote MSC phenotype in long-term culture while retaining their multipotency. By combining the high-throughput screening methodology with scale-up studies examining the MSC phenotype with ever greater scrutiny this study aims to identify polymers with superior maintenance properties that can also reveal cell surface interaction relationships. An overview of the strategy employed to achieve this is given in figure 3.1.

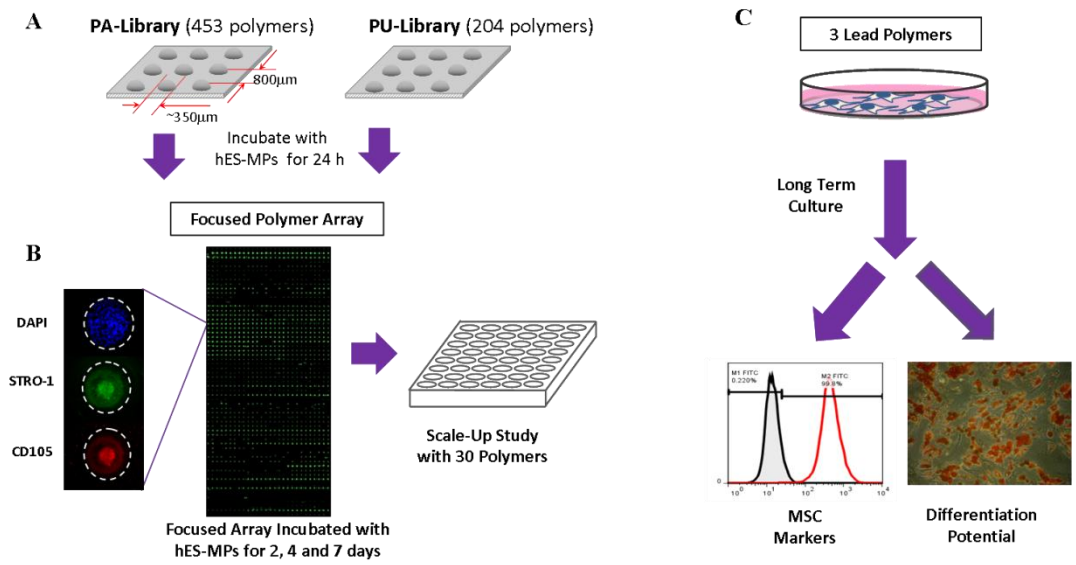

***Figure 3.1**. An outline of the polymer microarray platform to identify and verify lead polymers for long-term MSC cultured in 10% FCS containing media. A) In an initial screen hES-MPs were incubated for 24 h on polymer microarrays and the polymers evaluated for cell binding. B) A focused screen with microarrays containing 171 polymers from the initial screen were evaluated. Each polymer feature was evaluated for cell number (DAPI), viability, and STRO-1 and CD105 marker intensity. The top 30 polymers were coated on cover slips (Ø 10 mm) and after 7 days of culture, cells were stained with DAPI and CellTracker™Green and for STRO-1, CD105 and CD271. C) 3 'lead' polymers were validated in long-term cultures with hES-MPs (5 passages) and ADMSCs (10 passages) on polymer coated coverslips. Extensive MSC marker analysis (CD73, CD90, CD105, STRO-1, HLA-DR, CD146, CD271, CD140b, CD34 and CD14) was carried out using flow cytometry. ADMSCs were differentiated down the adipogenic and osteogenic lineages at passage 5.*

For the screening and scale-up experiments hES-MPs were used as a stable and robust surrogate for adult derived MSCs (Karlsson et al. 2009). The analysis of both hES-MPs and ADMSCs with multiple MSC markers during screening, scale-up and long-term passaging, combined with the high-throughput polymer microarray platform, provided an effective strategy for the identification of two synthetic substrates that could act as effective defined alternative to biological substrates, a necessary requirement for advancing MSC clinical applications.

3.1.1 Chapter aims

The aim of this chapter is to widen the current surfaces that are used for the maintenance of MSCs. Using the high-throughput polymer microarray platform it is hoped that polyacrylates and polyurethanes can be identified that can bind and facilitate the growth of MSCs in long-term culture while maintaining the MSC phenotype multipotency. This would identify synthetic surfaces could act as synthetic alternatives to biologically derived surfaces to make MSCs more amenable to therapeutic applications. The polymer microarray platform also has the potential to reveal components of how MSCs interact with the surface and the important factors for maintaining their 'stemness'.

3.2 RESULTS AND DISCUSSION

3.2.1 Screening on polymer microarrays

Two polymer libraries, a 'PA-library' (consisting of 453 co-polymers synthesised from acrylate, acrylamide and vinyl monomers) and a 'PU-library' (204 polyurethanes), were investigated using polymer microarray technology. These polymers were constructed to include a diverse range of monomers (appendix 1.1A–C) with a range of physico–chemical properties, such as variation in charge, lipophilicity, and wettability. The polymer libraries used in this study had been developed in two previous studies (Hitoshi et al. 2004; Tourniaire et al. 2006). The two libraries were printed onto agarose coated glass slides with each polymer printed in quadruplicate (Figure. 3.1A) (Pernagallo et al. 2008). In the initial screen, hES-MPs were incubated for 24 h on the microarrays to enable the identification of polymers that facilitated cell binding, as assessed by counting DAPI stained nuclei on each polymer feature. Slides were imaged with a Nikon 50i microscope using the software Pathfinder (IMSTAR). Each feature was imaged via bright field and the DAPI channel ($\lambda_{Ex}/\lambda_{Em}$ 358/461 nm). From this initial screen, 171 polymer candidates were identified (Figure 3.2). Based on cell binding from the initial screen, a new 'focused array' (171 polymers, n = 6) was fabricated (Fig. 3.1B).

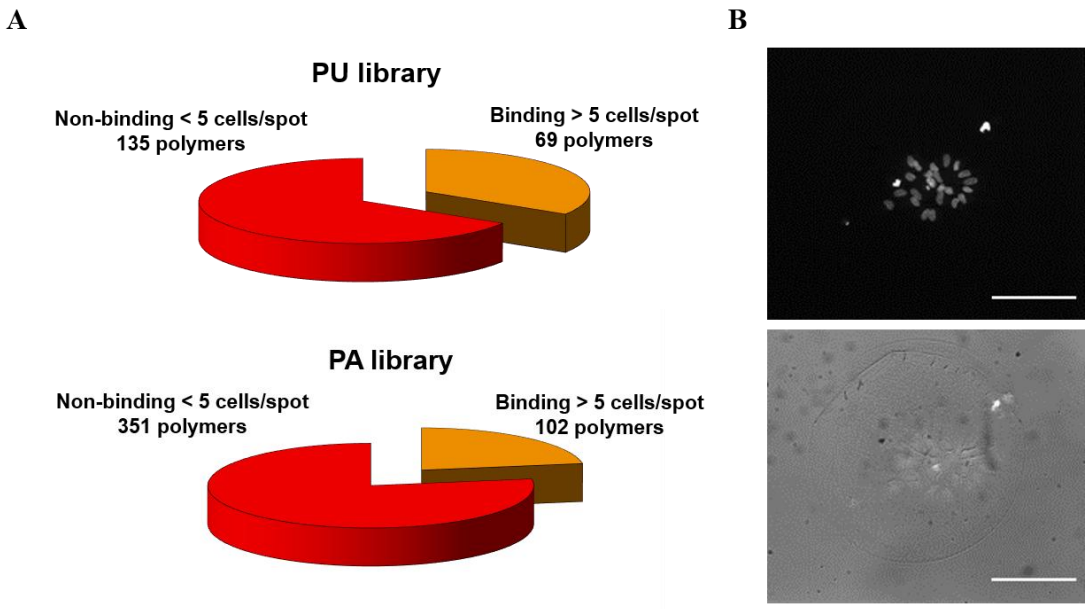

Figure 3.2 *A) Results of the initial 24 h binding screen (hES-MPs) on the 204 member PU-library and the 453 member PA-library. 69 polymers form the PU-library and 102 polymers from the PA-library were selected for the 'focused' screen. B) An example of a DAPI stained nuclei and bright field images of a polymer binding cells (24 h binding screen). Scale bar 100µM.*

The new arrays were incubated with hES-MPs for 2, 4 or 7 days, and analysed for cell binding on each polymer. In order to compensate for any variation in feature size between different polymers, the features were measured and the cell counts given as cells/mm^2.

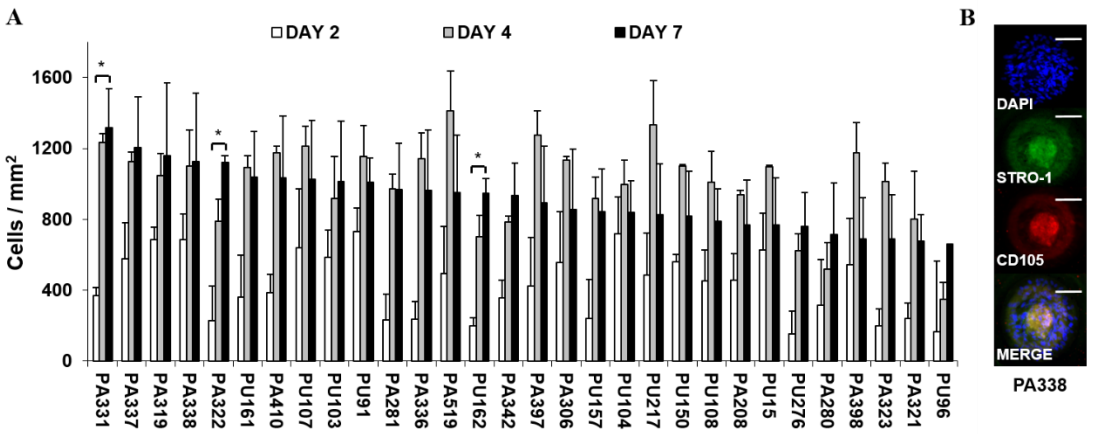

Figure 3.3*. A) Top 30 polymer candidates for hES-MP binding and growth (cells/mm^2) after 2, 4 and 7 days of culture on the 'focused' 171-member polymer microarray. B) Staining and imaging of the polymer* ***PA338*** *with DAPI (nuclei stain) and the markers STRO-1 and CD105 following cellular incubation on the array. Scale bar 100µM.*

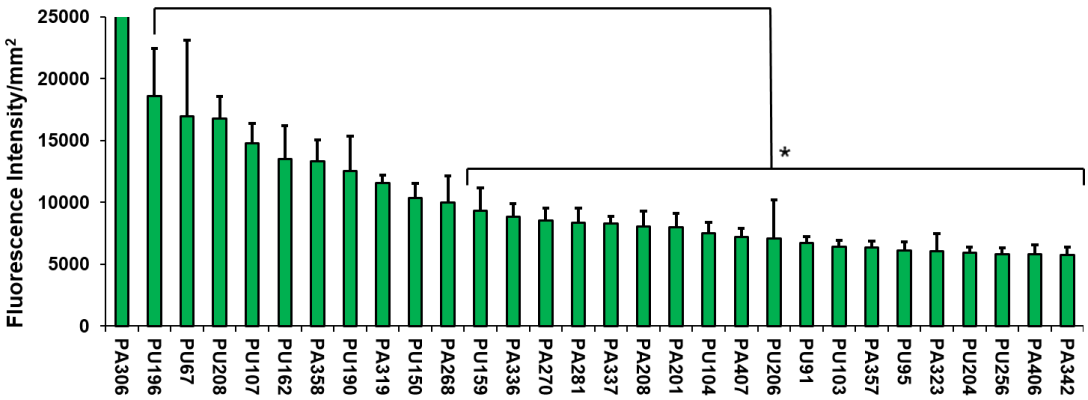

***Figure 3.4**. The top 30 polymers in terms of cell viability measured by fluorescence intensity/mm^2 (λ_{Ex}/ λ_{Em} 495/519 nm) from staining of cells on the 'focused' polymer microarray with CellTracker Green at day 7. Note that polymer **PA306** is auto-fluorescent.*

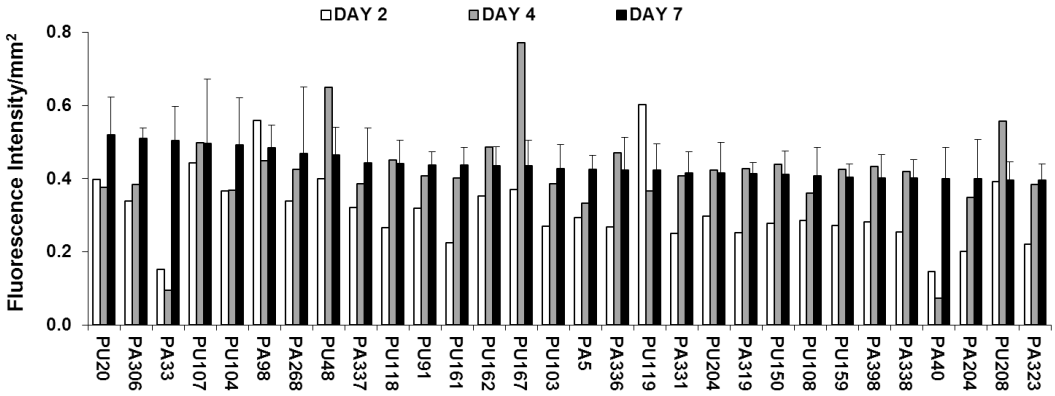

***Figure 3.5**. The top 30 polymers in terms of STRO-1 staining (λ_{Ex}/λ_{Em} 495/519 nm) from the 'focused' polymer microarray measured as fluorescence intensity/mm^2.*

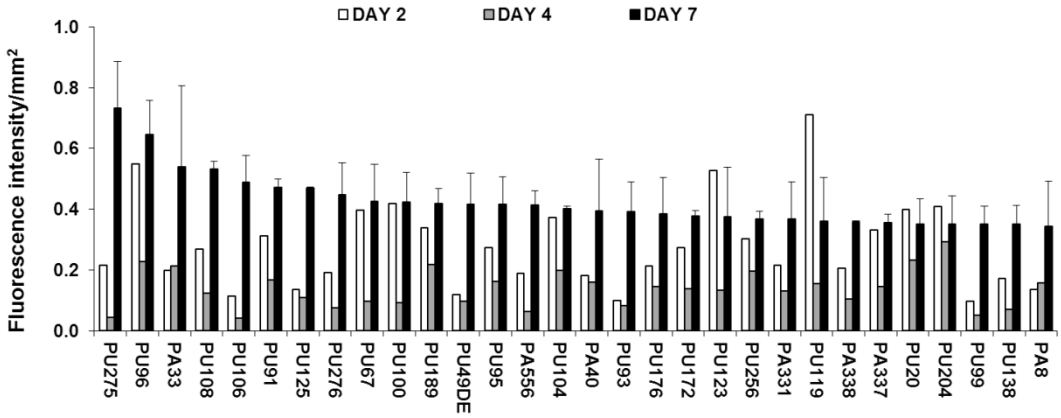

***Figure 3.6**. The top 30 polymers in terms of CD105 staining (λ_{Ex}/λ_{Em} 555/565 nm) from the 'focused' polymer microarray measured as fluorescence intensity/mm^2.*

To select substrates that would potentially favour the multipotent stem cells over less potent progenitors, criteria for selecting candidates for larger scale studies took into consideration marker intensities as well as cell count and viability.

***Table 3.1**. The top 30 performing polymers from the 171 member 'focused' polymer microarray were ranked for each criterion, i.e., cell count (cells/mm^2), STRO-1 intensity, CD105 intensity and cell viability and averaged to give an overall ranking.*

POLYMER	STRO-1 RANK	CD105 RANK	CELL COUNT	VIABILITY RANK	OVERALL RANKING
PU91	12	7	10	23	**1**
PA337	10	26	2	17	**2**
PU104	6	16	19	20	**3**
PU103	16	35	9	24	**4**
PU108	24	4	22	36	**5**
PA338	27	25	4	35	**6**
PU107	5	73	8	5	**7**
PA336	18	49	12	14	**8**
PA331	20	23	1	52	**9**
PA306	3	75	17	1	**10**
PU204	21	28	32	28	**11**
PU161	13	47	6	49	**12**
PA319	22	82	3	9	**13**
PU67	38	10	68	3	**14**
PU162	14	86	14	6	**15**
PU20	2	27	48	47	**16**
PU95	40	14	46	26	**17**
PU190	34	36	49	8	**18**
PU256	44	22	41	29	**19**
PU118	11	44	51	41	**20**
PU96	61	2	31	54	**21**
PU276	46	9	26	70	**22**
PU157	35	63	18	45	**23**
PA204	29	45	65	28	**24**
PU150	23	115	21	10	**25**
PA398	26	72	28	57	**26**
PU208	30	118	34	4	**27**
PU176	47	19	69	61	**28**
PA410	63	66	7	62	**29**
PA357	67	64	43	25	**30**

The best polymers in terms of number of cells/mm^2, cell viability, STRO-1 intensity and CD105 intensity were ranked with the 30 highest-ranking polymers selected for more detailed studies (Table 3.1).

3.2.2 Lead identification

The top 30 polymer candidates were coated onto glass coverslips and incubated with hES-MPs for 7 days using gelatin and tissue culture plastic as controls, followed by staining with DAPI, CD105, STRO-1, and an additional marker CD271 (CD271 was included to provide additional criteria for lead polymer selection).

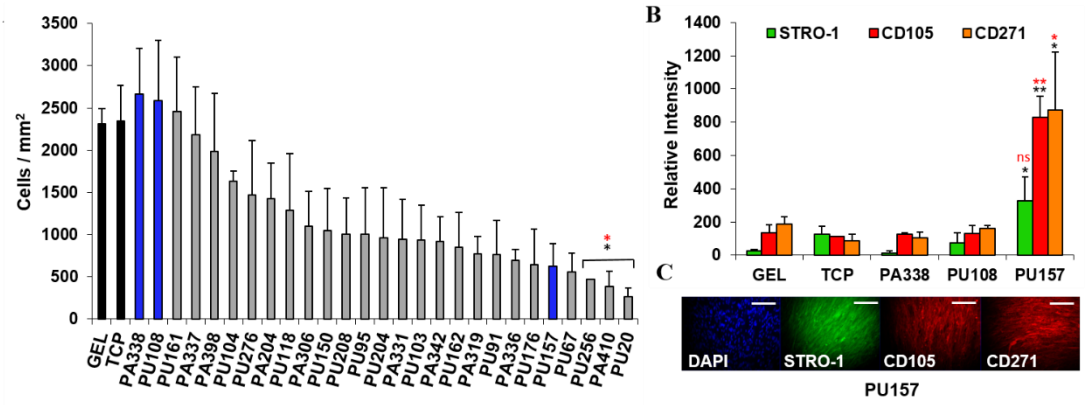

***Figure 3.7**. A) The number of hES-MPs/mm^2 for each of the polymer candidates after 7 days incubation on polymer coated coverslips (n = 3, error bars represent SEM). The blue bars represent polymers selected as 'leads' and the black bars represent the controls. B) Relative marker intensity for STRO-1, CD105 and CD271 for hES-MPs grown on the 3 'lead' polymers **PU157**, **PU108** and **PA338**, and gelatin (GEL) and tissue culture plastic (TCP) (n = 3). Statistical significance compared with the GEL and TCP controls is denoted with black and red star respectively. C) Examples of images of cells grown on the 'lead' polymer **PU157** stained for DAPI, STRO-1, CD105 and CD271. Scale bar 100µM.*

After 7 days of culture, 5 polymers showed better or similar levels of cell growth compared to gelatin or tissue culture plastic (Fig. 3.7), however, statistical comparison shows that only the bottom three candidates had significantly lower growth when compared with the gelatin control. The two top polymers, **PA338** and **PU108**, closely resembled gelatin in terms of marker expression and were chosen as

'lead' substrates (Fig. 3.7 and Fig. 3.8). On larger surfaces, **PU157** showed relatively modest cell growth but significantly enhanced **STRO-1**, **CD105**, and **CD271** intensities (Fig. 3.7B and C), and was therefore taken forward as the third 'lead' polymer for long-term culture and characterisation with hES-MPs and ADMCSs.

3.2.3 Long-term culture and characterisation of hES-MPs on lead polymers

For extended culture on the lead polymers **PU157**, **PU108** and **PA338** (Fig. 3.8), a variety of MSC markers were used to fully probe the suitability of the substrates for long-term MSC culture. In addition to CD105, STRO-1 and CD271, seven additional markers were used. This included positive markers CD90 and CD73, and negative markers CD14 and CD34, chosen because they are used as part of the minimal criteria for defining MSCs (Dominici et al. 2006).

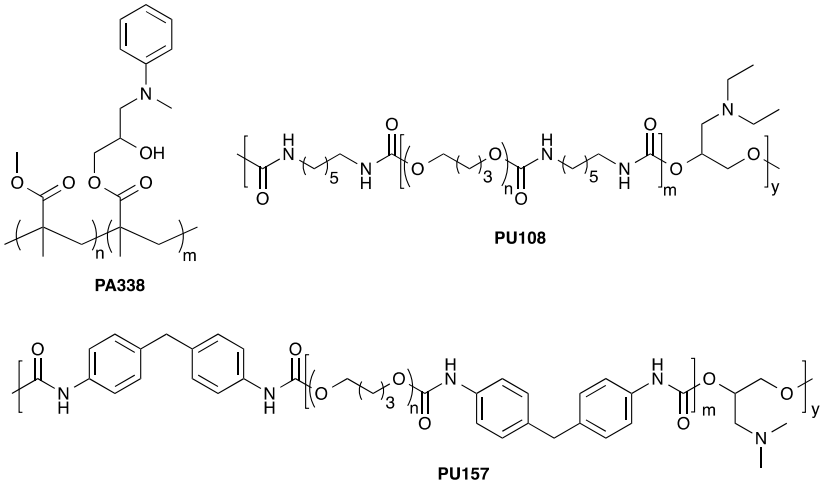

***Figure 3.8**. Structures of the copolymers **PU157**, **PU108** and **PA338**. **PU157** was synthesised from poly(butyleneglycol) (mw 250) and 4,4'-methylenediphenyldiisocyanate with 3-(dimethylamino)-1,2-propanediol as an extender, **PU108** from poly(butyleneglycol) (mw 1000) and hexamethylenediisocyanate with 3-(diethylamino)-1,2-propanediol as an extender. **PA338** is a poly(methylmethacrylate-co-glycidylmethacrylate) (synthesised in 1:1 monomer ratio) modified with N-methylaniline. The lead structures where drawn using CHEMDRAW by Dr Annamaria Lilienkampf.*

CD34 positive populations are present in MSCs obtained from adipose tissue (Corselli et al. 2012) and MSC marker expression in general has been shown to depend on the source (Nery et al. 2013). CD146 and CD140b were selected as these are considered as *in vivo* MSC markers (Crisan et al. 2008), while HLA-DR is a standard negative marker for MSCs as well as an indicator of the immune modulatory state of MSCs (HLA-DR is up regulated when MSCs are primed into their immune modulatory state) (Singer et al. 2011). Prior to the long-term culture on the 'lead' polymers, hES-MPs were characterised at 'passage 0', *i.e.*, the point of removal from gelatin, for the expression of CD105, STRO-1, CD271, CD90, CD73, CD34, CD14, CD146, CD140b, and HLA-DR (Fig. 10A). Here, cells were positive for CD73 and STRO-1 (100% and 99%, respectively), positive for CD105 and CD90 (91% and 83%, respectively), and moderately positive for CD34, CD146 and CD14 but had been significantly down-regulated by passage 5. hES-MPs grown on the 'lead' polymers were assessed with these 10 markers at passage 5 to monitor the marker conservation or changes in the marker expression levels.

Flow cytometry analysis at passage 5 showed that hES-MPs cultured on **PU108**, **PU157** and **PA338** expressed similar levels of the markers to cells grown on gelatin (Fig. 3.9A, Appendix 2.1). However CD105, which is considered one of the essential markers for MSCs, expression was reduced on cells grown on all 'lead' polymers, but levels were comparable with gelatin. Interestingly, hES-MPs are currently derived through serial passaging of hESCs on gelatin (Karlsson et al. 2009) Notably, CD105 was significantly reduced and almost completely lost at passage 5 on tissue culture plastic (Fig. 3.9A).

The marker CD90, which is bimodal in hES-MPs (Karlsson et al. 2009; Li et al. 2013), showed a substantial increase in the negative fraction with culture on **PA108** when compared to other substrates (Fig. 3.9A and Fig. 3.10). Comparison with the 'p0'showed a significant fall in CD90 on this polymer (55%). However, hES-MPs cultured on **PU157** and **PA338** maintained CD90 at levels similar to tissue culture plastic and gelatin (73%, 74% 70% and 82% of positive cells, respectively), although **PA338** did show a significant fall in expression (Fig. 3.9A). Decreasing levels of CD90 have been associated with the loss of the immune modulatory properties of

MSCs (Campioni et al. 2009). The ability of **PU157** and **PA338** to maintain marker expression (including CD105 and CD90) similar to gelatin indicates that they may act as chemically defined alternatives to gelatin for serial passaging of hESCs to produce hES-MPs.

3.2.4 Long-term culture and characterisation of ADMSCs on the lead polymers

ADMSCs grown on **PU157**, **PU108** and **PA338**, closely resembled the gelatin control with most of the MSC markers at passage 5 (Fig. 3.9B, Appendix 2.2). At passage 5, ADMSCs grown on tissue culture plastic, gelatin, **PU157**, **PU108** and **PA338** were positive for CD105, although a significant loss in marker intensity was observed with all substrates when compared with 'passage 0' (Fig. 3.9B and Fig. 3.11).

A further reduction in the CD105 marker intensity was observed by passage 10 with **PU157** and **PA338** (49% and 49% of positive cells, respectively), although with cells grown on gelatin and tissue culture plastic the levels were maintained (85% and 81%, respectively) (Fig. 3.9B and 3.11, Appendix 2.3).

At the start ('passage 0'), ADMSCs showed a 44% positive population for STRO-1. By passage 5 there was a significant positive shift in STRO-1 intensity with tissue culture plastic, which became even more pronounced by passage 10 with 70% of cells being positive (Fig. 3.5 and 3.11). High expression of STRO-1 has been associated with an increase in adipogenic and osteogenic markers PPAR-G and RUNX2, respectively, and up-regulation of either of these markers could reduce the ability of the cells to differentiate down the other lineage (Isenmann et al. 2009).

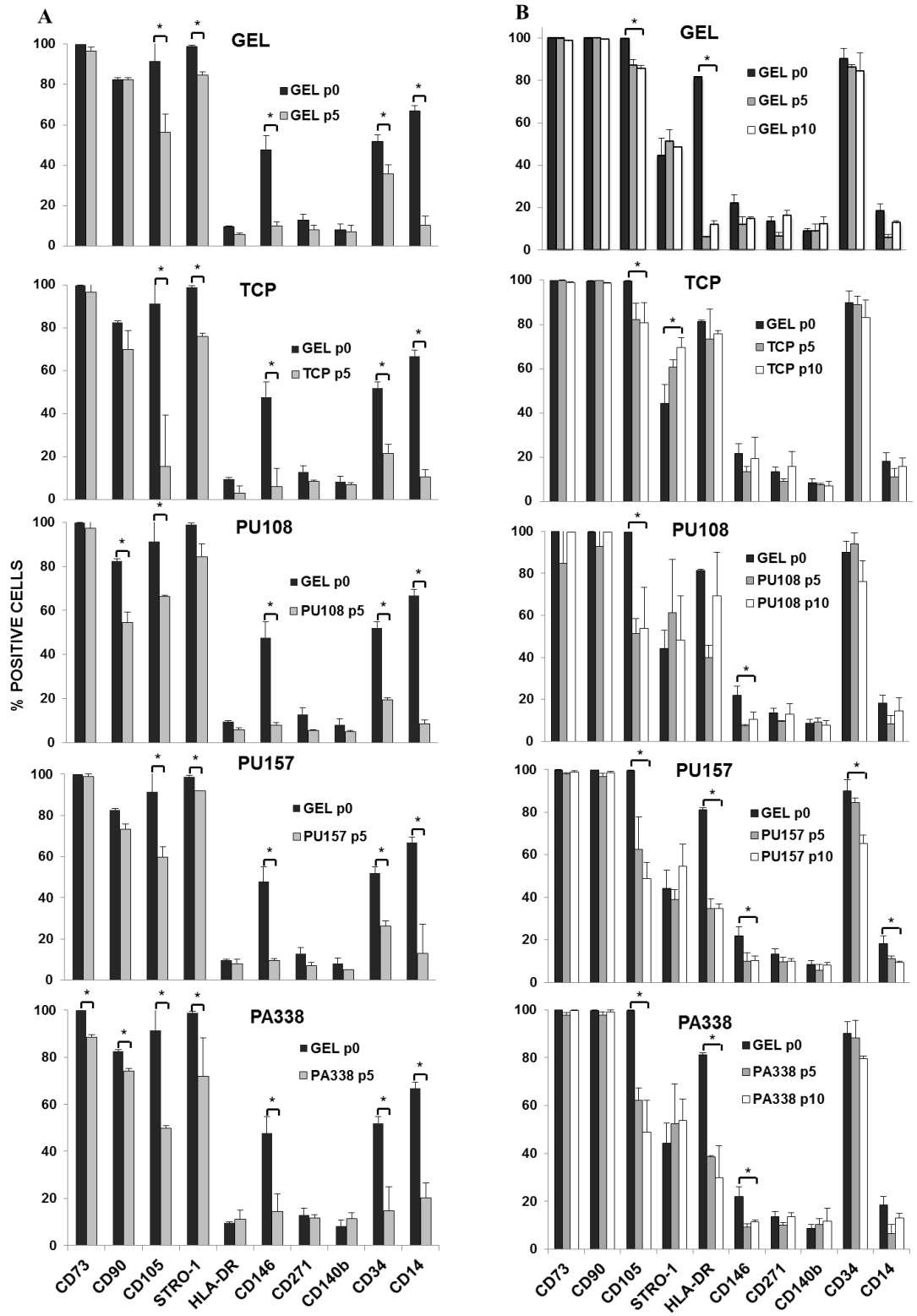

***Figure 3.9**. Flow cytometry analysis of 10 MSC markers for hES-MPs (A) and ADMSCs (B) prior to the culture on **PU157**, **PU108** and **PA338**, termed 'passage 0' (p0), and at passage 5 (p5) and 10 (p10) (ADMSCs only) on **PU157**, **PU108**, **PA338**, gelatin (GEL), and tissue culture plastic (TCP).*

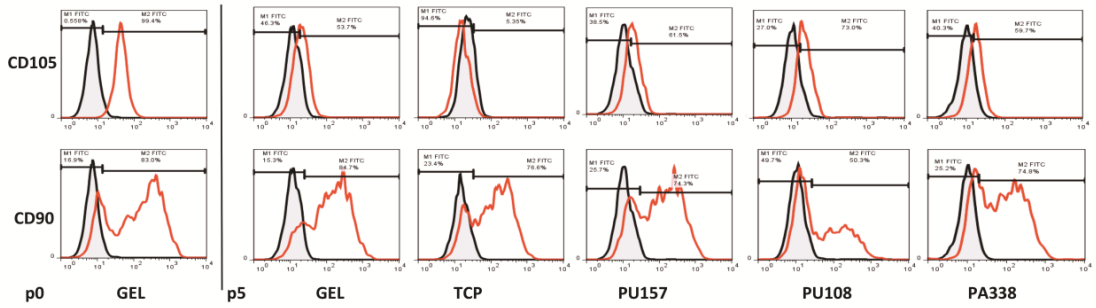

***Figure 3.10**. Representative flow cytometry traces of the markers CD105 and CD90 with hES-MPs at 'p0' and p5 on gelatin (GEL), tissue culture plastic (TCP), **PU157**, **PU108** and **PA338** (red trace for stained cells, black for unstained cells).*

PPAR-G is a nuclear receptor and master regulator (along with C/EBPα) of terminal adipogenisis involving the coordinating the expression of many hundreds of genes (Farmer 2005). RUNX2 is an early transcription factor in osteoblast differentiation, it binds to the promoter region OSE2 found in the promoter region of all major osteoblast marker genes (Bruderer et al. 2013).

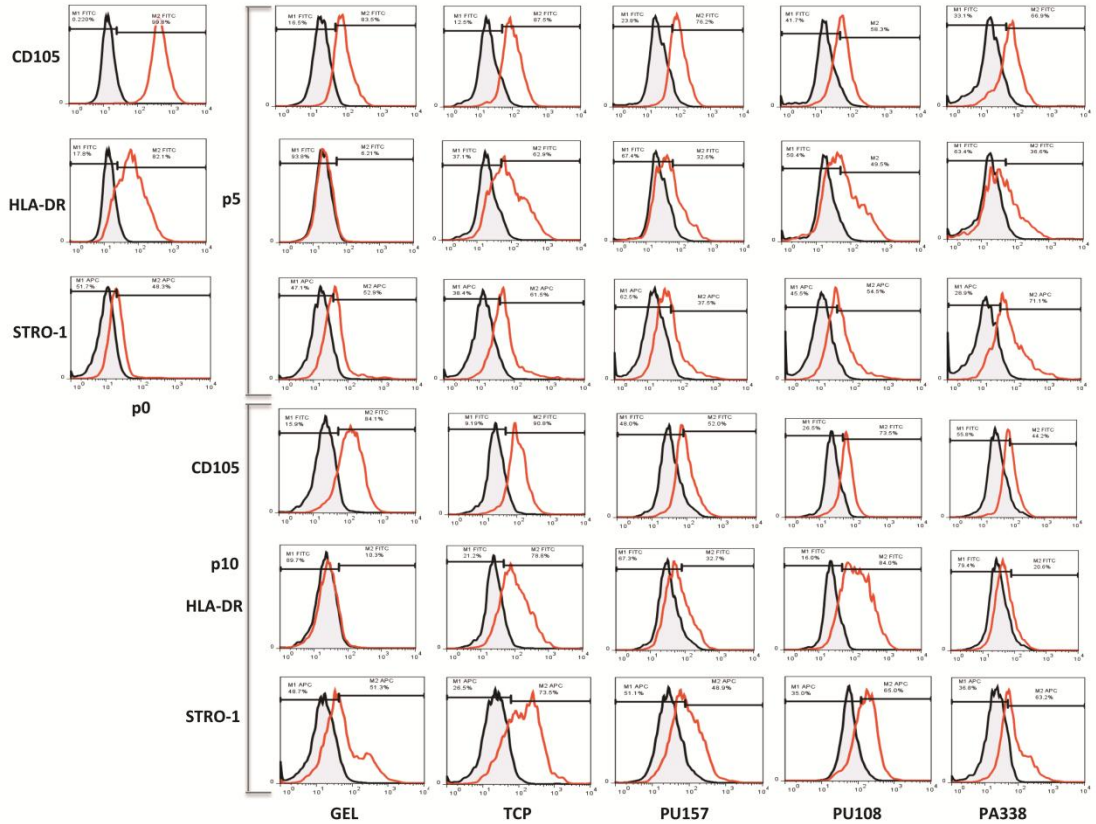

***Figure 3.11**. Representative flow cytometry traces of the markers CD105, HLA-DR and STRO-1 with ADMSCs at 'p0' , p5 and p10 on gelatin (GEL), tissue culture plastic (TCP), **PU157**, **PU108** and **PA338** (red trace for stained cells, black for unstained cells).*

3.2.5 Differentiation of ADMSCs

At passage 5, ADMSCs grown on **PU157**, **PU108**, **PA338**, gelatin, and tissue culture plastic were differentiated down the adipogenic and osteogenic lineages to evaluate if they retained their differentiation potential.

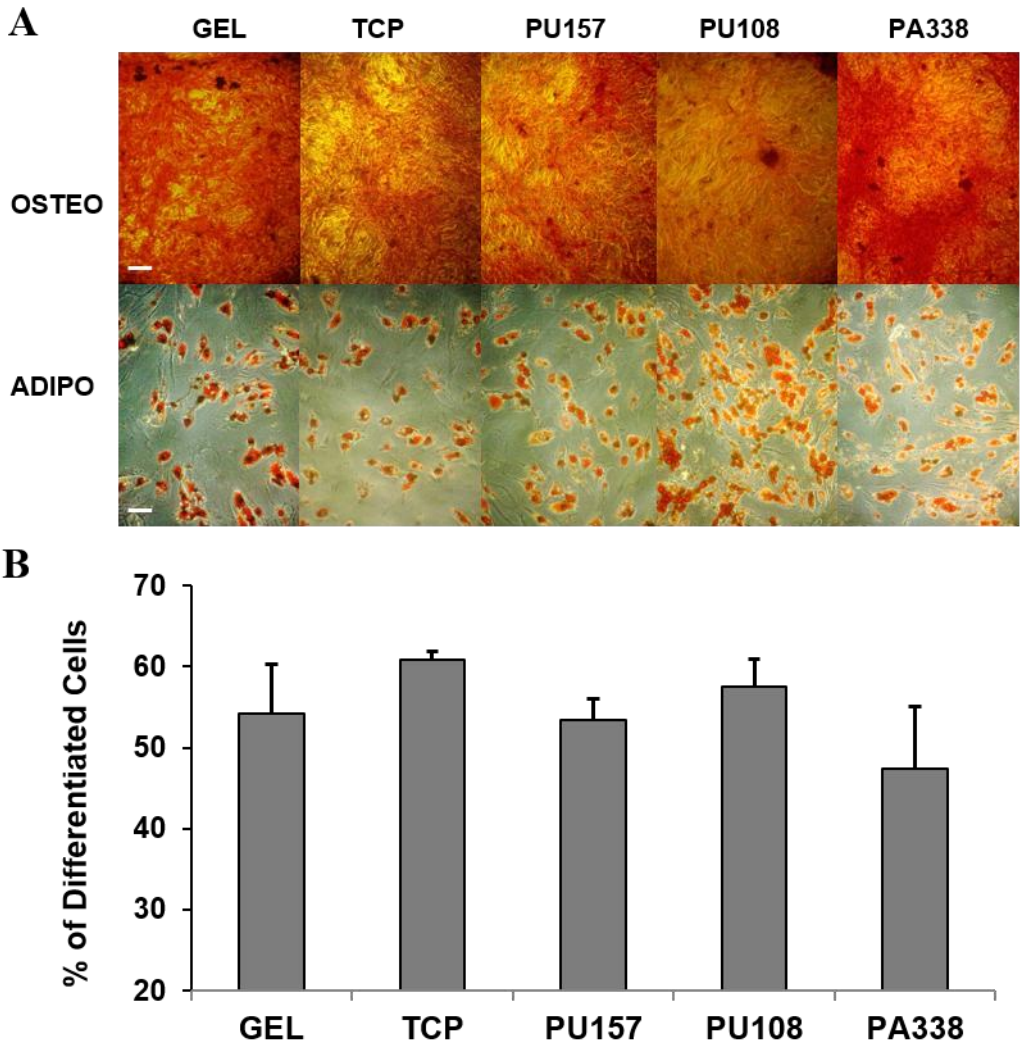

Figure 3.12 *A) Histological staining of ADMSCs differentiated down the osteogenic lineage with red staining indicating calcium deposits (Alizarin Red) and ADMSCs differentiated down the adipogenic lineage with red spots indicating fat droplets (Oil red O) Scale bar 100µM. B) The percentage of ADMSCs that differentiated down the adipogenic lineage after 5 passages on gelatin (GEL), tissue culture plastic (TCP),* ***PU157****,* ***PU108*** *and* ***PA338*** *(n = 3 with error bars representing SD, for each replicate 12 images were taken and analysed). ADMSCs were also stained for DAPI, the number of differentiated cells/total cell number gave the % differentiation per image.*

Histological staining of the cells with Alizarin Red and Oil red O showed that the ADMSCs had differentiated down the osteogenic and adipogenic lineages, respectively, proving that the cells had clearly maintained their multi-lineage potential (Fig. 3.12A). The ADMSCs grown on **PU157** (53%), **PU108** (57%), **PA338** (47%), gelatin (54%), and tissue culture plastic (61%) showed no significant difference in the percentage of cells capable of differentiating down the adipogenic lineage (Fig. 3.12B).

Image analysis of the Alizarin Red S stained cells showed that **PA338** (71%)**, PU157** (38%), **PU108** (30%), gelatin (58%) and tissue culture plastic (83%) had different levels of staining, however, the high variability meant there was no significant difference in the level of Alizarin Red S staining (Fig. 3.13).

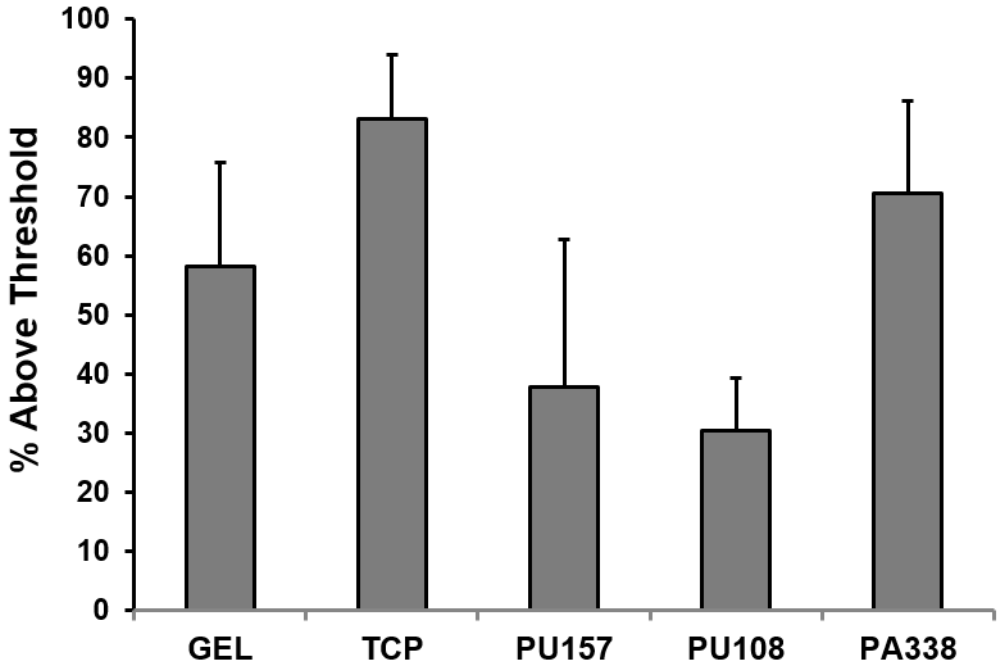

Figure 3.13. *Comparison of the amount of Alizarin red S positive pixels from osteogenic differentiation images of ADMSCs after 5 passages on gelatin (GEL), tissue culture plastic (TCP),* ***PU157****,* ***PU108*** *and* ***PA338****. Osteogenic comparison was carried-out using ImageJ by setting the image/adjust/colour threshold option. The 'analyse particles' option quantified the percentage of pixels above threshold. The values correspond to the percentage of positive pixels on an image that are above a defined minimum threshold (n = 3, error bars given as SD, 12 images per replicate were analysed) (Mehlem et al. 2013).*

A similar ability of ADMSCs to differentiate at passage 5, regardless of which substrate they were grown on, suggests that the differences seen in marker expression at this passage has no significant effect on their differentiation capacity.

3.2.6 Polymer analysis

To investigate if the chemical composition of the polymer surface can be correlated to cell binding/growth and stem cell maintenance, the monomers present in the top candidates from the scale up studies were analysed. The top ten performing polymers from the PA-library showed some monomers to be highly preferred over others, with only 10 monomers making up the 10 copolymers (Fig. 3.14).

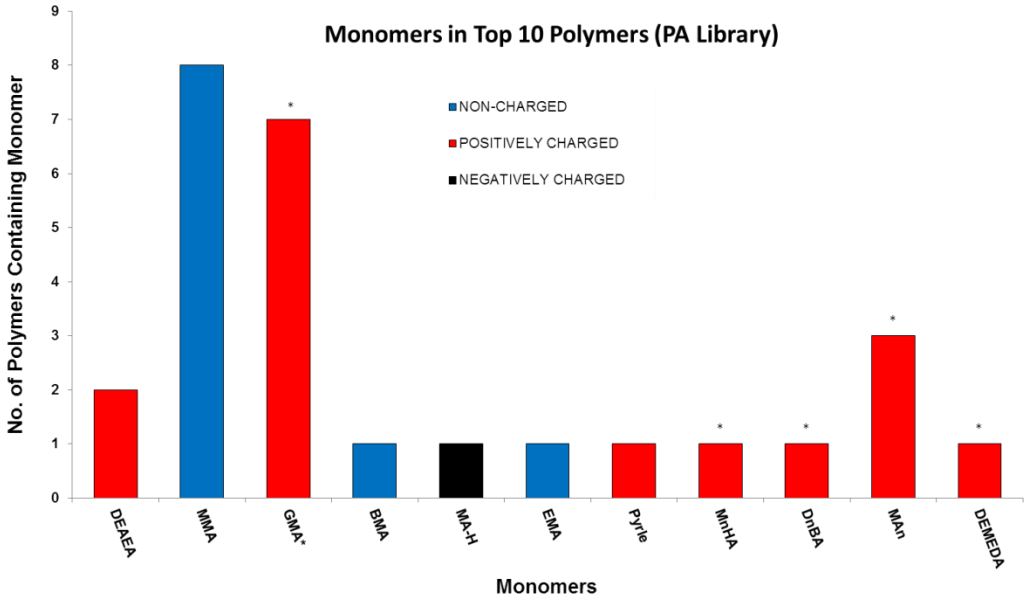

***Figure 3.14**. The monomers found in the top 10 polymers in the PA library in the scale up experiment. The GMA* containing polymers were subsequently functionalised with a variety of amines (signified by *). The figure legend shows the likely properties of the monomers at physiological pH (MAn is an aniline derivative and mostly uncharged).*

Methyl methacrylate (MMA) was present in 8 out of 10 polymers. This would correspond to the work of Curran (2006 & 2010) and Benoit (2008) that showed the methyl (–CH3) functional group to be critical in maintaining the mesenchymal stem cell state. A second monomer GMA (modified) was present in 7 of the top 10 polymers, the modified monomers; MnHA, DnBA, MAn and DEMEDA all contained a hydroxyl (-OH), methyl (-CH3) and tertiary amine (-N) groups. In

addition, the presence of an aryl ring seemed beneficial for the top PA candidate (**PA338** is a copolymer of MMA and *N*-methylaniline functionalised glycidyl methacrylate (GMA) designated MAn) (Fig. 3.14, Appendix 1A-B for chemical structures). The presence of 3 groups (-CH3, -OH, -N) instead of one adds to the previous studies.

Analysis of the top 10 polyurethanes from the scale up experiments showed 4,4'-methylenebis(phenylisocyanate) (MDI) and poly(butyleneglycol) (PTMG) were present in 8 and 5 polymers, respectively, both of which were present in the lead **PU157** along with 3-dimethylamino-1,2-propanediol (DMAPD) (Fig. 3.15 and 3.16, for chemical structures of the monomers see appendix 1.1C). The MDI monomer contains two aryl groups and the DMAPD monomer contains a tertiary amine (-N). Interestingly, the lead PU candidate **PU157** does not contain a methyl group (-CH3) (or hydroxyl group (-OH)). Taken together with the PA monomers and the lead candidate **PA338** this could indicate that the critical components may be the aryl group and tertiary amine.

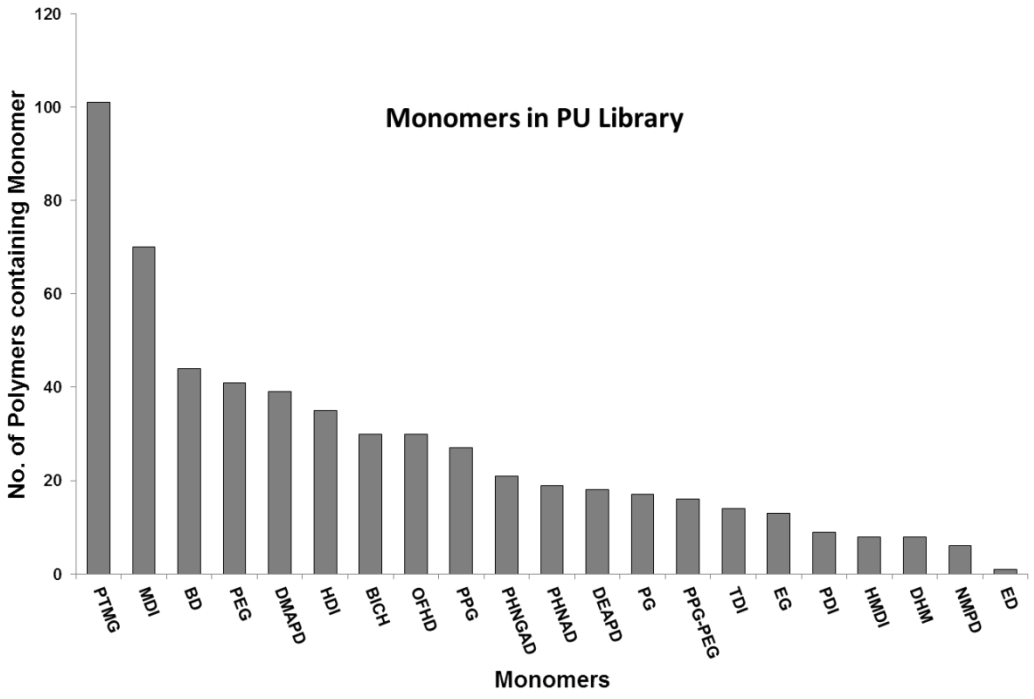

***Figure 3.15**. Monomer distribution in the polyurethane-based PU-library.*

Certain monomers, *e.g.* poly(ethylene glycol) (PEG), seemed disadvantageous in terms of binding and promotion of growth. PEG was a well-represented monomer in the polymer library (Fig. 3.15) but did not appear in the top polymers (Fig. 3.16) or in the top 30 performing polymers (Table 3.1). Whether this is due to its hydrophilic nature, stiffness or surface topography requires additional analysis but this is surprising due to its use in many cell studies.

Adhesion of cell on the surface is a complex process depending on a combination of cell–protein and polymer–protein interactions, and the physico–chemical properties of the surface as well as the topography and nano-topography of the surface. In stem cell culture, the ability of the substrate to maintain the cells in their stem cell state adds another level of complexity to the material–cell interactions. Therefore, although some common features could be found on the chemical composition of non-binding versus lead polymers, drawing direct 'structure–function relationships' for polymer surfaces and stem cell maintenance remains a challenge, further highlighting the advantages of a high-throughput approach for the discovery of new substrates.

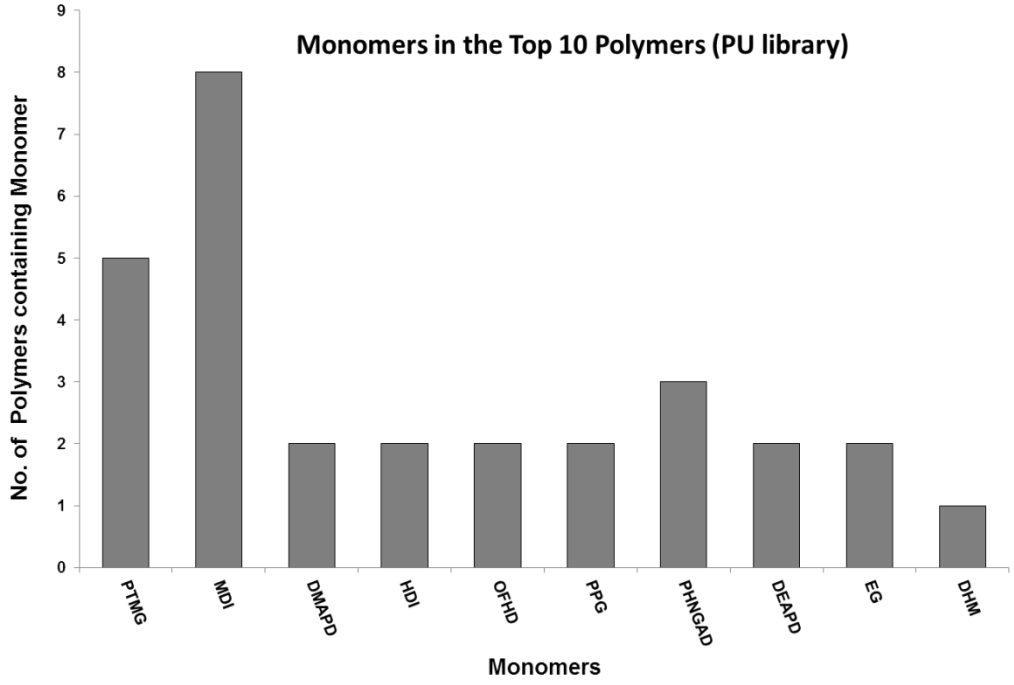

***Figure 3.16**. Monomer distribution in the top 10 PU polymers in the scale up experiment.*

3.2.7 Surface characterisation

Water contact angle (the angle a drop of water makes on the polymer surface) has previously been reported to be one of the most important determinants for cellular binding and growth for hESCs (Mei et al. 2010). Of the lead polymers, **PA338** and **PU157** had a water contact angle of 81° and 70°, respectively (representative control polymers, which showed no or poor cell binding or growth, had contact angles of 27–67°) (Table 3.2). However, **PU108** had a relatively small water contact angle of 46°, suggesting that water contact angle or the surface energy is a poor indicator of stem cell adhesion/growth with MSCs and the polymer libraries investigated.

Table 3.2. *Molecular weight, polydispersity index (PDI), water and formamide contact angles, and surface energy calculations of the 3 lead polymers* ***PU157, PU108*** *and* ***PA338****, and representative non-binding polymers* ***PA554*** *and* ***PU6****, and 'mid-range polymers'* ***PA63*** *and* ***PU212****.**

Surface	MW	PDI	Contact Angle H_2O (°)	Contact Angle $HCONH_2$ (°)	Surface Energy (dyne/cm)
PU6	**59000**	**2.0**	**26.5** ± 1.6	**27.1** ± 2.0	**66.0** ± 0.9
PA554	**110000**	**2.2**	**65.7** ± 0.5	**32.3** ± 0.6	**51.2** ± 0.7
PU212	**66000**	**2.2**	**61.8** ± 1.2	**32.3** ± 0.0	**49.8** ± 0.2
PA63	**52100**	**4.2**	**66.7** ± 1.9	**46.3** ± 5.1	**41.5** ± 3.1
PU108	**233000**	**2.5**	**46.1** ± 3.6	**27.6** ± 2.2	**54.0** ± 1.9
PU157	**41000**	**1.9**	**69.8** ± 1.2	**51.8** ± 1.5	**38.0** ± 0.9
PA338	**> 2,000,000**	**N.D**	**81.1** ± 0.7	**62.1** ± 0.6	**31.8** ± 0.6

** **PA63** is a copolymer of HBMA and PAA, and **PA554** of AH and HEMA. **PU212** was synthesised from PHNAD and HDI with PG as a chain extender, PU6 from PEG and BICH. For the monomer structures see appendix 2.1A-C. The contact angle and surface energy measurements were performed by W Hu and R Zhang.*

To investigate global protein binding on the polymer surfaces, polymer coated cover slips were treated with culture media (supplemented with 10% FCS) for 24 h, and adhered proteins analysed by gel electrophoresis (Fig. 3.17). With the exception of **PU108**, which showed slightly different protein binding pattern, **PU157**, **PA338**, **PA554**, **PU6**, **PA63** and **PU212**, including poor cell binding controls, showed protein binding similar to gelatin and tissue culture plastic, thus suggesting that the surface chemistry plays an important role in the cell adhesion and growth, although subtle changes in binding of low abundance proteins cannot be ruled out.

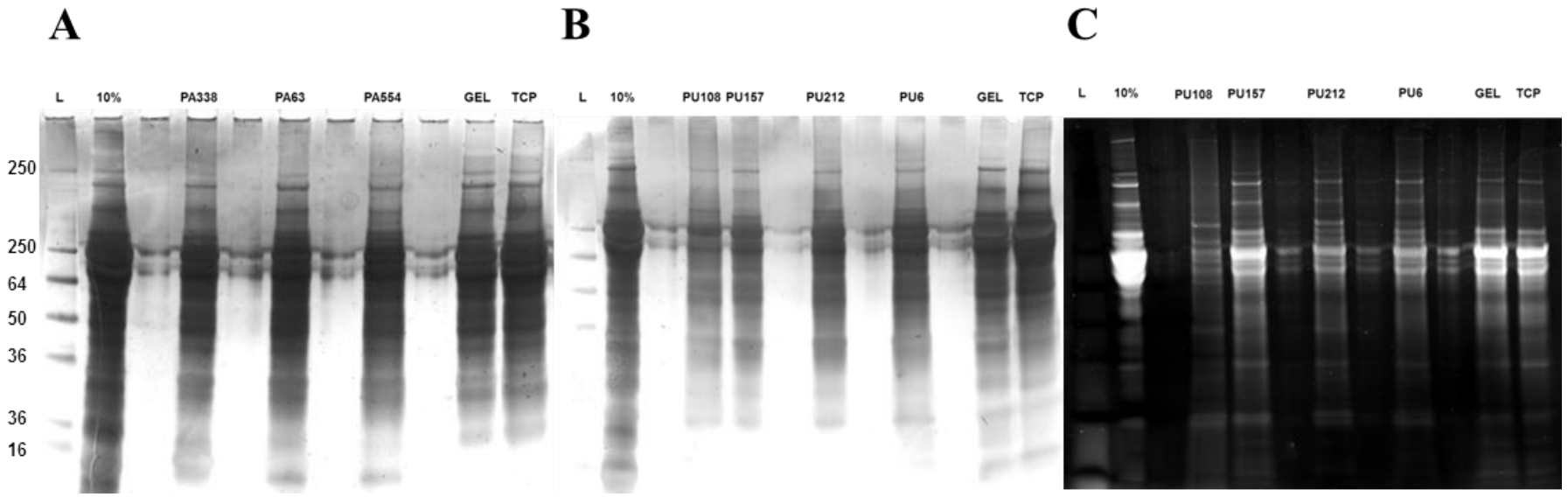

Figure 3.17. *Protein analysis on 4-12% gradient polyacrylamide gels (silver or fluorescent staining) after protein extraction from polymer-coated coverslips, gelatin and tissue culture plastic (TCP), incubated for 24 h with culture media (DMEM containing 10% FCS, 4 ng/mL bFGF, 200u/mL of L-glut, 1% pen/strep). The first lane on the left (L) contains a protein ladder (unit kDa) and the next lane contains culture media.*

3.3 CONCLUSIONS

Using hES-MPs in a 'three-step' screening strategy, which consisted of two iterative rounds of polymer microarray screens followed by a large scale 30 polymer study, a number of polymers were identified that could potentially support long-term MSC culture. Based on cell growth and the intensity of markers CD105, STRO-1 and CD271, two polyurethanes (**PU157** and **PU108**) and one polyacrylate (**PA338**), were identified as 'lead' substrates.

hES-MPs and ADMSCs were cultured on **PU157**, **PU108** and **PA338** for 5 and 10 passages, respectively, and analysed for 10 MSC markers. All substrates showed similar growth rates for both cell types. After 5 passages on the polymer substrates, both cell types expressed similar marker levels as control cells grown on gelatin, whereas on tissue culture plastic the marker CD105 was lost (hES-MPs). hES-MPs cultured on **PU108** showed an increase in the negative fraction for CD90 and ADMSCs cultured on **PU108** continued to express HLA-DR at passage 10. Irrespective of some variation in the marker expression between ADMSCs grown on different substrates, the cells were successfully differentiated into osteoblasts and adipocytes at passage 5. Overall, **PU157** and **PA338** showed the most similarity to gelatin and efficiently maintained growth and conserved phenotype over multiple passages for both hES-MPs and ADMSCs. Both these polymers contained an aryl group and a tertiary amine but only one PA338 contained a methyl group identified in previous studies as being able to maintain the MSC state. The application of the polymer microarray platform in conjunction with marker analysis proved an effective strategy for identifying two defined substrates **PU157** and **PA338**, as a potential alternative to gelatin which offers chemically defined synthetic polymer substrates for efficient long term MSC culture. This strategy can be applied to other cell types that require maintenance on serum free media, biological or poor performing synthetic substrates.

CHAPTER 4

Long-Term Mesenchymal Stem Cell Culture on a Defined Synthetic Hydrogel with Enzyme Free Passaging

Parts of this chapter have been previously were published in:

Duffy, C.R.E., Zhang, R., How, S.E., Lilienkampf, A., de Sousa, P.A. & Bradley, M., (2014) Long term mesenchymal stem cell culture on a defined synthetic substrate with enzyme free passaging. *Biomaterials*, 35(23), p5998–6005.

ADMSCs were supplied by Dr Chris West Ethical and approval for the collection of adipose tissue and subsequent research was granted by the South East Scotland Research Ethics Committee (Ref 10/S1103/45h).

4.1 INTRODUCTION

In chapter 3, polymer microarrays where applied to the identification of defined polymers that could retain the MSC phenotype and multilineage capacity in long-term culture. The benefit of the polymer microarray approach was clearly demonstrated with two polymers identified **PA338** and **PU157** that could maintain the phenotype of the MSCs in long-term culture. The application of hydrogels to stem cell culture has become and an increasingly active area in stem cell applications because of their similarity to native tissues and because of the wide range of applications due to their ability to encapsulate proteins/small molecules (Censi et al. 2012), alter stiffness/elasticity (Engler et al. 2006), change properties with various environmental cues such as pH (Yin et al. 2006), light (Hu et al. 1995), temperature (Wells et al. 2011).

Moreover, hydrogels have been used to investigate mechanical dosing using hydrogels with photo-cleavable cross linkers. These experiments showed that the hardness of the growth substrate directly influenced the expression of differentiation markers (PPARγ and RUNX2) in MSCs and that the length of time MSCs where exposed to such mechanical factors influenced their ability to differentiate down the adipo or osteogenic lineages (Yang et al. 2014). Studies where the mechanical properties remain constant and the functional group presented to the MSCs varies has revealed that small molecule functional groups alone can induce cells towards differentiation depending on the functional group, with charged phosphate groups inducing osteogenisis and hydrophobic *t*-butyl groups inducing adipogenesis (Benoit et al. 2008).

The opportunity to apply the polymer microarray platform to MSCs would allow the identification of hydrogels that could maintain the MSC phenotype in long term culture. This platform would allow the presentation of functional groups at different concentrations on surfaces with different mechanical properties. In the previous chapter the application of a polymer microarray identified a number of candidates that could have been taken forward in long term culture, three of which were selected. However, MSCs grown on these substrates still required trypsinisation at passage, a process that will 'shave off' a multitude of vital cellular surface proteins (Khalil et al. 2014) and is also animal derived. This is clearly an undesirable process if the stem cell 'state' is to be maintained, and which must also lead to variation and uncertainty in apparent surface marker expression.

As discussed in section 1.4.4, maintaining the stem cell state is a fine tuned interaction with the extracellular matrix. Treatment with trypsin destroys the extracellular matrix components that the cells are attached to and have secreted. The destruction of the niche at each passage will require a reassessment of the new substrate through integrin interactions with the extracellular matrix (Li et al. 2013). So-called 'smart' hydrogels add an additional dimension as they can respond to environmental cues. A relatively large hydrogel microarray containing over 2000 hydrogels had been previously developed by Zhang et al. incorporating monomers with thermo-responsive properties (Zhang et al. 2008). It was hypothesised that the

hydrogels identified in this work could be applied to MSCs to identify substrates that can maintain the MSC phenotype *and* remove the need for enzymatic treatment at passage. This aim of this chapter was to focus on removal of the additional component of enzymatic/chemical passaging to eliminating yet another component of MSC culture while maintaining the growth and phenotype of the MSCs.

4.2 RESULTS AND DISCUSSION

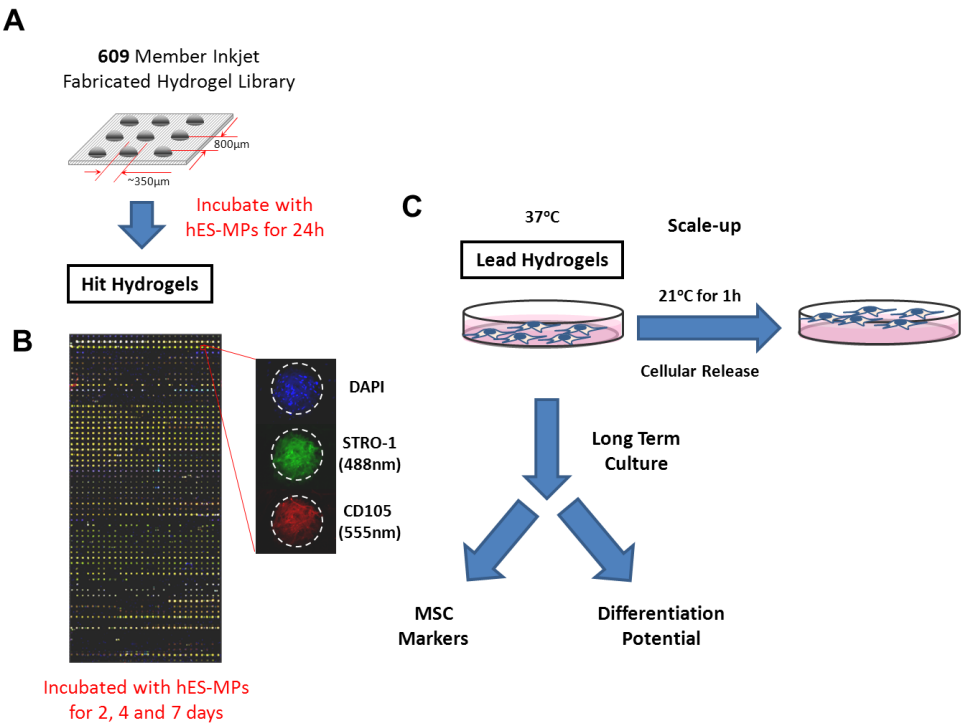

Figure 4.1*.Overview of the polymer microarray system for the identification of thermo-modulatable hydrogels. A) An inkjet synthesised 609-member hydrogel library (each hydrogel in quadruplicate) was fabricated. hES-MPs were incubated on the arrays for 24 hours to assess binding. The top binding hydrogel 'hits' were identified. B) A second 'hit array' was inkjet synthesised and incubated with HES-MPs cells for 2, 4 and 7 days and assessed for growth and the two MSC markers CD105 and STRO-1. C) The top 30 hits identified in step 2 were scaled-up and coated onto coverslips and incubated for 7 days with hES-MPs and assessed for growth with the markers CD105, STRO-1 and CD271. The top 10 leads were further assessed for their thermo-modulatable abilities. The top candidates were examined for long-term cell growth and maintenance of phenotype using marker expression and differentiation capacity.*

A 609-member hydrogel microarray was applied to MSC cell culture. Iterative screens and scale-up experiments identified a family of thermo-modulatable hydrogels for long-term culture of MSCs (Fig. 4.1). hES-MPs were incubated with a 609 member inkjet synthesised hydrogel array with each hydrogel in situ synthesised in quadruplicate (20nL per hydrogel spot). Hydrogels that showed good cell binding and good morphology were selected for a new 'hit array'. The best candidates from the 'hit' array were tested for their ability to trigger cellular release upon temperature reduction. The best candidates in terms of growth and thermo-modulation and phenotype where taken forward as lead candidates for long-term passage and characterisation.

4.2.1 Screening – Hit hydrogel identification

609 hydrogels were initially assessed for cell binding by looking at the number of cells attached to each feature (determined using nuclear stain DAPI) and morphology of cells that bound after 24 hours incubation (Fig. 4.2). This was achieved by imaging each of the features on the array with a Nikon Eclipse 50i microscope using the IMSTAR software and the obtained images were analysed with the software PathFinder. This hydrogel library was printed onto 2 microscope slides and the screen was repeated 3 times with hES-MPs. This high-throughput system allowed each individual feature to be imaged and subsequently analysed in up to 4 separate channels allowing multiple MSC markers to be quantified in terms of fluorescence intensity. On polymer features identified as 'hits', the cells were ideally spread with a fibroblast-like morphology as opposed to being 'clumped' or having proportions of cells with very bright (DAPI) small nuclei indicating apoptosis.

This initial screen identified 88 hydrogels as 'hits' (Fig. 4.2), which were synthesised by inkjet printing onto glass slides to fabricate a 'hit array' for further evaluation. In the 'hit array' the number of replicate features was increased from 4 to 9. Figure 4.2 shows the printing pattern of the 'hit' array with the ratio of each monomer. The structure of the monomers and the cross linker used to construct the hydrogel library is shown in Table 4.1.

M1	M2	Criteria	Cell No	Cell No	Cell No	Cell No	Cell No	Cell No	Cell No
			1:7	1:3	3:5	1:1	5:3	3:1	7:1
DMOBAA	NIPA	CMD	9	1	2	5	5	3	5
DEAA		CMD	6	9	14	18	14	17	12
DMAEMA		CMD	3	3	3	3	3	4	8
AEtMA-Cl		CMD	1	17	2	2	5	8	3
EOA		CMD	11	11	14	6	12	5	5
PEMA		CMD	1	2	1	1	2	1	1
DMAEMA	DMOBAA	CMD	3	11	11	5	8	10	16
EOA		CMD	3	2	3	6	3	5	8
AEtMA-Cl		CMD	2	1	2	5	10	3	4
DMAEMA	NANPPA	CM	1	1	1	6	12	4	5
DEAEA		R	1	1	1	1	1	1	1
AAm		R	1	1	2	1	1	1	1
EOA		R	1	1	1	1	1	1	2
DMAEMA	DEAA	CMD	3	3	3	3	3	4	8
EOA		CMD	4	4	3	3	3	4	3
AEtMA-Cl		CMD	6	4	3	5	7	4	3
DEAEA		CMD	1	2	4	1	2	2	4
HEMA		CM	8	2	2	1	1	1	1
CEA		R	2	2	1	1	1	1	1
CEAO		R	1	1	1	1	1	1	1
DMAA	DMAEMA	CMD	4	3	7	3	3	4	2
DEAEA		CMD	4	5	4	3	5	5	4
AAm		CMD	2	6	4	1	1	1	1
AEtMA-Cl		CMD	4	14	14	4	7	6	3
HBA		CMD	6	10	7	4	5	3	1
HEMA		CMD	4	4	6	3	2	2	2
HPMA		CMD	6	6	4	4	2	1	4
PEG6MA		CMD	3	4	2	2	2	1	3
AAH		CMD	7	7	6	6	5	2	2
CEA		CM	5	6	3	1	1	1	1
CEAO		CMD	5	6	7	2	3	2	1
EOA		R	7	6	3	3	3	2	5
PEMA		R	1	1	1	1	1	1	1
AEtMA-Cl	DEAEA	CMD	5	4	1	4	4	7	6
EOA		CM	6	3	2	2	1	5	4
HPMA		CM	12	7	2	2	1	1	1
PEMA		R	1	1	1	1	1	1	1
EOA	PEMA	CM	1	3	9	1	2	1	5

Monomer Combination	Ratio of Each Monomer		
DMOBAA/NIPA	1/7	1/1	7/1
DEAA/NIPA	1/3	1/1	3/1
DMAEMA/NIPA	1/3	1/1	7/1
AEtMA-Cl/NIPA	1/3	1/1	3/1
EOA/NIPA	1/3	1/1	5/3
PEMA/NIPA		3/5	
DMAEMA/DMOBAA	1/3	5/3	7/1
EOA/DMOBAA	1/3	1/1	3/1
AEtMA-Cl/DMOBAA	1/1	5/3	3/1
DMAEMA/NANPPA	1/1		5/3
DEAEA/NANPPA		1/1	
AAm/NANPPA		3/5	
EOA/NANPPA		3/5	
DMAEMA/DEAA	1/3	1/1	3/1
EOA/DEAA	1/3	1/1	3/1
AEtMA-Cl/DEAA	1/3	1/1	3/1
DEAEA/DEAA	1/3		3/5
HEMA/DEAA		1/7	
CEA/DEAA		3/5	
CEAO/DEAA		3/5	
DMAA/DMAEMA	1/3	1/1	3/1
DEAEA/DMAEMA	1/3	1/1	3/1
AAm/DMAEMA	1/3	1/1	3/1
AEtMA-Cl/DMAEMA	1/3	1/1	3/1
HBA/DMAEMA	1/3	1/1	3/1
HEMA/DMAEMA	1/3	1/1	3/1
HPMA/DMAEMA	1/3	1/1	3/1
PEG6MA/DMAEMA	1/3	1/1	3/1
AAH/DMAEMA	1/3	1/1	3/1
CEA/DMAEMA	1/3	1/3	3/5
CEAO/DMAEMA	1/3	3/5	1/1
EOA/DMAEMA		1/3	
PEMA/DMAEMA		1/3	
AEtMA-Cl/DEAEA	3/5	1/1	3/1
EOA/DEAEA	1/7		3/1
HPMA/DEAEA	1/7		3/1
PEMA/DEAEA		3/1	
EOA/PEMA		3/5	

88 'HIT' HYDROGEL CANDIDATES

Figure 4.2. *The results of the primary screen assessing cell binding. The table (left) is an example of one of the three screens performed (form monomer abbreviations see table 3.1). Red boxes indicate selected hydrogels used to construct the 'hit array' (right) containing replicates of the 88 'hit hydrogels'. For the selection of candidates, a number of criteria were considered, i.e. cell count (C), morphology (M) and also chemical composition of the hydrogel (D). Candidates with good cell morphology and good binding were selected for further evaluation (C, M). Candidates with high cell numbers but poor morphology were not selected. For hydrogels, which showed good morphology and binding in all monomer ratios, selected candidates were taken forward (D).*

Table 4.1*.Monomers used in the inkjet microarray fabrication. 15% of methylene bisacrylamide (MBA) was used as a cross-linker.*

Monomer A	Structure	Monomer B	Structure	Monomer B	Structure
NIPAA	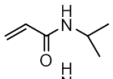	DMAA		HPMA	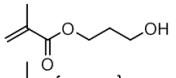
DMOBAA	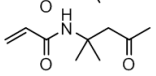	Aam		PEG6MA	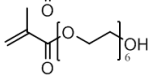
NANPPA	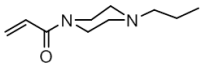	EOA	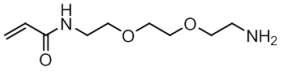	AAH	
DEAA	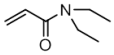	AEtMA-Cl	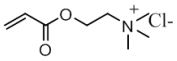	CEA	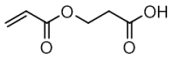
DMAEMA	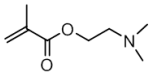	HEMA	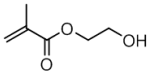	CEAO	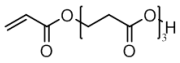
DEAEA	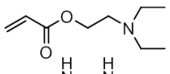	HBA	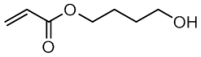	PEMA	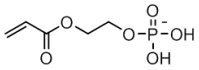
MBA	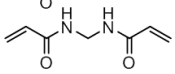				

For a hydrogel to act as an effective substrate it must not only bind cells but also promote cell growth while maintaining the cellular phenotype. The 'hit arrays' (n = 3) were incubated with hES-MPs, and subsequently fixed and assessed at day 2, 4 and 7 for cell number (Fig. 4.3A), and immunostained for two well established markers of MSC phenotype, STRO-1 and CD105 (Fig. 4.3B). As the hydrogel features vary in size, a simple cell count per spot would be inaccurate. In order to compensate for variations in the feature size, the area of each feature was measured and used to quantify the cells/mm^2. Fig. 4.3A shows the top 10 hydrogels from the second screen. For all hydrogels, the cell count on day 7 was higher than day 2, clearly showing the top candidates promoted growth as well as binding. The immune staining of hES-MPs on the hydrogel feature (Fig. 4.3B) shows that some hydrogels maintained the expression of CD105 and STRO-1. Comparison of the distribution of monomers used to construct the polymer library (Fig. 4.4 top) and the monomer representation of the top 30 candidates (Fig. 4.4 bottom) shows some monomers were clearly favoured, in particular AEtMA-Cl.

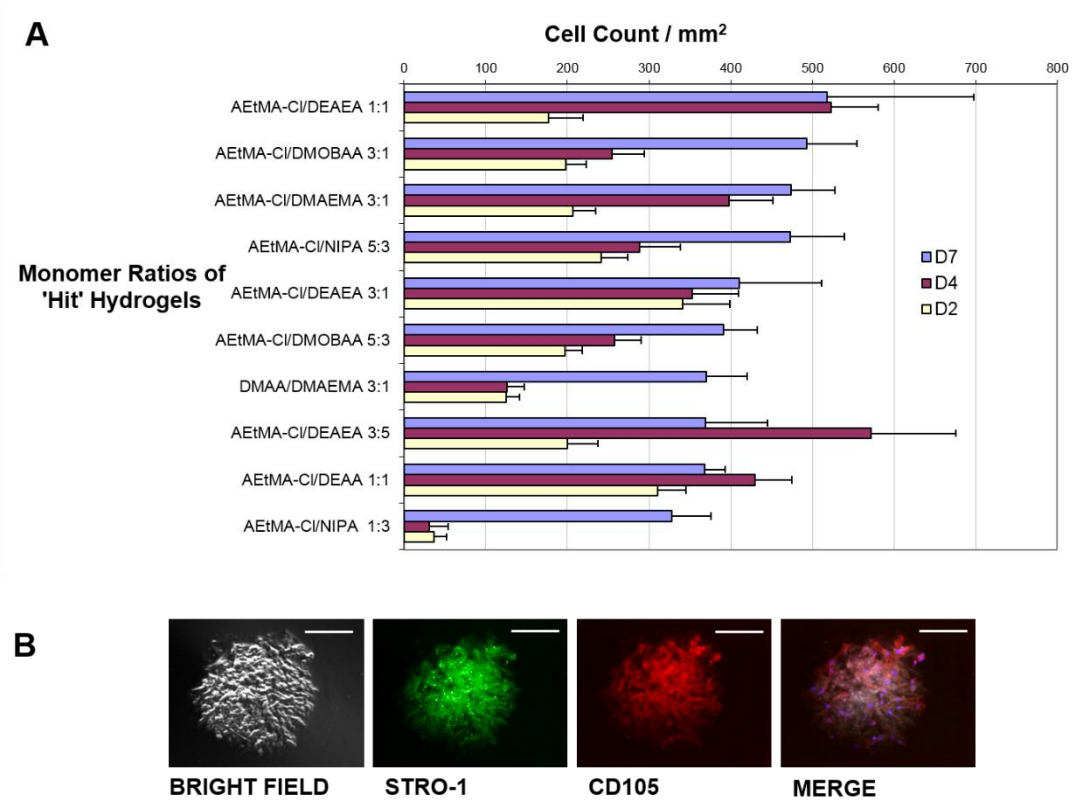

Figure 4.3 *A) Analysis of the top 10 candidates from the 'hit array' after for 2, 4 and 7 day incubation. The vertical axis indicates the monomer combinations and ratio used to formulate the hydrogel with (15% MBA as the cross-linker). The data are ordered according to the day 7 results. Analysis shows a general trend of cell growth between days 2 and day 7 indicating that the substrates support binding and growth of hES-MPs. Error bars represent the standard deviation from four separate slides. Scale bar 100μM B) An example of the output from the IMSTAR imaging system showing clear STRO-1 and CD105 staining. The DAPI stained nuclei can be seen in the merged image.*

Examination of the structure of AEtMA-Cl (Table 4.1) indicates that a quaternary amine group might be favoured for cell binding and growth on these hydrogels. This amine containing monomer is positively charged, similar to coatings used to promote cell binding. Cell binding on plasma treated polystyrene (tissue culture plastic) is thought to be the result of increasing the density of carboxyl groups on the surface (Ramsey et al. 1984). However, the large amounts of serum in the media means that direct structure–attachment relationships can be difficult to interpret as the surfaces and the cell membranes can use the serum components as intermediaries in this process.

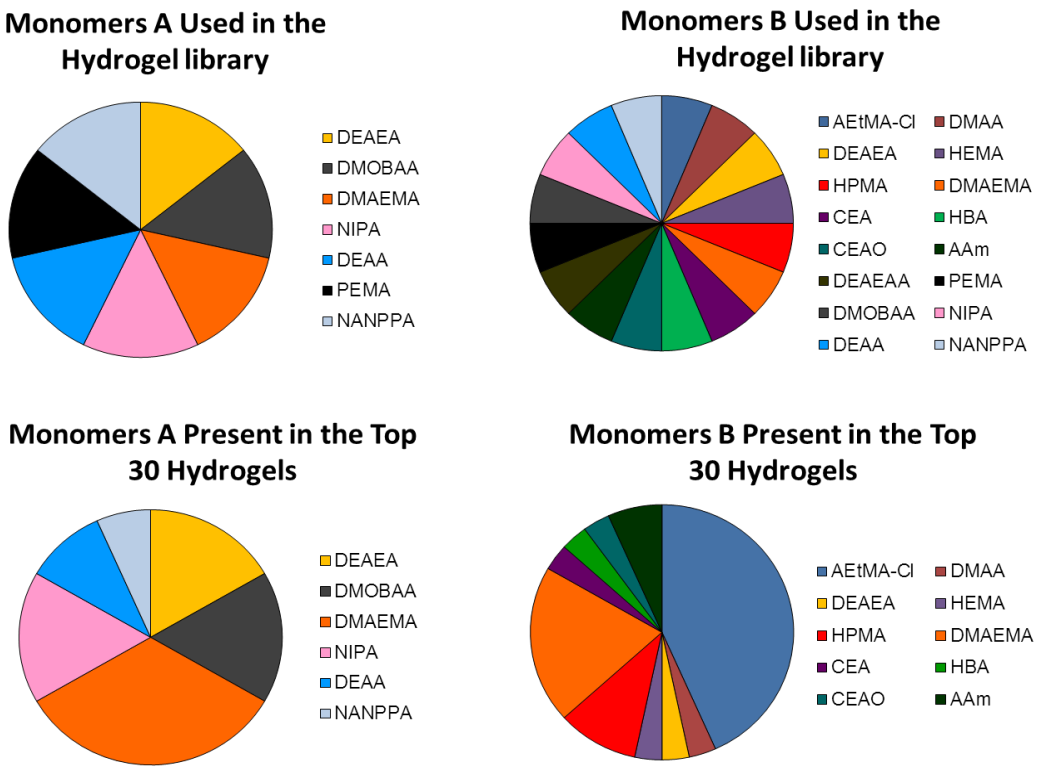

Figure 4.4*.Top, Representation of the different monomers A and B used in combination to construct the hydrogel library. Lower, monomers A and B occurring in top 30 hydrogels based on cell count after 7 day incubation with hES-MPs. The pie chart shows that some monomers are clearly favoured (e.g. DMAEMA and AEtMA-Cl).*

4.2.2 Screening – Lead optimisation

The top 30 hydrogels identified in the focused screen were re-assessed with hES-MPs after 7 days for growth (cell number) and then for their ability to trigger cellular release following temperature reduction (Fig. 4.1C, Table 4.2).

Cells were grown on hydrogel coated coverslips (10 mm diameter), fixed and immune-stained after 7 days for the expression of CD105, STRO-1 and CD271. The lead hydrogels all facilitated binding and promoted growth with the markers STRO-1 and CD105 observed in cells after 7 days of culture (Fig. 4.5B).

***Table 4.2**. The top 30 candidates identified from the screens. The top 10 hydrogels in terms of growth and thermo-detachment after re-assessment are shown in red with their corresponding monomers and monomer ratios. The cross linker ratio is 15%.*

Monomer 1	Monomer 2	Monomer Ratio	Hydrogel
AEtMA-Cl	DEAEA	8:8	
AEtMA-Cl	NIPAA	10:6	
AEtMA-Cl	DMAEMA	12:4	
AEtMA-Cl	DMOBAA	12:4	
AEtMA-Cl	DMOBAA	10:6	HGL3
AEtMA-Cl	DEAA	8:8	HGL1
AEtMA-Cl	DMOBAA	10:6	
DMAA	DMAEMA	12:4	
AEtMA-C	DEAEA	6:10	
HEMA	DMAEMA	12:4	
AEtMA-Cl	DEAA	12:4	HGL4
AEtMA-Cl	NIPAA	12:4	
HPMA	DMAEMA	12:4	
AEtMA-Cl	NIPAA	4:12	
DEAEA	DMAEMA	12:4	
DMAEMA	DMOBAA	10:6	HGL2
HPMA	DEAEA	4:12	HGL5
DMAEMA	DMOBAA	14:2	HGL9
AEtMA-Cl	DMAEMA	8:8	
AEtMA-Cl	DMOBAA	8:8	
DMAEMA	NIPAA	8:8	
DMAEMA	NANPPA	10:6	
CEA	DMAEMA	6:10	
HBA	DMAEMA	12:4	HGL8
DMAEMA	NANPPA	8:8	
DMAEMA	NIPAA	14:2	HGL7
HEMA	DEAEA	2:14	
HEMA	DMAEMA	8:8	
AAm	DMAEMA	8:8	HGL10
DMAEMA	DMOBAA	4:12	HGL6

The hydrogel candidates triggered cellular release after being subjected to room temperature (21 °C) for 1 hour (red diamonds) with the exception of hydrogel **HGL4**. Based on the cell count, high levels of thermo-detachment at 21 °C, and MSC marker intensities (Fig. 4.5A), hydrogel **HGL1** was taken forward for long-term culture and characterisation. Interestingly, analysis of the marker intensities of STRO-1, CD105 and CD271 for the top 30 candidates showed that one of the hydrogels **HGL6** had significantly higher intensities of STRO-1, CD105 and CD271 compared to the gelatin control (Fig. 4.5B). This suggested that this substrate could

potentially promote the MSC stem cell phenotype over other less potent cells in the mixed MSC population (MSCs are composed of a heterogeneous population of cells with varying degrees of potency (Pevsner-Fischer et al. 2011)). A substrate that could promote the 'true' MSC phenotype over other cell types would result in more clinically relevant homogeneous MSC population. **HGL6** also showed good thermo-detachment and reasonable cell growth (Fig. 4.5A). **HGL6** was therefore also chosen for long-term passage and characterisation. The structures of **HGL1** poly(AEtMA-Cl-co-DEAA) and **HGL6** poly(DMAEMA-co-DMOBAA) are shown in Fig. 4.5C.

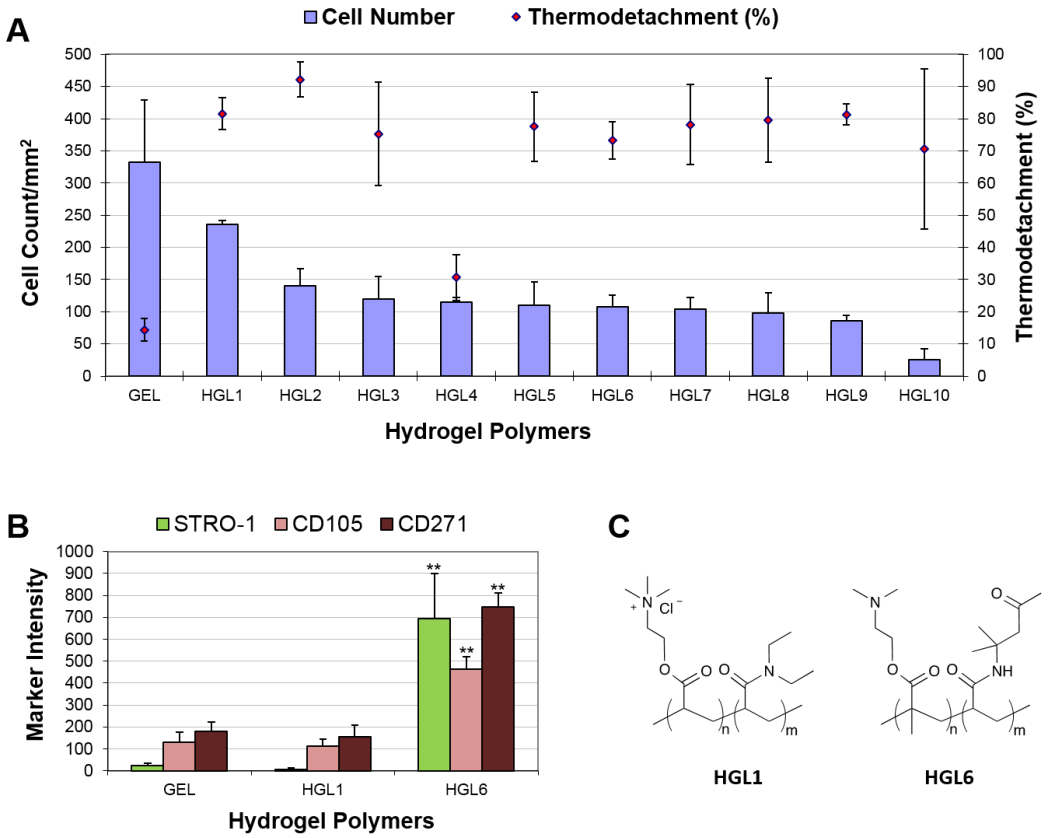

Figure 4.5. *Thermo-detachment of the top hydrogel candidates identified from the 'hit array' and marker intensity and structures of the lead candidates. A) Comparison of the thermo-detachment of the top 10 candidates compared to the gelatin control. The blue columns represent the total cell counts after 7 days at 21 °C incubation on hydrogel coated coverslips. Red diamonds represent the % thermo-detachment after 1h (n = 3, error bars given as SD). B) Normalised fluorescence intensity of the top candidates compared to controls for the MSC markers STRO-1, CD105 and CD271 (n = 3, error bars given as SEM). C) Structure of* ***HGL1*** *and* ***HGL6****.*

Note the amine groups present in **HGL1** and **HGL6** as they were present in the lead candidates **PA388** and **PU157** discussed in chapter 3.

Prior to initiation of long-term culture and characterisation, the conditions for thermo-detachment passaging were optimised. Fig. 4.6A shows the results of four different test conditions. Applying the passaging protocol immediately after removal from the incubator showed no significant difference to controls. A 30 minute exposure to 12 °C resulted in a significant difference ($p<*$) from the gelatin control. A 30 minute at exposure at 21 °C resulted in an additional improvement ($p<**$). 60 minutes at 21 °C proved optimal, with a significant difference between **HGL1** and the gelatin control ($p<***$). Fig. 4.6B shows cells on **HGL1** before and after thermo-detachment under the optimal conditions. Treatment of cells at 21 °C for 60 minutes was chosen as the passaging method for long-term characterisation of **HGL1** and **HGL6**.

To further assess the thermo-detachment properties, the proportions of each monomer in **HGL1** were varied, and the effects on thermo-detachment evaluated. Having lower amounts of the monomer DEAA present in the hydrogel polymer resulted in a significant reduction in the percentage of cell that thermo-detached during the 21°C, 1h treatment regime (Fig. 4.6B). The lower critical solution temperature (LCST) of DEAA homopolymer is 32 °C. Temperatures below the LCST results in a rapid transition from the solid gel phase into a liquid solution phase.

4.2.3 Long-term culture and characterisation of hES-MPs and ADMSCs on HGL1 and HGL6

hES-MPs were grown in DMEM containing 10%FCS for 5 passages on **HGL1** and **HGL6**, utilising the thermo-detachment regime, and characterised at p5 by flow cytometry, and compared to cells grown on gelatin and tissue culture plastic. After 5 passages of growth using the thermo-detachment method, the cells were stained for STRO-1, CD73, CD105, CD90 and CD34, CD14 and HLA-DR. These markers were chosen as the minimal criteria in defining the MSC phenotype as the MSC marker

phenotype varies considerably according to the source of the tissue from which they are derived (Nery et al. 2013).

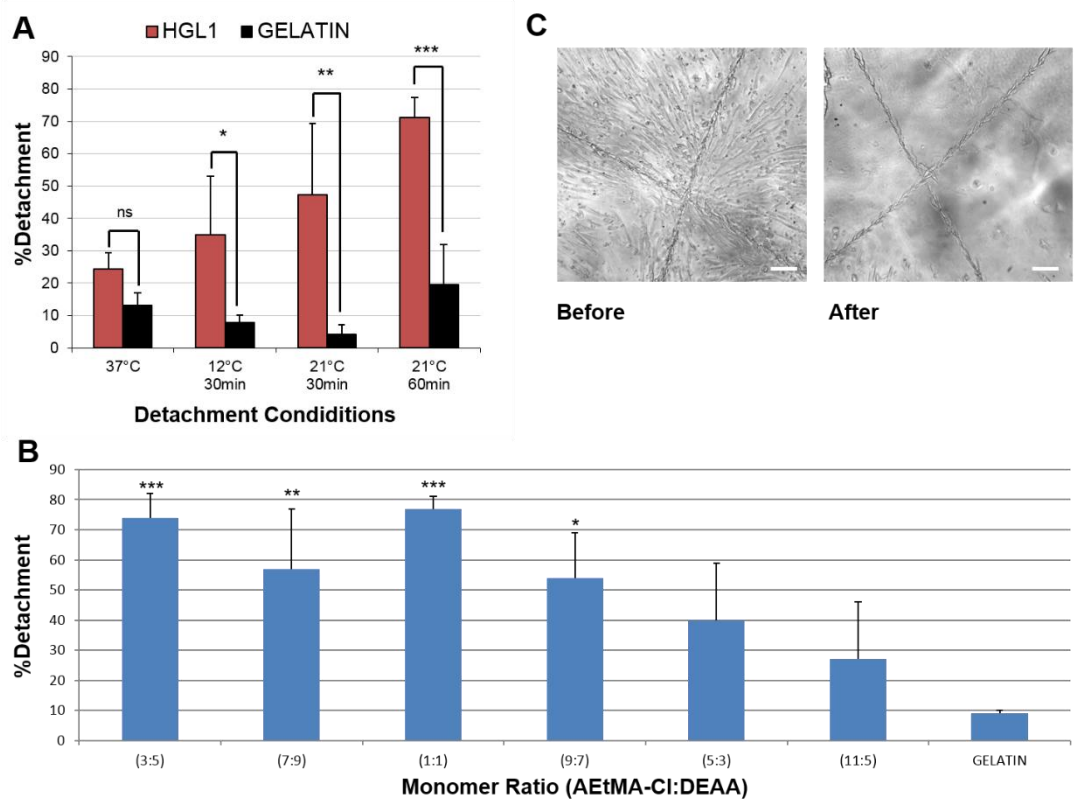

Figure 4.6.*Optimisation of thermo-detachment conditions and the effect of alteration of the monomer ratios on the thermo-detachment. A) Percentage of thermo-detached cells at different temperatures and times. n=3, Error bars denote SD. Scale bar 100µM B) Effect of alteration of the monomers composing* ***HGL1,*** *(****HGL1*** *has a 1:1 ratio). Significance denotes comparison with the gelatin control C)* ***HGL1*** *with cells before and after thermo-detachment. (n=3).*

Comparison with the gelatin control (p0) showed a small reduction in STRO-1 positive cells after 5 passages. Interestingly, one of the key markers used to define MSCs, CD105, showed a dramatic reduction both on gelatin and **HGL6**, and was completely lost when the cells were grown on tissue culture plastic (Fig. 3.7A and B). Remarkably, **HGL1** maintained this marker at original levels. Thus, passaging cells on **HGL1** using thermo-detachment confers advantages over other synthetic substrates, such as tissue culture plastic, as well as gelatin with this MSC defining

marker. This may also implicate trypsin passaging in the loss of this marker. The absence of enzymatic or chemical passaging methods could therefore potentially play a role in maintaining the multipotency of these cells. CD105 (also known as endoglin) forms part of the TGFβ receptor complex and is a Type I homo-dimeric transmembrane glycoprotein. CD105 has been shown to be absent in freshly isolated MSCs but is quickly up-regulated, which is associated with increased proliferation after isolation (Braun et al. 2013).

A

hES-MPs p11	GEL				HGL1		HGL6		TCP	
	p0	STDEV	p5	STDEV	p5	STDEV	p5	SDEV	p5	STDEV
STRO-1	95.9	2.8	**64.3**	8.2	**81.7**	8.0	**77.6**	12.5	**63.3**	23.9
CD105	70.5	22.4	**12.7**	1.2	**76.7**	28.7	**19.7**	2.5	**2.6**	4.2
CD73	99.8	0.1	**90.7**	4.7	**85.0**	11.5	**96.7**	3.2	**98.7**	0.8
CD90	73.6	1.1	**73.6**	1.7	**56.9**	4.2	**27.8**	3.9	**62.8**	9.2
CD34	15.1	0.4	**16.5**	5.3	**29.6**	1.7	**1.6**	0.1	**9.7**	4.5
CD14	13.3	2.3	**1.2**	0.6	**20.2**	7.9	**1.4**	0.2	**10.4**	6.0

B

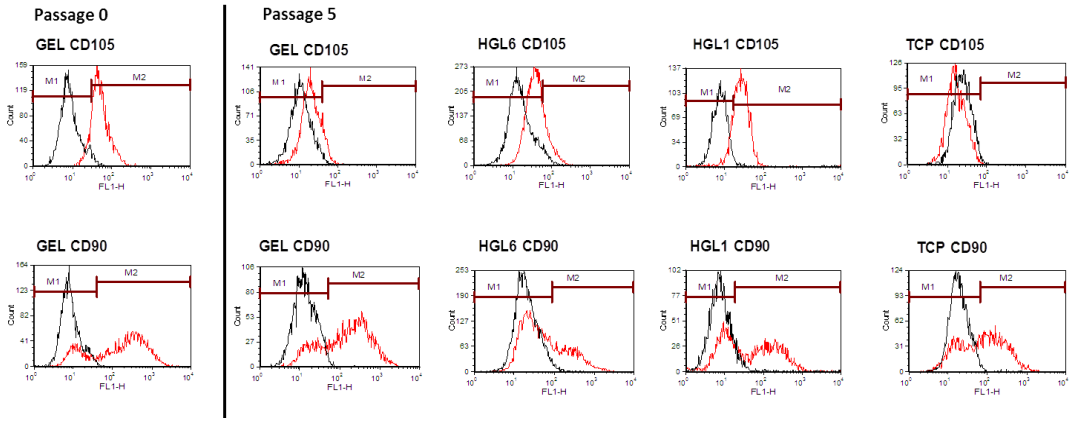

Figure 4.7*.Flow cytometry analysis of 6 MSC markers after 5 passages using the thermo-detachment protocol with hES-MPs. A) Table showing the percentage of positive cells for each of the markers before passaging (p0) on the four substrates; gelatin (GEL),* ***HGL1****,* ***HGL6*** *and tissue culture plastic (TCP) and after 5 passages. Values constitute mean +/- standard deviation of n=3 treatment groups. B) Histograms of two markers, CD105 and CD90 prior to passaging (p0) and after passaging (p5) on the four substrates. M1 represents the negative staining gate and M2 represents the positive staining gate. The black histogram signifies unstained cells and the red histogram signifies stained cells.*

Another critical marker CD90 (also known as Thy-1), had a bimodal distribution in hES-MPs (Fig. 4.8) (Karlsson et al. 2009; Li et al. 2013), remained unchanged on gelatin over 5 passages, whereas the negative fraction was enhanced on **HGL6** (Fig.

4.7A and B). This cell surface protein, with an immunoglobulin domain, is a minimal marker for MSCs (Dominici et al. 2006), however, it is weakly expressed in hES-MPs when compared to ADMSCs (Fig. 4.8).

It has also been reported that decreased intensity of CD90 is associated with the loss of the immune-modulatory properties of MSCs (Campioni et al. 2009). The comparatively low expression of this marker in hES-MPs in general, compared to adult derived MSCs, may explain the fact why hES-MPs do not possess the property of immune modulation associated with adult derived MSCs (Li et al. 2013).

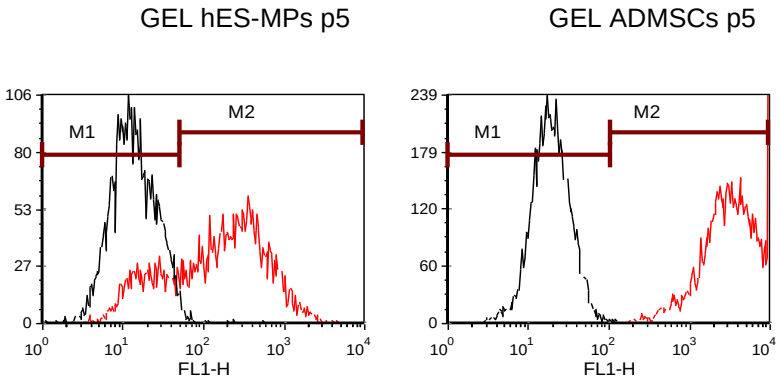

Figure 4.8. Flow cytometry traces for marker *CD90 with hES-MPs and ADMSCs grown on gelatin control (GEL) for 5 passages.*

To test the ability of these substrates to maintain adult MSCs and demonstrate their clinical potential, ADMSCs were cultured on the **HGL1** and **HGL6** for 10 passages, with differentiation potential assessed at passage 5 (Fig. 4.10) and MSC markers assessed by flow cytometry at p5 and p10 (Fig. 4.9). With ADMSCs the overall marker expression for cells grown on gelatin and **HGL1** were comparable, although **HGL6** showed a complete loss of STRO-1 at p5 (Fig. 4.9A) with other markers being maintained. However, cells grown on **HGL6** could not be effectively expanded beyond this point, although this cannot be linked directly with the loss of STRO-1 this marker has been associated with proliferation (Walsh et al. 2000). These cells were generally positive for CD34 and negative for CD146, however, recent studies have shown that cells derived from the stromal vascular fraction contain multiple

populations, one of which are $CD34^+$ and $CD146^-$ (known as adventitial cells) have the characteristic MSC phenotype (Corselli et al. 2013). These ADMSCs display the MSC phenotype and differentiation analysis showed them to be multipotent (Fig. 4.10).

A

ADMSCs	GEL						HGL1				HGL6		TCP			
p5	p0	STDEV	p5	STDEV	p10	STDEV	p5	STDEV	p10	STDEV	p5	SDEV	p5	STDEV	p10	STDEV
STRO-1	20.8	4.8	28.7	3.3	23.6	8.7	51.9	15.5	34.4	10.2	3.4	1.5	39.2	5.3	46.6	7.8
CD105	99.0	0.3	84.1	2.7	48.6	3.2	63.4	4.6	38.0	4.4	75.5	14.2	52.1	11.1	46.3	17.4
CD73	99.8	0.2	99.7	0.1	98.4	0.6	97.2	1.0	98.2	0.7	96.2	1.7	93.7	10.6	98.5	0.2
HLA-DR	55.6	5.7	1.9	0.6	0.7	0.6	17.3	2.4	3.8	3.4	37.7	6.8	47.3	4.3	61.7	1.7
CD90	98.8	0.4	95.4	1.5	79.9	1.0	93.9	1.0	93.2	2.8	87.7	5.6	94.4	4.6	92.0	2.1
CD34	72.5	1.7	82.2	2.2	52.3	21.9	54.5	6.9	38.1	9.3	62.6	6.2	78.4	5.3	60.0	17.4
CD14	3.5	2.1	1.0	0.0	3.8	2.8	3.8	0.9	0.8	0.4	3.0	0.8	4.8	0.8	7.7	1.9

B

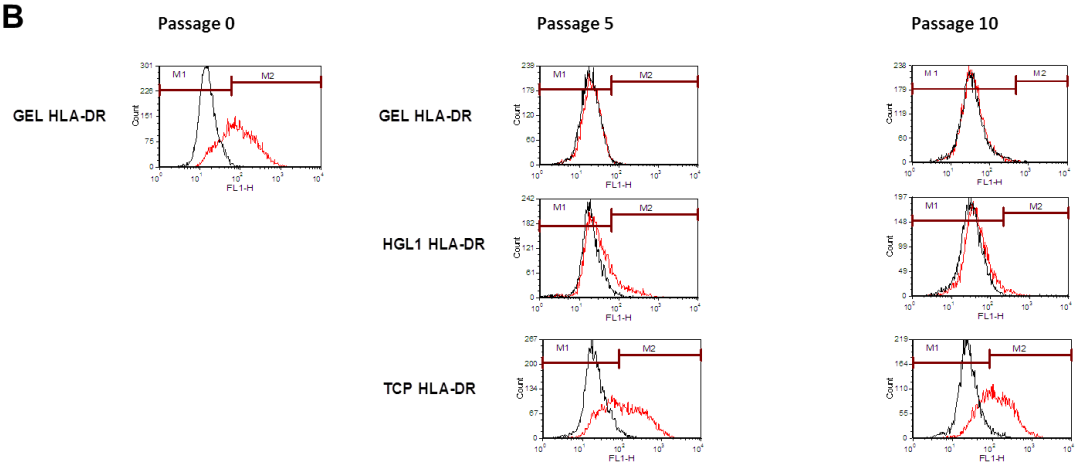

Figure 4.9.*Flow cytometry data for MSC markers on ADMSCs grown on gelatin (GEL), **HGL1**, **HGL6** and tissue culture plastic (TCP) for 5 and 10 passages. A) Table showing the percentage positive cells for the MSC markers before multiple passing (p0) and after cells were grown on GEL, **HGL1**, **HGL6** and TCP for p5 and p10. Values constitute mean +/- standard deviation of n=3 treatment groups. B) Flow traces for the HLA-DR marker at p0, p5 and p10 for GEL, **HGL1** and TCP. M1 (black) shows the trace for unstained ADMSCs and M2 (red) shows the trace for cells stained for this marker*

The immune-privileged state of MSCs is associated with the low expression of Human Leucocyte Antigen-DR (HLA-DR) (Chan et al. 2008). Interestingly, HLA-DR was down regulated on cells grown on gelatin and **HGL1** at p5 but not **HGL6** or tissue culture plastic (Fig. 4.9B). If applied in therapy, cells expressing HLA-DR would be recognised by the immune system as foreign, when donors are HLA mismatched. Currently, MSCs are not recognised by the immune systems of non-

matched patients (Imanishi et al. 2008). Therefore, the dramatic down regulation of this marker on cells grown on both gelatin and **HGL1**, reinforces the ability of **HGL1** to act as a synthetic alternative to gelatin. By contrast the inability of tissue culture plastic to down regulate this marker reinforces it as an inappropriate substrate for maintenance of this cell type. The absence of STRO-1, the continued expression of HLA-DR at p5, and the substantial loss of the MSC defining marker CD90, also suggests that **HGL6** is not an ideal substrate for long-term MSC culture (Fig. 4.9B). The flow cytometry analysis shows a loss of CD105 with the hES-MPs grown on tissue culture plastic (Fig. 4.7) and also shows very consistent correlation between the positive control, gelatin, and **HGL1** for both hES-MPs and ADMSCs (Fig. 4.7 and Fig. 4.9). In terms of marker expression, **HGL1** is superior to gelatin.

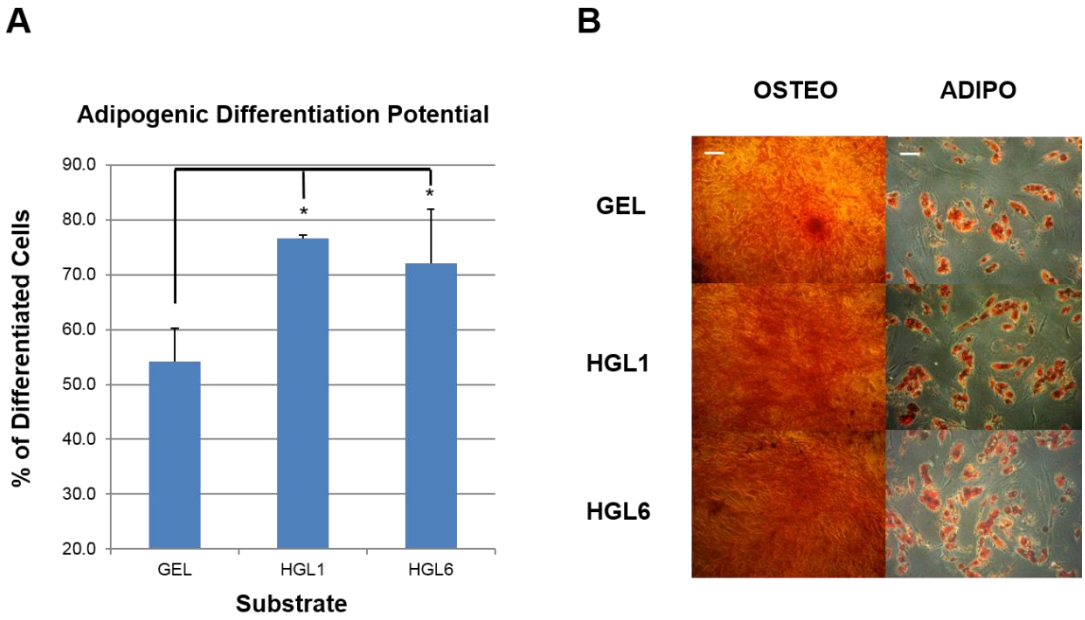

Figure 4.10*.Osteocyte and adipocyte differentiation of ADMSCs maintained for 5 passages on **HGL1** and **HGL6** using thermo-detachment passaging compared with the gelatin control passaged using enzymatic (trypsin) passaging. Scale bar 100µM A) Percentage of cells that differentiated into adipocytes on the 3 substrates (n = 3, 12 images/replicate). B) Alizarin red and Oil red O staining of cells differentiated for 28 days in osteogenic and adipogenic induction media, respectively.*

Differentiation analysis of ADMSC after 5 passages on **HGL1**, **HGL6** and gelatin down the adipo and osteo lineages is shown in Fig. 4.10. Fig. 4.10B shows clear oil red O staining of the fat droplets and alizarin red staining of the calcium deposits, demonstrating that they have retained lineage potency characteristic of these cells. Fig. 4.10A shows the proportion of cells that differentiated and clearly indicates that cells passaged on both hydrogels showed a significantly higher proportion of cells capable of differentiating down this lineage than when passaged on the control substrate gelatin. It is not possible from this data to determine whether the difference in differentiation potential is as a result of the non-enzymatic passaging methodology or is a consequence of the hydrogel substrate.

4.3 CONCLUSIONS

Using a microarray platform, defined synthetic hydrogels have been rapidly identified that allow for enzyme free passaging of ADMSCs while maintaining their potency and phenotype. One hydrogel substrate, poly(AEtMA-Cl-co-DEAA) cross-linked with 15% MBA, allowed long-term culture of hES-MPs and ADMSCs. This new substrate provides a significant improvement over current methods of long-term passaging for MSCs, improving their potential for future clinical applications. The ability of hydrogel **HGL1** to maintain and allow gentle passaging without destruction of extracellular matrix in the absence of chemical or enzymatic treatment makes it an attractive alternative to animal derived gelatin. In addition, the **HGL1** substrate and the thermo-detachment regime maintains critical MSC markers, in some cases better than gelatin, suggesting a potential role for the isolation of these cells in the complete absence of a biological substrate and enzymatic/chemical passaging.

CHAPTER 5

Knowledge-based small molecule screen to identify growth factor replacements in MSC culture

5.1 INTRODUCTION

The identification of the critical components within growth media that allows the long-term culture of stem cells has been pivotal in attempts to progress such cells clinical application. However, the critical growth factors necessary in defined media, such as TGF-β, bFGF, insulin, PDGR-ββ, are typically from recombinant bacterial origin and are hugely expensive. Similarly, the key components required to differentiate cells down their desired lineages (*e.g.* TGF-β3, Insulin and BMP-4) or activating cells into an immune-modulatory state (*e.g.* IFN-γ and TNF-α) are of recombinant origin. This imposes burdens on generating clinically relevant cell numbers for biomedical/tissue engineering applications due to the enormous expense of such growth factors, variability and their origins. An attractive alternative is to replace these vital growth factor components with robust, readily obtainable, synthetic small molecules.

5.1.1 Substitution of growth factors in stem cell reprogramming with small molecules

Screening of small molecules has been successfully applied to allow the replacement of some or all of the biological factors used to reprogram differentiated cells into induced pluripotent stem cells (iPS) (see section 1.1.4.) (Takahashi et al. 2007). Initially, screens of large numbers of small molecules identified two small molecules, CHIR99021 (CHIR) and PD0325901 (structures in Fig. 5.1), which could replace cMyc and Sox 2 in the reprogramming process (Silva et al. 2008). Interestingly, this study revealed a pre-pluripotent state that morphologically resembled pluripotent stem cells and resulted in the loss of somatic markers. However, Nanog was undetectable and this state failed to inactivate the X chromosome or form chimeras.

This study hypothesised that stem cells would be more amenable to reprogramming due to less stringent epigenetic restrictions than somatic cells. Neural stem cells (NSCs) where retrovirally transfected with the four factors, Oct4, Sox2, Klf4 and cMyc. Within 3 days cells took on the pre-pluripotent state, subsequently cells were cultured in media containing mitogen activated protein kinase signalling (Mek/Erk) and glycogen synthase kinase-3 (GSK3) inhibitors (PD0325901 and CHIR respectively) and leukaemia inhibitory factor (LIF). This resulted in the rapid conversion into the true pluripotent or 'ground state'. It was subsequently found that Sox2 and cMyc were dispensable, however, Sox2 is normally expressed in NSCs and the removal of cMyc reduced the efficiencies of iPS formation to levels similar to MEF reprogramming. This did however reveal the importance of Mek/Erk and GSK3 in the maintenance of the pluripotent state.

Other screening studies have identified small molecule combinations that included previously identified factors CHIR, valproic acid (VPA), and 616452, in combination with a random library to identify the small molecule tranylcypromine (tranyl) that allowed, in combination with the other factors, only Oct4 for reprogramming (Fig. 5.1). These small molecule screens used improvement in reprogramming efficiency of MEFs transfected with Oct4/Sox2/Klf4 as the readout for the compound identification (Li Y et al. 2011). It is now possible to reprogram fibroblasts into iPS in the absence of genetic manipulation using a combination of 7 small molecules (CHIR, VPA, 616452, tranyl, forskolin, 3-deazaneplanocin A and Arotinoid acid) (Hou et al. 2013) (Fig. 5.1). These studies demonstrated that substitution of protein factors is achievable even in processes that previously required multiple protein factors.

5.1.2 Substitution of factors in stem cell culture with small molecules

Maintaining the stem cell state using small molecules in the absence of growth factors was first achieved with mESCs. Using expression of Oct4 as a readout, a high-throughput small molecule screen was performed which identified the small molecule SC1 that could maintain mESCs in the absence of serum and LIF (Chen et

al. 2006). This was achieved though the inhibition of two differentiation inducing proteins, Ras GTPase-activating protein (RasGAP) and mitogen activate protein kinase 3 (MAPK3). Importantly, the identification of such small molecules helped reveal part of the underlying network involved in the signalling that maintains the pluripotent state. In hESCs culture, it was found that the two of the compounds used to replace cMyc and Sox2 during cell reprogramming, CHIR (glycogen synthase kinase-3 inhibitor (GSK3)) and PD0325901 (a MEK inhibitor) in combination with the ROCK inhibitor (Y27632) and bFGF, were able to maintain hESCs on a fibronectin substrate for 20 passages (Tsutsui et al. 2011) (Fig. 5.1). However, the culture conditions were not defined.

In a study designed to identify compounds that showed promoted Oct4 expression in H9 hESCs, Genzalez et al. used a defined serum free system that lacked the bFGF and TGF-β growth factors to screen 50,000 compounds. Here, hESCs were plated onto 384-well plates on an undefined matrigel surface, and compounds were added. High content microscopy identified 11 candidates, one of which dorsomorphin (Fig. 5.1), an inhibitor of bone morphogenic protein type I (BMP1) receptors and showed the highest levels of Oct4 staining in a dose dependent manner. Dorsomorphin was able to maintain hESCs for 5 passages in this minimal media formulation. Pluripotency was verified by differentiating EB into mesoderm, endoderm and ectoderm. Teratoma studies also confirmed the formation of all three germ layers (Fig.1.1). Dorsomorphin was found to inhibit the up-regulation of BMP2 and BMP4 mRNA, which spontaneously occurs in the absence of bFGF (Gonzalez et al. 2011). To date, no defined single formulation using only small molecules in the absence of growth factors for long-term culture (>5 passages) of stem cells has been published, however, a combination of the work by Tsutsui and Gonzales would seem a promising strategy.

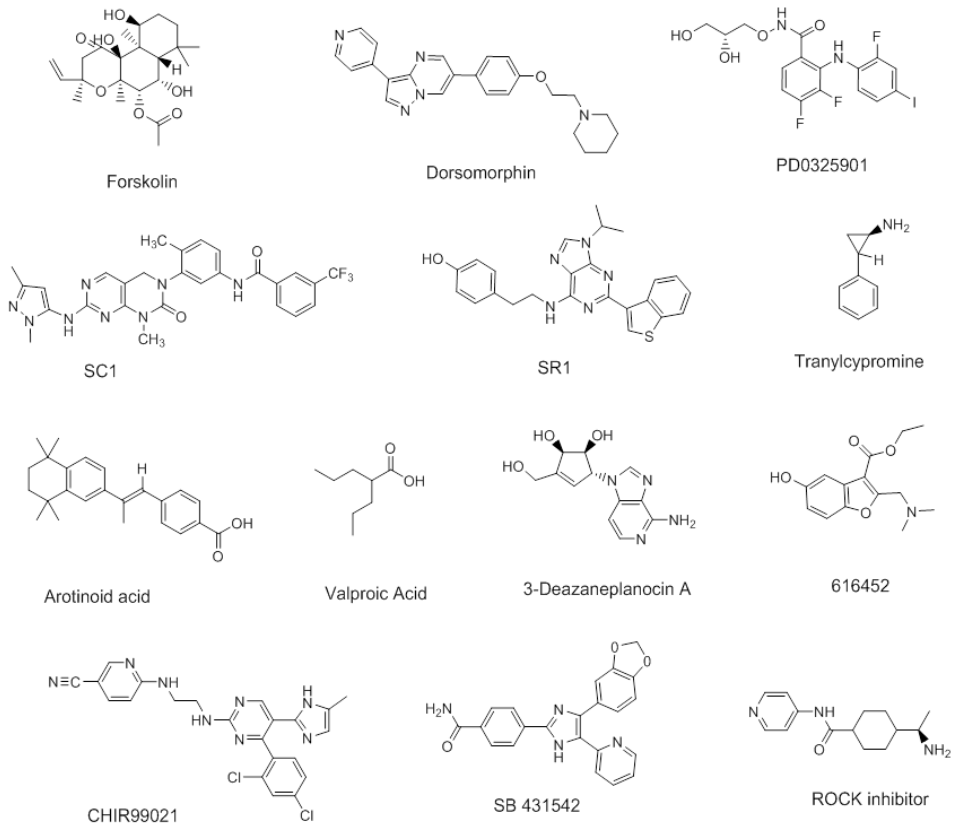

***Figure 5.1**. Structures of small molecules that can substitute for protein factors, differentiate or enhance stem cell phenotype. SC1, CHIR99021, PDO325901, valproic acid, 616452, artinoid acid, tranylcypromine, 3-deazaneplanocin A and forskolin enhance or directly reprogram diffentiated cells into induced pluripotent stem cells (iPS). Dorsomorphin acts as a small molecule substitute for bFGF, SR1 enhances the HSC phenotype in vitro and ROCK inhibitor promotes clonal growth and can be used with other factors to maintain stem cell growth.*

5.1.3 Small molecule mediated enhancement/differentiation of stem cells

Haematopoietic stem cells (HSCs) have been the most widely used cells in stem cell therapy. One of the major limitations of the application of these cells has been the rapid loss of phenotype during *in vitro* culture, signified by the loss of CD34 and CD166. A small molecule screen of 100,000 heterocyclic compounds identified a small molecule, Stem Regenin 1 (SR1) (Fig. 5.1) that resulted in a rapidly expandable cell population of HSCs with a 50-fold increase in CD34 expression and

a 17-fold improvement in engraftment when treated HSCs were transplanted into SCID mice when compared to untreated cells (Boitano et al. 2010). SR1 acted by the inhibition of the aryl hydrocarbon receptor (AhR), which acts as a quiescence regulator of haematopoiesis requiring down regulation for HSCs to escape from quiescence (Singh et al. 2009). Therefore, SR1 provides an escape route allowing considerable expansion and engraftment of the HSC population. AhR has also been implicated in other stem cell populations such as skin stem cells (SSCs) and NSCs (Panteleyev & Bickers 2006; Singh et al. 2009). This clearly demonstrated that a small molecule could enhance the stem cell phenotype and create a homogenous stem cell population from a heterogeneous starting population.

Small molecules have also been applied to the derivation, maintenance and differentiation of multipotent stem cells. NSCs can be derived from ESCs in a two-step process using low serum conditions with LIF, followed by treatment with bFGF (Tropepe et al. 2001). This results in cells with the NSC phenotype and differentiation potential. A novel approach using LIF and a combination of small molecules CHIR, SB431542 (SB) (Fig. 5.1) (a TGF-β and activin receptor inhibitor) and a γ-secretase inhibitor (presenilin) was also able to produce cells with the NSC phenotype. In addition, this method resulted in a rapid and homogenous NSC population that could be maintained thereafter with LIF, CHIR and SB (Li et al. 2011b).

In MSC culture, small molecules have been used as differentiation factors for osteogenic differentiation (ascorbic acid, β-glycerophosphate, and dexamethasone) or adipogenic differentiation (dexamethasone, isobutyl methyl xanthine, and indomethacin) in combination with FCS (Jaiswal et al. 1997; Augello et al. 2010). Small molecules have also been identified that can differentiate MSCs into hepatocytes (Ouyang et al. 2012) and cardiomyocytes (Song et al. 2011).

5.1.4. Chapter aims

The power of small molecules to control and manipulate cells is enormous as they can substitute for protein factors and maintain or alter cell potency. In addition, they

can differentiate cells into progenitor stem cell types or terminally differentiated cells. Small molecule modulators also enable pathway analysis allowing the role of that pathway to be better understood, thus revealing of the role of important pathways.

Many of the pathways that control the stem cell state of hESCs and hMSCs are the same (e.g. Insulin signalling, TGF-β and bFGF). Although work has been done to identify small molecules that differentiate MSCs, little has been done in terms of finding small molecules that can maintain the MSC state in the absence of serum and growth factors, or enhance their phenotype.

In this chapter, a 'knowledge-based' small molecule screen was performed on MSCs to identify small molecules that could:

1) Enhance growth and substitute for the protein growth factors in culture media.

2) Enhance phenotype with the aim of producing a more stable homogenous stem cell population.

3) Act as differentiation factors.

5.2 RESULTS AND DISCUSSION

5.2.1 Screening strategy for the identification of small molecules

Rather than performing a 'blind screen' some of the key pathways/proteins associated with hESCs and the MSC phenotype were identified (Table 5.1, Appendix 3) and using pathway analysis software (GeneGo), drug molecules that acted as agonists or antagonists of these pathways were identified and scrutinised.

To focus the screen, and to aid future regulatory approval, only small molecules that had FDA/EU regulatory approval were considered. Other factors, such as their ability to affect multiple pathways, and solubility, were also considered in the compound selection. In all, 200 compounds were identified for the MSC screens (Fig. 5.2, Appendix 4.1). The screening strategy and overall results are shown in figure 5.3 and 5.4. The knowledge-based small molecule library was tested using hES-MPs at 3 concentrations (1 µM, 10 µM and 100 µM) in 384-well plates (n = 4). After 7 day treatment, the cells were fixed and stained for the MSC marker STRO-1 (this was extended to STRO-1 and CD105 in the validation screen and STRO-1, CD105 and CD271 in the third screen).

***Table 5.1**. MSC markers and the main pathways associated with the MSC phenotype*

MSC Stemness Marker	Pathway
Protein tyrosine receptor type F	PDGF-ββ
Endolase 2	Bfgf
RAB3B	TGF-β
THY-1	Integrin
Frizzled 7	IGF-1
Dickkopf 3	GPCR
Biglycan	IL-1 receptor type II
Decorin	IL-6
Thrombospondin	Insulin Receptor signalling
Steroid sensitive gene 1	Pyrimidine metabolism
CD73	NFKB
Inhibin B	Wnt/B-catenin

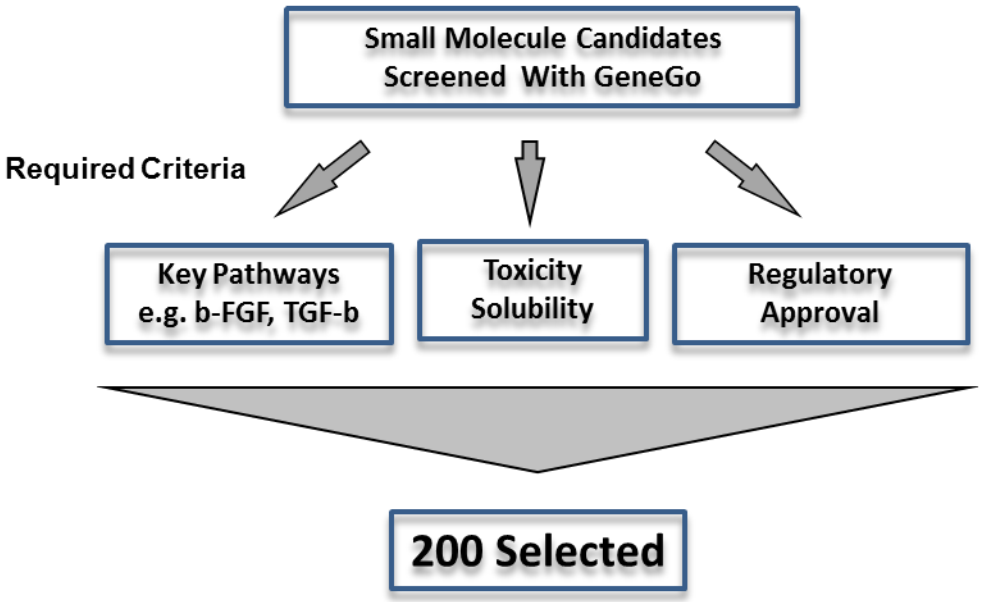

***Figure 5.2**. Selection criteria of the small molecules used in the first hES-MP screen.*

Plates were scanned with the Opera high-throughput high-content imaging system (Perkin Elmer) and analysed using the ACAPELLA analysis software. This provided 9 images per well and nuclear counts, and measured fluorescence from each image. A number of criteria were used to a potential candidates, 1) statistically significant growth or STRO-1 expression (evaluated by a fluorescent antibody) above the vehicle controls, 2) images from each well were visually examined for changes in cell morphology, to potentially identify small molecules that promote differentiation or alter potency. These criteria identified 73 potential candidates for the validation stage of screening (Fig. 5.3). Cell growth was analysed to validate candidates identified in the first screen. This also acted as a validation of the screening process itself.

The candidates identified in this 'primary' screened were validated in a second round of screening which analysed the additional marker CD105. This round of screening identified 22 candidates to take forward for a third screen. This screen was performed at 6 concentrations (as opposed to 3) and the additional phenotypic marker CD271 was analysed. This identified candidates that could significantly

enhance some of the phenotypic markers of MSCs. Literature research was performed on the function of these candidates and further validation was performed with flow cytometry (Fig. 5.4).

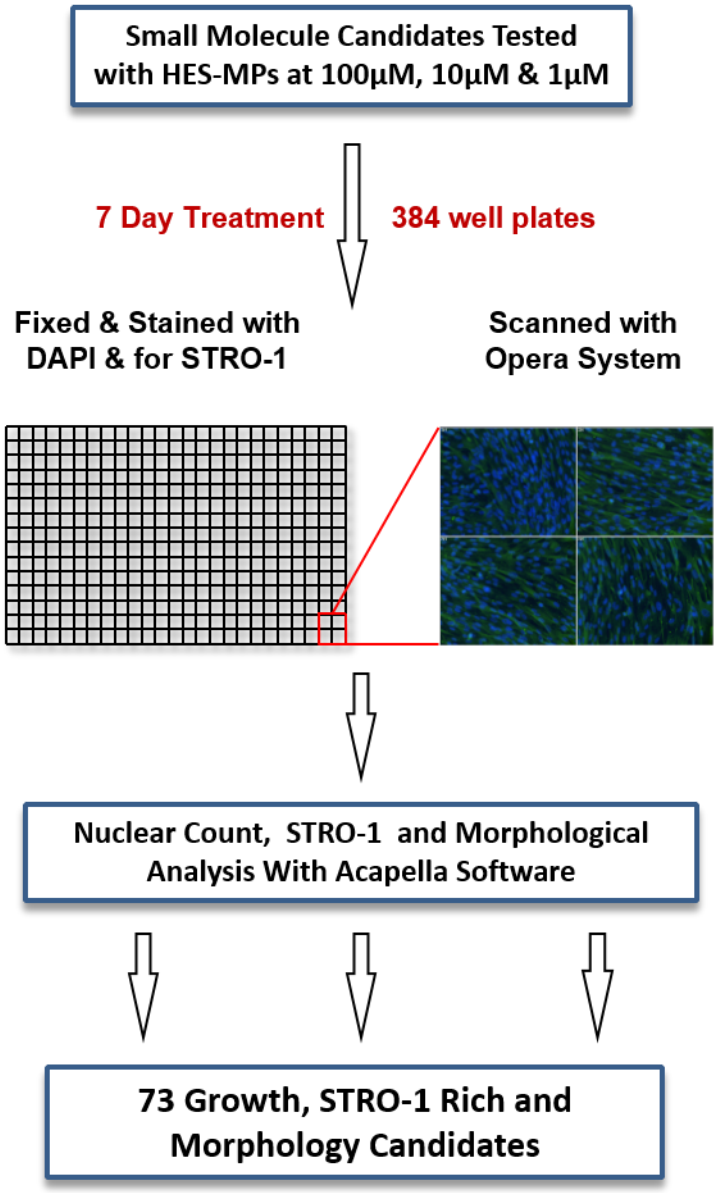

***Figure 5.3**. Overview of the knowledge-based screening strategy to identify candidates that can substitute for growth factors, enhance phenotypic marker expression or induce differentiation. First screen showing incubation of hES-MPs in 384-well plates treated for 7 days with small molecules at 1µM, 10µM and 100µM concentrations in the serum containing media. Scanning with the Opera high throughput microscope and analysis with ACAPELLA software identified 73 initial candidates.*

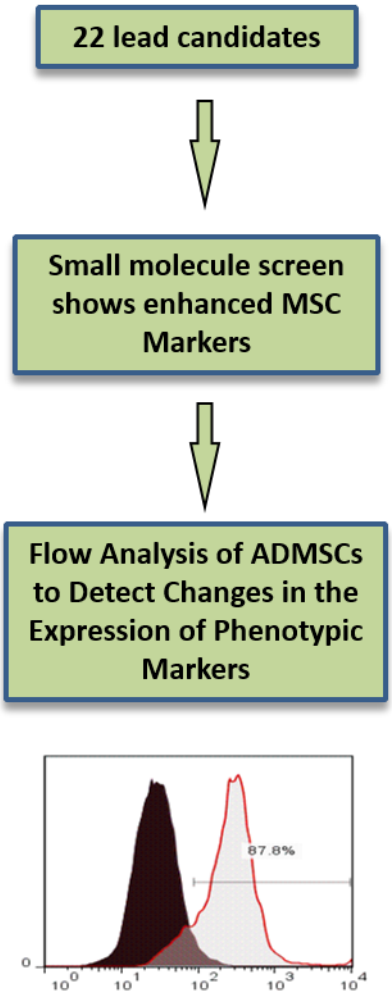

***Figure 5.4**. The 73 identified candidates were to identify 22 lead candidates. These were subsequently rescreened at 6 concentrations in defined and undefined media and 5 candidates where selected. Candidates were further scrutinise with flow cytometry and 2 candidates that could potentially alter MSC phenotype were identified.*

Small molecules that significantly enhanced STRO-1 and/or CD105 were selected for further analysis. A screen was performed in serum free and serum containing media to identify if any of the small molecules candidates were acting in a serum dependent or serum independent manner to significantly enhance STRO-1 and/or CD105 and/or CD271. Finally, the phenotype enhancing candidates were examined using flow cytometry to verify and analyse the phenotypic effect in greater detail.

5.2.2 Identification of small molecules that support cell growth

5.2.2.1 Optimisation of cell density for high-throughput screening

200 small molecules were prepared in 1 mM stock solutions (in DMSO) prior to screening. Prior to the screen, cell density optimisation was performed to determine the appropriate cell density (Fig. 5.5) for which 6 small molecules were chosen. hES-MPs were seeded on 96-well plate at various densities (n = 3) and incubated for 24 hours in hES-MP media, after which cells were washed twice with PBS and media containing the small molecules (100 µM) was added. Treating the cells with the highest concentration of drugs allowed a more accurate assessment of cell density for the subsequent screen. The two controls were untreated cells with no drugs in DMEM containing 10% FCS (supplemented with 4ng/ml bFGF) and vehicle controls containing the same media but also containing the same concentration of solvent used for dissolving the drugs at 100µM (0.1% DMSO).

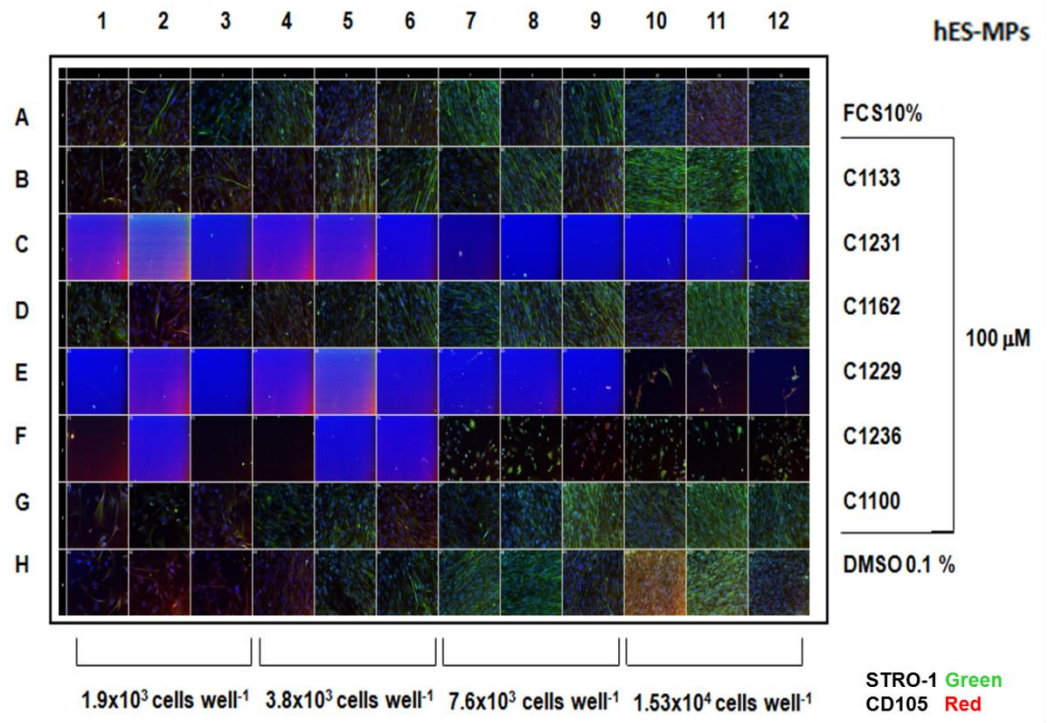

***Figure 5.5**. Plate montage of a 96-well plate stained with DAPI, STRO-1 and CD105. Four cell densities were examined for six small molecules (100 µM, n = 3). A vehicle control (0.1%, DMSO bottom row) and an untreated control (10 % FCS) were included. Areas of blue represent cytotoxic concentrations resulting in 'blank' wells.*

hES-MPs were cultured with the small molecules for 7 days with media changes every 2 days with media containing the small molecule. A cell counting script was performed on the plate, which showed that 3.8×10^3 cells per well was the optimum seeding density. At this density, cells had not reached confluence as with the higher concentrations, and the lower seeding density produced very little cell growth (Fig. 5.5).

5.2.2.2 Screening

The first screen was performed with 200 small molecules (Fig. 5.2). After 7 days incubation with hES-MP media containing 3 concentrations of the small molecules (1 µM, 10 µM and 100 µM), cells were fixed with 4% formaldehyde, stained with DAPI, immunostained with STRO-1 and the plates scanned using a high-throughput microscope. For each well of the 384-well plate, square 9 quadrants were selected as a chosen sampling area to apply to each well. Images of the areas were taken in the DAPI ($\lambda_{Ex}/\lambda_{Em}$ 340/488 nm) and FITC ($\lambda_{Ex}/\lambda_{Em}$ 495/519 nm) channels (Fig. 5.6).

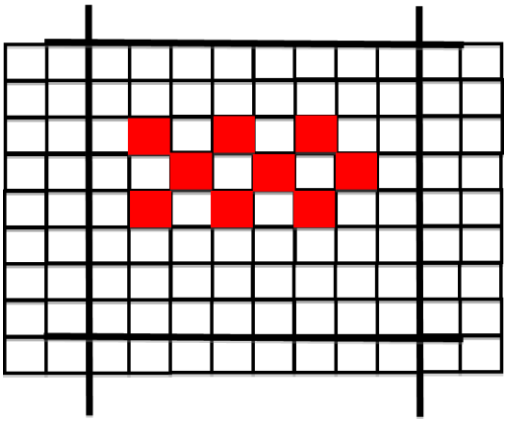

Figure 5.6*. Area of a single well of a 384-well plate. 9 areas were selected and scanned. Each quadrant was imaged in each channel to obtained nuclear counts and quantification of fluorescence (up to a maximum of 4 channels).*

Each image was processed using ACAPELLA using prewritten scripts that were optimised by varying the parameters for cell counts and fluorescence detection. Each small molecule concentration was represented by 4 quadruplicate wells. Images were

analysed and the raw output was processed. Statistical analyses with Instate was used to identify candidates that were statistically significant compared to untreated controls using the Dunnett's test.

5.2.2.3 Identification of small molecule candidates that could enhance hES-MP growth

The results of the first small molecule screen at 1 µM are shown in figure 5.7. At this concentration only one small molecule, curcumin (black bars), showed significant growth above the DMSO controls and in the subsequent validation screen (i.e. candidates that were identified as significant in the first screen were rescreened).

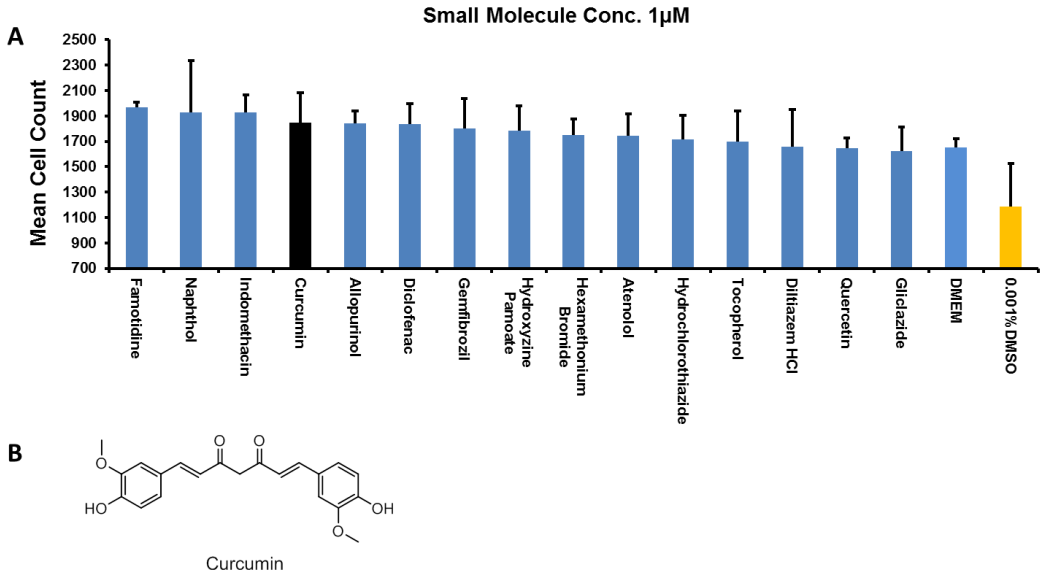

***Figure 5.7**. Results of the small molecule screens (1µM) showing candidates that had a significant effect on hES-MP growth (blue bars) above the vehicle control (yellow bars) and the one validated candidate from a second screen (black bar) (n = 4, error bars given as SD). A) 15 candidates with a significant effect on hES-MP growth from the initial screen of 200 small molecules. B) Structure of curcumin.*

Curcumin has been shown to promote osteogenisis and inhibit adipogenisis in MSCs through the up-regulation of heme oxygenase (HO)-1 expression (Cremers et al. 2014), which is the rate-limiting enzyme in the degradation of heme to biliverdin,

carbon monoxide and free iron. Curcumin has been widely studied regarding its anti-inflammatory properties (Aggarwal et al. 2010), but not specifically as a promoter of growth in MSCs.

At 10 µM (Fig. 5.8), three candidates, epinephrine, hydroquinone and *L*-noradrenaline, showed significantly higher cell growth than vehicle controls (in the second validation screen) although curcumin was not identified. A study of rat MSCs, showed that both epinephrine and noradrenaline (norepinephrine) increased proliferation in MSCs in a dose dependent manner with 10 µM showing a significant increase over controls (Kido et al. 2012). Epinephrine and noradrenaline activate the β2-adrenergic receptor (β2AR) signalling, which has been shown to mediate osteogenisis via the cyclic AMP/PKA pathway (Kellenberger et al. 1998; Huang et al. 2009).

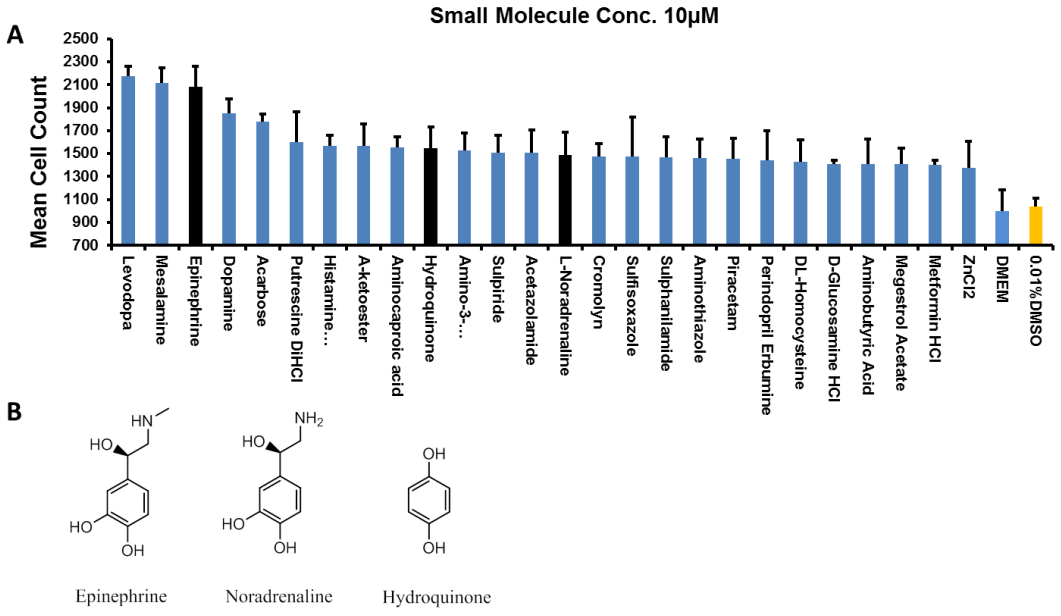

***Figure 5.8**. Results of the small molecule at 10 µM, showing candidates with significantly higher growth than vehicle controls. A) 26 significant candidates (blue bars) from the first screen compared to the vehicle control (yellow bar) of which 3 were validated in a second screen (black bars) (n = 4, error bars given as SD). B) Structures of epinephrine, hydroquinone and L-noradrenaline.*

At the highest concentration (100µM), 8 candidates were growth enhancers in both screens (Fig. 5.9). Adenine, D-glucosamine-HCL, synephrine, pyridine-2,5-dicarboxylic acid, choline chloride, mesalamine, Caffeine and DL-Homocysteine. D-glucosamine-HCl has been shown to promote chondrogenesis in chondrocytes and

MSCs by promoting the extracellular matrix proteins collagen II and aggrecan and by down regulate the matrix enzyme metalloproteinase 13 (Derfoul et al. 2007). Mesalamine is used in the treatment of chronic ulcerative colitis. In these patients, mesalamine has been shown to inhibit Wnt/β-catenin signalling through reduced PI3K/Akt-mediated β-catenin activation, in addition to down regulation of the downstream elements of signalling such as cMyc, GPR49 and MMP7 (Brown et al. 2010). Other studies have shown increased PPARγ activity in response to mesalamine treatment (Rousseaux et al. 2005). Increased PPARγ expression reduces β-catenin by cytosolic retention (Fujisawa et al. 2008) and proteasomal targeting (Liu et al. 2006). By contrast to the findings of this screen with MSCs, in epithelial cells β-catenin signal inhibition has been proposed to prevent endothelial stem cell activation and proliferation.

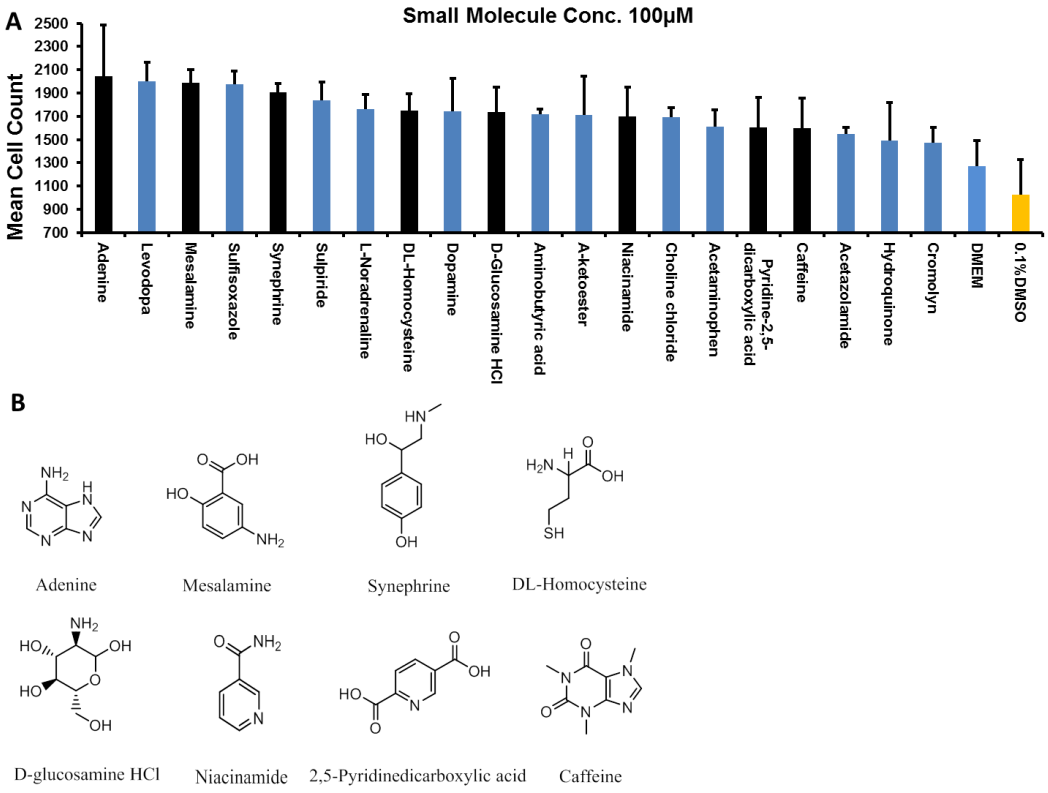

Figure 5.9*.100 μM screen showing candidates with significantly higher growth than vehicle controls. A) 20 significant candidates (blue bars) from the first screen compared to the vehicle control (yellow bar).Black bars represent validated candidates from the second screen (n = 4, error bars given as SD) B) Structures of Adenine, mesalamine, caffeine, DL-homocysteine, niacinamide, synephrine and D-glucosamine.*

5.2.2.4 Validation of screening assay

Examination of small molecules that could promote growth and their validation suggest that the platform is robust. In particular, the validation of two candidates epinephrine and L-noradrenalin corresponded to other published work (Kido et al. 2012). However, the 1µM, 10µM and 100µM screens did not contain overlapping molecules. Perhaps the screening conditions where too favourable for growth to begin with (10% FCS supplemented with 4ng/ml bFGF), optimisation of the screening procedure in low serum conditions may have more readily identified candidates that substantially increased growth above basal conditions thereby identifying candidates capable of substituting for growth factors. The lack of overlap at the different concentrations would suggest that the significance observed at each concentration was a consequence of the size of the screen itself (200) which will inevitably produce statistical significance by chance. The lack of overlap could also be a result of the concentration gap being too wide with a 10 fold difference between each concentration, a narrower range could therefore potentially reveal a dose response.

5.2.3. Identification of small molecules that enhance MSC phenotype

Small molecules that enhanced stem cell phenotype, in particular compounds that enhanced MSC marker expression were re-screened (along with the growth candidates). In the initial screen images taken of each well for all small molecule concentrations were individually examined and assessed for STRO-1 expression and morphological differences. Candidates that resulted in changes of cell morphology and had enhanced STRO-1 expression were selected for the second screen (Appendix 4.2, Table 4.2.1–3). In the second screen, the marker CD105 (antibody $\lambda_{Ex}/\lambda_{Em}$ 555/565 nm) was added to provide an additional layer of scrutiny. Small molecules that significantly enhanced STRO-1 (antibody $\lambda_{Em}/\lambda_{Ex}$ 495/519 nm) expression are shown in figure 5.10.

There was a degree of overlap between candidates from the STRO-1 screen and the CD105 screen. Sulfamilamide and aminobutyric acid significantly enhance both

markers at 1µM. Cumin (c1173), spermine (F436) and niacin significantly enhanced both markers at 10µM. Hermethonium Bromide (c1186), oleic acid (FF168), retinyl acetate (FF169), megestrol acetate (c1222), diltiazem HCL (c1179), pentoxifylline (c1201) and famotidine (c1182) significantly enhance both markers at 100µM.

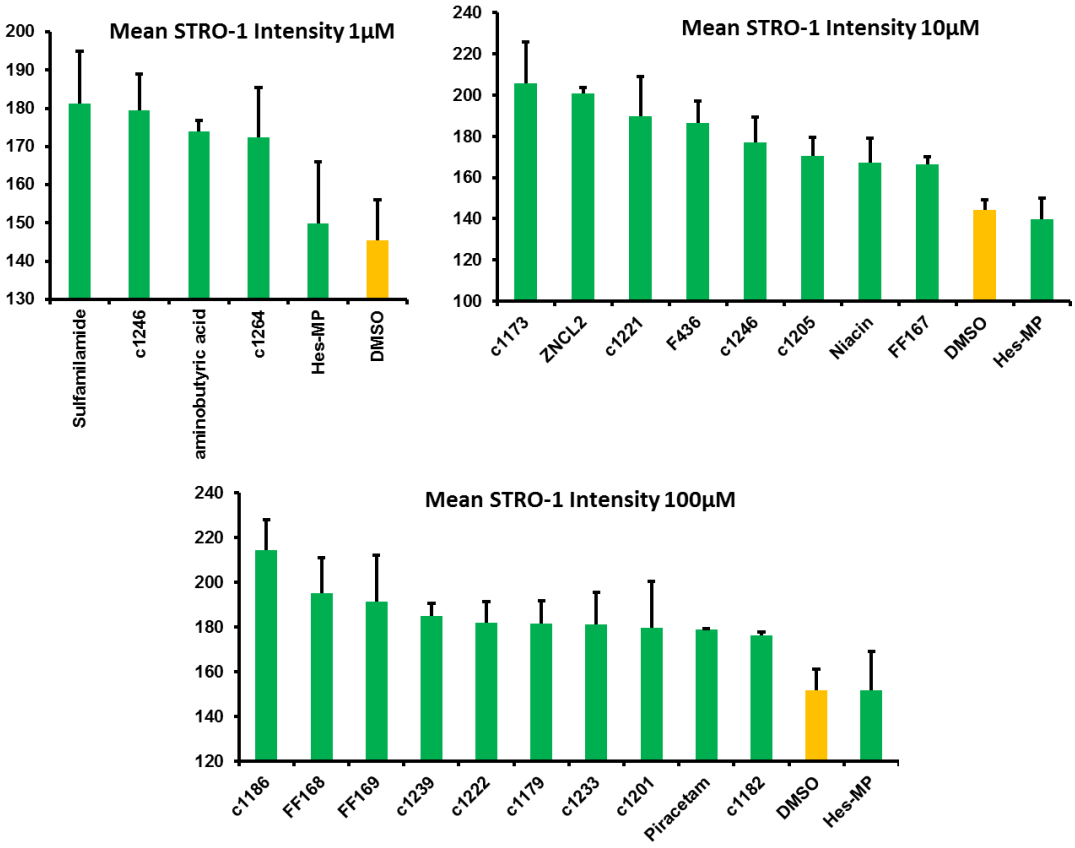

Figure 5.10. *Results of a screen showing small molecule candidates with significantly enhanced STRO-1 expression over vehicle control (DMSO yellow bars) at 1 µM, 10 µM and 100 µ (n = 4, error bars given as SD).*

Interestingly, some small molecules clearly enhanced one marker but not another, for example C1163 (tocopherol) showed the largest enhancement of CD105 at 10 µM concentration (Fig. 5.11) but did not appear to significantly enhance STRO-1. Only one drug appeared to enhance a marker at more than one concentration. Telmisartan (c1246) enhanced STRO-1 at 1µM and 10µM concentrations.

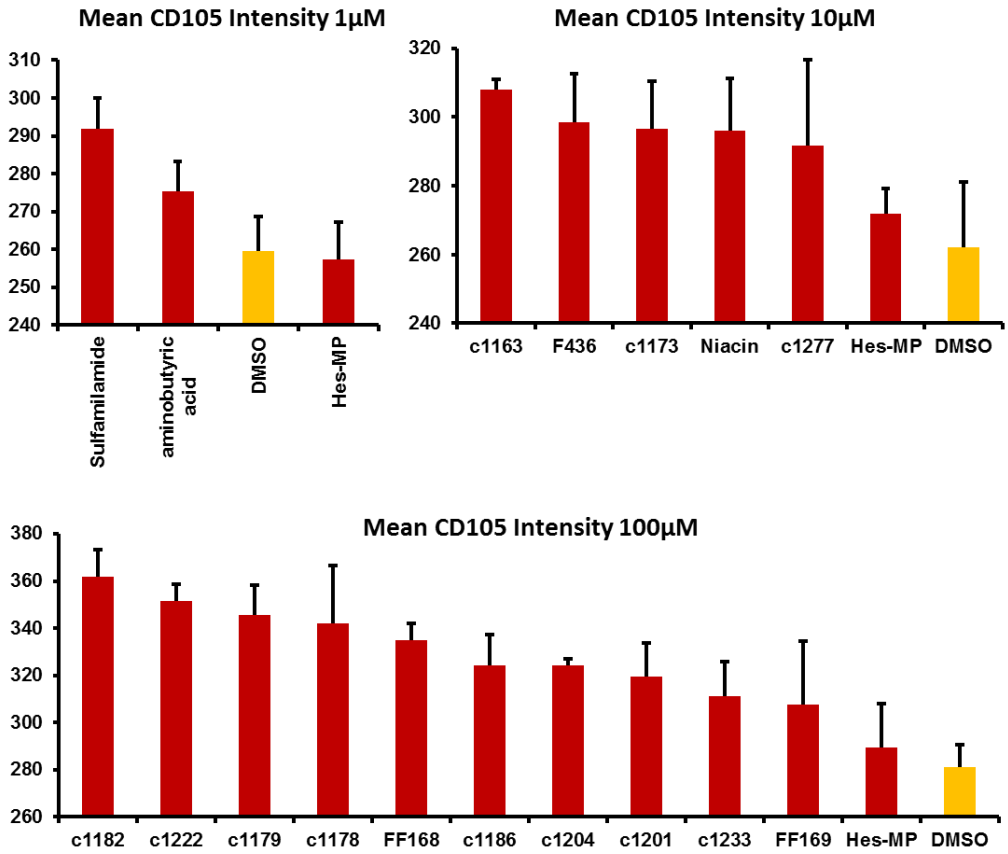

Figure 5.11. *Screen showing small molecules that significantly increased CD105 expression compared with the vehicle control (DMSO, yellow bars) (n = 4, error bars given as SD)*

5.2.3.1 Small molecule STRO-1, CD105 and CD271 enhancers in undefined (10% FCS containing) media

In a new screen, the identified candidates were tested using serum containing media and also using a defined media formulation (see table 2.1 materials and methods). It was reasoned that testing the small molecules in the absence of serum could potentially identify small molecules that were serum independent or were serum restricted in their effect.

In this focused screen, a third MSC marker, CD271 ($\lambda_{Em}/\lambda_{Em}$ 650/668 nm), was also evaluated. In addition, the small molecules were examined at 6 concentrations (0.3–100 µM) to identify if growth or the STRO-1, CD105 and CD271 expression

increased in a dose dependent manner. This would also reduce the 10 fold gaps between the different drug concentrations.

Figure 5.12 shows the effect of the small molecule estriol on hES-MPs marker expression. Clearly, estriol has a significant effect on the three MSC markers examined with the most pronounced effect on the marker STRO-1 at 100µM. Estriol, a ligand of the estrogen receptor alpha (ER-α), is produced at high levels and is part of the modulation of the immune system during pregnancy resulting in a suppression of proteins responsible for inflammation *e.g.* IL-1, IL-2 and IFN-γ (Robinson & Klein 2012). This anti-inflammatory immune suppression has also been demonstrated in mice with experimental autoimmune encephalomyelitis (EAE) (mouse model of multiple sclerosis (MS)), where estriol treatment resulted in amelioration of the EAE in treated mice. In male mice, splenocytes treated with myelin oligodendrocyte glycoprotein-35-55 peptide (which induces EAE) and estriol showed significant reductions in the pro-inflammatory cytokines IFN-γ, TNF-α, interleukin-2 (IL-2), and IL-6 (IL-6), and a significant increase in the anti-inflammatory cytokine IL-5 (Palaszynski et al. 2004).

Other studies have shown estriol prevents the progression of multiple sclerosis through its anti-inflammatory effects, whereas the other estrogen receptor hormone estradiol did not have this effect but still improved long-term outcomes (Tiwari-Woodruff & Voskuhl 2009). The effect of estrogen receptor signalling on MSCs has shown that they can act as potent inducers of neural differentiation. Estradiol was shown to decrease the neural stem cell marker nestin and increase the expression of the oligodendrocyte marker A2B5, particularly in MSCs derived from female patients (estriol was not tested) (Tiftikcioglu et al. 2012). The anti-inflammatory properties of estriol are well established and now used as part of the treatment for MS. MSCs are able to modulate the immune system and produce many of the anti-inflammatory effects observed with estriol treatment and have been applied as a cell therapy for many auto-immune diseases (see section 1.2). It has also been shown that the STRO-1 positive fraction of MSCs is responsible for the property of immune-modulation (Nasef et al. 2008). Taking into consideration that estriol significantly

enhances STRO-1 expression in hES-MPs, the interesting question therefore is does estriol affect the immune modulatory properties of MSCs?

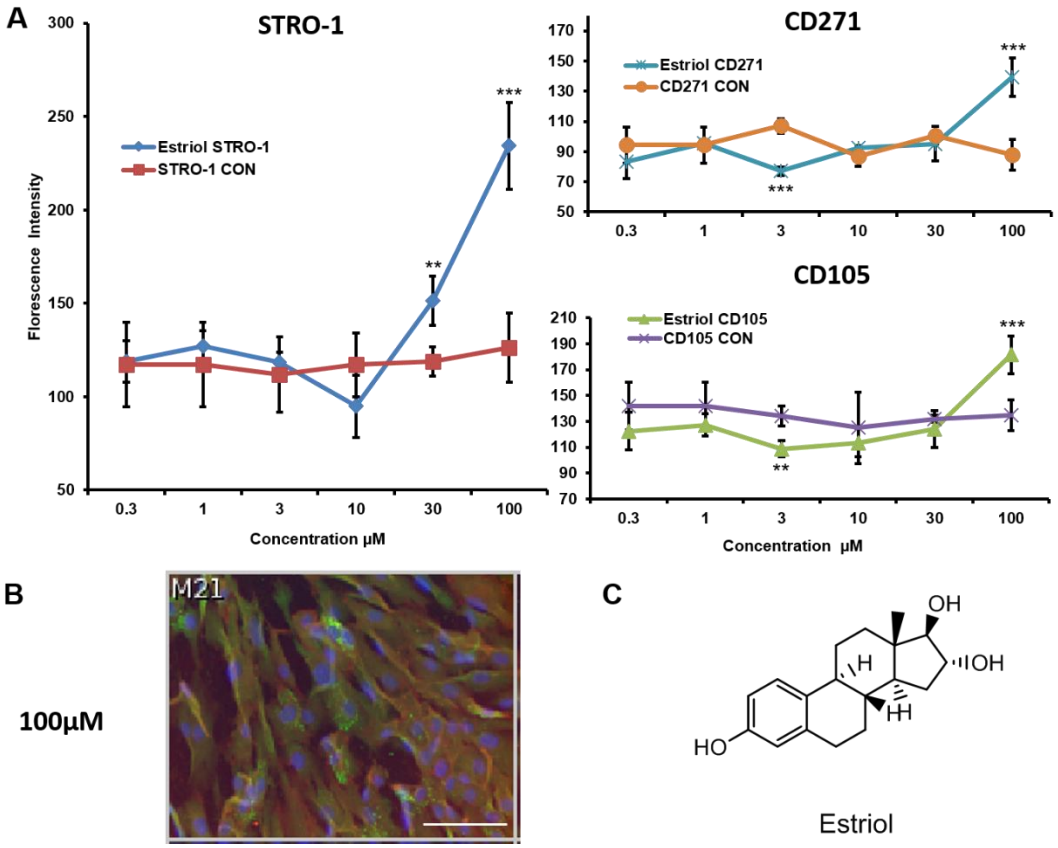

Figure 5.12. *The effect of estriol on MSC markers STRO-1, CD105 and CD271 at 6 concentrations. A) The STRO-1, CD105 and CD271 graphs showing increased fluorescence intensity with increased concentration of estriol. The effect of the small molecule is more pronounced with the STRO-1 marker being significantly higher at both 30 µM and 100 µM concentration. CD105 and CD271 are significantly higher at 100µM (n = 4, error bars given as SD). Scale bar 50µM. B) Fluorescence image of cells taken of a well in the STRO-1(green), CD271 (red) and DAPI (blue) channels at 100 µM treatment. It can be clearly seen in the merged images that some of the hES-MPs show extremely bright STRO-1 fluorescence (green) in the region surrounding the nucleus. Significant denotes comparison with the control at a given drug concentration. C) Structure of estriol.*

Telmisartan also significantly increased MSC marker expression in hES-MPs (Fig. 5.13). Telmisartan, which is used as a treatment for hypertension, has been shown to inhibit the angiotensin type 1 receptor (AGTR1). This receptor is involved in the control of blood pressure through activation by angiotensin II leading to

vasoconstriction and increased blood pressure. However, telmisartan has also been shown to have anti-inflammatory and anti-oxidative properties in experimentally induced myocarditis, an autoimmune disease of the heart. Telmisartan treatment significantly reduced mRNA levels of the pro-inflammatory cytokines IL-1, IL-6, TNF-α and IFN-γ. Serum levels of the anti-inflammatory IL-10 were also significantly elevated (Sukumaran et al. 2010). Other studies showed that the anti-inflammatory response of telmisartan was mediated by peroxisome proliferator-activated receptor gamma (PPAR-γ) in mouse model of Parkinson's disease (Garrido-Gil et al. 2012).

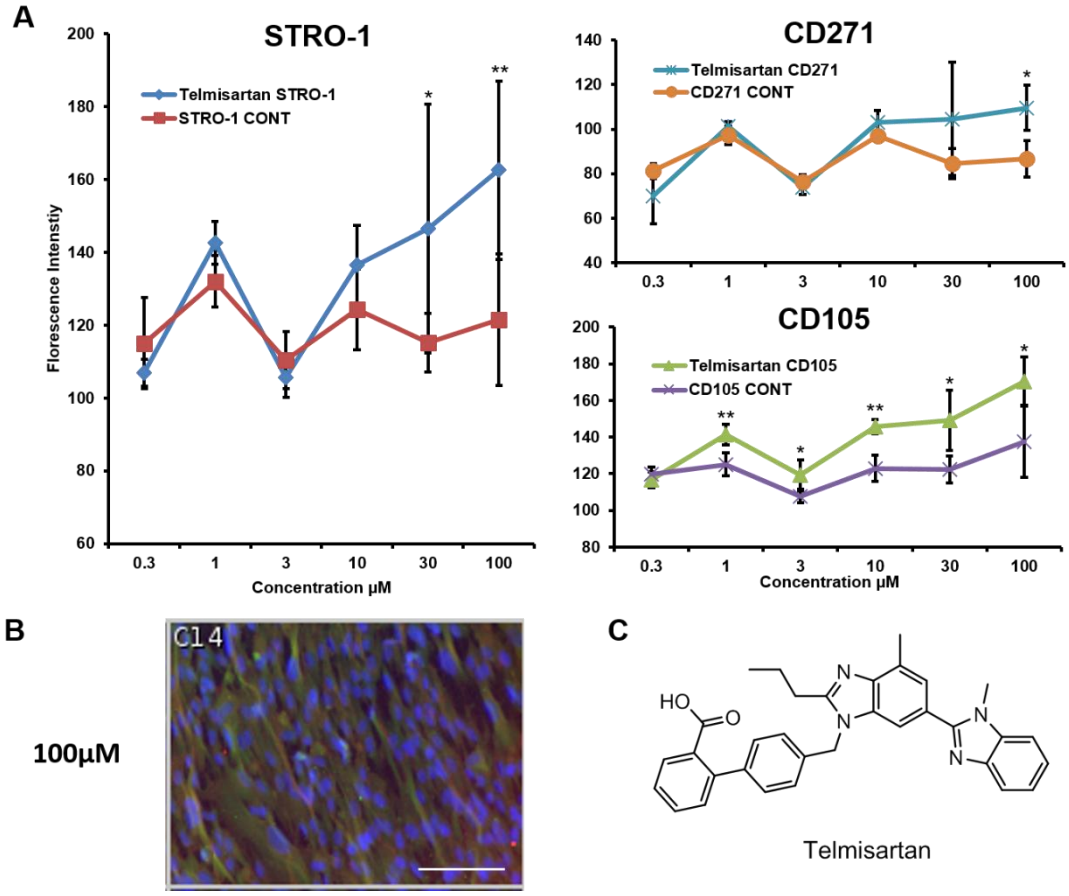

Figure 5.13. *The effect of telmisartan on hES-MPs at 6 concentrations. A) STRO-1, CD271 and CD105 marker expression showing the most pronounced effect at the two highest concentrations, 30 and 100 µM (n = 4, error bars given as SD). Significant denotes comparison with the control at a given drug concentration. B) Image of STRO-1(green), DAPI (blue) and CD271 (red) at 100µM treatment. Scale bar 50µM. C) Structure of telmisartan.*

Activation of PPAR-γ by telmisartan has also been shown to attenuate T-lymphocyte inflammation in the adipose tissue of insulin resistant obese mice (Foryst-Ludwig et al. 2010). PPAR-γ is a regulator of ostegenic and adipogenic differentiation but how telmisartan affects this process in MSCs is unknown. However, the use of other AGTR1 blockers has been shown to enhance differentiation of MSCs towards the cardiac lineage (Numasawa et al. 2011).

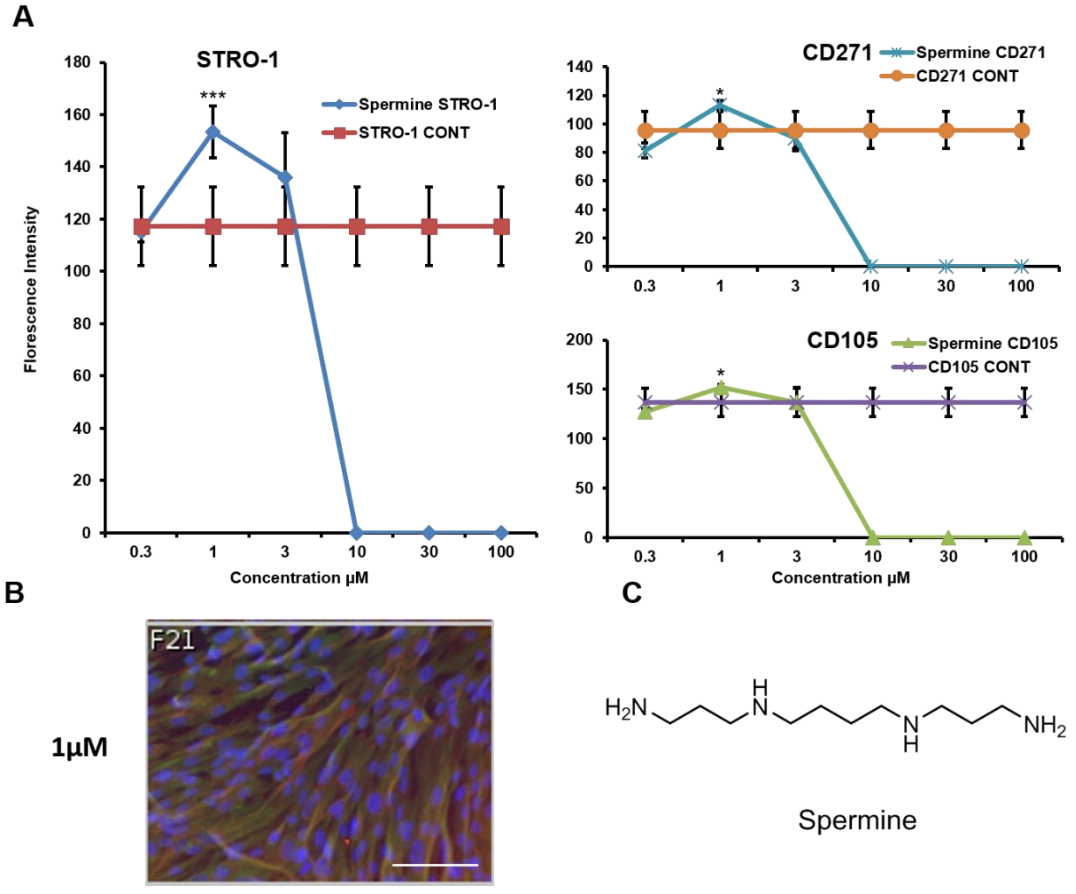

Figure 5.14. *The effect of spermine on hES-MPs at 6 concentrations. A) The effect on STRO-1, CD271 and CD105 marker expression shows a significant increase at 1 µM on STRO-1 and the toxic effects of spermine above 10 µM (n = 4, error bars given as SD). Significant denotes comparison with the control at a given drug concentration. B) Florescent Image of spermine treated hES-MPs at 1 µM stained with DAPI (blue), STRO-1 (green) and CD271 (red). Scale bar 50µM. C) Structure of spermine.*

Spermine (Fig. 5.14) is associated with compaction of DNA and initiation of protein synthesis in mitochondria and is essential for cell growth (Pegg & McCann 1982). Spermine has been shown to regulate inflammation and protect mice against lethal sepsis by down regulation of inflammatory factors such as IL-6, monocyte chemo-attractant protein-1 (MCP-1), macrophage inflammatory protein-2 (MIP-2), and TNF-α (Zhu et al. 2009).

Recently, spermine has been shown to enhance osteogenisis of ADMSCs by β-catenin activation. The application of spermine (5 μM) promoted early osteogenic markers, such as Runx-2, followed by increased β-catenin expression and activation, which lead to the induction of Osterix expression, a mature osteogenic marker (Guidotti et al. 2013). This study was performed using 3D culture, so the effect of this small molecule on these genes in a traditional 2D culture is yet to be determined. Figure 5.14 shows significantly increased expression of all three markers, peaking at 1 μM spermine with concentrations of above 10 μM being toxic.

5.2.3.2 Small molecule STRO-1, CD105 and CD271 enhancers in defined media

To identify small molecules in a serum independent environment, the small molecules were screened concurrently in a serum free media. This identified two small molecule candidates, atenolol and niacin, as potential MSC enrichment candidates. The effect of atenolol is shown in figure 5.15A, with both STRO-1 and CD271 increasing significantly in a dose dependent manner with the highest levels of expression obtained at 100 μM. Atenolol is a beta adrenergic receptor blocker (β-blocker) (in contrast to epinephrine and noradrenalin which are agonists) and is a prescribed treatment for hypertension.

Some of the small molecules chosen in the library are considered nutrients (e.g. niacin) but the fact that they affect signalling pathways categorises them as ‘nutraceuticals’.

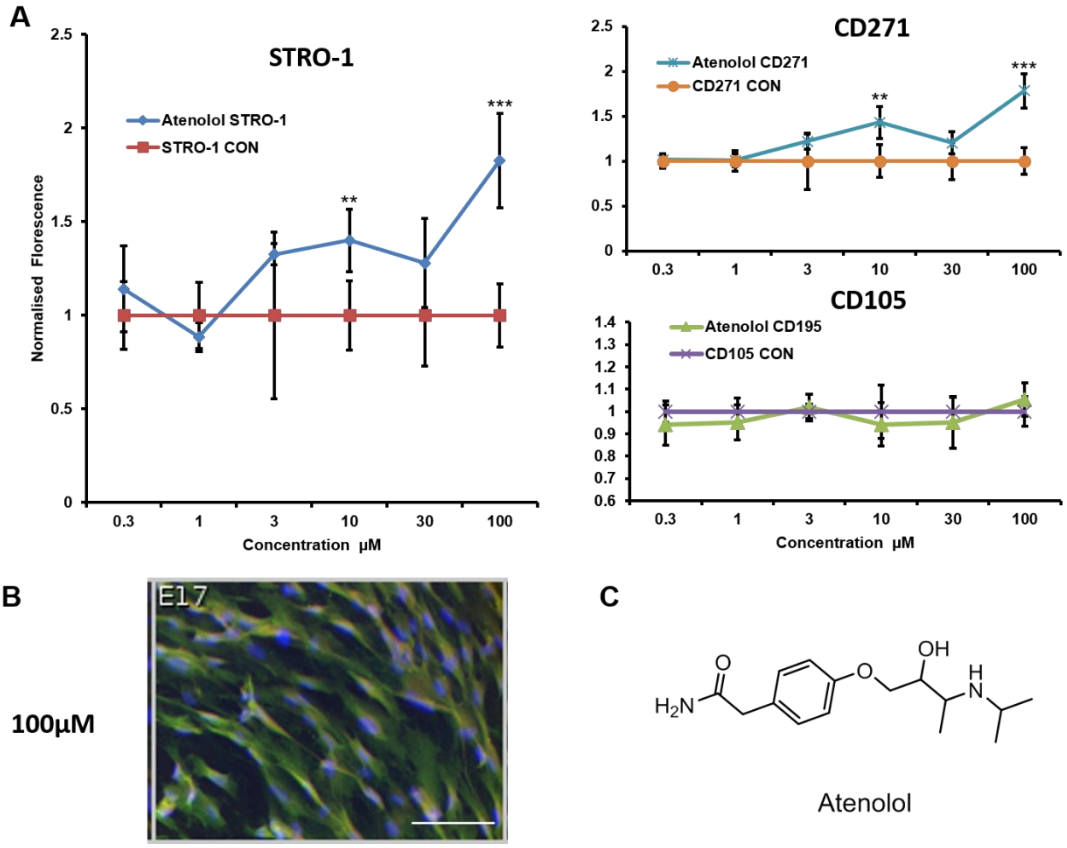

Figure 5.15. *The effect of atenolol on hES-MPs at 6 concentrations in serum free conditions. A) The effect on STRO-1, CD271 and CD105 marker expression shows a significant increase at the 100 µM on STRO-1 and CD271 but not CD105 (n = 4, error bars given as SD). Significant denotes comparison with the control at a given drug concentration. B) Florescent Image of atenolol treated hES-MPs at 100 µM stained with DAPI (blue), STRO-1(green) and CD271 (red). Scale bar 50µM C) Structure of Atenolol.*

In this respect, niacin has been shown to suppress inflammatory cytokines in adipose tissue (fractalkine, RANTES, and MCP-1) as well as up-regulate anti-inflammatory cytokines (adiponectin) (Digby et al. 2010). Niacin, which is used to treat atherosclerosis, activates the orphan G-protein couple receptor GPR109A. It has been demonstrated that activation of this receptor in immune cells is essential for the anti-inflammatory effect in mice with atherosclerosis (Lukasova et al. 2011). Figure 5.16 shows the effect of niacin on the three MSC markers under no serum conditions. Interestingly, the significant increase seems to only occur with the STRO-1 marker and not with CD271 and CD105. At 3 µM, there is a 2.5-fold increase in STRO-1 intensity as compared with controls.

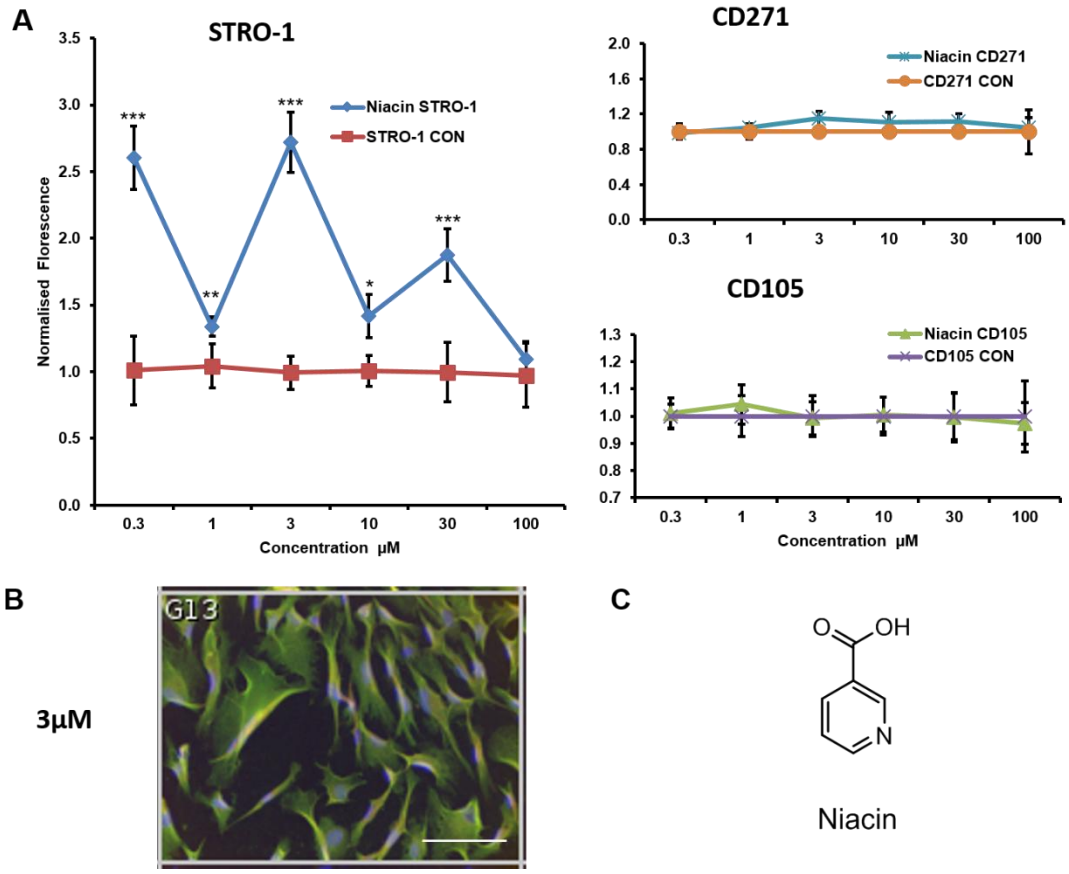

Figure 5.16. *Normalised results of the third small molecule screen in serum free media with hES-MPs showing the effect of niacin at 6 concentrations. A) The effect on STRO-1, CD271 and CD105 marker expression shows a significant increase at 100 µM on STRO-1 and CD271 but not CD105 (n = 4, error bars given as SD). Significant denotes comparison with the control at a given drug concentration. B) Image of atenolol treated hES-MPs at 3 µM stained with DAPI (blue), STRO-1(green) and CD271 (red). Scale bar 50µM. C) Structure of niacin.*

5.2.3.3 STRO-1, CD105 and CD271 expression with a known differentiation factor

As a comparison, results for retinoic acid, which is a neural differentiation factor of hESCs (Murashov et al. 2005), is shown in figure 5.17. Retinoic acid operates by activating retinoic acid receptors (RARs), which regulate hundreds of genes depending on the cell type (Maden 2007).

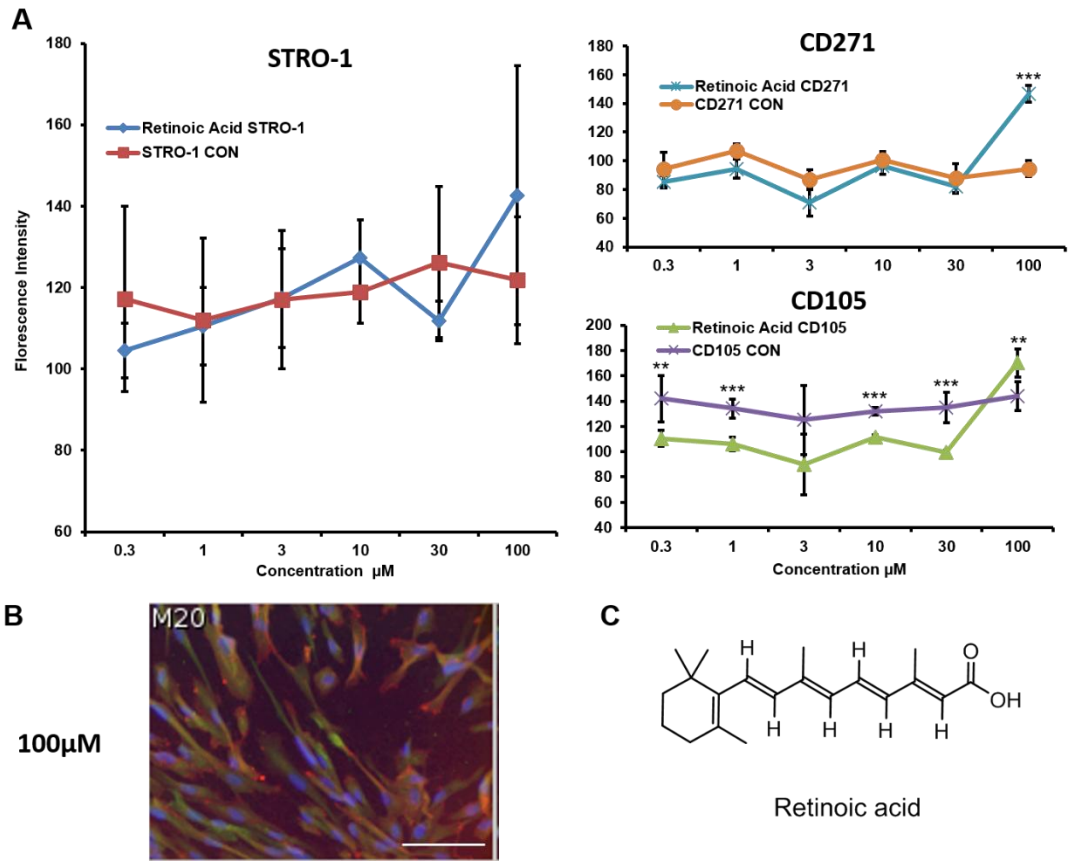

Figure 5.17. *Results of the third small molecule screen in serum containing media with hES-MPs showing the effect of retinoic acid at 6 concentrations. A) The effect on the CD271 marker expression shows a significant increase at 100 µM but not STRO-1 or CD105 (n = 4, error bars given as SD). Significant denotes comparison with the control at the same drug concentration. B) Florescent image of retinoic acid treated hES-MPs at 100 µM stained with DAPI (blue), STRO-1(green) and CD271 (red). Intense CD271 staining can be observed at the boundaries of the cells. Scale bar 50µM. C) Structure of retinoic acid.*

MSCs have also been shown to differentiate into neurons (Tropel et al. 2006) but whether retinoic acid is used in this process was not disclosed. Recently, retinoic acid has been shown to pre-induce MSCs towards the neuronal lineage (Gong et al. 2013). The up-regulation of CD271 in MSCs treated with retinoic acid has not been reported. The up-regulation of CD271 also known as low affinity nerve growth factor; the non-significant effect on STRO-1 and the down regulation of CD105 would suggest that that retinoic acid is acting as a differentiation factor. CD271 is also a marker for neural stem cells and a pure population of NSCs has been isolated using GFAP and CD271 alone (Van Strien et al. 2014). This suggests that CD271 is a good neural marker and its up-regulation compared to the other markers in this

study would indicate that retinoic acid is inducing the cells towards the neural lineage.

5.2.4 Small molecules as potential enhancers of immune-modulation

The majority of small molecule candidates that have been identified in this screening process to promote STRO-1 and CD271 (and to a lesser extent CD105), have been associated with the reduction of inflammation. As stated in section 1.2.2, there are hundreds of clinical trials underway that apply MCSs as a therapy in the modulation of the immune system for a number of autoimmune diseases. The anti-inflammatory effects of these compounds, e.g. reduction of IL2, IL2, IL-6, MCP-1, RENTES, TNF-α, INF-γ, MIP-2, fractalkine and induction of the anti-inflammatory cytokines IL-5, IL-10 and adiponectin, have all been characterised as part of the immune modulatory properties of MSCs (Singer et al. 2011). The interesting question is what effect, if any, do these anti-inflammatory compounds have body's anti-inflammatory machinery, in this case of MSCs? Does the activation of anti-inflammatory pathways recruit or suppress the natural anti-inflammatory properties of MSCs? To test this hypothesis, a literature search was performed to identify markers, specifically surface markers, associated with the immunomodulation state in MSCs.

Prior to application of MSCs for therapy, MSCs are stimulated with pro-inflammatory cytokines IFN-γ and/or TNF-α (Caplan et al. 2011; Polchert et al. 2008). IFN-γ forms part of the adaptive and innate immune response. It is primarily secreted by natural killer cells and natural killer T cells, and is an activator of macrophages and inducer of MHC-II molecules for foreign cell recognition. Overexpression of IFN-γ is associated with many autoimmune diseases. In MSCs, IFN-γ treatment activates indoleamine 2,3 dioxygenase (IDO), the master regulator of immune-modulation in human MSCs (Croitoru-Lamoury et al. 2011). TNF-α is a pro-inflammatory regulator of immune cells produced by activated macrophages. Both IFN-γ and TNF-α differentially regulate immune-modulation in MSCs (English et al. 2007). Stimulation by IFN-γ not only causes the up regulation of IDO but also other proteins critical for the immune-modulation function of MSCs. One of the

primary properties of MSC immune-modulation is the ability to inhibit T cell proliferation. When MSCs are treated with IFN-γ, MSCs up regulate a number of surface proteins critical for the suppression of T-cell proliferation. B7-1 (also known as programmed death ligand 1) is an inhibitory surface protein that has been shown through siRNA knockdown studies to be essential in T-cell suppression (Sheng et al. 2008). Other surface proteins, which are up regulated by IFN-γ and critical for T-cell suppression, include intercellular adhesion molecule-1 (ICAM-1). The up-regulation of these surface proteins by INF-γ and inflammatory cytokines (TNF-α or IL-1) allow the MSCs to directly attach to the T-cells and induce cell death. This is achieved through the production of nitric oxide by inducible nitric oxide synthase (another key component of MSC immune modulation) (Ren et al. 2010). Other surface markers, such as HLA-DR and HLA-ABC (MHC class I and II molecules used for cell recognition), are up regulated by IFN-γ but are not necessarily essential for the immune function of MSCs, however, these markers offer a potential means of identifying 'activated' MSCs.

5.2.4.1 Flow cytometry analysis of MSCs after treatment with IFN-γ, TNF-α or small molecules in serum containing and serum free media.

Prior to the application of MSCs in graft versus host disease, MSCs are treated with IFN-γ to activate them into their immune-modulatory state (Polchart et al. 2008). The activation occurs through the up-regulation of IDO (Croitoru-Lamoury et al. 2011) by stimulation with TNF-α and IFN-γ. The immune-suppression of MSCs directly correlates with TNF-α and IFN-γ induction of IDO (Francios et al. 2012). The identification of small molecules with known anti-inflammatory properties raised the possibility that these compounds may be affecting the immune-modulatory properties of MSCs. If the small molecule candidates affect the immune-modulatory properties of MSCs, they may also affect surface proteins critical for or associated with immunomodulation such as ICAM-1, HLA-DR, and B7-1.

In order to evaluate the immune-modulatory effects of the candidate small molecules, ADMSCs were treated with estriol, atenolol, telmisartan, spermine and

niacin at their most effective concentrations (see section 5.2.3). As controls, ADMSCs were also treated with IFN-γ and TNF-α. After 4 days of treatment, which had been shown to be the optimal treatment time of MSCs for the expression of IFN-γ associated markers (Chan et al. 2008), cells were trypsinised and immuno-stained for ICAM-1, HLA-DR, HLA-ABC, B7-1, B7-2, and STRO-1. ICAM-1 has previously been shown to be up-regulated upon IFN-γ. HLA-DR and HLA-ABC are normally not expressed in MSCs but are expressed at high levels after IFN-γ treatment. The surface protein B7-1 has been shown to be critical for immune-modulation and to be up-regulated by IFN-γ stimulation. Its related homologue B7-2 was included for comparison and STRO-1 was included to verify the results of the screening. Stained cells were analysed by flow cytometry. It should be noted that atenolol and niacin were tested in serum free media. The concentrations for IFN-γ (20 ng/mL) and TNF-α (10 ng/mL) were obtained from the literature (English et al. 2007).

In this preliminary screen, atenolol, telmisartan and niacin showed no change in the expression of MSC immune markers. However, estriol at 100 µM, and spermine at 1 µM and 3 µM, showed a decrease in ICAM-1 expression. Treatment of ADMSCs with IFN-γ up-regulated HLA-ABC, HLA-DR and ICAM-1. TNF-α resulted in the up-regulation of HLA-ABC and ICAM-1 (Fig. 5.18).

For the cells treated with estriol at 100 µM, flow cytometry analysis of markers STRO-1 and ICAM-1 showed a minor shift to the STRO-1+ and ICAM-1+ quadrant (Fig. 5.19). The ADMSCs treated with spermine showed a reduction in the STRO-1- and ICAM-1+ quadrant (Fig. 5.19).

The expression of STRO-1 and ICAM-1 in treated and untreated cells is compared in figure 5.20. In this preliminary screen, treatment with estriol at 100 µM and spermine at 3µM reduces the proportion of ICAM-1+ cells and increases the proportion of STRO-1+ cells (Fig. 5.20A, B and C). The flow data correlates to what was seen in the small molecule screens in relation to increased expression of STRO-1.Treatment of ADMSCs with IFN-γ increased the STRO-1+ and ICAM-1+ fraction (Fig. 5.20A and B, purple histogram). Comparison with the untreated control suggests that there was some induction of STRO-1 expression.

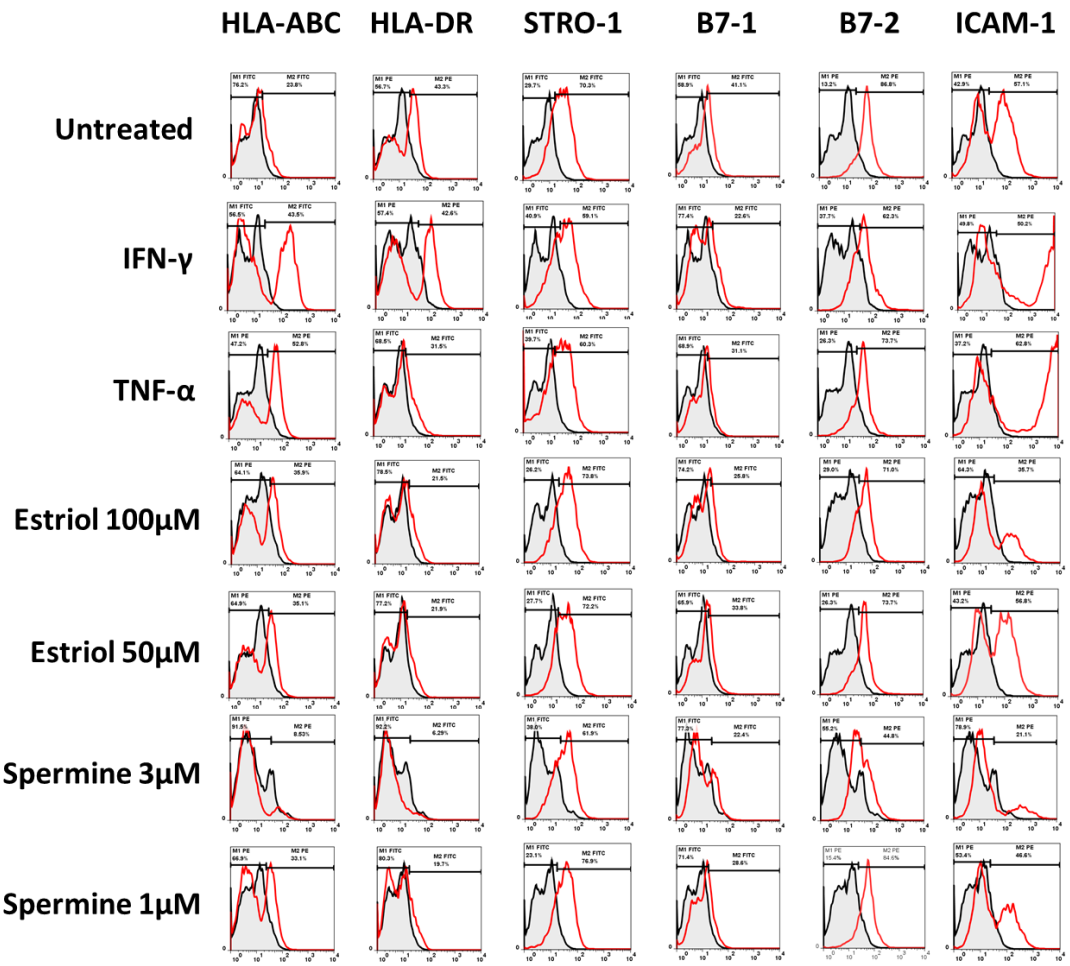

Figure 5.18*. Flow cytometry analysis of ADMSCs after 4 days of treatment with estriol at 50 and 100 µM, and spermine at 1 and 3µM. IFN-γ and TNF-α were used at 10 and 20 ng/mL, respectively. The six immune-associated surface markers HLA-ABC, HLA-DR, STRO-1, B7-1, B7-2 and ICAM-1were compared with the untreated, IFN-γ and TNF-α controls.*

As can be seen in figure 5.19, the ICAM-1+ fraction reacts to IFN-γ stimulation by substantially up-regulating this surface protein. By contrast, a high proportion of the STRO-1+ and ICAM-1- cells do not appear to respond to IFN-γ stimulation.

Additional experiments are required to confirm the down-regulation of ICAM-1 receptor in spermine treated cells. ICAM-1 binds two integrins belonging to the β_2 superfamily LFA-1 ($\alpha_L\beta_2$), and is critical in leucocyte migration and activation of T-cells (Zuckerman et al. 1998). It has a critical role in the immune-modulatory properties of MSCs (Ren et al. 2010). ICAM-1 is constitutively expressed in wide variety of cell types (Kim et al. 2012).

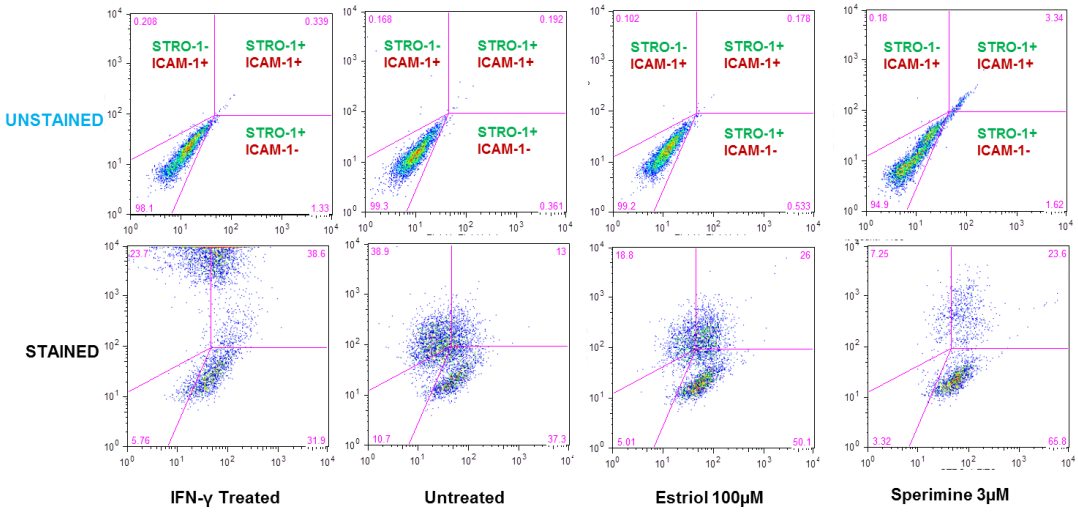

Figure 5.19. *STRO-1 and ICAM-1 marker analysis for IFN-γ, untreated, estriol (100µM) and spermine treated (3µM) ADMSCs.*

Suppression of ICAM-1 expression has been demonstrated in TNF-α activated human bronchial epithelial cells using the anti-inflammatory compound eupatilin. Here, eupatilin supressed ICAM-1 by inhibiting the phosphorylation of Akt resulting in the down-regulation of nuclear factor kappa-light-chain-enhancer of activated B cells (NF-κB) (a regulator of the immune response) (Jung et al. 2012).

Similarly, lactoferrin (also an anti-inflammatory compound) suppressed TNF-α induced ICAM-1 expression in human umbilical vascular endothelial cells (HUVECs) by preventing NF-KB binding to a NF-KB site of the ICAM-1 promoter (Kim et al. 2012). These preliminary results indicate that spermine reduces the expression of ICAM-1. If confirmed, it would be interesting to see if spermine is able to suppress TNF-α (and INF-γ) induced ICAM-1 expression.

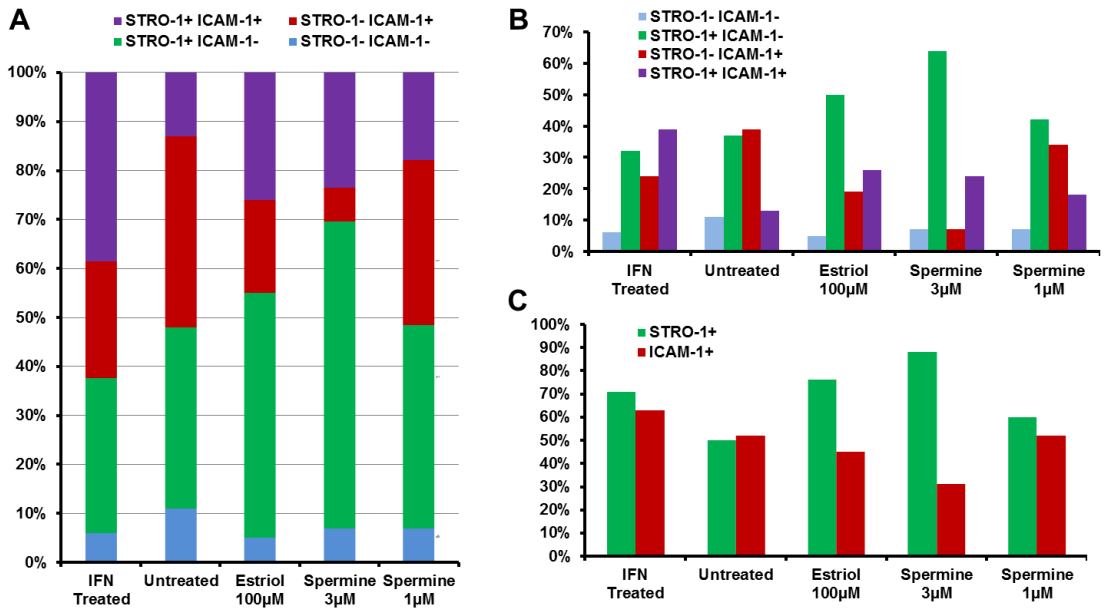

Figure 5.20. *Analysis of STRO-1 and ICAM-1 expression. A) Percentage each marker combination in each of the 5 treatment groups. B) Breakdown of the proportions into individual bar graphs. C) Proportion of ADMSCs positive for STRO-1 and ICAM-1.*

5.3 CONCLUSIONS

A 'knowledge based' approach was used to examine the known MSC and ESC pathways involved in the maintenance and differentiation of these cells. This approach used 200 FDA/EU approved small molecules.

This focused small molecule library identified 5 compounds, of which 4 were known anti-inflammatory agents, which enhanced the expression of MSC markers STRO-1, CD105 and CD271. The known anti-inflammatory immune-modulatory properties of MSCs led to the investigation of the effect of these small molecules on signature immune-modulatory surface proteins. In a preliminary screen, two small molecules, spermine and estriol, were found to up-regulate STRO-1 expression and down-regulate the cell surface protein ICAM-1. Since the small molecule library included small molecules with a wide variety of activity, the disproportionate identification of anti-inflammatory compounds that effect the phenotype of MSCs (which also have anti-inflammatory activity) raises the interesting question of what effect does an anti-inflammatory environment (small molecule) have on the anti-inflammatory activities

of MSCs. If MSCs have their activities suppressed or activated in the presence of anti-inflammatory compounds, then this would have important clinical implications.

CHAPTER 6

FUTURE WORK

The work of this thesis achieved a number of advances in mesenchymal stem cell culture, it identified two defined polymer substrates **PA338** and **PU157** that could promote growth and maintain the MSC phenotype and differentiation capacity in long term culture. The process used to identify these candidates was through multiple screens, scale up and long term passage examining progressively more phenotypic markers through the screening and scale-up process. This means that additional value will be obtained from examination of their surface structure and physical properties. Examination of the stiffness/elasticity and how cells interact with the surface at the micro to the nanoscale level using scanning electron microscopy may identify polymer properties and motifs that can be compared with other studies. Examination of integrin expression profiles with an integrin antibody panel covering all human integrin combinations could potentially identify alteration/up-regulation of specific integrins.

These polymers extend the list of biomaterials for MSC culture and potentially other cell types as the extracellular matrix components these polymers substitute for, such as collagen/gelatin are widely used in cell culture. The alteration of surface rigidity through a photo-cleavable cross-linked has shown surface rigidity to heavily determine the multipotency of MSCs. Tissue culture plastic is currently used in the isolation of MSCs, the stiffness of which (elastic modulus ~3GPa) is several order of magnitude higher than substrates shown to predispose cells to the osteogenic lineage (Yang et al. 2014). The use of these polymers in the isolation of MSCs may enhance their multipotency by avoiding the changes induced by extremely stiff substrates such as tissue culture plastic but additional material characterisation is required.

In addition, **PA338** and **PU157** could be applied to 3D culture systems where MSCs are use as either seeded scaffolds or as scaffolds that recruit MSCs and other cells or scaffolds that promote growth and are subsequently differentiated with soluble factors/differentiation media.

The advent of 3D printing adds the prospect of using these polymers as a component for localizing MSCs in conjunction with other polymers recruiting other cells (such as endothelial). High resolution 3D printing to produce complex 3D scaffolds is a potential future path for polymer microarray technology.

This work also identified a 'smart' thermo-modulatable hydrogel **HGL1** that allowed MSCs to be passaged by modest temperature reduction in the absence of harsh enzymatic trypsin passaging. This added an additional dimension to polymer microarray technology. The identification of a smart hydrogel that can trigger cellular release could be modified further as micro-carriers potentially allowing large scale MSC production with temperature controlled cellular release. The superior retention of MSC markers over the gelatin control makes this substrate potentially superior for the isolation of MSCs and retention of phenotype in long term culture. The fact that this is also a hydrogel and its retention of the MSC phenotype opens it up to MSC encapsulation studies.

Monomer analysis of the polymers that promoted growth in chapter 3 revealed PEG to be particularly poor monomer for MSC binding and growth. Many of the important studies that have examined MSC behaviour while encapsulated (Benoit et al. 2008) or on surfaces (Yang et al. 2014) have used PEG based hydrogels. Applying **HGL1** as the major hydrogel component may improve future studies involving hydrogel encapsulation or hydrogel property modification where MSCs are used. Encapsulation with perfusion bioreactor technology or even a vascular network is possible with such a hydrogel as was used with encapsulated hepatocytes with patterned vascular networks (using human umbilical cord vascular endothelial cells) for perfusable engineered tissues (Miller et al. 2012).

The power of the microarrays at identifying polymers in the presence of serum should certainly be applied to defined media systems now available for MSC culture. This would result in culture conditions where all the components would be known removing the confounding element of unknown protein components to experimental analysis. This is particularly true for cell substrate interaction analysis as the key extracellular components for cell binding are contained within the FCS component. Culture in the absence could more clearly define the role of MSC substrate

interaction in the absence of integrin binding proteins. This would remove potential interactions due to the binding of the proteins to the polymers and the cells binding to the proteins. From the work in chapter 3 and 4 it is impossible to determine whether the cells favour a polymer because the chemistry of the polymer binds particular proteins to that polymer and that this proteins are required for the growth and maintenance of the MSC phenotype or if the MSCs are interacting with the chemistry of the surface directly.

Ultimately, the achievement of chapters 3 and 4 was to have taken the goal of MSC culture in the absence of biological components a step further. As we move forward with tissue engineering and regenerative medicine, the need for platforms that can identify defined substrates that allow for the expansion and isolation of different stem cell populations will be an essential tool realising the full potential of regenerative medicine. Importantly, the polymer microarray platform allows the phenotype of the stem cell to be analysed. Advances in the understanding of the stem cell phenotypes will facilitate their isolation using this system even where components such as preferred functional group, surface rigidity/elasticity, and nano-topography remain unknown they can be elucidated through the high-throughput approach.

In addition, this work also used a 'knowledge based' small molecule library and a high-throughput high content imaging system for screening to identify 5 small molecules that enhanced the MSC marker phenotype. In further preliminary work, two small molecules estriol and spermine with known anti-inflammatory properties down regulated the essential MSC immune-modulation surface protein ICAM-1. In future work, the down regulation observed in this initial study should be confirmed. Other studies have reported small molecules (also with anti-inflammatory properties) that down regulated ICAM-1 after its up-regulation with TNF-α treatment. This should also be tested with these two small molecules. The unexpected identification of small molecules with anti-inflammatory properties being identified as MSC marker enhancers raised the interesting question. What is the effect of anti-inflammatory signals on the MSCs state and importantly MSCs immune modulatory state? Given the number of clinical trials using MSCs as a cell therapy, studies that

reveal the different aspects of the immune properties of this cell type have immediate wide ranging implications. How the activated MSCs cytokine profile alters in the presence of anti-inflammatory drugs can be easily tested using Elisa assays for pro and anti-inflammatory cytokines with MSCs compared to cells treated with and without activation factors.

The current screening process was however unable to identify candidates that were able to substitute for growth factors such as bFGF, TGF-β and PDGF-ββ. A potential major flaw in the screening process was the overly favourable conditions in the background of the small molecule screening. The drugs were screened in the presence of DMEM with 10%FCS supplemented with 4ng/ml of bFGF. The process which identified the small molecules was very rigorous, because of this one possibility would be to optimise the conditions of MSC growth in the absence of bFGF and under optimised low serum conditions in which the readout gives a clear signal in the absence of the key growth factors bFGF, TGF-β and PDGF-ββ.

Addition of the small molecules in low serum in the absence of any growth factors should give a more consistant readout. Identified candidates could then be analysed individually and in combination with other identified small molecules (it is known that the growth factors act synergistically (Ng et al. 2008)). Such identified candidates would require testing in serum free conditions such as that described by Jung *et al* but in the absence of one or more of the growth factors. The ultimate formulation would have to be tested in long term culture MSC culture and undergo differentiation analysis and cell characterisation. This approach may prove to be more successful than the one employed in this study, it is also possible however that the candidates were not in fact able to substitute for growth factors alone or in combination with other small molecules but this has not been exhaustively tested.

In all, this work represents a significant advance in the development of new culture systems for mesenchymal stem cells.

CHAPTER 7

REFERENCES

Aggarwal, B.B., (2010) Targeting inflammation-induced obesity and metabolic diseases by curcumin and other nutraceuticals. *Annu Rev Nutr*, 30, p173–199.

Amit, M. et al., (2003) Human feeder layers for human embryonic stem cells. *Biol Reprod*, 68(6), p2150–2156.

Anderson, D.G., Levenberg, S. & Langer, R., (2004) Nanoliter-scale synthesis of arrayed biomaterials and application to human embryonic stem cells. *Nat Biotechnol*, 22(7), p863–866.

Apel, A. et al., (2009) Suitability of human mesenchymal stem cells for gene therapy depends on the expansion medium. *Exp Cell Res*, 315(3), p498–507.

Ardehali, R. et al., (2013) Prospective isolation of human embryonic stem cell-derived cardiovascular progenitors that integrate into human fetal heart tissue. *Proc Natl Acad Sci*, 110(9), p3405–3410.

Arthur-Farraj, P.J. et al., (2012) c-Jun reprograms Schwann cells of injured nerves to generate a repair cell essential for regeneration. *Neuron*, 75(4), p633–647.

Asahi, K. et al., (2003) Patent GB 2408331: Arrays for screening polymeric materials.

Augello, A. & De Bari, C., (2010) The regulation of differentiation in mesenchymal stem cells. *Hum Gene Ther*, 21(10), p1226–1238.

Augello, A. et al., (2007) Cell therapy using allogeneic bone marrow mesenchymal stem cells prevents tissue damage in collagen-induced arthritis. *Arthritis Rheum*, 56(4), p1175–1186.

Baroli, B., (2007) Hydrogels for tissue engineering and delivery of tissue-inducing substances. *J Pharm Sci*, 96(9), p2197–2223.

Budyanto L., Goh Y.Q. & Ooi C.P., (2009) Fabrication of porous poly(L-lactide) (PLLA) scaffolds for tissue engineering using liquid-liquid phase separation and freeze extraction. *J Mater Sci Mater Med*, 20(1), p105–111.

Baker, M., (2011) Stem cells in culture: defining the substrate. *Nature methods*, 8(4), p293–297.

Barberi, T. et al., (2005) Derivation of multipotent mesenchymal precursors from human embryonic stem cells. *PLoS Med*, 2(6), p554–560.

Bartholomew, A. et al., (2002) Mesenchymal stem cells suppress lymphocyte proliferation in vitro and prolong skin graft survival in vivo. *Exp Hematol*, 30(1), p42–48.

Benoit, D.S. et al., (2008) Small functional groups for controlled differentiation of hydrogel-encapsulated human mesenchymal stem cells. *Nat Mater*, 7(10), p816–823.

Bernet, J.D. et al., (2014) p38 MAPK signaling underlies a cell-autonomous loss of stem cell self-renewal in skeletal muscle of aged mice. *Nature Med*, 20(3), p265–271.

Bickenbach, J.R., (1981) Identification and behavior of label-retaining cells in oral mucosa and skin. *J Dent Res*, 60, p1611–1620.

Bischoff, R., (1975) Regeneration of single skeletal muscle fibers in vitro. *Anat Rec*, 182(2), p215–235.

Bischoff, R., (1986) Proliferation of muscle satellite cells on intact myofibers in culture. *Dev Biol*, 115(1), p129–139.

Bjerknes, M. & Cheng, H., (2002) Multipotential stem cells in adult mouse gastric epithelium. *Am J Physiol Gastrointest Liver Physiol*, 283(3), G767–G777.

Boerckel, J.D. et al., (2011) Effects of protein dose and delivery system on BMP-mediated bone regeneration. *Biomaterials*, 32(22), p5241–5251.

Boitano, A.E. et al., (2010) Aryl hydrocarbon receptor antagonists promote the expansion of human hematopoietic stem cells. *Science*, 329(5997), p1345–1348.

Brafman D.A. et al., (2010) Long-term human pluripotent stem cell self-renewal on synthetic polymer surfaces. *Biomaterials*, 31(34), p9135–9144.

Brocchini, S. et al., (1997) A combinatorial approach for polymer design. *J Am Chem Soc*, 119(19), p4553–4554.

Brooke, G. et al., (2008) Molecular trafficking mechanisms of multipotent mesenchymal stem cells derived from human bone marrow and placenta. *Stem Cells Dev*, 17(5), p929–940.

Brown, J.B. et al., (2010) Mesalamine inhibits epithelial beta-catenin activation in chronic ulcerative colitis. *Gastroenterology*, 138(2), p595–605.

Brown, S.E., Tong W. & Krebsbach PH., (2009). The derivation of mesenchymal stem cells from human embryonic stem cells. *Cells Tissues Organs*, 189(1-4), 256–260.

Bruderer, M. et al., (2013) Role and regulation of RUNX2 in osteogenesis. *Eur Cell Mater*, 28, p269–286.

Buczacki, S.J. et al., (2013) Intestinal label-retaining cells are secretory precursors expressing Lgr5. *Nature*, 495(7439), p650–659.

Bühring, H.J. et al., (2007) Novel markers for the prospective isolation of human MSC. *Ann N Y Acad Sci*, 1106, p262–271.

Burdick, J.A. & Prestwich G.D., (2011) Hyaluronic acid hydrogels for biomedical applications. *Adv Mater*, 23(12), H41–56.

Braun, J. et al., (2013) Concerted regulation of CD34 and CD105 accompanies mesenchymal stromal cell derivation from human adventitial stromal cell. *Stem Cells Dev*, 22(5), p815–827.

Braun, K. et al., (2003) Manipulation of stem cell proliferation and lineage commitment: visualisation of label-retaining cells in wholemounts of mouse epidermis. *Development*, 130(21), p5241–5255.

Campioni, D. et al., (2009) A decreased positivity for CD90 on human mesenchymal stromal cells (MSCs) is associated with a loss of immunosuppressive activity by MSCs. *Cytometry B*, 76(3), p225–230.

Carbone, E.J. et al., (2014) Small molecule delivery through nanofibrous scaffolds for musculoskeletal regenerative engineering. *Nanomedicine*, 10(8), p1691–1699.

Casado, J.G. et al., (2014) Mesenchymal stem cell-coated sutures enhance collagen depositions in sutured tissues. *Wound Repair Regen*, 22(2), p256–264.

Castro-Malaspina, H. et al., (1980) Charachterization of human bone marrow fibroblast colony-forming cells (CFU-F) and their progeny. *Blood*, 56(2), p289–301.

Celiz, A.D. et al., (2014) Chemically diverse polymer microarrays and high throughput surface characterisation: a method for discovery of materials for stem cell culture. *Biomater Sci*, 2(11), p1604–1611.

Censi, R. et al., (2012) Hydrogels for protein delivery in tissue engineering. *J Control Release*, 161(2), p680–692.

Chan, W.K. et al., (2008) MHC expression kinetics and immunogenicity of mesenchymal stromal cells after short-term IFN-γ challenge. *Exp Hematol*, 36(11), p1545–1555.

Chang, J.W. et al., (2014) Tissue-engineered tracheal reconstruction using three-dimensionally printed artificial tracheal graft: preliminary report. *Artif Organs*, 38(6), E95-E105.

Chase, L.G. et al. (2010) A novel serum-free medium for the expansion of human mesenchymal stem cells. *Stem Cell Res Ther*, 1(1), p8.

Chastain, S.R. et al., (2006) Adhesion of mesenchymal stem cells to polymer scaffolds occurs via distinct ECM ligands and controls their osteogenic differentiation. *J Biomed Mater Res A*, 78(1), p73–85.

Chen, .F.M. et al., (2009) In vitro cellular responses to scaffolds containing two microencapulated growth factors. *Biomaterials*, 30(28), p5215–5224.

Chen, G. et al., (2011) Chemically defined conditions for human iPS cell derivation and culture. *Nat Methods*, 8(5), p424–429.

Chen, S. et al., (2006) Self-renewal of embryonic stem cells by a small molecule. *Proc Natl Acad Sci*, 103(46), p17266–17271.

Cockburn, K. & Rossant J., (2010) Making the blastocyst: lessons from the mouse. *j Clin Invest*, 120(4), p995–1003.

Codega, P. et al., (2014) Prospective identification and purification of quiescent adult neural stem cells from their in vivo niche. *Neuron*, 82(3), p545–559.

Cohen, J., (2013) Mesenchymal stem cell transplantation in multiplesclerosis. *J Neurol Sci*, 333(1-2), p43–49.

Collins C.A. et al., (2005) Stem cell function, self-renewal and behavioural heterogeneity of cells from the adult muscle satellite cell niche. *Cell*, 122(2), p289–301.

Corselli, M. et al., (2012) The tunica adventitia of human arteries and veins as a source of mesenchymal stem cells. *Stem Cells Dev*, 21(8), p1299–1308.

Cotsarelis, G., Sun T. & Lavker R.M. (1990) Label-retaining cells reside in the bulge area of pilosobaceous unit: implications for follicular stem cells, hair cycle, and skin carcinogenesis. *Cell*, 61(7), p1329–1337.

Cremers, N.A. et al., (2014) Curcumin-induced heme oxygenase-1 expression prevents H2O2-induced cell death in wild type and heme oxygenase-2 knockout adipose-derived mesenchymal stem cells. *Int J Mol Sci*, 15(10), p17974–917979.

Crisan, M. et al., (2008) A perivascular origin for mesenchymal stem cells in multiple human organs. *Cell Stem Cell*, 3(3), p301–313.

Crist, C.G., Montarras, D. & Buckingham, M., (2012) Muscle satellite cells are primed for myogenesis but maintain quiescence with sequestration of Myf5 mRNA targeted by microRNA-31 in mRNP granules. *Cell Stem Cell*, 11(1), p118–126.

Croitoru-Lamoury, J. et al., (2011) Interferon-γ regulates the proliferation and differentiation of mesenchymal stem cells via activation of indoleamine 2,3 dioxygenase (IDO). *PLoS One*, 6(2), e14698.

Cui, X. et al., (2012) Thermal inkjet printing in tissue engineering and regenerative medicine. *Recent Pat Drug Deliv Formul*, 6(2), p149–55.

Curran, J.M., Chen R. & Hunt J.A, (2006) The guidance of human mesenchymal stem cell differentiation in vitro by controlled modifications to the cell substrate. *Biomaterials*, 27(27), p4783–4793.

Curran, J.M. et al., (2011) The use of dynamic surface chemistries to control msc isolation and function. *Biomaterials*, 32(21), p4753–4760.

Curran, J.M. et al., (2010) Introducing dip pen nanolithography as a tool for controlling stem cell behaviour: unlocking the potential of the next generation of smart materials in regenerative medicine. *Lab Chip*, 10(13), p1662–1670.

Dala, J., Grady, K. & Domen J., (2012) Role of mesenchymal stem cell therapy in Crohn's disease. *Pediatric Research*, 71(4), p445–451.

Dalby, M.J. et al., (2007) The control of human mesenchymal cell differentiation using nanoscale symmetry and disorder. *Nat Mater*, 6(12), p997–1003.

Dalby, M.J., Gadegaard, N. & Oreffo, R.O., (2014) Harnessing nanotopography and integrin-matrix interactions to influence stem cell fate. *Nat Mater*, 13(6), p558–569.

Dalby M.J. et al., (2004) Investigating the limits of filopodial sensing: a brief report using SEM to image the interaction between 10 nm high nano-topography and fibroblast filopodia. *Cell Biol Int*, 28(3), p229–236.

Danmark, S. et al., (2012) Integrin-mediated adhesion of human mesenchymal stem cells to extracellular matrix proteins adsorbed to polymer surfaces. *Biomed Mater*, 7(3), e035011.

Das, R.K. et al., (2013) Influence of nanohelical shape and periodicity on stem cell fate. *ACS Nano*, 7(4), p3351–3361.

Dennis, J.E. et al., (2002a) The STRO-1+ marrow cell population is multipotential. *Cells Tissues Organs*, 170(2-3), p73–82.

Dennis, J.E. & Charbord P., (2002b) Origin and differentiation of human and murine stroma. *Stem Cells*, 20(3), p205–214.

Derfoul, A. et al. (2007) Glucosamine promotes chondrogenic phenotype in both chondrocytes and mesenchymal stem cells and inhibits MMP-13 expression and matrix degradation. *Osteoarthritis Cartilage*, 15(6), p646–655.

Digby, J.E. et al., (2010) Anti-inflammatory effects of nicotinic acid in adipocytes demonstrated by suppression of fractalkine, RANTES, and MCP-1 and upregulation of adiponectin. *Atherosclerosis*, 209(1), p89–95.

Ding, L. et al., (2012) Endothelial and perivascular cells maintain haematopoietic stem cells. *Nature*, 481(7382), p457–462.

Discher, D.E., Mooney D.J & Zandstra P.W., (2009) Growth factors, Matrices, and forces combine and control stem cells. *Science*, 324(5935), p1673–1677.

Dolley-Sonneville, P.J., Romeo L.E. & Melkoumian Z.K., (2013) Synthetic surface for expansion of human mesenchymal stem cells in xeno-free, chemically defined culture conditions. *PLoS One*, 8(8), e70263.

Dominici, M. et al., (2006) Minimal criteria for defining multipotent mesenchymal stromal cells. The International Society for Cellular Therapy position statement. *Cytotherapy*, 8(4), p315–317.

Duan, Y. et al., (2010) Differentiation and characterization of metabolically functioning hepatocytes from human embryonic stem cells. *Stem Cells*, 28(4), p674–686.

Ducheyne, P. & Qiu, Q., (1999) Bioactive ceramics: the effect of surface reactivity on bone formation and bone cell function. *Biomaterials*, 20(23-24), p2287–2303.

Elder, B.D., Eleswarapu S.V. & Athanasiou K.A., (2009) Extraction techniques for the decellularization of tissue engineered articular cartilage constructs. *Biomaterials*, 30(22), p3749–3756.

Engler, A.J. et al., (2006) Matrix elasticity directs stem cell lineage specification. *Cell*, 126(4), p677–689.

English, K. et al., (2007) IFN-gamma and TNF-alpha differentially regulate immunomodulation by murine mesenchymal stem cells. *Immunol Lett*, 110(2), 91–100.

Esenhauer, P. et al., (2013) Endogenous distal airway progenitor cells, lung machanics, and disproportionalte lobar growth following long-tem pospneumonectomy in mice. *Stem Cells*, 31(7), p1330–1339.

Falanga, V. & Sabolinski M., (1999) A bilayered living skin construct (APLIGRAF) accelerates complete closure of hard-to-heal venous ulcers. *Wound Repair Regen*, 7(4), p201–207.

Fan, T. et al., (2011) Preparation of thermoresponsive and pH-sensitivity polymer magnetic hydrogel nanospheres as anticancer drug carriers. *Colloids Surf B Biointerfaces*, 88(2), p593–600.

Farmer, S.R., (2005) Regulation of PPAR gamma activity during adipogenesis. *Int J Obes*, 29 Suppl 1, S13–16.

Fioretta, E.S. et al., (2012) Polymer-based scaffold designs for in situ vascular tissue engineering: controlling recruitment and differentiation behavior of endothelial colony forming cells. *Macromol Biosci*, 12(5), p577–590.

Fiorina, P. et al., (2009) Immunomodulatory function of bone marrow-derived mesenchymal stem cells in experimental autoimmune type 1 diabetes. *J Immunol*, 183(2), p993–1004.

Fickert, S., Fiedler J. & Brenner R.E., (2003) Identification, quantification and isolation of mesenchymal progenitor cells from osteoarthritic synovium by fluorescence automated cell sorting. *Osteoarthritis Cartilage*, 11(11), p790–800.

Foryst-Ludwig, A. et al., (2010) PPARgamma activation attenuates T-lymphocyte-dependent inflammation of adipose tissue and development of insulin resistance in obese mice. *Cardiovasc Diabetol*, 9, p64.

Foster, L.J. et al., (2005) Differential expression profiling of membrane proteins by quantitative proteomics in a human mesenchymal stem cell line undergoing osteoblast differentiation. *Stem Cells*, 23(9), p1367–1377.

François, M. et al., (2012) Human MSC suppression correlates with cytokine induction of indoleamine 2,3-dioxygenase and bystander M2 macrophage differentiation. *Mol Ther*, 20(1), p187–195.

Friedenstein, A.J. et al., (1974) Precursors for fibroblasts in different populations of hematopoietic cells as detected by the in vitro colony assay method. *Exp Hematol*, 2(2), p83–92.

Frith, J.E. et al., (2012) Development of defined culture conditions for the expansion of human mesenchymal stromal cells for clinical applications. *Stem Cells and Cancer Stem Cells*, 8, p13–26

Fujisawa, T. et al., (2008) Peroxisome proliferator-activated receptor gamma (PPARgamma) suppresses colonic epithelial cell turnover and colon carcinogenesis through inhibition of the beta-catenin/T cell factor (TCF) pathway. *J Pharmacol Sci*, 106(4), p627–638.

Garrido-Gil, P. et al. (2012) Involvement of PPAR-γ in the neuroprotective and anti-inflammatory effects of angiotensin type 1 receptor inhibition: effects of the receptor

antagonist telmisartan and receptor deletion in a mouse MPTP model of Parkinson's disease. *J Neuroinflammation*, 9, 38.

Gimble, J.M., Katz A.J. & Bunnell B.A., (2007) Adipose-derived stem cells for regenerative medicine. *Circ Res*, 100(9), p1249–1260.

Girdlestone, J. et al., (2009) Efficient expansion of mesenchymal stromal cells from umbilical cord under low serum conditions. *Cytotherapy*, 11(6), p1–11.

Goessler, U.R. et al., (2006) In vitro analysis of integrin expression during chondrogenic differentiation of mesenchymal stem cells and chondrocytes upon dedifferentiation in cell culture. *Int J Mol Med*, 17(2), p301–307.

Gonfiotti, A. et al., (2014) The first tissue-engineered airway transplantation: 5-year follow-up results. *Lancet*, 383(9913), p238–244.

Gong, M. et al., (2013) Retinoic acid receptor beta mediates all-trans retinoic acid facilitation of mesenchymal stem cells neuronal differentiation. *Int J Biochem Cell Biol*, 45(4), p866–875.

Gonzalez, R. et al., (2011) Dorsomorphin promotes human embryonic stem cell self-renewal. *Angew Chem*, 50(15), p3439–3441.

Gopal, K., Amirhamed HA. & Kamarul T., (2014) Advances of human bone marrow-derived mesenchymal stem cells in the treatment of cartilage defects: A systematic review. *Exp Biol Med*, 239(6), p663–669.

Gronthos, S. et al., (2001) Characterization of surface protein expression on human adipose tissue-derived stromal cells. *J Cell Physiol*, 189(1), p54–63.

Gronthos, S. et al., (1994) The STRO-1+ fraction of adult human bone marrow contains the osteogenic precursors. *Blood*, 84(12), p4164–4173.

Gronthos, S. et al., (2001) Integrin-mediated interactions between human bone marrow stromal precursor cells and the extracellular matrix. *Bone*, 28(2), p174–181.

Guidotti, S. et al., (2013) Enhanced osteoblastogenesis of adipose-derived stem cells on spermine delivery via β-catenin activation. *Stem Cells Dev*, 22(10), p1588–1601.

Enhanced osteoblastogenesis of adipose-derived stem cells on spermine delivery via β-catenin activation.

Hansen, A. et al., (2014) High-density polymer microarrays: Identifying synthetic polymers that control human embryonic stem cell growth. *Adv Healthc Mater*, 3(6), p848–853.

Hansen, A. et al., (2011) Polymers for the rapid and effective activation and aggregation of platelets. *Biomaterials*, 32(29), p7034–7041.

Hay, D.C. et al., (2011) Unbiased screening of polymer libraries to define novel substrates for functional hepatocytes with inducible drug metabolism. *Stem Cell Res*, 6(2), p92–102.

Heckmann, L. et al., (2006) Mesenchymal progenitor cells communicate via alpha and beta integrins with a three-dimensional collagen type I matrix. *Cells Tissues Organs*, 182(3-4), p143–154.

Heijkants, R.G.J.C. et al., (2006) Preparation of a polyurethane scaffold for tissue engineering made by a combination of salt leaching and freeze-drying of dioxane. *J Mater Sci*, 41(8), p2423–2428.

Hirokawa, Y. & Tanaka T., (1984) Volume phase transition in a nonionic gel. *J Chem Phys*, 81(12), p6379–6380.

Hook, A.L. et al., (2012) Combinatorial discovery of polymers resistant to bacterial attachment. *Nat Biotechnol*, 30(9), p868–875.

Hong, K.U. et al., (2004) Basal cells are a multipotent progenitor capable of renewing the bronchial epithelium. *Am J Patho*, 164(2), p577–588.

Hou, P. et al., (2013) Pluripotent stem cells induced from mouse somatic cells by small-molecule compounds. *Science*, 341(6146), p651–654.

Hu, Z., Zhang X. & Li Y., (1995) Synthesis and application of modulated polymer gels. *Science*, 269(5223), p525–527.

Huang, H.H. et al., (2009) Functional α1- and β2-adrenergic receptors in human osteoblasts. *J Cell Physiol*, 220(1), p267–275.

Hudson, J.E. et al., (2011) A defined medium and substrate for expansion of human mesenchymal stromal cell progenitors that enriches for osteoand chondrogenic precursors. *Stem Cells Dev*, 20(1), p77–87.

Hungerford, J.E. & Little, C.D., (1999) Developmental biology of the vascular smooth muscle cell: building a multilayered vessel wall. *J Vasc Res,* 36(1), p2–27.

Hsu Y.C. & Fuchs E. (2012) A family business: stem cell progeny join the niche to regulate homeostasis. *Nat Rev Mol Cell Biol*, 13(2), p103–114.

Imaizumi Y. et al., (2012) Mitochondrial dysfunction associated with increased oxidative stress and α-synuclein accumulation in PARK2 iPSC-derived neurons and postmortem brain tissue. *Mol Brain*, 5, p35.

Imaizumi, Y. & Okano, H., (2014) Modeling human neurological disorders with induced pluripotent stem cells. *J Neurochem*, 129(3), p388–399.

Imanishi, Y. et al., (2008) Allogenic mesenchymal stem cell transplantation has a therapeutic effect in acute myocardial infarction in rats. *J Mol Cell Cardiol*, 44(4), p662–671.

Inzana, J.A. et al., (2014) 3D printing of composite calcium phosphate and collagen scaffolds for bone regeneration. *Biomaterials*, 35(13), p4026–4034.

Isenmann, S. et al., (2009) TWIST family of basic helix-loop-helix transcription factors mediate human mesenchymal stem cell growth and commitment. *Stem Cells*, 27(10), p2457–2468.

Jaiswal, N. et al., (1997) Osteogenic differentiation of purified, culture-expanded human mesenchymal stem cells in vitro. *J Cell Biochem*, 64(2), p295–312.

James, A.W. et al., (2012) Perivascular stem cells: a prospectively purified mesenchymal stem cell population for bone tissue engineering. *Stem Cells Transl Med*, 1(6), p510–519.

Jiang, T. et al., (2010) Potent in vitro chondrogenisis of CD105 enriched human adipose-derived stem cells. *Biomaterials*, 31(13), p3564–3571.

Joly-Duhamel, C., Hellio, D. & Djabourov, M., (2002) All gelatin networks: 1.Biodiversity and physical chemistry. *Langmuir*, 18(19), p7208–7217

Jung, J. et al., (2012) 5,7-Dihydroxy-3,4,6-trimethoxyflavone inhibits intercellular adhesion molecule 1 and vascular cell adhesion molecule 1 via the Akt and nuclear factor-κB-dependent pathway, leading to suppression of adhesion of monocytes and eosinophils to bronchial epithelial cells. *Immunology*, 137(1), p98–113.

Jung, S. et al., (2010). Identification of growth and attachment factors for the serum-free isolation and expransion of human mesenchymal stromal cells. *Cytotherapy*, 12(5), p637–657.

Kan, C.W. et al., (2004) Thermoresponsive N,N-dialkylacrylamide copolymer blends as DNA sieving matrices with a thermally tunable mesh size. *Electrophoresis*, 25(7-8), p1007–1015.

Kanczler, J.M. et al., (2008) The effect of mesenchymal populations and vascular endothelial growth factor delivered from biodegradable polymer scaffolds on bone formation. *Biomaterials*, 29(12), p1892–1900.

Kaplan, M. & Hinds, J.W., (1977) Neurogenesis in the adult rat: electron microscopic analysis of light radioautographs. *Science*, 197(4308), p1092–1094.

Karlsson, C. et al., (2009) Human embryonic stem cell-derived mesenchymal progenitors-potential in regenerative medicine. *Stem Cell Res*, 3(1), p39–50.

Kasuya, J. & Tanishita, K., (2012) Microporous membrane-based liver tissue engineering for the reconstruction of three-dimensional functional liver tissues in vitro. *Biomatter*, 2(4), p290–295.

Katz, A.R. & Tumer R.J., (1970) Evaluation of tensile and absorption properties of polyglycolic acid sutures. *Surg Gynecol Obstet*, 131(4), p701.

Kehat, I. et al., (2001) Human embryonic stem cells can differentiate into myocytes with structural and functional properties of cardiomyocytes. *J Clin Invest*, 108(3), p407–414.

Kellenberger, S. et al., (1998) Formoterol and isoproterenol induce c-fos gene expression in osteoblast-like cells by activating β2-adrenergic receptors. *Bone*, 22(5), p471–478.

Kestendjieva, S. et al., (2008) Characterization of mesenchymal stem cells isolated from the human umbilical cord. *Cell Biol Int*, 32(7), p724–732.

Khalil, A.S., Xie, A.W. & Murphy, W.L. (2014) Context clues: The importance of stem cell–material interactions. *Chemical Biology*, 9(1), p45–56.

Kido, A. et al., (2012) Effect of mesenchymal stem cells on hypoxia-induced desensitization of β2-adrenergic receptors in rat osteosarcoma cells. *Oncol Lett*, 4(4), p745–750.

Kim, C.W. et al., (2012) Human lactoferrin suppresses TNF-α-induced intercellular adhesion molecule-1 expression via competition with NF-κB in endothelial cells. *FEBS Lett*, 586(3), p229–234.

Kim, H.A., Mindos T. & Parkinson D.B., (2013) Plastic fantastic: Schwann cells and repair of the peripheral nervous system. *Stem Cells Transl Med*, 2(8), p553–557.

Kisiday, J.D. et al., (2011) Expansion of mesenchymal stem cells on fibrinogen-rich protein surfaces derived from blood plasma. *J Tissu Eng Regen Med*, 5(8), p600–611.

Kortesidis, A. et al., (2005) Stromal-derived factor-1 promotes the growth, survival, and development of human bone marrow stromal stem cells. *Blood*, 105(10), p3793–3801.

Khan, F. et al., (2010) Strategies for cell manipulation and skeletal tissue engineering using high-throughput polymer blend formulation and microarray techniques. *Biomaterials*. 31(8), p2216–2228.

Kiel, M.J. et al., (2005) SLAM family receptors distinguish hematopoietic stem and progenitor cells and reveal endothelial niches for stem cells. *Cell*, 121(7), p1109–1121.

Kiel, M.J. et al., (2007) Haematopoietic stem cells do not asymmetrically segregate chromosomes or retain BrdU. *Nature*, 449(7159), p238–242.

Klees, R.F. et al., (2005) Laminin-5 induces osteogenic gene expression in human mesenchymal stem cells through an ERK-dependent pathway. *Mol Biol Cell*, 16(2), p881–890.

Koepsel, J.T. et al., (2012) Combinatorial screening of chemically defined human mesenchymal stem cell culture substrates. *J Mater Chem*, 22(37), p19474–19481.

Kopher, R.A. et al., (2010) Human embryonic stem cell-derived CD34+ cells function as MSC progenitor cells. *Bone*, 47(4), p718–28.

Kuang, S. et al., (2006) Distinct roles for Pax7 and Pax3 in adult regenerative myogenesis. *J Cell Biol*, 172(1), p103–113.

Kuang, S et al., (2007) Asymmetric self-renewal and commitment of satellite stem cells in muscle. *Cell*, 129(5), p999–1010.

Kunisaki, Y. et al., (2013) Arteriolar niches maintain haematopoietic stem cell quiescence. *Nature*, 502(7473), p637–643.

Lao, L.H. et al., (2011) Poly(lactide-co-glycolide)/ hydroxyapatite nanofibrous scaffolds fabricated by electrospinning for bone tissue engineering. *J Mater Sci Mater Med*, 22(8), p1873–1884.

Laurencin, C.T., Khan, Y. & El-Amin, S.F., (2006) Bone graft substitutes. *Expert Rev Med Devices*, 3(1), p49–57.

Lazarus, H.M. et al., (2005) Cotransplantation of HLA-identical sibling culture-expanded mesenchymal stem cells and hematopoietic stem cells in hematologic malignancy patients. *Biol Blood Marrow Transplant*, 11(5), p389–398.

Le Douarin, N.M. et al., (2004) Neural crest cell plasticity and its limits. *Development*, 131(19), p4637–4650.

Le, N. et al., (2005) Analysis of congenital hypomyelinating Egr2Lo/Lo nerves identifies Sox2 as an inhibitor of Schwann cell differentiation and myelination. *Proc Natl Acad Sci USA*, 102(7), p2596–2601.

Lee, M.W. et al., (2004) Mesenchymal stem cells from cryopreserved human umbilical cord blood. *Biochem Biophys Res Commun*, 16(1), p273–278.

Lee, R.H. et al., (2009) The CD34-like protein PODXL and α6-integrin (CD49f) identify early progenitor MSCs with increased clonogenicity and migration to infarcted heart in mice. *Blood*, 113(4), p816–826.

Li, O. et al., (2013) Human embryonic stem cell-derived mesenchymal stroma cells (hES-MSCs) engraft in vivo and support hematopoiesis without suppressing immune function: implications for off-the shelf ES-MSC therapies. *Plos One*, 8(1), e55319.

Li, W. et al., (2011b) Rapid induction and long-term self-renewal of primitive neural precursors from human embryonic stem cells by small molecule inhibitors. *Proc Natl Acad Sci*, 108(20), p8299–82304.

Li, Y. et al., (2011) Generation of iPSCs from mouse fibroblasts with a single gene, Oct4, and small molecules. *Cell Res*, 21(1), p196–204.

Liberski, A., Zhang, R. & Bradley, M., (2009) Inkjet fabrication of polymer microarrays and grids--solving the evaporation problem. *Chem Commun*, 21(3), p334–336.

Liu, J. et al., (2006) Functional interaction between peroxisome proliferator-activated receptor gamma and beta-catenin. *Mol Cell Biol*, 26(15), p5827–5837.

Liu, X., Holzwarth J.M. & Ma P.X., (2012) Functionalized synthetic biodegradable polymer scaffolds for tissue engineering. *Macromol Biosci*, 12(7), p911–919.

Liu Y. et al., (2013) Six1 regulates MyoD expression in adult muscle progenitor cells. *PLoS One*, 8(6), e67762.

Long, T. et al., (2014) The effect of mesenchymal stem cell sheets on structural allograft healing of critical sized femoral defects in mice. *Biomaterials*, 35(9), p2752–2759.

Ludwig, T.E. et al., (2006) Derivation of human embryonic stem cells in defined conditions. *Nat Biotechnol*, 24(2), p185–187

Lukasova, M. et al., (2011) Nicotinic acid inhibits progression of atherosclerosis in mice through its receptor GPR109A expressed by immune cells. *J Clin Invest*, 121(3), p1163–1173.

Macchiarini, P. et al., (2008) Clinical transplantation of a tissue-engineered airway. *Lancet*, 372(9662), p2023–2030.

Maden, M., (2007) Retinoic acid in the development, regeneration and maintenance of the nervous system. *Nat Rev Neurosci*, 8(10), p755–765.

Maheshwari, G. et al., (2000) Cell adhesion and motility depend on nanoscale RGD clustering. *J Cell Sci*, 113(10), p1677–1686.

Majumdar, MK. et al., (2000) Isolation, characterization, and chondrogenic potential of human bone marrow-derived multipotential stromal cells. *J Cell Physiol*, 185(1), p98–106.

Mant, A. et al., (2006) Polymer microarrays: identification of substrates for phagocytosis assays. *Biomaterials*, 27(30), p5299–5306.

Martin M.J. et al., (2005) Human embryonic stem cells express an immunogenic nonhuman sialic acid. *Nature Med*, 11(2), p228–232.

Mason, C., (2007) Regenerative Medicine 2.0. *Regenerative medicine*, 2, p11–18.

Mauney, J.R., Kaplan, D.L. & Volloch, V., (2004) Matrix-mediated retention of osteogenic differentiation potential by human adult bone marrow-derived mesenchymal stem cells during ex vivo expansion. *Biomaterials*, 25(3), p3233–3243.

Mauney, J.R., Volloch, V. & Kaplan, D.L., (2005) Matrix-mediated retention of adipogenic differentiation potential by human adult bone marrow-derived mesenchymal stem cells during ex vivo expansion. *Biomaterials*, 26(31), p6167–6175.

Maxson, S. et al., (2012) Concise review: role of mesenchymal stem cells in wound repair. *Stem Cells Transl Med*, 1(2), p142–149.

McBeath, R. et al., (2004) Cell shape, cytoskeletal tension, and RhoA regulate stem cell lineage commitment. *Developmental Cell*, 6(4), p483–495.

McKinnell, I.W. et al., (2008) Pax7 activates myogenic genes by recruitment of a histone methyltransferase complex. *Nat Cell Biol*, 10(1), p77–84.

McMurray, R.J. et al., (2011) Nanoscale surfaces for the long-term maintenance of mesenchymal stem cell phenotype and multipotency. *Nat Mater*, 10(8), p637–644.

Mehlhorn, A.T. et al., (2007) Differential effects of BMP-2 and TGF-beta1 on chondrogenic differentiation of adipose derived stem cells. *Cell Prolif*, 40(6), p809–823.

Mehlem, A. et al., (2013) Imaging of neutral lipids by oil red O for analyzing the metabolic status in health and disease. *Nat Protoc*, 8(6), p1149–1154.

Mei, Y. et al., (2010) Combinatorial development of biomaterials for clonal growth of human pluripotent stem cells. *Nat Mater*, 9(9), p768–778.

Mei, Y. et al., (2010b) A high throughput micro-array system of polymer surfaces for the manipulation of primary pancreatic islet cells. *Biomaterials*, 31(34), p8989–8995.

Melkoumian, Z. et al., (2010) Synthetic peptide-acrylate surfaces for long-term self-renewal and cardiomyocyte differentiation of human embryonic stem cells. *Nat Biotechnol*, 28(6), p606–610.

Méndez-Ferrer, S. et al., (2010) Mesenchymal and haematopoietic stem cells form a unique bone marrow niche. *Nature*, 466(7308), p829–834.

Mendes, S.C., Robin C. & Dzierzak E., (2005) Mesenchymal progenitor cells localize within hematopoietic sites throughout ontogeny. *Development*, 132(5), p1127–1136.

Mikami, Y. et al., (2011) CD271/P75ntr Inhibits the differentiation of mesenchymal stem cells into osteogenic, adipogenic, chondrogenic and myogenic lineages. *Stem Cells & Dev*, 20(5), p901–913.

Miller, J.S. et al., (2012) Rapid casting of patterned vascular networks for perfusable engineered three-dimensional tissues. *Nat Mater*, 11(9), p768–774.

Mizomoto, H., (2004) The synthesis and screening of polymer libraries using a high throughput approach. PhD Thesis, University of Southampton.

Morikawa, S. et al., (2009) Development of mesenchymal stem cells partially originate from the neural crest. *Biochem Biophys Res Commun*, 379(4), p1114–1119.

Moss, F.P. & Leblond, C., (1971) Satellite cells as the source of nuclei in muscles of growing rats. *Anat Rec*, 170(4), p421–435.

Murashov, A.K. et al., (2005) Directed differentiation of embryonic stem cells into dorsal interneurons. *FASEB J*, 19(2), p252–254.

Murray, I.R. et al., (2014) Natural history of mesenchymal stem cells, from vessel walls to culture vessels. *Cell Mol Life Sci*, 71(8), p1353–1374.

Nagahama, K., Ouchi, T. & Ohya, Y., (2008) Temperature-induced hydrogels through self-assembly of cholesterol-substituted star PEG-b-PLLA copolymers: an injectable scaffold for tissue engineering. *Adv Funct Mater*, 18(8), p1220–1231.

Numasawa, Y. et al., (2011) Treatment of human mesenchymal stem cells with angiotensin receptor blocker improved efficiency of cardiomyogenic transdifferentiation and improved cardiac function via angiogenesis. *Stem Cells*, 29(9), p1405–1414.

Nasef, A. et al., (2009) Selected Stro-1-enriched bone marrow stromal cells display a major suppressive effect on lymphocyte proliferation. *Int J Lab Hematol*, 31(1), p9–19.

Niehage, C. et al., (2011) The cell surface proteome of human mesenchymal stromal cells. *PLoS One*, 6(5), e20399.

Nery, A.A. et al., (2013) Human mesenchymal stem cells: from immunophenotyping by flow cytometry to clinical applications. *Cytometry A*, 83(1), p48–61.

Ngadaonye, J.I. et al., (2012) Photopolymerised thermo-responsive poly(N,N-diethylacrylamide)-based copolymer hydrogels for potential drug delivery applications. *J Polym Res*, 19, p9822–9837.

Ng, F. et al., (2008) PDGF, TGF-beta, and FGF signaling is important for differentiation and growth of mesenchymal stem cells (MSCs): Transcriptional profiling can identify markers and signaling pathways important in differentiation of MSCs into adipogenic, chondrogenic, and osteogenic lineages. *Blood*, 112(2), p295–307.

Nyeng, P. et al., (2008) FGF10 maintains distal lung bud epithelium and excessive signalling leads to progenitor state arrest, distalization, and goble cell metaplasia. *BMC Dev Biol*, 8(2).

Oguro, H. Ding, L. & Morrison, S.J., (2013) SLAM family markers resolve functionally distinct subpopulations of hematopoietic stem cells and multipotent progenitors. *Cell Stem Cell*, 13(1), p102–116.

Ouyang, J. et al., (2012) Hepatic differentiation of rat mesenchymal stem cells by a small molecule. *ChemMedChem*, 7(8), p1447–1452.

Owens, G.K., (1995) Regulation of differentiation of vascular smooth muscle cells. *Physiol Rev*, 75(3), p487–517.

Palaszynski, K.M. et al., (2004) Estriol treatment ameliorates disease in males with experimental autoimmune encephalomyelitis: implications for multiple sclerosis. *J Neuroimmunol*, 149(1-2), p84–89.

Panda, S. et al., (2012) Combined effects of quercetin and atenolol in reducing isoproterenol-induced cardiotoxicity in rats: possible mediation through scavenging free radicals. *Cardiovasc Toxicol*, 12(3), p235–242.

Panteleyev, A.A. & Bickers, D.R., (2006) Dioxin-induced chloracne--reconstructing the cellular and molecular mechanisms of a classic environmental disease. *Exp Dermatol*, 15(9), p705–730.

Park, I.H. et al., (2008) Disease-specific induced pluripotent stem cells. *Cell*, 134(5), p877–886.

Pegg, A.E. & McCann, P.P., (1982) Polyamine metabolism and function. *Am J Physiol*, 243(5), C212–221.

Peng, L. et al., (2008) Comparative analysis of mesenchymal stem cells from bone marrow, cartilage, and adipose tissue. *Stem Cells Dev*, 17(4), p761–773.

Pernagallo, S., Diaz-Mochon, J.J. & Bradley, M., (2009) A cooperative polymer-DNA microarray approach to biomaterial investigation. *Lab Chip*, 9(3), p397–403.

Pernagallo, S. et al., (2012) Novel biopolymers to enhance endothelialisation of intra-vascular devices. *Adv Healthc Mater*, 1(5), p646–656.

Pernagallo, S. et al., (2011) Colonising new frontiers—microarrays reveal biofilm modulating polymers. *J Mater Chem*, 21, p96–101.

Pevsner-Fischer, M., Levin, S. & Zipori, D., (2011) The origins of mesenchymal stromal cell heterogeneity. *Stem Cell Rev*, 7(3), p560–568.

Phelps, E.A. et al., (2010) Bioartificial matrices for therapeutic vascularisation. *Proc Natl Acad Sci*, 107(8), p3323–3328.

Pitchford, S.C. et al., (2009) Differential mobilization of subsets of progenitor cells from the bone marrow. *Cell Stem Cell*, 4(1), p62–72.

Pittenger, M.F. et al., (1999) Multilineage potential of adult human mesenchymal stem cells. *Science*, 284(5411), p143–147.

Pivoriuūnas, A. et al., (2010) Proteomic analysis of stromal cells derived from the dental pulp of human exfoliated deciduous teeth. *Stem Cells Dev*, 19(7), p1081–1093.

Polchert, D. et al., (2008) IFN-gamma activation of mesenchymal stem cells for treatment and prevention of graft versus host disease. *Eur J Immunol*, 38(6), p1745–1755.

Poole, K. et al., (2005) Molecular-scale topographic cues induce the orientation and directional movement of fibroblasts on two-dimensional collagen surfaces. *J Mol Biol*, 349(2), p380–386.

Quarto, R. et al., (2001) Repair of large bone defects with the use of autologous bone marrow stromal cells. *N Engl J Med*. 344(5), p385–386.

Ramsey, W.S., Hertl, W., Nowlan, E.D. & Binkowski, N,J., (1984) Surface treatments and cell attachment. *In Vitro*, 20(10), p802–808.

Reckhenrich, A.K. et al., (2014) Surgical sutures filled with adipose-derived stem cells promote wound healing. *PLoS One*, 9(3), e91169.

Rémy-Martin, J.P. et al., (1999) Vascular smooth muscle differentiation of murine stroma: a sequential model. *Exp Hematol*, 27(12), p1782–1795.

Ren, G. et al., (2010) Inflammatory cytokine-induced intercellular adhesion molecule-1 and vascular cell adhesion molecule-1 in mesenchymal stem cells are critical for immunosuppression. *J Immunol*, 184(5), p2321–2328.

Reyes, M. et al., (2002) Origin of endothelial progenitors in human postnatal bone marrow. *J Clin Invest*, 109(3), p337–346.

Richards, M. et al., (2002) Human feeders support prolonged undifferentiated growth of human inner cell masses and embryonic stem cells. *Nature Biotechnology*, 20(9), p933–936.

Robinson, D.P. & Klein, S.L., (2012) Pregnancy and pregnancy-associated hormones alter immune responses and disease pathogenesis. *Horm Behav*, 62(3), p263–271.

Rodin, S. et al., (2010) Long-term self-renewal of human pluripotent stem cells on human recombinant laminin-511. *Nat Biotechnol*, 28(6), p611–615.

Romagnoli, C., D'Asta, F. & Brandi, M.L., (2013) Drug delivery using composite scaffolds in the context of bone tissue engineering. *Clin Cases Miner Bone Metab*, 10(3), p155–161.

Roth, E.A. et al., (2004) Inkjet printing for high-throughput cell patterning. *Biomaterials*, 25(17), p3707–3715.

Rousseaux, C. et al., (2005) Intestinal antiinflammatory effect of 5-aminosalicylic acid is dependent on peroxisome proliferator-activated receptor-gamma. *J Exp Med*, 201(8), p1205–1215.

Ruel-Gariépy, E. & Leroux, J.C., (2004) In situ-forming hydrogels--review of temperature-sensitive systems. *Eur J Pharm Biopharm*, 58(2), p409–426.

Russel, K.C. et al., (2010) In vitro high-capacity assay to quantify the clonal heterogeneity in trilineage potentail of mesenchymal stem cells reveals a complex hierarchy of lineage commitment. *Stem cells*, 28(4), p788–798.

Schaller, M.D., (2010) Cellular functions of FAK kinases: insight into molecular mechanisms and novel functions. *J Cell Sci*, 123(7), p1007–1013.

Schugar, R.C. et al., (2009) High harvest yield, high expansion and phenotype stability of CD146 mesenchymal stromal cells from whole primitive human umbilical cord tissue. *J Biomed Biotech*, doi: 10.1155/2009/789526.

Serra, T. et al., (2013) 3D printed PLA-based scaffolds: a versatile tool in regenerative medicine. *Organogenesis*, 9(4), p239–244.

Sheng, H. et al., (2008) A critical role of IFNgamma in priming MSC-mediated suppression of T cell proliferation through up-regulation of B7-H1. *Cell Res*, 18(8), p846–857.

Shi, H. et al., (2013) Mesenspheres of neural crest-derived cells enriched from bone marrow stromal cell subpopulation. *Neurosci Lett*, 532, p70–75.

Silva, J. et al., (2008) Promotion of reprogramming to ground state pluripotency by signal inhibition. *PLoS Biol*, 6(10), e253.

Simmons, .P.J. & Torok-Storb, B., (1991) Identification of stromal cell precursors in human bone marrow by a Novel monoclonal antibody STRO-1. *Blood*, 78(1), p55–62.

Singer, N. & Caplan, A., (2011) Mesenchymal stem cells: Mechanisms of inflammation. *Annu Rev Pathol Mech Dis*, 6, p457–478.

Singh, K.P. et al., (2009) The aryl hydrocarbon receptor has a normal function in the regulation of hematopoietic and other stem/progenitor cell populations. *Biochem Pharmacol*, 77(4), p577–587.

Smart, I. & Leblond, C., (1961) Evidence for division and transformations of neuroglia cells in the mouse brain, as derived from radioautography after injection of thymidine-H3. *J Comp Neurol*, 116(3), p349–367.

Soleimani, V.D. et al., (2012) Snail regulates MyoD binding-site occupancy to direct enhancer switching and differentiation-specific transcription in myogenesis. *Mol Cell*, 47(47), p457–468.

Song, H. et al., (2011) Cardiomyocytes from phorbol myristate acetate-activated mesenchymal stem cells restore electromechanical function in infarcted rat hearts. *Proc Natl Acad Sci*, 108(1), p296–301.

Song, J.J. et al., (2013) Regeneration and experimental orthotopic transplantation of a bioengineered kidney. *Nat Med*, 19(5), p646–651.

Sottile, V., Thomson, A. & McWhir, J., (2003) In vitro osteogenic differentiation of human ES cells. *Cloning Stem Cells*, 5(2), p149–155.

Spangrude, G.J., Heimfeld, S. & Weissman, I.L., (1988) Purification and characterization of mouse hematopoietic stem cells. *Science*, 241(4861), p58–62.

Sugiyama, T. et al., (2006) Maintenance of the hematopoietic stem cell pool by CXCL12-CXCR4 chemokine signaling in bone marrow stromal cell niches. *Immunity*, 25(6), p977–988.

Sukumaran, V. et al., (2011) Telmisartan ameliorates experimental autoimmune myocarditis associated with inhibition of inflammation and oxidative stress. *Eur J Pharmacol*, 652(1-3), p126–135.

Sun, J.Y. et al., (2012) Highly stretchable and tough hydrogels. *Nature*, 489(7414), p133–136.

Takashima, Y. et al., (2007) Neuroepithelial cells supply an initial transient wave of MSC differentiation. *Cell*, 129(7), p1377–1388.

Takahashi, K**.** & Yamanaka, S., (2006) Induction of pluripotent stem cells from mouse embryonic and adult fibroblast cultures by defined factors. *Cell*, 126(4), p663–676.

Takahashi, K. et al, (2007) Induction of pluripotent stem cells from adult human fibroblasts by defined factors. *Cell*, 131(5), p861–872.

Tare, R.S. et al., (2009) A microarray approach to the identification of polyurethanes for the isolation of human skeletal progenitor cells and augmentation of skeletal cell growth. *Biomaterials*, 30(6), p1045–1055.

Tarkowski, A.K., (1959) Experiments on the development of isolated blastomers of mouse eggs. *Nature*, 184, p1286–1287.

Tiwari-Woodruff, S. & Voskuhl, R.R., (2009) Neuroprotective and anti-inflammatory effects of estrogen receptor ligand treatment in mice. *J Neurol Sci*, 286(1-2), p81–85.

Thomson, J.A. et al., (1998) Embryonic stem cell line from human blastocysts. *Science*, 282(5395), p1145–1147.

Tiftikcioglu, B.I. et al., (2012) Neurosteroid Hormones Modulate the Differentiation of Adult Human Multipotent Mesenchymal Stromal Cells. *J Stem Cell Res Ther*, S4:003.

Tobita, M. & Mizuno, H., (2013) Adipose-derived stem cells and periodontal tissue engineering. Int J Oral Maxillofac Implants, 28(6), e487–493.

Tourniaire, G. et al., (2006) Polymer microarrays for cellular adhesion. *Chem Commun*, 20, p2118–2120

Trappmann, B. et al., (2012) Extracellular-matrix tethering regulates stem-cell fate. *Nat Mater*, 11(7), p642–649.

Tropepe, V. et al., (2001) Direct neural fate specification from embryonic stem cells: a primitive mammalian neural stem cell stage acquired through a default mechanism. *Neuron*, 30(1), p65–78.

Tropel, P. et al., (2006) Functional neuronal differentiation of bone marrow-derived mesenchymal stem cells. *Stem Cells*, 24(12), p2868–2876.

Tsutsui, H. et al., (2011) An optimized small molecule inhibitor cocktail supports long-term maintenance of human embryonic stem cells. *Nat Commun*, 2, p167.

Uccelli, A. & Prockop D.J., (2010) Why should mesenchymal stem cells (MSCs) cure autoimmune disease? *Current Opinion in Immunology*, 22(6), p768–774.

Uygun, B.E. et al., (2010) Organ reengineering through development of a transplantable recellularized liver graft using decellularized liver matrix. *Nat Med*, 16(7), p814–820.

Van Strien, M.E. et al., (2014) Isolation of neural progenitor cells from the human adult subventricular zone based on expression of the cell surface marker CD271. *Stem Cells Transl Med*, 3(4), p470–480.

Van Vlierberghe, S., Dubruel P. & Schacht E., (2011) Biopolymer-based hydrogels as scaffolds for tissue engineering applications: a review. *Biomacromolecules*, 12(5), p1387–408.

Volckaert, T., Cambell, A. & De Langhe, S., (2013) c-Myc regulates proliferation and Fgf10 expression in airway smooth muscle after airway epithelial injury in mouse. *PLoS One*, 8(8), e71426.

Wakitani, S., Saito, T. & Caplan, A.I., (1995) Myogenic cells derived from rat bone marrow mesenchymal stem cells exposed to 5-azacytidine. *Muscle Nerve*, 18(12), p1417–1426.

Walsh, S. et al., (2000) Expression of the developmental markers stro-1 and alkaline phosphatase in cultures of human marrow stromal cells: Regulation by fibroblast growth factor (FGF)-2 and relationship to the expression of FGF receptors 1-4. *Bone*, 27(2), p185–195.

Walsh, S. et al., (2001) High concentrations of dexamethasone suppress the proliferation but not the differentiation or further maturation of human osteoblast precursors in vitro: relevance to glucocorticoid-induced osteoporosis. *Rheumatology*, 40(1), p74–83.

Wang, H. et al., (2004) Mesenchymal stem cells in the Wharton's jelly of the human umbilical cord. *Stem Cells*, 22(7), p1330–1337.

Wells, L.A. et al., (2011) Generic, anthracene-based hydrogel crosslinkers for photo-controllable drug delivery. *Macromol Biosci*, 11(7), p988–998.

Winton, D,.J. & Ponder B.A., (1990) Stem-cell organization in mouse small intestine. *Proc Biol Sci*, 241(1300), p13–18.

Wischerhoff, E. et al., (2000) Direct Observation of the Lower Critical Solution Temperature of Surface-Attached Thermo-Responsive Hydrogels by Surface Plasmon Resonance. *Angew Chem*, 39(24), p4602–4604.

Wu, M., Bridle, H. & Bradley, M., (2012) Targeting Cryptosporidium parvum capture. *Water Res*, 46(6), p1715–1722.

Wu, X. et al., (2002) A small molecule with osteogenesis-inducing activity in multipotent mesenchymal progenitor cells. *J Am Chem Soc*, 124(49), p14520–14521.

Yang, MT. et al., (2011) Assaying stem cell mechanobiology on microfabricated elastomeric substrates with geometrically modulated rigidity. *Nat Protoc*, 6(2), p187–213.

Yang, C. et al., (2014) Mechanical memory and dosing influence stem cell fate. *Nat Mater*, 13(6), p645–652.

Yannarelli, G. et al., (2014) Donor mesenchymal stromal cells (MSCs) undergo variable cardiac reprogramming in vivo and predominantly co-express cardiac and stromal determinants after experimental acute myocardial infarction. *Stem Cell Rev*, 10(2), p304–315.

Yin, X., Hoffman, A.S. & Stayton, P.S., (2006) Poly(N-isopropylacrylamide-co-propylacrylic acid) copolymers that respond sharply to temperature and pH. *Biomacromolecules*, 7(5), p1381–1385.

Younger, E.M. & Chapman, M.W., (1989) Morbidity at bone graft donor sites. *J Orthop Trauma*, 3(3), p192–195.

Youssef, W., Wickett, R.R. & Hoath S.B., (2001) Surface free energy characterization of vernix caseosa. Potential role in waterproofing the newborn infant. *Skin Res Technol*, 7(1), p10–17.

Zammit, P.S., Partridge, T.A. &, Yablonka-Reuveni, Z., (2006) The skeletal muscle satellite cell: the stem cell that came in from the cold. *J Histochem Cytochem*, 54(11), p1177–1191.

Zannettino, A.C.W. et al., (2008) Multipotential human adipose-derived stromal stem cells exhibit a perivascular phenotype in vitro and in vivo. *J Cell Physiol*, 214(2), p413–421

Zeng, X. et al., (2004) Dopaminergic differentiation of human embryonic stem cells. *Stem Cells*, 22(6), p925–940.

Zhang, R. et al., (2008). Inkjet fabrication of hydrogel microarrays using in situ nanolitre-scale polymerisation. *Chem Commun*, 21, p1317–1319.

Zhang, R. et al., (2009) Microarrays of over 2000 hydrogels-identification of substrates for cellular trapping and thermally triggered release. *Biomaterials*, 30(31), p6193–6201.

Zhang, R. et al., (2013) A thermoresponsive and chemically defined hydrogel for long-term culture of human embryonic stem cells. *Nature Comm*, 4, p1335–1342.

Zhao, X. et al., (2014) In vitro vascularization of a combined system based on a 3D printing technique. *J Tissue Eng Regen Med*. doi: 10.1002/term.1863. [Epub ahead of print]

Zhu, S. et al., (2009) Spermine protects mice against lethal sepsis partly by attenuating surrogate inflammatory markers. *Mol Med*, 15(7-8), p275–282.

Zuk, P.A. et al., (2001) Multilineage cells from human adipose tissue: implications for cell-based therapies. *Tissue Eng*, 7(2), p211–226.

Zuckerman, LA., Pullen, L. &, Miller, J., (1998) Functional consequences of costimulation by ICAM-1 on IL-2 gene expression and T cell activation. *J Immunol*, 160(7), p3259–3268.

APPENDICES

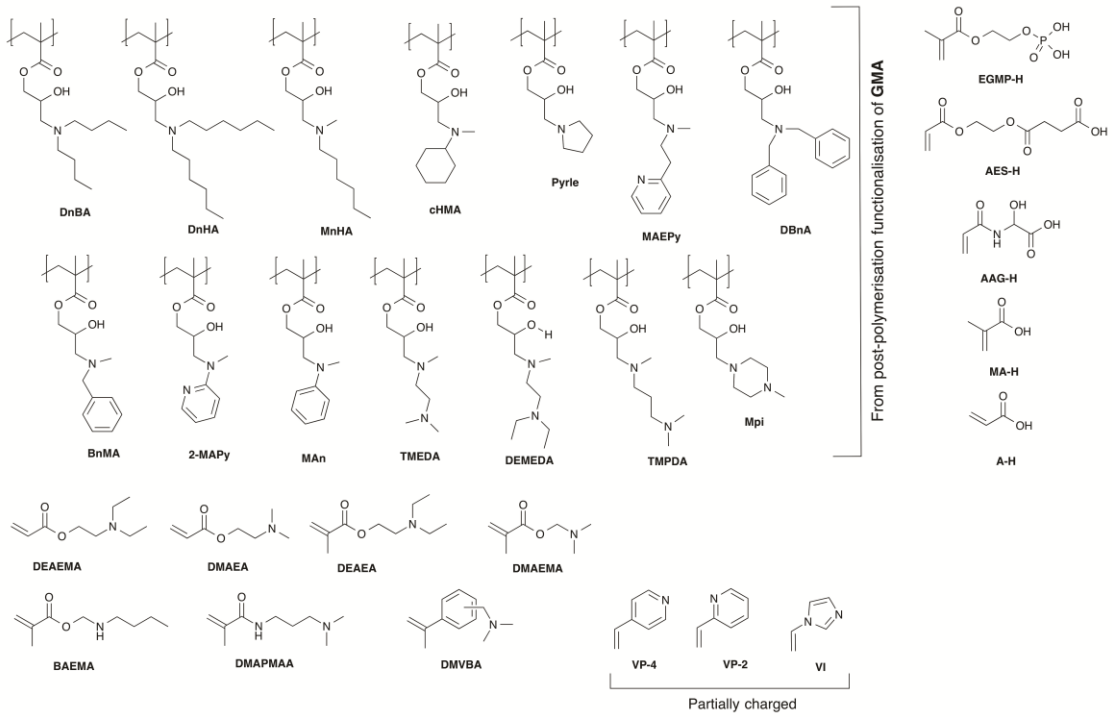

Appendix 1.1A Charged monomers in the "PA" library Monomers that are likely to be positively charged at physiological pH.

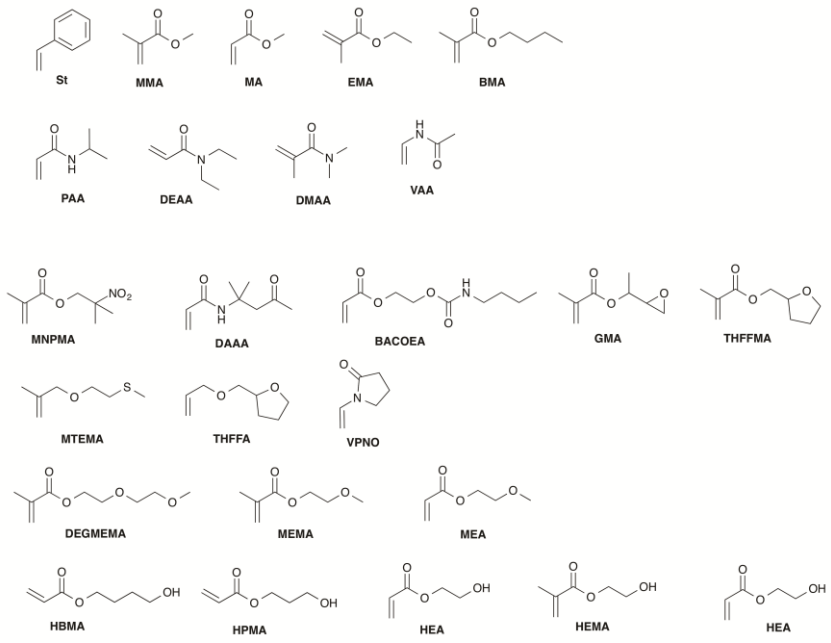

Appendix 1.1B Other "PA" library monomers – Monomers with varying degrees of hydrophilicity/hydrophobicity.

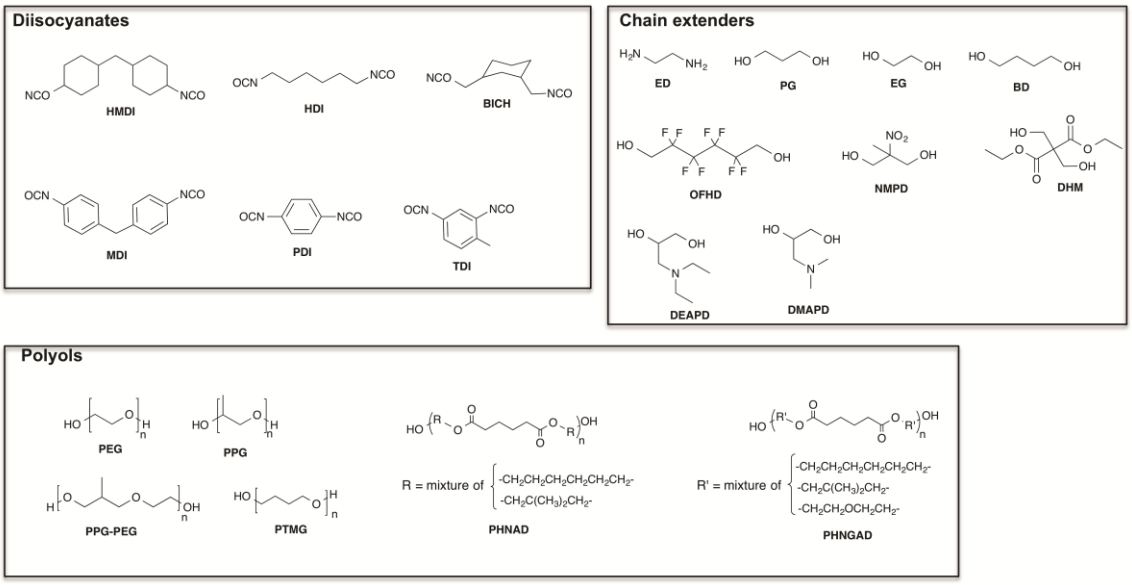

Appendix 1.1C Monomers used to construct the PU library.

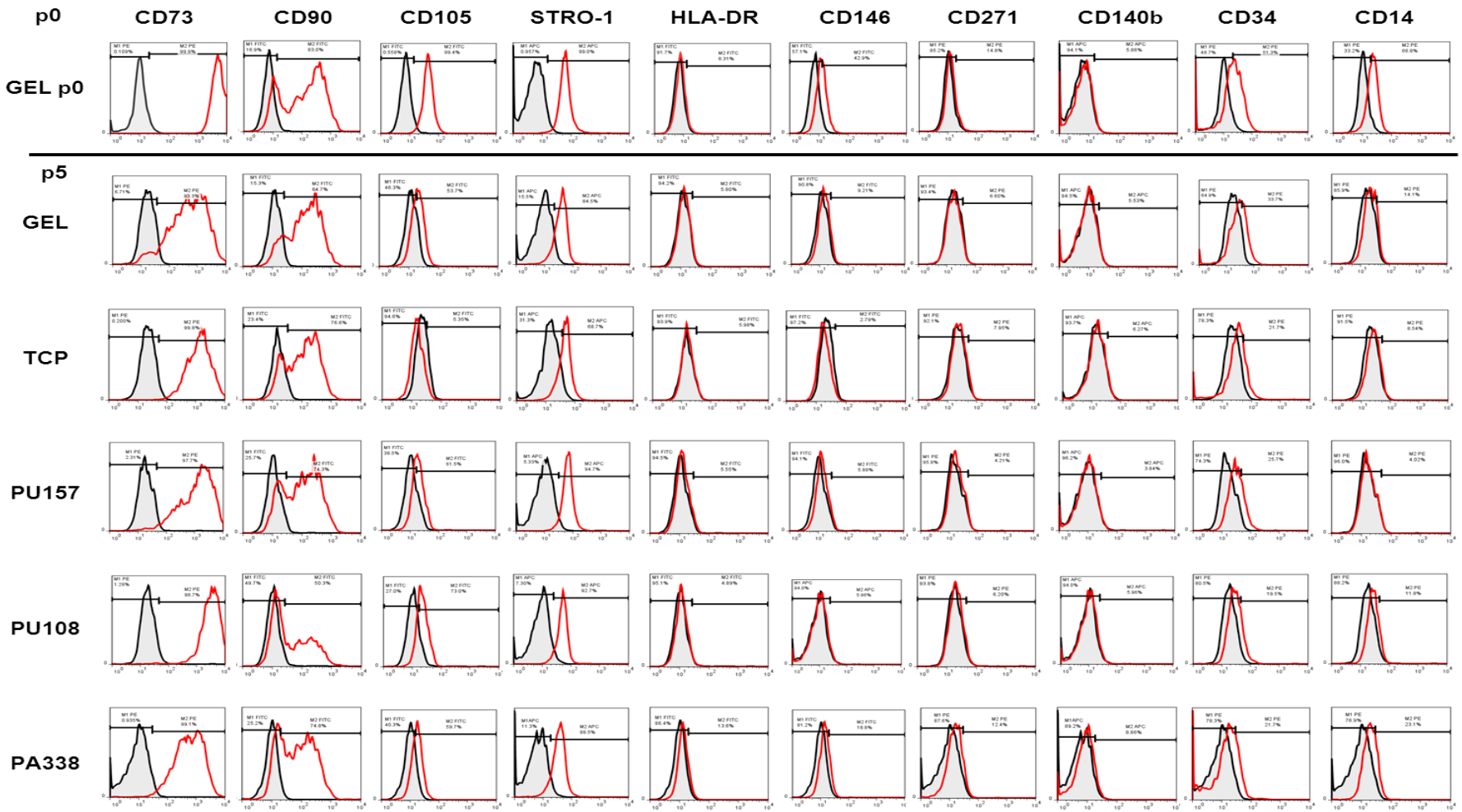

Appendix 2.1. *Representative flow cytometry traces for hES-MPs stained with 10 MSC markers at 'passage 0' (p0) prior to long term culture, and after 5 passages (p5) on gelatin (GEL), tissue culture plastic (TCP),* ***PU157****,* ***PU108*** *and* ***PA338****. The red trace represents the stained cells and the black shaded trace represents the unstained cells for that substrate (n = 3).*

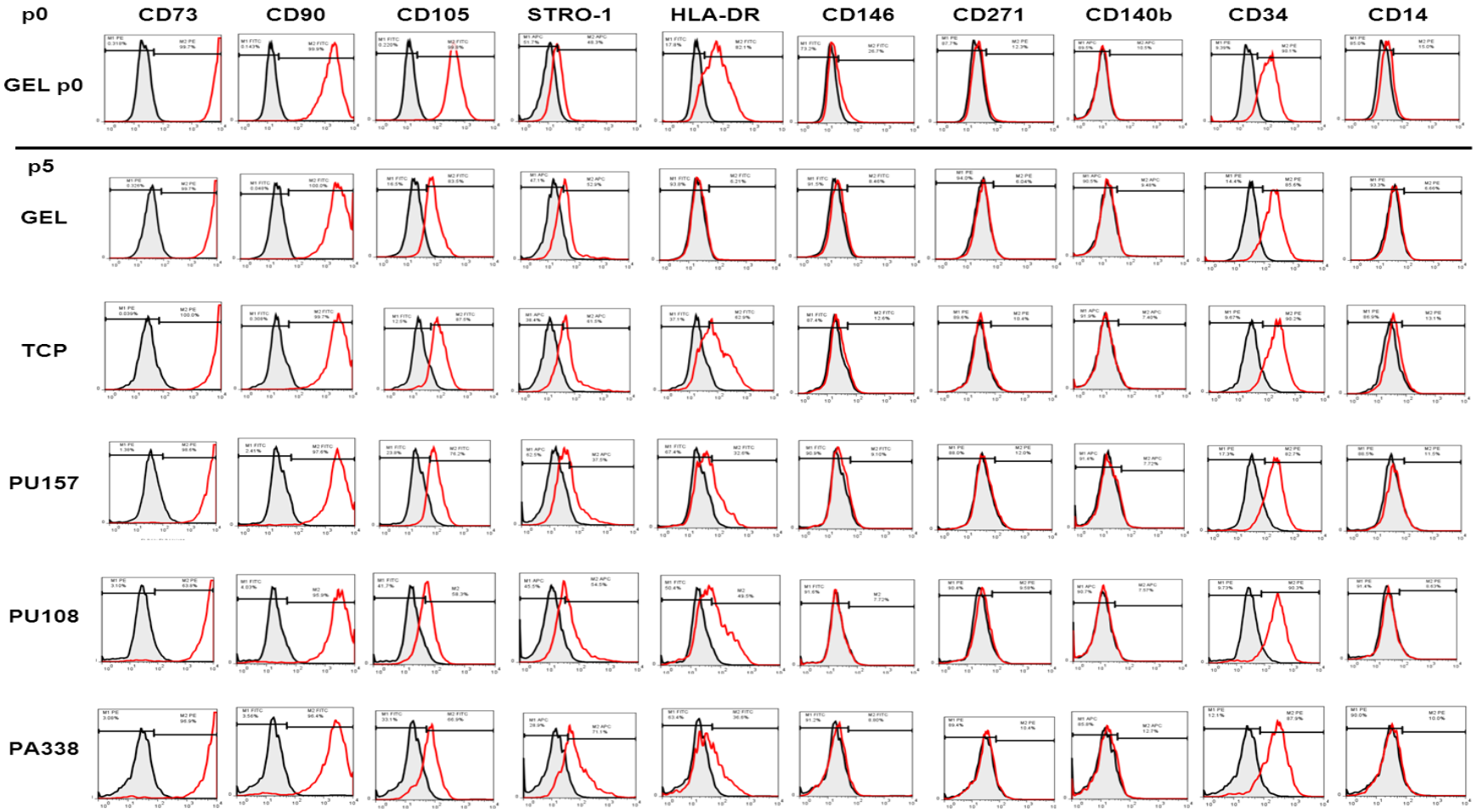

***Appendix 2.2**. Representative flow cytometry traces for ADMSCs stained with 10 MSC markers at 'passage 0' (p0) prior to long term culture, and after 5 passages (p5) on gelatin (GEL), tissue culture plastic (TCP), **PU157**, **PU108** and **PA338**. The red trace represents the stained cells and the black shaded trace represents the unstained cells for that substrate (n = 3).*

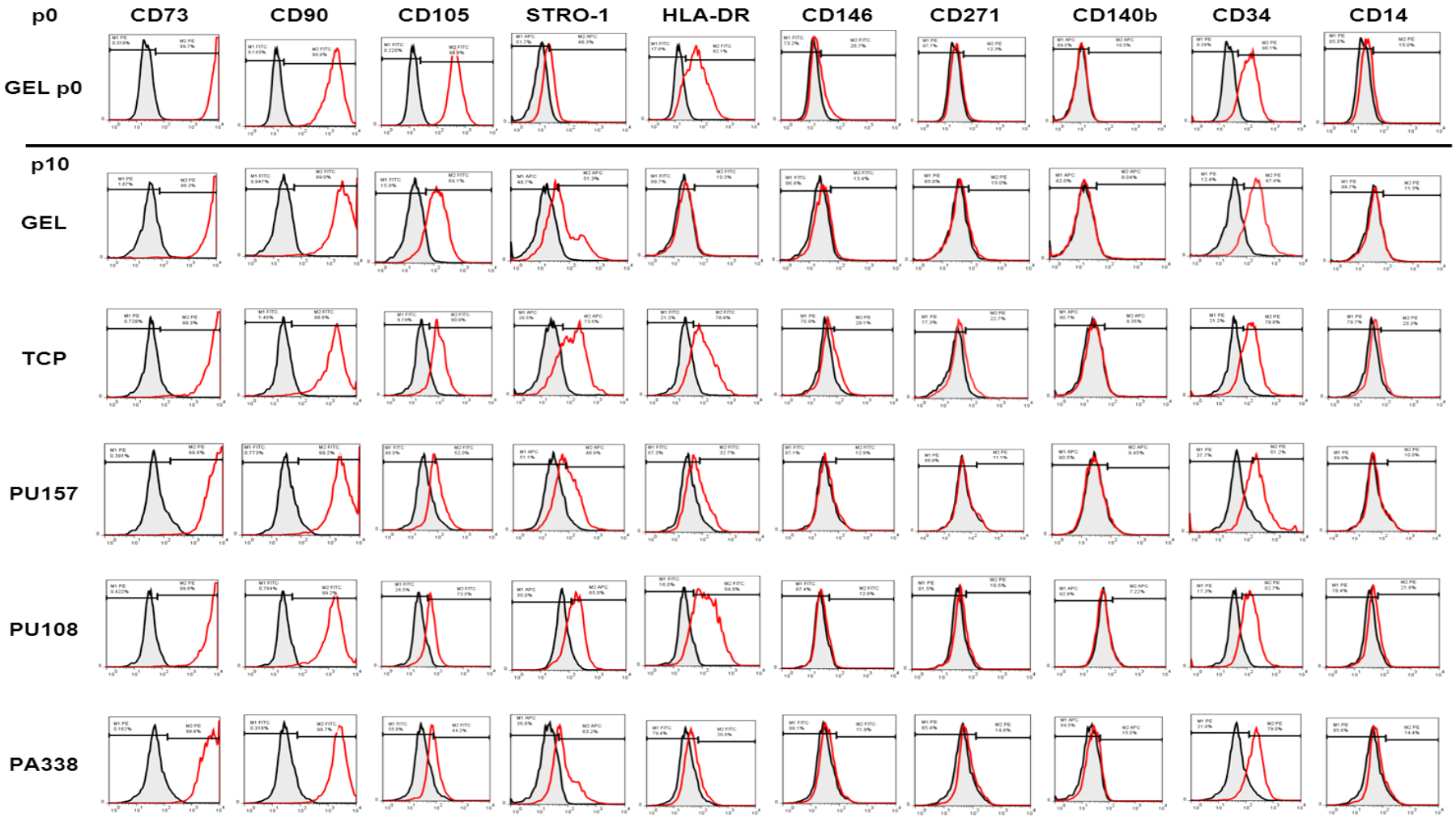

***Appendix 2.3**. Representative flow cytometry traces for ADMSCs stained with 10 MSC markers at 'passage 0' (p0) prior to long term culture, and after 10 passages (p10) on gelatin (GEL), tissue culture plastic (TCP), **PU157**, **PU108** and **PA338**. The red trace represents the stained cells and the black shaded trace represents the unstained cell for that substrate (n = 3).*

Appendix 3: Gene expression

Genes expressed selectively in MSC (n = 3) compared with fibroblasts, osteoblasts, chondrocytes and adipocytes (n = 3). The criterion of selection was a more than twofold higher expression in MSC than in any of the other cells.

Fold average and Gene name

Over 100-fold CHI3L1, FLG, KRT19

30–100-fold DGKG, F2RL1, HB2B, KRT18, KRTAP1-1, LOC401097, SLC14A1

15–30-fold CDCP1, CFI, CNTNAP3, FRMD5, GATA6, HNT, KRTAP1-5, KRTAP2–2, KRTHA4,LOC285758, LOC389734, LYPDC1, RARRES1, RGS4, SOX11, TRPC4

10–15-fold CD33L3, DCBLD2, ENG, ESM1, IFI30, IL6, LOC152742, LOXL2, LXN, PAK3, RAB27B,RAC2, TGM2, ZNF423

5–10-fold ADAMTS1, ARHGAP22, BDNF, BRCC2, C13orf31, CCL26, CCND1, CCNE2, CPA4, EGFL3, ETV1, FAM40B, HECW2, HGF, HMGA2, IER3, ITGA2, KCTD16, KIAA0746, KIAA1913, KLF12, KRTAP2-1, LAMA3, LOC157693, LOC399947, LRB2BP, MET, NALP1, NETO2, NTN4, PASK, PDE5A, PLCXD2, PODXL, PRDM16, SAMD3, SLC16A4, SLC4A4, SLC9A7, SMURF2, TFPI2, TMEM166

2–5-fold ABHD2, ABI3BP, ADAMTS5, ADD3, ADORA1, ARL7, ATP6V1G3, BRIP1, C1GALTI, C5orf13, C6orf105, CAMK2D, CAPZA1, CDC25A, CDH6, CPNE8, DKFZp313A2432, DKFZp761P0423, EDEM1, ETV5, FAM36A, FAM44A, FCHSD2, FHL2, FN1, FLJ35409, FOXP1, GDF15, GLIPR1, HTR7, HRB2, IGFBP3, KIAA1189, KIAA1946, KIF18A, LAMA1, LOX, MALAT1, MAP4K4, MCFD2, MCOLN3, MSCP2, NEK7, NHS, NUPL1,OCIAD2, PAPPA2, PHLDB2, PKIA, PLAC3, PSCDBP, RAMP, SH3RF1, SIM2, SKI, SLC25A37, SLC26A4, SLC30A7, SLC4A4, SMC2L1, SMYD3, SNK25, SSH1, TMEM49,UGCG, VEGFC, VMP1

Appendix 4.1 Small molecule library

CODE	SMALL MOLECULE
c1160	HYDOXYBUTANOIC ACID / Γ-HYDROXYBUTYRIC ACID SODIUM SALT
c1161	HYDROXY-L-TRYPTOPHAN
c1162	ALLOPURINOL
c1163	TOCOPHEROL
c1164	4-AMINOANTIPYRINE, REAGENT GRADE, AMINOPHENAZONE, US WITHDRAWN
c1165	AMINOSALICYLIC ACID
c1166	DL-AMPHETAMINE SULFATE SALT
c1167	ATENOLOL
c1168	NAPHTHOL
c1169	BEZAFIBRATE
c1170	BROMHEXINE HYDROCHLORIDE
c1171	CARBAMOYLCHOLINE CHLORIDE
c1172	CHLORPROPAMIDE
c1173	CURCUMIN
c1174	CYPROHEPTADINE HYDROCHLORIDE
c1175	DECAMETHONIUM BROMIDE
c1176	DEQUALINIUM CHLORIDE HYDRATE
c1177	DIAZOXIDE
c1178	DICLOFENAC (NA SALT)
c1179	DILTIAZEM HCL
c1180	DIMENHYDRINATE
c1181	DIPYRIDAMOLE
c1182	FAMOTIDINE
c1183	GEMFIBROZIL
c1184	GLICLAZIDE
c1185	HALOPERIDOL.
c1186	HEXAMETHONIUM BROMIDE
c1187	HISTAMINE DIHYDROCHLORIDE
c1188	HYDRALAZINE
c1189	HYDROCHLOROTHIAZIDE
c1190	HYDROXYZINE PAMOATE (2 PARTS)
c1191	IBUPROFEN
c1192	INDOMETHACIN
c1193	INOSINE
c1194	ISONIAZIDE
c1195	LEVODOPA
c1196	MOXISYLYTE HYDROCHORIDE
c1197	NILUTAMIDE
c1198	NIZATIDINE
c1199	OUABAIN OCTAHYDRATE
c1200	PENTOBARBITAL NA SALT
c1201	PENTOXIFYLLINE

c1202	PHENYLEPHRINE HYDROCHLORIDE
c1203	PILOCARPINE HCL
c1204	PIPERINE
c1205	PRIMAQUINE BISPHOSPHATE
c1206	PRIMIDONE
c1207	PUTRESCINE DIHCL
c1208	PYRIDOXINE
c1209	QUERCETIN
c1210	RIBOFLAVIN
c1211	SULFASALAZINE
c1213	TANNIC ACID
c1214	TETRAHYDROZOLINE HYDROCHLORIDE
c1215	TOLAZAMIDE
c1216	TOLFENAMIC ACID
c1217	VALPROIC ACID NA SALT
c1218	VERAPAMIL HYDROCHLORIDE
c1219	YOHIMBINE HYDROCHLORIDE
c1220	AMINO-3-HYDROXYBUTYRIC ACID
c1221	ESTRIOL
c1222	MEGESTROL ACETATE
c1223	BERBERINE CHLORIDE
c1224	ACARBOSE
c1225	SIBUTRAMINE HCL
c1226	CHLOROQUINE DIPHOSPHATE SALT
c1227	ENALAPRIL MALEATE
c1228	CINNARIZINE
c1229	S-(+)-CHLORPHENIRAMINE MALEATE SALT
c1230	OLMESARTAN MEDOXOMIL
c1231	TETRAETHYLTHIURAM DISULFIDE
c1232	OMEPRAZOLE
c1233	RETINOIC ACID (CONTROL)
c1234	BIFONAZOLE
c1235	CANRENONE
c1236	CHLORHEXIDINE ACETATE
c1237	CLOPIDOGREL SULFATE
c1238	ANIRACETAM
c1239	BECLOMETHASONE DIPROPIONATE
c1240	BENFORIAMINE
c1241	CHLORPROMAZINE
c1242	DIACEREIN
c1243	BIS(2,2,2-TRIFLUOROETHYL) ETHER
c1244	PHENFORMIN HCL
c1245	TAMOXIFEN CITRATE
c1246	TELMISARTAN
c1247	THALIDOMIDE
c1249	AMANTADINE HYDROCHLORIDE
c1250	AMILORIDE HYDROCHLORIDE
c1251	TESTOSTERONE
c1252	METOPROLOL (+)-TARTRATE SALT
c1253	SULFAGUANIDINE
c1254	FLUOROURACIL

c1255	PHENYL-1,3-INDANDIONE
c1256	QUINACRINE DIHCL
c1257	PROTAMINE SULFATE SALT FROM SALMON
c1258	FLUORO-ALPHA-METHYL-4-BIPHENYLACETIC ACID
c1259	VALSARTAN
c1260	CLORSULON
c1261	METFORMIN - HCL
c1262	ROFECOXIB
c1263	ISOTRETINOIN
c1264	PERINDOPRIL ERBUMINE
c1265	TADALAFIL
c1266	AMINO-6-(TRIFLUOROMETHOXY) BENZOTHIAZOLE
c1267	M-HYDROXYPHENYL ACETATE
c1270	NICOTINE DITARTRATE
c1272	PREDNISOLONE
c1273	TAURINE
c1277	QUINAZOLINAMINE
c1280	CHLORZOXAZONE
c1281	FENOFIBRATE
F422	BIOTIN
F423	CEPHALOTHIN SODIUM
F424	CHOLECALCIFEROL
F425	CLOFIBRATE
F426	ERGOCALCIFEROL
F427	GLIBENCLAMIDE
F428	HEPARIN NA
F429	L-NORADRENALINE
F430	MEXILETINE HYDROCHLORIDE
F431	SYNEPHRINE
F432	D-PANTETHINE
F433	D-PANTHENOL
F434	PERPHENAZINE
F435	SPERMIDINE
F436	SPERMINE
F437	SULFISOXAZOLE
F438	SULPIRIDE
F440	TRIMEBUTINE MALEATE
F441	TRIPROLIDINE HYDROCHLORIDE
F442	BUSPIRONE HYDROCHLORIDE.
F443	ESTRADIOL
F444	BACLOFEN
F445	CIMETIDINE
F447	EPINEPHRINE
F448	DESIPRAMINE HYDROCHLORIDE
F449	CODEINE
f450	TRANS-2-PHENYLCYCLOPROPYLAMINE HYDROCHLORIDE
f451	PINDOLOL
f452	L-THYROXINE
F453	TROPICAMIDE
F454	NEOMYCIN SOLUTION
F455	PHOSPHOMYCIN DISODIUM
FF167	HYALURONIC ACID NA SALT

FF168	OLEIC ACID
FF169	RETINYL ACETATE
FF170	TETRACYCLINE HCL
FF171	TRIFLUOPERAZINE DIHYDROCHLORIDE
FF172	LEVONORGESTREL
FF173	DL-HOMOCYSTEINE ?(EXPENSIVE)
A111	D-THREONINE
A139	D-SERINE
A200	AMINOCAPROIC ACID
Aminobutyric acid	GAMMA-AMINOBUTYRIC ACID
Aminothiazole	AMINOTHIAZOLE
Asprin	ACETYL SALICYLIC ACID (ASPRIN)
B68	UREA
c145	BENZOIC ACID
c17	ADENINE
c240	HYDROQUINONE.
c398	CHOLINE CHLORIDE
Caf	CAFFEINE
Clotrimazole	CLOTRIMAZOLE
D-Glucosamine HCl	D-GLUCOSAMINE HYDROCHLORIDE
Ethyl paraben	ETHYL PARABEN (ETHYL 4-HYDROXYBENZOATE)
F228	TACRINE HYDROCHLORIDE
Fampridine	FAMPRIDINE (4-PYRINAMINE)
Fe(NO3)3	FE+++ FERRIC NITRATE
Gly	GLYCEROL
Li	LICL
Menadione	MENADIONE
Mesna	MESNA (2-MERCAPTOETHANESULFONIC ACID)
Methimazole	METHIMAZOLE
Niacin	NIACIN (NICOTINIC ACID)
Prasterone	PRASTERONE (TRANS-DEHYDROXYANDROSTERONE)
Quin	QUININE SEMISULFATE.H2O
Sulfanilamide	SULFANILAMIDE
Thiamine	THIAMINE MONOPHOSPHORIC ACID CHLORIDE
Vitamine C	ASCORBIC ACID
ZnCl2	ZN++ (ZINC CHLORIDE)
PIRACETAM	PIRACETAM
Benzoperoxide	BENZOPEROXIDE
Acetaminophen	ACETAMINOPHEN
Acetylcysteine	ACETYLCYSTEINE (H2O)
Mannitol	D-MANNITOL
c1292	PYRIDINE-2,5-DICARBOXYLIC ACID
c1306	CHROMIUM(III) CHLORIDE

Appendix 4.2. Selected candidates from first screen

Table 4.2.1 *– Drugs showing a statistically significant improvement over vehicle control for growth (DAPI) or marker expression (% STRO-1) and/or morphology at a concentration of 1 μM.*

Small Molecule (1μM)	n	Mean Nuclei Count	STDEV	P	% Stro1 positive cells	STDEV	P	Morphology
C1182 Famotidine	4	1964.5	43.1	P<0.01 w.r.t. DMSO control	76.3	4.2		Fibroblast
C1168 Naphthol	4	1929.8	408	P<0.01 w.r.t. DMSO control	74.5	10.4		Fibroblast
C1192 Indomethacin	4	1927.3	134.9	P<0.01 w.r.t. DMSO control	75.8	1.3		Fibroblast
C1173 Curcumin	4	1845.5	234.9	P<0.01 w.r.t. DMSO control	76.2	3.4		Fibroblast
C1162 Allopurinol	4	1843	94.8	P<0.01 w.r.t. DMSO control	76.6	7.7		Fibroblast
C1178 Diclofenac (Na Salt)	4	1835.3	159.3	P<0.01 w.r.t. DMSO control	79.1	3.9		Fibroblast
C1183 Gemfibrozil	4	1798.8	236.8	P<0.01 w.r.t. DMSO control	74	4.1		Fibroblast
C1190 Hydroxyzine Pamoate	4	1781	198.8	P<0.01 w.r.t. DMSO control	73.8	5.4		Fibroblast
C1186 Hexamethonium Bromide	4	1751	125	P<0.01 w.r.t. DMSO control	76.3	4.5		Fibroblast
C1167 Atenolol	4	1745	171.3	P<0.01 w.r.t. DMSO control	72.1	6.2		Fibroblast
C1189	4	1712	189.6	P<0.01 w.r.t.	70.8	4.3		Fibroblast

Hydrochlorothiazide				DMSO control				
C1163 Tocopherol	4	1695	242.3	P<0.05 w.r.t. DMSO control	72	5.5		Fibroblast
C1179 Diltiazem HCl	4	1656.8	293.7	P<0.05 w.r.t. DMSO control	76.7	4.2		Fibroblast
C1209 Quercetin	4	1645.5	78.4	P<0.05 w.r.t. DMSO control	69.9	1.9		Fibroblast
C1184 Gliclazide	4	1623.5	190.1	P<0.05 w.r.t. DMSO control	72.5	4.5		Fibroblast
C1264 Perindopril Erbumine	4	422.5	492.5		87	10.7	P<0.01 w.r.t. DMSO control	Variable
C1221 Estriol	4	238.5	269.7		86	12.1	P<0.01 w.r.t. DMSO control	Variable
C1246 Telmisartan	4	311.5	405.1		84.2	13.7	P<0.05 w.r.t. DMSO control	Variable
FF167 Hyaluronic acid Na Salt	4	323	364.1		82.2	15.5	P<0.05 w.r.t. DMSO control	Fibroblast
A-ketoester Alpha-ketoester	4	1242.3	145.4		68.7	5		Fibroblast
C1292 Pyridine-2,5-dicarboxylic acid	4	1166.8	152.3		64.1	7.6		Fibroblast
C1277 Quinazolinamine	4	1102.3	123		64.3	4.5		Large elongated cells
C1169 Bezafibrate	4	907.8	455.2		66.5	1.6		Large elongated cells
C1172	4	750	540.1		66.3	7.9		Large elongated

Chlorpropamide								cells
C1205 Primaquine Bisphosphate	4	1056	355.6		64.4	3.8		Large elongated cells
C1233 Retinoic Acid	4	482.5	89.7		62.1	3.9		Large elongated cells
F455 Phosphomycin Disodium	4	1234.3	119.1		64.1	4.9		Fibroblast
FF168 Oleic Acid	4	1305.8	61.1		62.1	8.4		Fibroblast
FF169 Retinyl Acetate	4	1150.5	201.6		61.7	3.5		Fibroblast / large elongated cells
DMEM	4	1653.3	66.7		77	8.4		Fibroblast
0.001%DMSO	4	1187.8	335.5		68.1	4.7		Fibroblast

Table 4.2.2 *– Drugs showing a statistically significant improvement over vehicle control for growth (DAPI) or marker expression (% STRO-1) and/or morphology at a concentration of 10 µM.*

Small Molecule (10µM)	n	Mean Nuclei Count	STDEV	P	% Stro1 positive cells	STDEV	P	Morphology
C1195 Levodopa	4	2174.8	86.6	P<0.01 w.r.t. DMSO control	68.6	1.8		Fibroblast
Mesalamine	4	2117	127.3	P<0.01 w.r.t. DMSO control	70.5	2.7		Fibroblast
F447 Epinephrine	4	2079.8	178.7	P<0.01 w.r.t. DMSO control	70.2	2.5		Fibroblast
C1286 Dopamine (3-Hydroxytyramine Hydrobromide)	4	1850.3	127.4	P<0.01 w.r.t. DMSO control	69.2	3		Fibroblast

C1224 Acarbose	4	1778.5	64.1	P<0.01 w.r.t. DMEM	72.5	4.5		Fibroblast
C1207 Putrescine DiHCl	4	1601.5	265.5	P<0.01 w.r.t. DMEM	52.4	33		Fibroblast
C1187 Histamine Dihydrochloride	4	1567.3	94.7	P<0.01 w.r.t. DMEM	69.3	3.4		Fibroblast
A-ketoester Alpha-ketoester	4	1566.3	190	P<0.01 w.r.t. DMSO control	71.4	2.7		Fibroblast
A200 Aminocaproic acid	4	1556.8	86.4	P<0.01 w.r.t. DMEM	65.7	4.1		Fibroblast
C240 Hydroquinone	4	1548	183.2	P<0.01 w.r.t. DMSO control	66.2	3.8		Fibroblast
C1220 Amino-3-Hydroxybutyric Acid	4	1529.8	151.2	P<0.01 w.r.t. DMEM	72.9	5		Fibroblast
F438 Sulpiride	4	1510.5	150.6	P<0.01 w.r.t. DMSO control	68.3	3.6		Fibroblast
Acetazolamide	4	1510.3	192.8	P<0.01 w.r.t. DMSO control	68.8	2.9		Fibroblast
F429 L-Noradrenaline	4	1485.3	200.3	P<0.01 w.r.t. DMSO control	67.7	4.6		Fibroblast
C1285 Cromolyn	4	1475.3	112	P<0.05 w.r.t. DMSO control	72.5	2.5		Fibroblast
F437 Sulfisoxazole	4	1474.3	345.1	P<0.05 w.r.t. DMSO control	65.4	10.5		Fibroblast
Sulphanilamide	4	1469.8	175.1	P<0.05 w.r.t. DMSO control	70.4	2.1		Fibroblast

Aminothiazole	4	1461.3	167	P<0.05 w.r.t. DMSO control	68.9	3.6		Fibroblast
Piracetam	4	1453	177.3	P<0.01 w.r.t. DMEM	73.5	2		Fibroblast
C1264 Perindopril Erbumine	4	1442.5	257.4	P<0.05 w.r.t. DMSO control	71.1	6.4		Fibroblast
FF173 DL-Homocysteine	4	1430.3	189.6	P<0.05 w.r.t. DMEM	68.3	2.1		Fibroblast
D-Glucosamine HCl	4	1410	28.9	P<0.05 w.r.t. DMEM	72.7	3.8		Fibroblast
Aminobutyric Acid	4	1407.3	221.6	P<0.05 w.r.t. DMEM	67.8	4.8		Fibroblast
C1222 Megestrol Acetate	4	1407	142.6	P<0.05 w.r.t. DMSO control	70.5	4.5		Large elongated cells
C1261 Metformin HCl	4	1402.3	38.6	P<0.05 w.r.t. DMSO control	63.2	5.2		Fibroblast
ZnCl2 Zn++ (Zinc Chloride)	4	1373.5	230.6	P<0.05 w.r.t. DMEM	71.6	3.9		Large elongated cells
C1292 Pyridine-2,5-dicarboxylic acid	4	1265	317.3		69.6	3.6		Large elongated cells
C1277 Quinazolinamine	4	1137.8	161.7		66.3	4.3		Large elongated cells
C1235 Canrenone	4	549.8	154.5		65.5	3.5		Large elongated cells
C1233 Retinoic Acid	4	618.8	95.3		68.3	2.2		Large elongated cells
C1205 Primaquine Bisphosphate	4	609.8	65.6		67.7	2.1		Large elongated cells

F436 Spermine	4	233	215.5		62.8	7.1		Large elongated cells
DMEM	4	1002	182.7		70.5	5.5		Fibroblast
0.01%DMSO	4	1036.3	77.8		68.6	3		Fibroblast

Table 4.2.3 *– Drugs showing a statistically significant improvement over vehicle control for growth (DAPI) or marker expression (% STRO-1) and/or morphology at a concentration of 100 µM.*

Small Molecule (100µM)	n	Mean Nuclei Count	STDEV	P	% Stro1 positive cells	STDEV	Morphology
C17 Adenine	4	2046	441.4	P<0.01 w.r.t. DMSO control	68.9	1.4	Fibroblast
C1195 Levodopa	4	1998	164.6	P<0.01 w.r.t. DMSO control	71	1.6	Fibroblast
Mesalamine	4	1989.8	110.4	P<0.01 w.r.t. DMSO control	77.5	5.6	Fibroblast
F437 Sulfisoxazole	4	1976.3	113.7	P<0.01 w.r.t. DMSO control	73.4	2.6	Fibroblast
F431 Synephrine	4	1908.5	72.5	P<0.01 w.r.t. DMSO control	72.3	3.2	Fibroblast
F438 Sulpiride	4	1840.3	154.5	P<0.01 w.r.t. DMSO control	77.4	1.1	Fibroblast
F429 L-Noradrenaline	4	1760.8	124.9	P<0.01 w.r.t. DMSO control	72.5	2.3	Fibroblast
FF173 DL-Homocysteine	4	1749.8	142.4	P<0.05 w.r.t. DMEM	70.4	4.2	Fibroblast
C1286 Dopamine (3-Hydroxytyramine Hydrobromide)	4	1741.5	287.5	P<0.01 w.r.t. DMSO control	73.4	3.1	Fibroblast
D-Glucosamine HCl	4	1739.3	209.5	P<0.05 w.r.t. DMEM	71	4.7	Fibroblast
Aminobutyric acid	4	1718.3	44.1	P<0.05 w.r.t. DMEM	70.8	2.4	Fibroblast

A-ketoester	4	1714	330.3	P<0.01 w.r.t. DMSO control	72	3.7	Fibroblast
Niacinamide	4	1700.5	247.9	P<0.01 w.r.t. DMSO control	74.6	4.8	Fibroblast
C398 Choline chloride	4	1690	82.5	P<0.01 w.r.t. DMSO control	66.6	3.6	Fibroblast
Acetaminophen	4	1610.8	146.7	P<0.01 w.r.t. DMSO control	69.6	1.3	Fibroblast
C1292 Pyridine-2,5-dicarboxylic acid	4	1604	256	P<0.01 w.r.t. DMSO control	76.7	2.5	Fibroblast
Caffeine	4	1598.8	260.5	P<0.01 w.r.t. DMSO control	67.7	2	Fibroblast
Acetazolamide	4	1545.5	56.8	P<0.05 w.r.t. DMSO control	70.7	3.1	Fibroblast
C240 Hydroquinone	4	1489.8	326.9	P<0.05 w.r.t. DMSO control	69.3	3.1	Fibroblast
C1285 Cromolyn	4	1470.5	134.2	P<0.05 w.r.t. DMSO control	73.7	6.3	Fibroblast
C1277 Quinazolinamine	4	1198.5	370.9		68.3	4.4	Large elongated cells
DMEM	4	1271.5	222.5		71	3	Fibroblast
0.1%DMSO	4	1026	301.7		70.4	3.5	Fibroblast

Appendix 4.3 *Optimisation of flow data for ADMSCs treated with 20ng/mL of IFN-γ and 10ng/mL of TNF-α for 4 days.*